Untersuchung des Tau-Proteins mit Hilfe von NMR-Spektroskopie

DISSERTATIONSSCHRIFT

zur Erlangung des Doktorgrades

der Naturwissenschaften

vorgelegt beim

Fachbereich Biochemie, Chemie und Pharmazie

der JOHANN WOLFGANG GOETHE-Universität

in Frankfurt am Main

von

MARCO DANIEL MUKRASCH

aus Frankfurt am Main

Frankfurt am Main

2007

vom Fachbereich Biochemie, Chemie und Pharmazie der

Johann Wolfgang Goethe-Universität als Dissertation angenommen.

Dekan: Prof. Dr. Harald Schwalbe

Gutachter: Prof. Dr. Christian Griesinger und Prof. Dr. Harald Schwalbe

Datum der Disputation: **..**

Ich möchte diese Dissertation Suse und meinen Eltern widmen.

Ihre Unterstützung war mir sehr wichtig.

Wenn nicht mehr Zahlen und Figuren

Sind Schlüssel aller Kreaturen

Wenn die so singen, oder küssen,

Mehr als die Tiefgelehrten wissen,

Wenn sich die Welt ins freye Leben

Und in die <freye> Welt wird zurück begeben,

Wenn dann sich wieder Licht und Schatten

Zu ächter Klarheit wieder gatten,

Und man in Mährchen und Gedichten

Erkennt die <alten> wahren Weltgeschichten,

Dann fliegt vor Einem geheimen Wort

Das ganze verkehrte Wesen fort.

(Georg Friedrich Philipp Freiherr von Hardenberg (1772-1801) auch genannt Novalis)

Danksagung

Während meiner gesamten Doktorarbeit wurde mir von einer Reihe von Leuten geholfen, ohne die es mir nicht möglich gewesen wäre, meine Dissertation in der vorliegenden Qualität zu verfassen. Während meiner täglichen Arbeiten bekam ich viel Unterstützung durch meine Betreuer und Kollegen im AK Griesinger. Alle Projekte waren an Kooperationen mit anderen Arbeitskreisen, der Arbeitsgruppen von Prof. E. Mandelkow (MPASMB) in Hamburg und von Dr. M. Blackledge (IBS) in Grenoble, geknüpft. Ebenfalls hatte ich das Glück, zu allen Zeitpunkten meiner Arbeit eine komfortable Finanzierung zu erfahren, die es mir erlaubte, mich vollständig auf meine Arbeit zu konzentrieren. Allen beteiligten Personen und Organisationen möchte ich nun einzeln danken, da sie es mir ermöglichten, meine Doktorarbeit zu schreiben.

Arbeitsgruppe von Prof. C. Griesinger (NMR based Structural Biology) am Max-Planck-Institut für biophysikalische Chemie (Karl Friedrich Bonhoeffer Institut) in Göttingen

Besonders schön für mich während meiner Zeit in Göttingen war das gute Verhältnis zu meinen Kollegen, die immer sehr hilfsbereit waren. Dies war eine wichtige Stütze für mich, besonders in Phasen, in denen Probleme auftauchten. Die Atmosphäre war entspannt und freundschaftlich. Insbesondere meinem Büro (Office 06/07) möchte ich hierfür danken. Dr. Daniela Fischer arbeitete mit mir am Tau-Projekt zusammen und verrichtete nahezu alle Arbeiten, die für die Publikation über Tau-Mutanten (Fischer et al., 2007) notwendig waren. Ebenso war sie eine große Hilfe für Teilprojekte, die primär von mir erledigt wurden, da sie eine wichtige Diskussionspartnerin war, mit der ich mich beraten konnte. Eine andere Mitstreiterin für das Tau-Projekt war Alice Soragni. Die Zusammenarbeit mit ihr war sehr fruchtbar und führte zu einer Reihe von interessanten Ergebnissen. Einigen anderen Kollegen schulde ich ebenfalls besonderen Dank: Dr. Vinesh Vijayan (Hilfe bei Problemen mit NMR-Spektrometern), Nils Lakomek (Hilfe bei der Herstellung von Polyacrylamidgelen für RDC-Messungen), Lukasz Skora (Unterstützung bei HR-MAS-Messungen), Jörg Fohrer (Tipps bei NMR-Messungen), Marcel Reese (Hilfe bei Computerproblemen), Dr. Carlos Bertoncini

Arbeitsgruppe von Prof. E. Mandelkow (Max-Planck-Arbeitsgruppen für strukturelle Molekularbiologie Hamburg)

Natürlich möchte ich der Max-Planck-Gesellschaft meinen Dank aussprechen. Ohne ihre finanzielle und materielle Unterstützung wären meine Arbeiten nicht denkbar gewesen.

Zusammenfassung der Dissertationsschrift

Das Tau-Protein gehört zu der Klasse der Mikrotubuli (MTs) - assoziierten Proteine (MAPs) und ist essentiell für die Aufrechterhaltung des Stoffwechsels in Neuronen. Darüber hinaus ist es ein Vertreter der intrinsisch ungeordneten Proteine (IUPs). Es spielt eine wichtige Rolle bei verschiedenen Demenzen, wie z.B. Morbus Alzheimer (Marx, 2007). Im Gehirn von Patienten, die an Morbus Alzheimer erkrankt sind, bilden sich neben β-Amyloid-Plaques „neurofibrilläre Geflechte", die aus Fibrillen (PHFs) bestehen. PHFs entstehen durch Aggregation des Tau-Proteins. Der Grund für die Aggregation von Tau, welches ein stark hydrophiles Protein ist, konnte noch nicht vollständig geklärt werden. Es ist jedoch bekannt, dass polyanionische Faktoren, wie z.B. Heparin, oder Mutationen diese Fibrillenbildung hervorrufen können (Barghorn et al. 2000).

Das Ziel der vorliegenden Doktorarbeit ist, mit Hilfe von NMR-Spektroskopie residuale Strukturelemente und Dynamiken in Tau zu detektieren, die dafür verantwortlich sein könnten, dass Tau als ungefaltetes Protein hochgeordnete Fibrillen mit einer „cross-β-Struktur" ausformen kann. Tau wurde deshalb in unterschiedlichen Zuständen charakterisiert: als lösliches Monomer, im MT-gebundenen Zustand und als PHF. Ebenfalls wurden Wechselwirkungen mit aggregationsinduzierenden Reagenzien, wie Polyglutamat und Heparin, und MTs untersucht. Zusätzlich zu Wildtyp-Tau wurden Experimente mit zwei Tau-Mutanten, P301L und ΔK280, durchgeführt, um die erhöhte Pathogenität in Tau-Mutanten besser zu verstehen. Die Ergebnisse sind in fünf Manuskripten enthalten, von denen vier (Mukrasch et al., 2005; Fischer et al., 2007; Mukrasch et al., 2007a; Mukrasch et al. 2007b) bereits veröffentlich sind.

NMR-Spektroskopie bietet sich als Technik zur Strukturaufklärung mit atomarer Auflösung im Falle von IUPs besonders an, da NMR direkt auf Proteinlösungen angewendet werden kann. Zur Behandlung der oben aufgeführten Fragestellungen wurden folgende NMR-Parameter bzw. – Methodiken verwendet: sekundärchemische Verschiebungen, residuale dipolare Kopplungen (RDCs), „chemical shift perturbation mapping", $^3J(H^N H^\alpha)$-Kopplungen, R2- bzw. R1ρ-Relaxationsraten und HR-MAS-Spektroskopie.

Das Tau-Protein kommt im Zentralnervensystem von Menschen in sechs verschiedenen Isoformen vor, von denen die größte htau40 mit 441 Resten ist. Da ein ungefaltetes Protein dieser Größe aufgrund der höchst problematischen NMR-

Signalzuordnung noch nie mit Hilfe von NMR-Spektroskopie detailliert untersucht werden konnte, wurden bei unseren Experimente zunächst Tau-Teilkonstrukte, K18 (130 Reste) und K32 (198 Reste), verwendet. K18 besteht aus einer Tau-Domäne, die durch vier „repeats" gebildet wird, die den Kern der PHFs formen und notwendig für MT-Assemblierung sind. K32 besteht aus derselben Region wie K18, besitzt aber zusätzlich zwei flankierende Domänen, die dem Konstrukt eine Affinität zu MTs verleihen, die der Bindungsstärke von htau40 nahezu gleichkommt. Aufbauend auf den Arbeiten mit diesen Konstrukten konnte die Signalzuordnung von htau40 gelöst werden. Damit stellt htau40 das größte Protein dar, dessen NMR-Resonanzzuordnung erfolgreich bewerkstelligt werden konnte.

Wir konnten in der „repeat"-Domäne von Tau Sequenzen mit partiellem β-Strukturcharakter identifizieren (^{274}Lys-Leu^{284}, ^{305}Ser-Asp^{315} und ^{336}Gln-Asp^{345}), die wir als Aggregationskeime betrachten. Zwischen diesen β-Struktursequenzen befinden sich „turn"-Regionen als flexible „linker". Als weitere Strukturelemente außerhalb der „repeats" konnten zwei Regionen (^{114}Leu-Thr^{123} und ^{428}Leu-Ala^{437}) mit α-Helixcharakter im N-terminalen Teil und nahe des C-Terminus gefunden werden. Außerdem gab es Segmente mit Tendenz zur Bildung von poly-Prolinhelices (^{175}Thr-Ser^{184}, ^{217}Thr-Lys^{224}, ^{234}Lys-Ala^{239}). Ebenfalls wurde festgestellt, dass die β-Strukturelemente sowohl aggregationsinduzierende Reagenzien als auch MTs binden. Tau-Mutanten zeigen eine deutlich verminderte Affinität zu MTs, wohingegen sie Heparin weiterhin binden. Hieraus ergibt sich folgendes Modell: Sind die Aggregationskeime in Tau aufgrund von MT-Instabilität, Phosphorylierung oder Mutationen nicht an MTs gebunden, können sie mit anderen Faktoren wechselwirken, wodurch Dimerisierung und weitere Aggregation eingeleitet werden können.

Weiterhin konnten wir in den Domänen, welche die „repeats" flankieren, MT-Bindungsstellen bestimmen, die als „jaws" bezeichnet werden. Experimente mit htau40 zeigten, dass die MT-Bindung auf die „repeat"-Domäne und die „jaws" beschränkt ist.

In HR-MAS-Messungen konnte gefunden werden, dass nur die MT-bindende Region (MTBR) den Kern von htau40-PHFs bildet und die übrigen Proteinbereiche weitestgehend eine konformationelle Flexibilität wie in monomerem Tau aufweisen.

In dieser Dissertation wurde htau40 zum ersten Mal detailliert mit atomarer Auflösung beschrieben. Residuale Strukturelemente und Bindungsregionen für polyanionische Moleküle konnten charakterisiert werden. Hieraus resultierte ein Modell, welches die Verbindung zwischen physiologischen und pathologischen Mechanismen erklärt.

Inhaltsverzeichnis

Abkürzungsverzeichnis

Aβ   Amyloid-β-peptide (Amyloid-β-Peptid)

AD   Alzheimer's disease (Morbus Alzheimer)

AMD   Accelerated Molecular Dynamics

APP   Amyloid protein precursor

ATP   Adenosine triphosphate (Adenosin-Triphosphat)

CaMK Ca^{2+}/Calmodulin-dependent kinase (Ca^{2+}/Calmodulin-abhängige Kinase)

CBD   Corticobasal degeneration (Kortikobasale Degeneration)

CD   Circular dichroism (Zirkulärer Dichroismus)

cdk5   Cyclin-dependent kinase 5 (Cyclin-abhängige Kinase 5)

CNS   Central nervous system (Zentrales Nervensystem)

CRINEPT   Cross-correlated relaxation-enhanced polarization transfer

CT   Constant time

EM   Electron microscopy (Elektronenmikroskopie)

EPR   Electron paramagnetic resonance (Elektronenspinresonanz)

FM   Flexible Meccano

FRET   Fluorescence resonance energy transfer (Fluoreszenz-Resonanz-Energie-

              Transfer)

FTDP-17   Frontotemporal dementia and Parkinsonism linked to Chromosom 17

GSK3   Glycogen synthase kinase 3 (Glykogen-Synthase-Kinase 3)

GTP   Guanosine triphosphate (Guanosin-Triphosphat)

(HA)CANNH   3D-Sequenz, bei der C^{α}_i und C^{α}_{i-1}-Atome korreliert werden

HNN   3D-Sequenz, bei der N_{i-1}, N_i und N_{i+1}-Atome korreliert werden

HSQC   Heteronuclear single quantum spectroscopy

IDP   Intrinsically disordered proteins (s. IUP)

INEPT   Insensitive Nuclei Enhanced by Polarization Transfer

IPAP   In-Phase-Anti-Phase

IUP   Intrinsically unfolded proteins (Intrinsisch ungeordnete Proteine)

MARK   Microtubule affinity regulating kinase

MAPs   Microtubule associated proteins (Mikrotubuli-assoziierte Proteine)

MTs   Microtubules (Mikrotubuli)

MTBR   Microtubule binding region (Mikrotubuli bindende Region)

MTOC   Microtubule-organizing center

NFD   Neurofibrillary degeneration (Neurofibrilläre Degeneration)

NFTs   Neurofibrillary tangles (Neurofibrilläre Geflechte)

NMR   Nuclear magnetic resonance (Nuklear Magnetische Resonanz)

NOE   Nuclear Overhauser effect (Nuklearer Overhauser Effekt)

PD   Parkinson's disease (Morbus Parkinson)

pGLU   Poly-glutamate

PKA   Protein kinase A

PKC   Protein kinase C

PHF   Paired helical filaments

PiD   Pick's disease (Morbus Pick)

PNS   Peripheral nervous system (Peripheres Nervensystem)

PRE   Paramagnetic Relaxation Enhancement

PSP   Progressive supranuclear palsy (progressive supranukleäre Blickparese)

R1-R4   Repeat sequences 1-4

RC   Random coil values ("Random coil"-Werte)

SDS   Sodium-dodecyl-sulfate

SFs   Straight filaments

S/N   Signal to noise ratio (Signal-zu-Rauschen-Verhältnis)

STEM   Scanning Transmission Electron Microscopy

TROSY   Transversal relaxation optimised spectroscopy

ZNS   Zentrales Nervensystem

1   Einleitung

Die vorliegende Dissertation beschäftigt sich mit dem Tau-Protein, welches eine wichtige Rolle in einer Reihe von Demenzerkrankungen, wie z.B. Morbus Alzheimer (AD), spielt (Marx, 2007). Die intermolekularen Wechselwirkungen und Konformationsänderungen, die Tau bei Demenzerkrankungen eingeht, sind noch nicht aufgeklärt. Gesichert jedoch ist, dass das Auftreten von Aggregaten dieses Proteins im Gehirn von demenzkranken Patienten einen entscheidenden Marker darstellt, der einen hohen Grad an Korrelation mit dem Verlauf der Krankheit aufweist (Braak and Braak, 1991). Die Aufklärung molekularer Mechanismen, die erklären könnten, wie ein hydrophiles und weitgehend ungefaltetes Protein Aggregate bilden kann, die aus hochgeordneten Fibrillen bestehen, ist deshalb von großem Interesse. Allerdings ist bisher ungesichert, ob die Fibrillen selbst oder die oligomeren Zwischenprodukte die für Neurone und Synapsen schädlichen Faktoren darstellen (Lansbury, 1999). Zumindest teilweise lässt sich die erhöhte Aggregationstendenz des Tau-Proteins durch Mutationen, wie z. B. P301L und ΔK280 (Barghorn et al., 2000), und damit einhergehenden Veränderungen, z.B. Bindung an Mikrotubuli, erklären. Außerdem sind Wechselwirkungen zu anderen Aggregate bildenden Proteinen, wie z.B. Amyloid-β-Peptid (AD) oder α-Synuclein (Morbus Parkinson (PD)), belegt, aber im Detail noch nicht erforscht (Geschwind, 2003; Goedert et al., 1998; Haass and Selkoe, 2007). Im Unterschied zu α-Synuclein, bei dem bezüglich der physiologischen Rolle in der Zelle nur die Bindung an Phospholipide belegt ist (Kahle et al., 2002)), ist die biologische Funktion des Tau-Proteins relativ ausführlich in der wissenschaftlichen Primärliteratur der letzten Jahrzehnte beschrieben (Reviews: Cassimeris and Spittle, 2001; Garcia and Cleveland, 2001). Tau ist ein Mikrotubuli-assoziiertes Protein (MAP) und gehört damit zu einer ganzen Klassen von Proteinen, die z. T. sequentielle und auch funktionale Homologien aufweisen. Vertreter dieser Proteinklasse sind durch ein komplexes Netzwerk bestehend aus regulatorischen Mechanismen, die zumeist durch Phosphorylierungsmuster der einzelnen Proteine bewerkstelligt werden, miteinander verknüpft (Dehmelt and Halpain, 2004; Dehmelt and Halpain, 2005). Hierbei werden dynamische Prozesse kontrolliert, die für das Überleben der Zelle essentiell sind.

Um die genannten Aspekte des Tau-Proteins, physiologische wie pathologische, auf einer molekularen bzw. atomaren Ebene zu untersuchen, wird als Technik der Wahl die

Nuklear Magnetische Resonanz-Spektroskopie (NMR) verwendet. Anders als Kristallographie ist sie nicht darauf angewiesen, Kristalle des Proteins zu erhalten, was sich für die Klasse der ungefalteten Proteine als sehr problematisch herausgestellt hat. NMR Spektroskopie kann in Lösung (Flüssig-NMR) oder amorphen Phasen (Festkörper-NMR) durchgeführt werden. Außerdem stellt sie eine Reihe von Werkzeugen zur Verfügung, die die Untersuchung von molekularer Dynamik mit atomarer Auflösung ermöglichen, wie z.B. residuale dipolare Kopplungen (RDCs) (Tjandra and Bax, 1997; Tolman et al., 1995; Bernadó et al., 2005a; Blackledge, 2005) und Relaxationszeiten (Palmer et al., 2001)).

Der erste Teil der Dissertation besteht aus einer Einleitung, in der primär die biologischen Grundlagen der Tauopathien erklärt werden. Die Einleitung beginnt mit einer kurzen Darstellung der Rolle von Proteinen und insbesondere deren Faltung im lebenden Organismus. Es werden Mechanismen beschrieben, die den entscheidenden aber auch kritischen Vorgang der Proteinfaltung kontrollieren. Weiterhin wird der pathologische Fall der Proteinfaltung, die sogenannten Aggregopathien, wie z.B. AD, erwähnt. Nach dieser allgemeinen Darstellung der Funktion bzw. Fehlfunktion von Proteinen konzentriert sich die Beschreibung auf das Cytoskelett der Zelle. Wie schon erwähnt, ist die biologische Rolle von Tau hier angesiedelt, weshalb es wichtig ist, die Basis der Funktion und des Aufbaus des Cytoskeletts zu beschreiben, wobei die Mikrotubuli eine besonders ausführliche Erwähnung erfahren. Im Anschluss wird auf die Funktion der MAPs eingegangen und die Rolle von Tau genauer definiert. Im darauf folgenden Abschnitt steht der pathologische Fall im Vordergrund. Der aktuelle Kenntnisstand der Aggregationsmechanismen des Tau-Monomers zu den „paired helical filaments" (PHFs) bzw. neurofibrillären Geflechten (NFTs) wird beschrieben. Die Einleitung schließt mit methodischen Aspekten der NMR-Spektroskopie. Insbesondere jene NMR-Methodiken werden erläutert, die zur Erlangung der experimentellen Resultate beigetragen haben. Danach folgen vier Publikationen, die nahezu alle Ergebnisse und neuen Erkenntnisse, die während der Promotion des Autors erzielt wurden, enthalten. Außerdem wird das Manuskript einer geplanten fünften Veröffentlichung hinzugefügt, welches die Ergebnisse der Arbeiten mit der größten Tau-Isoform htau40 enthält.

Die erste Publikation (Mukrasch et al., 2005) stellt den Grundstein für die folgenden Veröffentlichungen dar. Die experimentellen Prinzipien, die in dieser Arbeit zum ersten Mal auf ein Konstrukt (K18) (s. **Abb. 1**) des Tau-Proteins angewendet wurden, konnten für die weiteren Veröffentlichungen weitestgehend beibehalten werden. Entscheidend war die Zuordnung der Resonanzen im NMR-Spektrum des Konstrukts K18, die aufgrund der

geringen Dispersion in der ^{1}H-Dimension und der starken sequentiellen Monotonie, eine Herausforderung war (**Abb. 2**). K18 besteht ausschließlich aus einer Domäne des Tau-Proteins, die aus vier sogenannten „repeats" (4R) gebildet wird (**Abb. 1**). Dieser sequentielle Bereich von Tau stellt den Kern der Alzheimerfibrille dar, welcher aus einer Cross-β-Struktur besteht (Barghorn and Mandelkow, 2002). Die Region der 4 „repeats" (R1-R4) sollte alle strukturellen Eigenschaften enthalten, die der Aggregation von Tau zugrunde liegen. Überdies ist sie für die Assemblierung von Mikrotubuli notwendig und übt so einen Teil der biologischen Funktion des vollständigen Tau-Proteins in seiner zellulären Umgebung aus (Mandelkow, 2004). Aus diesem Grund sollten die Bindungsstellen von K18 an Mikrotubuli mittels „chemical shift perturbation mappings" bestimmt werden. Diese Technik wurde auch angewendet um herauszufinden, an welchen Stellen aggregationsinduzierende Reagenzien, wie pGLU und Heparin, an Tau binden. Zur Definition residualer Strukturen in der „repeat"-Domäne wurden sekundärchemische Verschiebungen (C$^\alpha$ und CO) herangezogen (Wishart and Sykes, 1994b). Wie von Dyson & Wright (2005) beschrieben, sollten mit Hilfe dieser Technik auch für ein ungefaltetes Protein Rückschlüsse bezüglich struktureller Tendenzen möglich sein. Alle diese Experimente wurden analog mit dem Konstrukt K19 durchgeführt, welches aus nur 3 „repeats" besteht, um mögliche Unterschiede zwischen der 3R- und 4R-Form von Tau zu untersuchen. Mit Hilfe dieser erworbenen Daten konnte ein Vorschlag für einen Aggregationsmechanismus erstellt werden: Bereiche mit partiellem β-Struktur-Charakter (G^{273}-L^{284}, G^{304}-L^{315} und G^{333}-D^{345}) fungieren als Aggregationskeime, die aber gleichzeitig auch Bindungsstellen für MTs und Heparin sind. Demnach können Polyanionen an diese Stellen binden, wenn sie nicht mehr durch MTs blockiert sind, repulsive positive elektrostatische Wechselwirkungen abschirmen und so die Aggregation einleiten.

Die für diese Publikation notwendigen 3D-NMR-Experimente wurden zum größten Teil von M. Zweckstetter gemessen. Es handelte sich hier um HACANNH- (Zweckstetter and Bax, 2001b) und HNN-Sequenzen (Panchal et al., 2001). Beide Experimente ergänzten sich sehr gut bezüglich der Konnektivitätsinformationen, da sie jeweils komplementäre Informationen lieferten. Die Titrationsexperimente hingegen wurden vom Verfasser der vorliegenden Dissertation durchführt, wie auch die Auswertung aller Experimente und das Lösen der Zuordnung. Wie bei allen folgenden Publikationen wurden alle präparativen Arbeiten durch die Arbeitsgruppe von Prof. E. Mandelkow (insbesondere J. Biernat und M. von Bergen) vorgenommen.
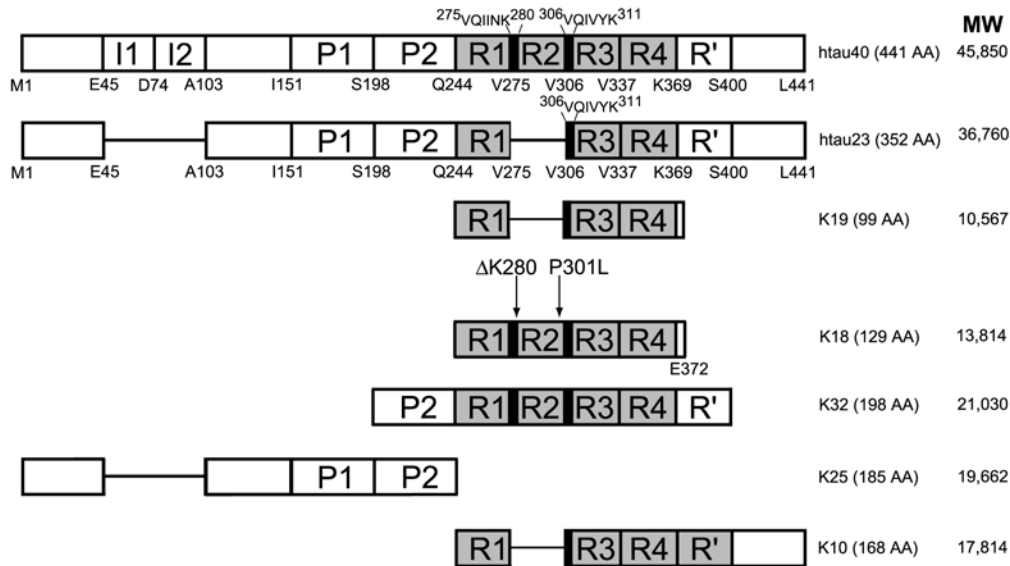
Abb. 1: Schematischer Aufbau der Tau-Konstrukte: Neben der größten (htau40) und kleinsten Tau-Isoform (htau23) sind alle in den Publikationen verwendeten Tau-Konstrukte aufgeführt. Schwarze Balken zeigen Hexapeptidmotive an. Die Mutationen ΔK280 und P301L sind für K18 eingezeichnet.

Die zweite Publikation (Fischer et al., 2007) konzentriert sich auf den Unterschied im Aggregations- und MT-Bindungsverhalten von Tau-Mutanten im Vergleich zum Wildtyp. Hierfür wurden zwei Mutationen innerhalb der „repeat"-Region (R1-R4), die bei realen Krankheitsverläufen *in vivo* eine Rolle spielen, untersucht. Die beiden folgenden Konstrukte wurden untersucht: K18-P301L und K18-ΔK280 (von Bergen et al., 2001) (**Abb. 1**). Die gesamte Arbeit beruht auf der Signalzuordnung von K18 aus der ersten Publikation. Bis auf eine Titration (P301L+MT mit NaCl wurde vom Autor dieser Dissertation gemessen) wurden alle NMR-Messungen und deren Auswertung von der Postdoktorandin D. Fischer durchgeführt. Als besonders interessant erwiesen sich Vergleiche der sekundärchemischen Verschiebungen der Mutanten mit denen des Wildtyps, da beide Mutanten zu einer verstärken Aggregation neigen, was eventuell mit einem höheren Gehalt an β-Struktur erklärt werden könnte. Außerdem sollte mit Hilfe von „chemical shift perturbation mapping" die veränderte Interaktion der beiden Konstrukte zu Heparin und Mikrotubuli quantifiziert werden. Das Ziel war, ein Modell für das veränderte Aggregations- und Bindungsverhalten der Tau-Mutanten zu postulieren. Hiernach verfügen die Mutanten über dieselben Aggregationskeime wie der Wildtyp, wobei jedoch ihre Affinität für MTs herabgesetzt ist, weswegen sie vermehrt im ungebundenen Zustand anzutreffen sind. Sie binden jedoch weitestgehend im gleichen Maße

an Polyanionen wie der Wildtyp und neigen so zur Aggregation, da die Aggregationskeime nicht durch Bindung an MTs geschützt sind.

Bei der dritten Publikation (Mukrasch et al., 2007b) wurde ein neues Tau-Konstrukt, K32, verwendet. Dieses Konstrukt verfügt zusätzlich zu der „repeat"-Domäne über zwei flankierende Regionen (P2 und R') (**Abb. 1**), die zur einer MT-Bindungsaffinität führt, die nahe der Affinität der längsten Tau-Isoform, htau40, liegt. P2 und R' enthalten Sequenzabschnitte, die in Veröffentlichungen der Arbeitsgruppe Mandelkow als „jaws" bezeichnet werden (Preuss et al., 1997). Sie sind unerlässlich für eine feste MT-Bindung, die es den „repeats" ermöglicht, ihre biologische Aufgabe, die Assemblierung der MTs, effizient zu erfüllen. Außerdem war ein Vergleich der sekundärchemischen Verschiebungen von K32 zu denen von K18 interessant, da die beiden umgebenden Domänen eventuell Veränderung der Sekundärstruktur der R1-R4-Domäne induzieren könnten. Alle für diese Publikation erforderlichen NMR-spektroskopischen Messungen (Ausnahme: eine K32+MT-Titration ohne NaCl von D. Fischer) sowie deren Auswertung (Signalzuordnung und Titrationsverläufe) wurden vom Verfasser der vorliegenden Arbeit durchgeführt. Hierbei ist zu erwähnen, dass wiederum M. von Bergen für die MT-Polymersierung verantwortlich war.

Die vierte Publikation (Mukrasch et al., 2007a) beruht auf einer Zusammenarbeit mit der Gruppe von Martin Blackledge (Grenoble). Hierbei wurden alle erforderlichen experimentellen Daten ausschließlich vom Verfasser der vorliegenden Arbeit erstellt. Alle Simulationen und theoretischen Arbeiten wurden durch P. Markwick durchgeführt, woraus sich die geteilte Erstautorenschaft ergibt. Im Fokus dieser Arbeit steht wiederum das Konstrukt K18, welches aus der R1-R4-Domäne besteht. Hierbei wurden strukturelle Informationen wie residuale dipolare Kopplungen, $^3J(H^N H^\alpha)$-Kopplungen und NOE-Signale gemessen und mit den Ergebnissen aus den sekundärchemischen Verschiebungen verglichen. Es ergab sich eine weitestgehende Übereinstimmung bei der Bestimmung von β-Strukturelementen und „turn"-Motiven (L^{253}-K^{254}, L^{284}-S^{285}, L^{315}-S^{316} und L^{346}-K^{347}). Mit Hilfe des Algorithmus „flexible meccano" (FM) (Bernadó et al., 2005a; Bernadó et al., 2005b) und „accelerated molecular dynamics" (AMD) konnten diese residualen Strukturen bestätigt werden. Überdies konnten durch Simulationen die „turns" bezüglich Dihedralwinkeln und ihrer Typen (βI-turn) genauer charakterisiert werden. FM und AMD bestätigten dieses Modell und sagten residuale dipolare Kopplungen sowie $^3J(H^N H^\alpha)$-Kopplungen akkurat voraus.

Aufbauend auf den Zuordnungsdaten der vorangegangenen Veröffentlichungen und der Zuordnung zusätzlicher Konstrukte (K10, K25) (s. **Abb. 1**) konnten die Amidresonanzen der größten der sechs Tau-Isoformen, htau40, erfolgreich zugeordnet werden (**Abb. 2**). Es wurde dieselbe Strategie wie bei den anderen Konstrukten verfolgt. Alle Spektren, deren anschließende Auswertung und die erforderliche Zuordnung wurden vom Autor der vorliegenden Dissertation durchgeführt. Parallel zu diesen Arbeiten erschienen einige Veröffentlichungen der Gruppe von G. Lippens (Landrieu et al., 2006; Lippens et al., 2006; Sibille et al., 2006; Sillen et al., 2007; Sillen et al., 2005a; Sillen et al., 2005b), die auf einer Zuordnung von 40-50% der Rückgratamidresonanzen von htau40 basieren. Dies war für uns eine weitere Motivation, da es nicht sicher war, ob es wirklich möglich sei, ein ungefaltetes Protein der Größe von htau40 (s. **Abb. 2**) vollständig mit NMR-Spektroskopie zu analysieren. Mit Hilfe erstens der separaten Zuordnung verschiedener Teilbereiche von htau40, zweitens Hochfeldspektrometern (900 MHz) mit Cryo-Probenkopf und drittens der (HA)CANNH- bzw. HNN- Sequenzen war es uns möglich, die Zuordnung zu lösen. Der Vorteil des (HA)CANNH-Experiments liegt in seiner hohen Auflösung, während die HNN-Sequenz die ^{15}N-Dimension mit ihrer hohen Dispersion nutzt. Basierend auf der Zuordnung konnten Sekundärstruktur und Dynamik des Proteinrückgrats beschrieben werden. Es wurde klar ersichtlich, dass sich die Mikrotubuli bindende Region (MTBR) von dem Rest des Proteins bezüglich Sekundärstruktur und Dynamik unterscheidet. Während die MTBR das größte Vorkommen von β-Struktur in R2 und R3 zeigt, konnten wir außerhalb der MTBR zwei Regionen (Leu^{114}-Thr^{123} and Leu^{428}-Ala^{437}) mit α-Helixcharakter ausmachen, von denen eine auf den zweiten Insert (I2) folgt und die andere sich am C-terminalen Ende des Proteins befindet. Zusätzlich konnten wir Thr^{175}-Ser^{184}, Thr^{217}-Lys^{224} und Lys^{234}-Ala^{239} als sequentielle Bereiche mit partiellem Polyprolin-helikalem Charakter identifizieren. RDCs und R1ρ-Relaxationsraten spiegeln überdies den Gegensatz der relativ rigiden MTBR zu den eher flexiblen flankierenden Regionen wider. Bei Bindungsstudien mit MTs war es möglich, die stärksten Bindungsstellen zu bestimmen, was wir in einer differenzierteren Form als die Gruppe von G. Lippens durchführen konnten, die eine Tendenz für eine sehr breite Region erkannte, aber nicht auf die genauen Bindungsstellen schließen konnte, da das ihnen vorliegende Assignment nicht vollständig war. Die von uns erzielten Ergebnisse bestätigten exakt die Bindungsdaten, die wir schon an K32 messen konnten. Da wir nun zum ersten Mal mit einer Tauform arbeiteten, die zusätzlich zu P2, R1-R4 und R' über die gesamte N-terminale Hälfte und den vollständigen C-terminalen Teil verfügt, untersuchten wir htau40-Fibrillen mit Hilfe von HR-MAS-NMR-Spektroskopie (900 MHz), um eventuelle flexible

Bereich innerhalb des Fibrillenkerns (Pro^{206}-Asp^{402}) und in den ihn umgebenden Regionen („fuzzy coat") genauer zu lokalisieren. Abschließend kann man sagen, dass die Arbeit mit htau40 einen sehr aufschlussreichen Schlusspunkt der vorliegenden Dissertation bildete, der es ermöglichte, die vorhergehenden Arbeiten zu bestätigen und sie in einen größeren Rahmen einzuordnen. Außerdem bedeutete es, die Grenzen für NMR-Spektroskopie bezüglich der Analyse von ungefalteten Proteinen auszudehnen.
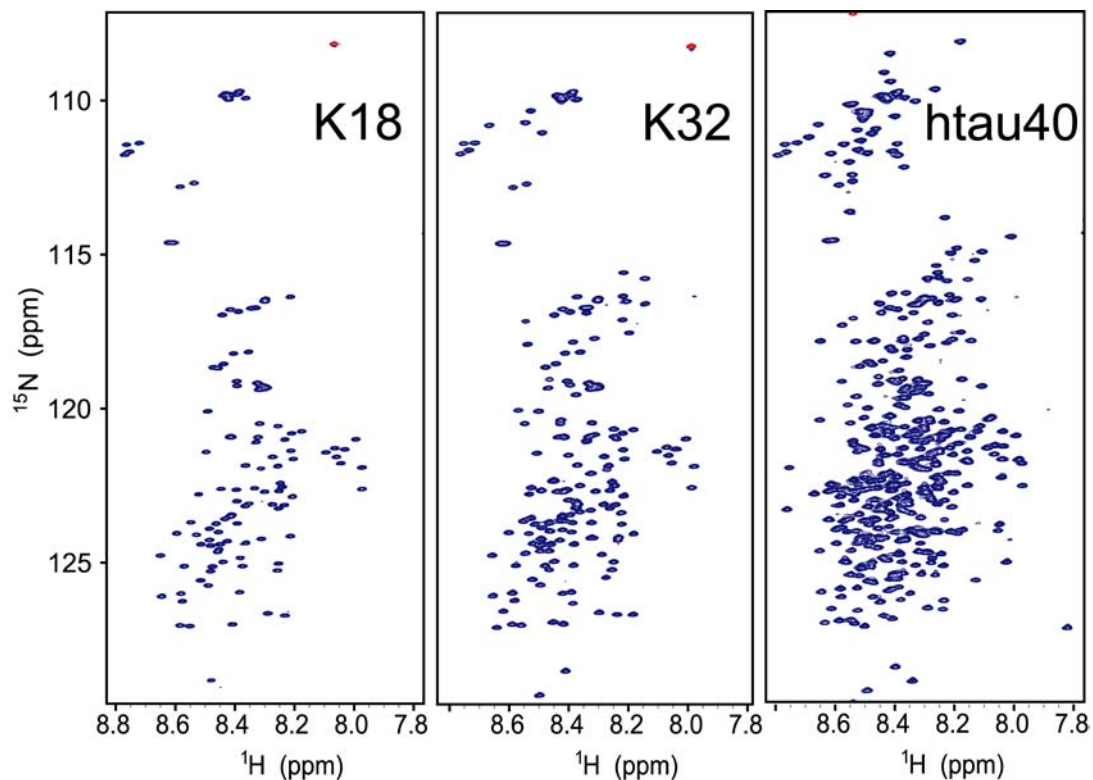
Abb. 2: ^{1}H, ^{15}N- HSQC-Spektren von K18, K32 und htau40. K18: 130 Reste (Zuordnung April 2004), K32: 198 Reste (Zuordnung Juni 2005) htau40: 441 Reste (Zuordnung Oktober 2006)

Folgende Publikationen bilden das Kernstück der vorliegenden Dissertation:

1. Marco D. Mukrasch, Jacek Biernat, Martin von Bergen, Christian Griesinger, Eckhard Mandelkow and Markus Zweckstetter **Sites of Tau Important for Aggregation Populate β-Structure and Bind to Microtubules and Polyanions** *J. Biol. Chem.* (2005) **280(26)**, 24978-24986

   Anteil des Autors: Zuordnung der Rückgratamidprotonen, Durchführung und Auswertung der Titrationsexperimente.

2. Daniela Fischer, Marco D. Mukrasch, Martin von Bergen, Aleksandra Klos-Witkowska, Jacek Biernat, Christian Griesinger, Eckhard Mandelkow and Markus Zweckstetter **Structural and Microtubule Binding Properties of Tau Mutants of Frontotemporal Dementias** *Biochemistry* (2007) **46**, 2574-2582

   Anteil des Autors: Die Arbeit ist auf der Signalzuordnung von K18 aufgebaut. Ein Titrationsexperiment wurde durch den Autor durchgeführt.

3. Marco D. Mukrasch, Martin von Bergen, Jacek Biernat, Daniela Fischer, Christian Griesinger, Eckhard Mandelkow and Markus Zweckstetter **The "Jaws" of the Tau-Microtubule Interaction** *J. Biol. Chem.* (2007) **282(16)**, 12230-12239

   Anteil des Autors: Messung aller Spektren (bis auf eine K32+MT-Titration) und deren Auswertung einschließlich der Lösung der Signalzuordnung für K32.

4. Marco D. Mukrasch[*], Phineus Markwick[*], Jacek Biernat, Martin von Bergen, Pau Bernado, Christian Griesinger, Eckhard Mandelkow, Markus Zweckstetter and Martin Blackledge **Highly Populated Turn Conformations in Natively Unfolded Tau Protein Identified from Residual Dipolar Couplings and Molecular Simulation** *J. Am. Chem. Soc.* (2007) **129**, 5235-5342 ([*] Beide Autoren haben zu gleichen Teilen zur Veröffentlichung beigetragen.)

   Anteil des Autors: Messung und Auswertung aller experimenteller Daten.

Ebenfalls wurde ein noch nicht veröffentlichtes Manuskript eingefügt, welches die Daten von htau40 enthält:

Marco D. Mukrasch, Sadasivam Jeganathan, Jacek Biernat, Christian Griesinger, Eckhard Mandelkow und Markus Zweckstetter **Structural Polymorphism of 441 Residue Tau at Atomic Resolution**

Anteil des Autors: Messung aller Spektren und deren Auswertung sowie die Zuordnung der htau40-Signale.

Unsere Arbeiten zeigen, dass NMR-Spektroskopie die Methode der Wahl ist, um ungefaltete Proteine mit atomarer Auflösung zu charakterisieren. Wir haben verschiedene Techniken zusammengestellt und erprobt, um möglichst effizient Fragen nach dem Grund für Taus Pathogenität und deren Zusammenhang mit der biologischen Funktion des Proteins beantworten zu können. Anhand der Untersuchung von htau40, einem Protein mit der Länge von 441 Resten, lässt sich ersehen, dass es die Kombination aus bereitstehenden NMR-Techniken ermöglicht, das Größenlimit der NMR-Spektroskopie für ungefaltete Proteine heraufzusetzen. Damit eröffnet sich die Möglichkeit, eine ganze Klasse von Biomakromolekülen detailliert zu erforschen, die zwar immer größere Aufmerksamkeit erfährt, sich bis jetzt jedoch einer näheren Charakterisierung weitestgehend entziehen konnte. Mit Hilfe unserer Daten kann das Aggregationsverhalten und auch die MT-Bindung des Tau-Proteins genauer verstanden werden. Insbesondere die wichtige Rolle der Domäne R1-R4 bei der Fibrillisierung konnte weitestgehend durch unsere Experimente erklärt werden. Es ist bekannt, dass insbesondere bei Aggregopathien Proteinaggregate entstehen, die Cross-β-Struktur aufweisen. Wir konnten am Beispiel Taus zeigen, dass auch schon in der monomeren Form klare Tendenzen vorhanden sind, β-Struktur zu formen. Besonders ausgeprägt ist dies für die Regionen R2 und R3. Demnach ist der große, wenn nicht sogar der ausschließliche Anteil der Tau-Pathogenität in diesen Sequenzen enthalten, was zusätzlich dadurch bestätigt wird, dass dieser Abschnitt mitten im Kern der Alzheimer-Fibrillen liegt. Deshalb ist es

gerechtfertigt, diese Regionen als Aggregationskeim zu bezeichnen, der von uns exakt identifiziert werden konnte (Gly^{273}-Leu^{284} und Gly^{304}-Leu^{315}). Therapien gegen AD sind darauf angewiesen, molekulare Zusammenhänge möglichst exakt zu überblicken, um z.B. Fibrillenbildung-inhibierende Substanzen zu entwickeln und deren genaue Wirkungsweise verstehen zu können. Durch die vorliegenden Zuordnungen ist dies zum ersten Male möglich geworden, da man nun mit NMR-spektroskopischen Methoden in der Lage ist, Interaktionen zwischen medizinischen Substanzen und dem Tau-Protein detailliert beschreiben zu können. Demnach könnten sich R2 und R3 als mögliche „targets" für aggregationshemmende Wirkstoffe herausstellen.

Interessanterweise spielt die aggregationsanfällige Region R2 und R3 eine wichtige Rolle bei der Bindung von Tau an Mikrotubuli und auch an aggregationsfördernde Substanzen wie Polyanionen. MTs könnten daher durch Bindung an die aggregationsanfällige Region die Aggregationskeime blockieren. Polyanionen binden jedoch auf dieselbe Weise an R2-R3 des ungebundenen Tau-Proteins und können so PHF-Bildung auslösen. Hieraus ergibt sich, dass als Grund für das Auftreten von Demenzen mit der Beteilung des Tau-Proteins ebenfalls Prozesse bzw. Mutationen in Betracht gezogen werden müssen, die die Stabilität von Mikrotubuli und auch die Affinität von Tau zu ihnen verändern können. Demnach sind Aggregopathien vielschichtige Prozesse, deren genaueren Charakterisierung es bedarf, um Methoden zu entwickeln, die diesem Krankheitstyp entgegenwirken, der insbesondere in einer zunehmend alternden Gesellschaft verheerende Folgen zeitigen kann.

1.1   Proteinfaltung – Die Basis für biologische Aktivität

Jeder Organismus muss, um zu überleben und erfolgreich auf seine Umwelt reagieren zu können, eine Fülle metabolischer Leistungen erbringen. Beispiele hierfür sind der grundlegende Aufbau biologischer Substanzen, aus welchen Zellen aufgebaut sind (wie Zellmembran und Organellen), die Weitergabe von Erbinformationen (Replikation von DNA) und deren Umsetzung in biologische Funktionen (Transkription und Translation von RNA). RNA kann einige Funktionen im Stoffwechsel von Organismen besetzen, wie z.B. Riboswitches (Winkler and Breaker, 2005) und micro-RNA (Aravin and Tuschl, 2005), die bei der Kontrolle der Genexpression eine Rolle spielen. Außerdem wird vermutet, dass sie am Beginn der Entwicklung des Lebens die maßgebliche Rolle als Katalysator gespielt hat (Chen et al., 2007). Trotzdem ist es unbestreitbar, dass Proteine gegenwärtig den größten Anteil an der katalytischen und regulatorischen Grundlage des Lebens bilden.

Im menschlichen Organismus verleihen 20 Aminosäuren (bzw. mit Hydroxyprolin 21) als Bausteine von Proteinen diesen eine praktisch unbegrenzte strukturelle und damit auch funktionelle Vielfalt. Diese Vielfalt wird zusätzlich durch posttranslationale Modifikationen, wie z.B. Methylierungen, Phosphorylierungen, Glykosylierungen und Sulfatierungen, erweitert. Aufgrund einer hohen Variationsbreite bezüglich Hydrophobizität, Hydrophilie, Ladung und sterischer Charakteristika können alle erforderlichen Eigenschaften ausschließlich in der Proteinsequenz (Primärstruktur) kodiert werden. Insbesondere am Beispiel der Enzyme wird der Grad der Entwicklung deutlich, den Proteine in der Evolution erfahren haben. Einige Enzyme erreichen eine derartige katalytische Perfektion, dass sie die Kinetik einiger metabolischer Prozesse zu einer diffusionskontrollierten Reaktion optimieren. Die Reaktionsgeschwindigkeit wird demnach einzig durch die neuerliche Versorgung des Enzyms mit Metaboliten bestimmt. Damit diese enorme Effizienz erreicht werden kann, ist eine sehr präzise Kontrolle der Bindung und Orientierung der Reaktanden notwendig. Grundlage hierfür ist die Proteinstruktur, die es ermöglicht, dass aktives Zentrum und eventuelle Coenzyme ihre Funktion optimal erfüllen können. Dies bedeutet, dass es für einige Proteinfunktionalitäten notwendig ist, dass eine translatierte Aminosäurekette durch Faltung eine 3D-Struktur erhält. Eine Zelle muss demnach für die Aufrechterhaltung ihrer Funktionen

über ein breites Instrumentarium verfügen, welches den Ablauf der Faltung eines Proteins exakt kontrolliert. Nur auf diese Weise können Proteine ihre Funktionalität erhalten und auch unter eventuellen Veränderungen äußerer Bedingungen (pH-Wert, Temperatur) beibehalten oder erneut erlangen. Darüber hinaus ist in vielen Studien in den vergangenen Jahren belegt worden, dass aus einer Fehlfaltung von Proteinen sogar Gefahren für das Leben von Zellen und so für den ganzen Organismus hervorgehen können (Dobson, 2003; Zerovnik, 2002).

1.1.1 Kontrolle der Proteinfaltung

Proteine weisen unterschiedlichste Grade an Komplexität auf. Diese Größenvielfalt reicht von relativ kleinen Proteinen wie Ubiquitin (76 Reste), dessen Funktion die Markierung eines zur Proteolyse bestimmten Proteins ist, bis hin zu gigantischen Multienzymkomplexen wie den Pyruvat-Dehydrogenase-Komplex (~ 4.6 MDa). Entsprechend dieser Variationsbreite sind verschiedene Mechanismen für eine Faltung nötig. Das Levinthalparadoxon spiegelt frühe Überlegungen bezüglich der kombinatorischen Vielfalt unterschiedlicher konformationeller Möglichkeiten einer Peptidkette wider. Hierbei wird deutlich, dass auch kleine Proteine ihre Struktur in keiner akzeptablen Zeitspanne erreichen könnten, wenn alle Konformere gleichermaßen energetisch zugänglich wären bzw. durchgespielt würden (Levinthal, 1968).

Durch die Forschung der letzten Jahre wurde deutlich, dass die Faltung von Proteinen bestimmten Prinzipien folgt, die eine zeitliche Effizienz und starke Qualitätskontrollen ermöglichen. Zahlreiche Proteine falten im Endoplasmatischen Retikulum (ER), in welchem ein komplexes Schema von Glykosylierungsschritten sicherstellt, dass nur Proteine erhalten bleiben, die eine korrekte Faltung aufweisen, da sonst pathogene Proteinaggregationen hervorgerufen werden könnten (Hammond and Helenius, 1995; Kaufman, 2002; Schroder and Kaufman, 2005). Es konnte beobachtet werden, dass Teile von Proteinen unabhängig voneinander falten. Diese sich praktisch autonom formenden Domänen weisen schon früh während des Faltungsprozesses weitestgehend dieselben strukturellen Eigenschaften auf wie im nativen Endzustand des Proteins. Hierdurch werden die statistisch möglichen Übergangszustände um zahlreiche Größenordnungen reduziert. Sekundärstrukturelemente können sehr schnell ausgebildet werden, z.B. α-Helices in 100 ns und β-Faltblätter in ~ 1 μs. Kleine Proteine mit starkem α-helikalem Anteil können sich in ca. 50 μs falten (Mayor et al.,

2003; Snow et al., 2002; Yang and Gruebele, 2003). Nachdem diese Sekundärstrukturen entstanden sind, liegt das Protein in der Form des sogenannten „molten globule" vor, welcher auch im Falle eines reversiblen Faltungsprozesses bei einer schrittweisen Denaturierung des Proteins erreicht werden kann (Klein-Seetharaman et al., 2002; Wirmer et al., 2004). Vergleicht man Protonenaustauschraten oder NMR-Parameter wie Relaxationszeiten (T2 bzw. T1ρ), J-Kopplungen und NOE-Raten der nativen Form mit den rudimentären Struktursegmenten eines Proteins unter modulierten denaturierenden Bedingungen (Fiebig et al., 1996), erkennt man große Übereinstimmungen. Im Übergangszustand ist die Ausbildung von Kontakten zwischen sogenannten „key residues" notwendig, welche auch im nativen Zustand vorliegen, damit sich der Faltungsprozess korrekt vollzieht (Dobson, 2003b) (s. **Abb. 3**). Demnach liegen die Domänen schon im frühen Faltungsstadium weitestgehend strukturiert vor. Hydrophobe Kontakte (Dyson et al., 2006) leiten primär die Proteinfaltung ein („hydrophober Kollaps"). Die energetische Grundlage hierfür ist, dass Aminosäurereste mit hydrophoben Seitenketten vorwiegend im Inneren des Proteins lokalisiert sein müssen, um den thermodynamisch stabilsten Zustand zu erreichen, da aufgrund des „Eisbergeffektes" ein möglichst minimierter Kontakt zum Solvens angestrebt wird. Hydrophile Reste bilden deshalb zumeist die dem wässrigen Milieu zugewandte Proteinoberfläche.
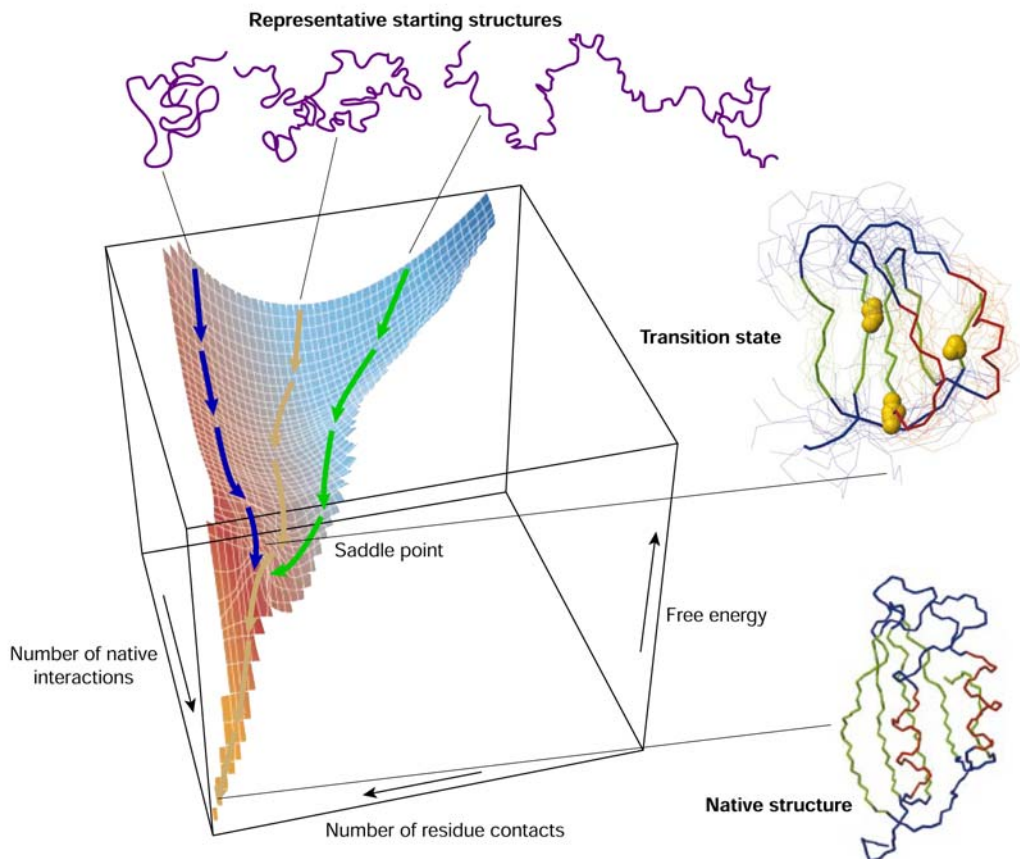
Abb. 3: Schematische Darstellung des energetischen Verlaufs der Proteinfaltung. Ein ungefaltetes Protein erreicht seine native Form durch Minimierung der Freien Enthalpie und Maximierung der Zahl der nativen und interresidualen Kontakte. Der Sattelpunkt stellt den Übergangszustand dar, in dem die Wechselwirkungen zwischen den Schlüsselresten (gelbe Kugeln) ausgebildet werden müssen (entnommen aus Dobson, 2003).

Kleinere Proteine können die in ihrer Sequenz angelegte Struktur ohne äußere Hilfe in sehr kurzer Zeit formen. Bei anderen Proteinen sind jedoch spezielle zelluläre Faktoren, wie Chaperone und Chaperonin, notwendig. Chaperone konnten in Zellen, die einem Hitzeschock ausgesetzt waren, zum ersten Mal beobachtet werden. Diese speziellen Hitzeschockproteine wurden von den betreffenden Zellen gebildet, um den Auswirkungen der höheren Temperatur auf die Proteinausstattung entgegenzuwirken oder rückgängig zu machen (Tissieres et al., 1974). Sie sind ebenfalls notwendig, um die Faltung von Proteinen zu beschleunigen, die ohne diese Hilfe kaum oder nur sehr langsam ihre native Form erlangen können. Chaperone erfüllen dies, indem sie metastabile Faltungszustände destabilisieren und es so dem Protein ermöglichen, schneller in den thermodynamisch stabilsten (nativen) Zustand zu gelangen. In

einigen Fällen ist hierzu ATP notwendig (Bukau and Horwich, 1998; Bukau et al., 2006; Hartl and Hayer-Hartl, 2002).

Fehlfaltung von Proteinen führt dazu, dass Proteinsegmente mit hydrophoben Sequenzen nicht im Inneren des Proteins angesiedelt werden, sondern nach außen weisen können. Diese fehlgefalteten Proteine sind anfällig für Aggregation, welche mit der Bildung von Oligomeren beginnt und über Protofibrillen zu sogenannten Amyloid-Fibrillen bzw. -Plaques fortschreitet. Die Bezeichnung „Amyloid" leitet sich aus der Beobachtung ab, dass sich diese Proteinaggregate ähnlich der Amylose mit Jod anfärben lassen (Virchow, 1854). Die Fähigkeit zur Aggregation ist bei allen Proteinen vorhanden (Chiti et al., 1999; Dobson, 1999), da die hauptsächliche energetische Stabilisierung der Aggregate durch Rückgratkontakte, wie z.B. hydrophobe Wechselwirkungen und Wasserstoffbrücken, zustande kommt. Gemeinsam ist allen Amyloidaggregaten, dass sie durch spezifische Farbstoffe wie Kongo-Rot angefärbt werden können. Ebenfalls verfügen alle Amyloide über eine „cross-β"-Struktur (Sunde and Blake, 1997; Sawaya et al., 2007). Die Aminosäuresequenz eines aggregierenden Proteins kann nur Details im Aufbau der Amyloide beeinflussen, deren allgemeinen Charakter jedoch nicht verändern (Chamberlain et al., 2000). Welche Aggregationsstufe – Oligomer, Protofibrille oder Amyloidfibrille – für die Zelle letztendlich toxisch ist und auf welchem molekularen Weg diese schädliche Wirkung vermittelt wird, ist noch nicht geklärt (Koo et al, 1999; Caughey and Lansbury, 2003).

1.1.2 Intrinsisch ungeordnete Proteine (IUPs)

Im obigen Abschnitt wurde die Wichtigkeit der 3D-Struktur von Proteinen bezüglich ihrer enzymatischen Funktion dargelegt. Dies wurde zum ersten Mal von Fischer 1894 dokumentiert, als er chirale Selektivität bei der Hydrolysierung glykosidischer Bindungen in extrazellulären Extrakten von Bierhefe beobachten konnte (Dunker et al., 2001). Er schlug das sogenannte „Schlüssel-Schloss-Prinzip" vor, das 1936 von Mirsky und Pauling (Mirsky and Pauling, 1936) bestätigt wurde, indem sie nachwiesen, dass Pepsin seine enzymatische Aktivität bei Denaturierung durch Harnstoff, Säuren oder Basen verliert. Diese Erkenntnisse führten zu der allgemein anerkannten Vorstellung, dass die Funktion eines Proteins immer von einer weitestgehend rigiden und wohldefinierten 3D-Struktur abhinge und ohne sie keine

Aktivität möglich sei. Zweifel an diesem Bild wurden allerdings laut, als Karush 1950 das Prinzip der „configurational adaptability" beschrieb, als er feststellte, dass Serumalbumin eine starke Affinität für ein Vielzahl kleiner hydrophober anionischer Moleküle zeigte, die jedoch sehr unterschiedliche Formen aufwiesen. Hieraus folgerte er, dass Serumalbumin in der Lage sein müsste, eine Vielzahl unterschiedlicher Konformationen einzunehmen (Karush, 1950a; Karush, 1950b). Unabhängig hiervon wurde von Koshland der „induced fit" vorgeschlagen (Koshland, 1953; Koshland, 1954). 1978 konnte dieser Effekt besonders eindrucksvoll am Beispiel der Glukosebindung durch Hexokinase demonstriert werden, bei welchem eine eindeutige Neuanordnung der Proteindomänen zueinander bei Ligandenbindung zu beobachten war (Bennett and Steitz, 1978). Im selben Jahr wurde gezeigt, dass ein Teil des Histons H5 in einem ungeordneten Zustand vorliegt (Aviles et al., 1978), der für Röntgenkristallographie nicht zugänglich ist, jedoch von NMR-Spektroskopie charakterisiert werden kann. Seitdem konnten zahlreiche intrinsisch ungeordnete Proteindomänen mit NMR identifiziert werden (Plaxco and Gross, 1997; Wright and Dyson, 1999). Demnach können Proteine in drei unterschiedlichen Zuständen biologische Funktionen ausüben:

- In der „klassischen" geordneten Form

- Im sogenannten „random coil"-Zustand, der keinerlei definierte 3D-Struktur aufweist

- Als „molten globule" – Form eines Proteins, welches sowohl teilstrukturierte als auch weitestgehend ungeordnete Bereiche enthält

Dies ist in **Abb. 4** als Proteintrinität dargestellt (Dunker et al., 2002a; Dunker et al., 2002b; Dunker et al., 2001; Dunker and Obradovic, 2001; Dunker and Obradovic, 2002; Radivojac et al., 2004; Uversky et al., 2005). Damit wird das Proteinstrukturparadigma um Proteine erweitert, die ihre Funktion nur dank ihrer mangelhaft definierten 3D-Struktur ausüben können und große konformationelle Flexibilität benötigen. Charakteristisch für alle nativ ungefalteten Proteine ist ihre hohe Hydrophilie aufgrund des hohen sequentiellen Anteils an geladenen Aminosäuren (Gast et al., 1995; Weinreb et al., 1996) und die weitgehende Abwesenheit von hydrophoben Regionen, was eine höhere Kompaktheit des Proteins unwahrscheinlich macht. Charakteristisch sind weiterhin eine geringe sequentielle Komplexität und eine hohe konformationelle Flexibilität. Ebenfalls sind einige Aminosäuretypen seltener, wie z.B. I, L, V, W, F, Y, C, N, und andere häufiger, wie z.B. E,

K, R, G, Q, S, P und A, vertreten (Uversky, 2002). Beispiele für IUPS sind die folgenden Proteine:

- Hüllenproteine von filamentösen Bakteriophagen gehen von einer geordneten Struktur zu „molten globule" über, wenn sie die Zellwand von Bakterien durchdringen. Dies könnte darauf hindeuten, dass Membranproteine in einem teilstrukturierten Zustand besser in eine Membran insertiert werden können (Griffith et al., 1981; Ji et al., 1998).

- Histone verlieren durch Acetylierung ihre rigide Struktur und ermöglichen so, dass die um sie gewundene DNA zugänglich für transkriptorische Enzyme wird (Oliva et al., 1990).

- Das Protein Calsequestrin verfügt über ungeordnete Sequenzabschnitte mit negativen Ladungen für die Bindung von Calciumionen (Krause et al., 1991).

- Der Cyclin-abhängige Kinaseninhibitor p21 verfügt im ungebundenen Zustand über keine Struktur. Die N-terminale Hälfte nimmt jedoch eine Struktur ein, wenn p21 eine Kinase bindet (Kriwacki et al., 1996).

- Der „V3 loop" des gp120 Proteins von HIV-1 wird zur Infektion benötigt und enthält ein 24 Reste langes Segment, das ungeordnet ist. Die konformationelle Flexibilität ermöglicht dem Virus sowohl an eine Vielzahl von Oberflächenrezeptoren von Zellen anzudocken als auch der Immunabwehr des Körpers zu entkommen (Balbach et al., 2000; Stanfield et al., 1999).

- Der Transkriptionsfaktor p53 aktiviert Gene, die den Zellzyklus anhalten oder Apoptose bzw. DNA-Reparatur einleiten. Das kann notwendig sein, um zu verhindern, dass sich eine normale Zelle zu einer Tumorzelle entwickelt. Die C-terminale Domäne von p53, die im ungebundenen Zustand weitestgehend ungeordnet ist, spielt bei der Regulierung von p53 eine wichtige Rolle. Bindet die C-terminale Domäne an DNA oder regulierende Faktoren, wird in ihr die Bildung einer α-Helix und eines „β-hairpin" induziert, wodurch die Aktivität von p53 moduliert wird (Weinberg et al., 2004).

Strukturelle Trinität
von Proteinen

Geordnete 3D-
Struktur

Molten globule (IDP
mit strukturierten
Bereichen)

Vollständig
ungeordnetes
Protein mit random-
coil
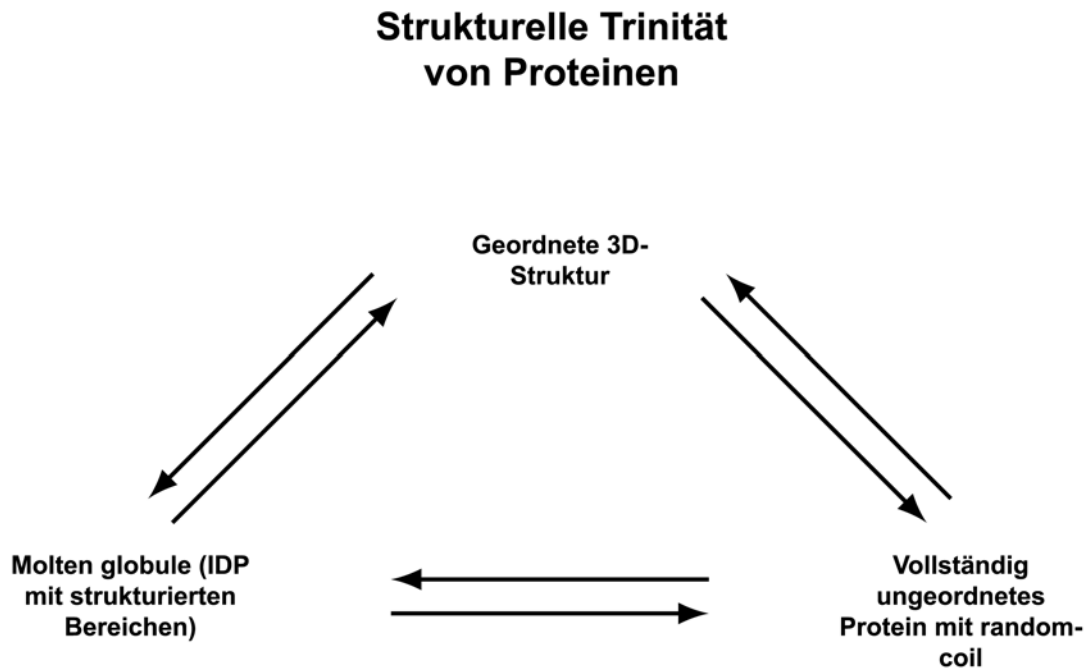
Abb. 4: Alternatives Struktur-Funktions-Modell von Proteinen. Proteine können alle drei Formen (geordnet, ungeordnet und molten-globule) als nativen Zustand einnehmen, in welchem sie ihre jeweilige Funktion erfüllen (aus Dunker et al., 2001).

Intrinsische Unordnung in einem Protein kann demnach Vorteile bieten. Es entsteht eine hohe Variabilität für ein Protein bezüglich seiner Bindungspartner (Wright and Dyson, 1999). p21 zum Beispiel kann an eine Vielzahl von Kinasen binden und diese inhibieren. Weiterhin ist es möglich, trotz hoher Bindungsspezifität eine geringe Affinität für einen Liganden zu erhalten, was ebenfalls notwendig sein kann, da es für katabolische Prozesse unerlässlich ist, dass Bindungspartner wieder dissoziieren können (Dunker et al., 2001). Bindet ein IUP an einen Liganden und bildet daraufhin eine geordnete Struktur aus, erhöht dieser Faltungsprozess die Freie Enthalpie, weshalb die Triebkraft für die Assoziation gemindert wird. Hieraus resultieren reduzierte Affinität und höhere Dissoziationskonstante.

Abseits ihrer biologischen Funktionen spielen IUPs in zahlreichen Krankheitsbildern eine entscheidende Rolle. Einige Beispiele sind: Morbus Alzheimer (Aggregate des β-Amyloidpeptids und Tau-Proteins), Morbus Niemann-Pick Typ C (neurofibrilläre Geflechte des Tau-Proteins), Down's Syndrom (Amyloid-β-Peptid), Morbus Parkinson (Lewy Bodies bestehend aus α-Synuclein) und Morbus Hallervorden-Spatz (Ablagerungen von α-Synuclein in Form von Lewy Bodies und Lewy Neurites) (Arawaka et al., 1998; Arima et al., 1998a;

Arima et al., 1998b; Galvin et al., 1999a; Galvin et al., 1999b; Tu et al., 1998; Wakabayashi et al., 1998a; Wakabayashi et al., 1998b).

1.2 Cytoskelett

Das Cytoskelett besteht aus den drei folgenden Komponenten: Mikrofilamente (Aktin), Intermediärfilamente (IFs) und Mikrotubuli (MTs). Es erfüllt verschiedene Funktionen:

- Formgebung der Zelle und Ausbildung von Polarität des Zellinneren, d.h. eine Verteilung von Zellorganellen nach apikaler/basaler Seite der Zelle.

- Bildung von Transportwegen, an denen Vesikel, Zellorganellen und mRNA, z.B. während der Translation, bewegt werden.

- Zelllokomotion durch Cilien- und Flagellenbewegung.

- Anordnung der Chromosomen während der Mitose/Meiose und deren Verteilung auf die Tochterzellen.

Alle drei Cytoskelettkomponenten stehen in statischem und dynamischem Kontakt, der durch Proteine wie MAPs übertragen wird. Diese hochkomplexen Vorgänge sind noch weitestgehend unerforscht (Rodriguez et al., 2003).

1.2.1 Intermediärfilamente und Mikrofilamente

Die Klasse der Intermediärfilamente (IFs) (Durchmesser ca. 10-12 nm) besteht aus einem breiten Spektrum von Proteinen, wie z. B. Keratine, Vimentin, Desmin, Laminproteine (Lamin A, B, C) und Neurofilamentproteine (NF-L, NF-M, NF-H). IFs werden durch 70 Gene kodiert und in fünf Klassen – vier im Cytoplasma und eine im Nukleus – eingeteilt (Omary et al., 2006). Charakteristisch für diese Gruppe von Proteinen ist, dass sie eine zentrale α-helikale Domäne aufweisen, die auf jeder Seite von globulären Domänen unterschiedlicher

Größen umgeben ist. Die α-helikalen Domänen unterschiedlicher IFs weisen eine hochkonservierte Aminosäuresequenz auf, wobei die Länge von ~310 Resten bei cytoplasmatischen IFs bis ~352 Resten bei Laminen des Nukleus variiert (Fuchs and Weber, 1994). Besonders stark konserviert sind die Sequenzmotive am Anfang bzw. Ende der α-helikalen Domäne (Helixinitiations- bzw. Helixterminationsmotive). Mutationen in diesen Bereichen können zu schwerwiegenden Krankheiten, sogenannten Keratinopathien, führen (Fuchs, 1996; Omary et al., 2004). Die zentrale α-helikale Domäne kann in Coil 1 (Segmente 1A und 1B) bzw. Coil 2 (Segmente 2A und 2B) unterteilt werden. Diese Segmente sind aus „repeats" geformt, welche aus hydrophoben Resten bestehen. Die „repeats" sind jeweils α-helikal strukturiert und über nichthelikale Linker verbunden (Parry and Steinert, 1999). Die Bauteile der zellulären filamentösen Strukturen sind nichtpolare IF-Tetramere, die aus zwei IF-Dimeren gebildet werden, die jeweils durch die Ausbildung einer „coiled-coil"-Struktur zweier α-helikalen Zentraldomänen entstehen. Die größte Sequenzdiversität zwischen verschiedenen IF-Typen sind in den N- bzw. C-terminalen Regionen zu beobachten, wodurch ihre unterschiedlichen Funktionen bestimmt werden (Fuchs and Weber, 1994). Die C-Termini können hierbei Wechselwirkungen zu Mikrotubuli, Mikrofilamenten, Zellorganellen und Mitochondrien ausbilden (Toivola et al., 2005), wobei die N-terminalen Domänen vorwiegend für die Zusammenlagerung von IFs notwendig sind. Die Funktionen von IFs können durch Phosphorylierung zahlreicher Stellen an C- und N-Termini moduliert werden.

Die Hauptfunktion von IFs sind die eines zellulären Stützgerüstes, welches Zellen Stabilität und Form verleiht (Parry and Steinert, 1999). Ein Beispiel hierfür ist Keratin der Typen I und II in Haaren, Haut und Fingernägeln. Dennoch weisen IFs eine hohe strukturelle Dynamik auf, welche durch Ereignisse in der Zelle, wie z.B. Mitose, beeinflusst wird. Weitere wichtige Funktionen von IFs sind Signalübertragung zwischen Zellmembran und Zellkern und Abstimmung von Positionierung und Funktion der Zellorganellen (Paramio and Jorcano, 2002).

Mikrofilamente (Durchmesser 5-8 nm) bestehen aus polymerisierten Monomeren des globulären Proteins Aktin. Im monomeren Zustand wird das Protein als G-Aktin bezeichnet und im polymerisierten als F-Aktin. F-Aktin entsteht, wenn sich G-Aktin in Gegenwart von ATP zu Strängen zusammenlagert, von denen jeweils zwei eine Doppelhelix bilden. G-Aktin besitzt eine Polarität und entsprechend gilt dies auch für die Mikrofilamente. In cytologischen Untersuchungen können Mikrofilamente mit S1, einem Fragment des Myosins, markiert werden. Durch die Markierung wird deutlich, dass F-Aktin ein Plusende („barbed end") und

ein Minusende („pointed end") besitzt. G-Aktin ist eine ATP-Hydrolase. Es bindet ATP und hydrolysiert es zu ADP, nachdem es in F-Aktin eingebaut wurde. Bei einer sehr schnellen Polymerisierung von G-Aktin zu F-Aktin bildet sich eine sogenannte „ATP-cap" aus, welche die Depolymerisierung des Filaments verhindert und so ein weiteres Wachstum von F-Aktin fördert. Mikrofilamente wachsen am Plusende ca. fünf- bis zehnmal so schnell wie am Minusende, welches auch stärker zu Depolymerisierung neigt. Hierdurch lässt sich ein sogenanntes „treadmilling" beobachten (Theriot, 1997), bei welchem Aktinmonomere entlang eines Mikrofilamentes vom Plusende zum Minusende wandern (Bretscher, 1999; Furukawa and Fechheimer, 1997; Sheterline et al., 1995).

Aktin ist für alle Motilitätsprozesse von Zellen notwendig: Bei der Wanderung von Leukozyten in den Blutgefäßen, bei Heilungsprozessen, bei der Ausbildung von Neuronen oder bei muskulären Bewegungen. Aktin formt entlang der Zellmembran im Inneren der Zelle eine kortikale Zone, deren Dynamik für Vorgänge, wie Aufnahme extrazellulärer Materialen, Zelllokomotion und Zellteilung, bestimmend ist (Pettit and Fay, 1998; Welch et al., 1997).

In der Zelle herrscht ein dynamisches Gleichgewicht zwischen G-Aktin und F-Aktin. Essentiell für die Regulation dieses Gleichgewichts sind die aktinbindenden Proteine, von denen mehr als 100 existieren. Diese Proteine sind ebenfalls unerlässlich für die Anordnung und Funktionen der Mikrofilamente in Zellen. Folgende Funktionen können sie ausüben:

- Bindung von G-Aktin und Inhibierung der Polymerisierung. Andernfalls läge das Gleichgewicht zwischen Monomer und Filament fast vollständig auf Seiten des Polymers.

- Blockierung der Enden, wodurch die Länge der Filamente kontrolliert wird. Blockierte Enden können nicht weiter G-Aktin anlagern und weiterwachsen.

- Vernetzung von Mikrofilamenten. F-Aktine können Netzwerke ausbilden, die Zellen, zum Beispiel im Bereich von Mikrovilli, die erforderliche Rigidität verleihen.

- Schneiden von Filamenten. Diese Klasse von Proteinen erniedrigt die Zellviskosität und bildet neue freie Enden von F-Aktin aus, die G-Aktin anlagern können.

- Depolymerisierung von F-Aktin. Dies ist für den schnellen Umsatz von Aktinfilamenten notwendig, wenn es zu strukturellen Änderungen des Cytoskeletts kommt.

- Bindung der Zellmembran. Viele nichtmuskuläre kontraktile Vorgänge werden durch Filamente unterhalb der Zellmembran ermöglicht. Hierzu gehören Zelllokomotion, Ein- und Ausstülpung der Zellen während Phagozytose und Mitose.

1.2.2 Mikrotubuli und Mikrotubuli-assoziierte Proteine (MAPs)

Mikrotubuli (MTs) bilden die größten Strukturen unter den Cytoskelettkomponenten. Sie formen Röhren von 24 nm Durchmesser. Ihre Länge kann zwischen einem und mehreren hundert Mikrometern variieren. Die Grundeinheit der MTs ist das α/β-Tubulin-Dimer, welches aus zwei Monomeren mit einer molekularen Masse von jeweils ca. 55.000 MDa besteht. In diesen α/β−Dimeren kann man zwei GTP-Moleküle beobachten. Eines ist nahe der Schnittstelle der beiden Monomere in der α-Einheit lokalisiert. Dieses GTP-Molekül ist nicht austauschbar und wird nie hydrolysiert. Im Gegensatz hierzu ist das zweite GTP-Molekül, welches an die Außenseite der β-Einheit gebunden ist, einem ständigen Durchsatz von Hydrolyse und Austausch während der MT-Assemblierung unterworfen. Ein Dimer kann einen longitudinalen Kontakt zu einem weiteren Dimer durch sogenannte „Kopf-Schwanz" (head-to-tail)-Kontakte ausbilden und so ein Protofilament formen, welches wiederum transversale Kontakte zu anderen Protofilamenten eingeht. In der Regel legen sich 13 dieser Protofilamente zu einer Röhre zusammen und bilden Singulett-MTs. In Strukturen wie Cilien, Flagellen, Centriolen und Basalkörper können auch Duplett-und Triplett-MTs gefunden werden. Da MTs durch die parallele Anordnung von α/β−Dimeren gebildet werden, die wiederum in der schon erwähnten „Kopf-Schwanz" Anordnung vorliegen, weisen MTs eine Polarität auf. Das (-)-Ende schließt mit einem Ring aus α-Untereinheiten ab, während das (+)-Ende aus β-Monomeren geformt wird.

MTs können einem sehr dynamischen Umsatz unterliegen (**Abb. 5**), wie er z.B. während der Zellteilung vorkommt, bei dem ständig MTs polymerisieren und wieder abgebaut werden. Im Gegensatz hierzu sind MTs in Flagellen oder Neuronen sehr stabil. Sogenannte „microtuble-organizing center" (MTOCs) (Vaughn and Harper, 1998) sind bei der Ausbildung und Orientierung von MTs notwendig. Das (-)-Ende bindet hierbei an einen Ring aus γ-Tubulin, der ein Bestandteil der MTOCs ist. Auf diese Weise wird auch die Ausrichtung der MTs bestimmt, so dass das (+)-Ende immer distal zu den MTOCs ist. Die Stabilität von MTs ist temperaturabhängig. Bei 4°C depolymerisieren sie, wohingegen sie

sich bei 37°C und der Anwesenheit von GTP assemblieren. Drei Charakteristika sind bezüglich des MT-Umsatzes zu beobachten:

- Liegt die Konzentration von α/β-Dimeren oberhalb der kritischen Konzentration (Cc), kommt es zur MT-Assemblierung, wohingegen MTs depolymerisieren, wenn die Cc unterschritten wird.

- Die anfängliche Assemblierungsrate kann durch Hinzugabe von MT-Fragmenten, die als Keime fungieren, beschleunigt werden.

- Das Wachstum, aber auch der Abbau von MTs durch Anlagerung und Ablösen von α/β-Dimeren, ist am (+)-Ende schneller.

Unter bestimmten Bedingungen ist auch ein sogenanntes „treadmilling" (WatermanStorer and Salmon, 1997) zu beobachten, wobei α/β-Dimere an einem Ende angefügt werden und an dem anderen Ende dissoziieren. MTs unterliegen einer dynamischen Instabilität, da sie ständig zwischen Auf- und Abbau oszillieren können. Hierbei wird der Wechsel von Wachsen zu Depolymerisierung als „Katastrophe" und als „Rettung" der Übergang in umgekehrter Richtung bezeichnet (Desai and Mitchison, 1997) (**Abb. 5**). Da in der Zelle die (-)-Enden mit den MTOCs verbunden sind, geht dieses dynamische Verhalten vorwiegend von den (+)-Enden aus. Bei einer Dimerkonzentration nahe der Cc treten Wachstum und Schrumpfen von verschiedenen MTs in unterschiedlichem Maße auf. Ein weitere Faktor, der auf die MT-Dynamik Einfluss hat, ist das Verhältnis zwischen GTP- und GDP-bindenden Tubulindimeren, die an das (+)-Ende gebunden sind. Wird das GTP schneller hydrolysiert, als dass neue Dimere mit GTP hinzukommen können, werden die MTs destabilisiert und depolymerisieren.
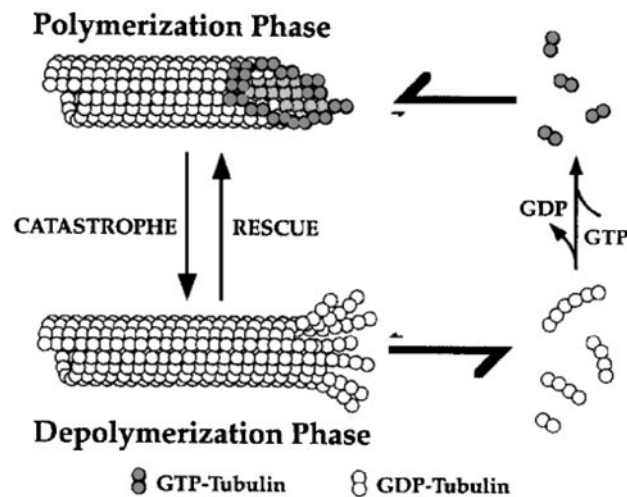
Abb. 5: Dynamische Instabilität von Mikrotubuli (MTs): Koexistenz von wachsenden und schrumpfenden MTs. GTP-Tubulin wird für die MT-Polymerisation benötigt, wohingegen GDP-Tubulin bei der Depolymerisation frei wird. Der Übergang von Wachstums- zu Depolymerisationsphase wird Katastrophe bzw. in umgekehrter Richtung Rettung genannt (übernommen aus Desai and Mitchison, 1997).

Diese dynamische Instabilität weicht von dem *in vitro* beobachteten Verhalten ab. *In vivo* kann es zu einem Wachstum am (+)-Ende der MTs kommen, welches um einen Faktor fünf bis zehn erhöht ist gegenüber den Daten *in vitro*. Ebenfalls kann der Wechsel von Depolymerisierung zu Wachstum bzw. umgekehrt *in vivo* bis zu zehnmal häufiger als *in vitro* vollzogen werden (Cassimeris, 1999; Cassimeris and Spittle, 2001; Desai and Mitchison, 1997). Außerdem ist es *in vivo* auch möglich, dass es zu Abbau am (-)-Ende kommt, obwohl dieses an MTOCs gebunden ist. Dies kann unter anderem bei der Wachstumsspindel während der Mitose beobachtet werden, wo das (+)-Ende fest an die Kinetochoren der Chromosomen gebunden ist und dennoch ein polwärts gerichteter Fluss von MT-Untereinheiten erkennbar ist (Mitchison and Salmon, 1992). Ebenfalls ist das Ablösen des (-)-Endes von den MTOCs oder das Abbrechen der MTs und so die Bildung neuer (-)-Enden möglich (WatermanStorer and Salmon, 1997). Besonders während der Zellteilung ist ein starker Umsatz an MT-Polymeren zu beobachten, wobei die Menge an Polymeren bei Beginn der Mitose stark zurückgeht und dann im weiteren Verlauf der Zellteilung wieder nahezu auf den ursprünglichen Stand der Interphase zurückkehrt (Cassimeris, 1999).

Verantwortlich für diese Dynamik *in vivo* sind sogenannte Mikrotubuli-assoziierte Proteine (MAPs), welche MTs stabilisieren, destabilisieren, assemblieren und auch schneiden können. Die Regulation der MAPs wird durch Phosphorylierung zellzyklusabhängiger Kinasen, wie z.B. der cdc2-Kinase, bewerkstelligt (Garner et al., 1988). Dynamische Prozesse bei MTs können mittels Phosphorylierungskaskaden Einfluss auf andere Zellkomponenten

nehmen, wie die Aktin-Myosin-Wechselwirkung mittels der Rho-Kinase (Rodriguez et al., 2003). Zu den MAPs, die MTs stabilisieren, gehören insbesondere die beiden großen MAP1A/1B- und MAP2/Tau-Familien. Diese beiden Gruppen unterscheiden sich in ihrer Thermostabilität und ihrem sequentiellen Aufbau (Schoenfeld and Obar, 1994), wobei für die MAP2/Tau-Familie gilt, dass ihre Angehörigen thermostabil sind und über charakteristische MT-bindende „repeat"-Sequenzen im C-terminalen Teil des Proteins verfügen. Außerdem weisen sie eine sogenannte N-terminale „projection domain" unterschiedlicher Länge auf, die für Kontakte mit anderen Zellorganellen oder Cytoskelettkomponenten verantwortlich ist (Dehmelt and Halpain, 2004). Gerade bei Zellmotilitätsprozessen scheinen Proteine wie MAPs, die zwischen den einzelnen Cytoskelettkomponenten vermitteln können, eine wichtige Rolle zu spielen. MAP1b (meist axonal), MAP2 (dendritisch) und Tau (axonal) sind die für Neuronen wichtigsten MAPs.
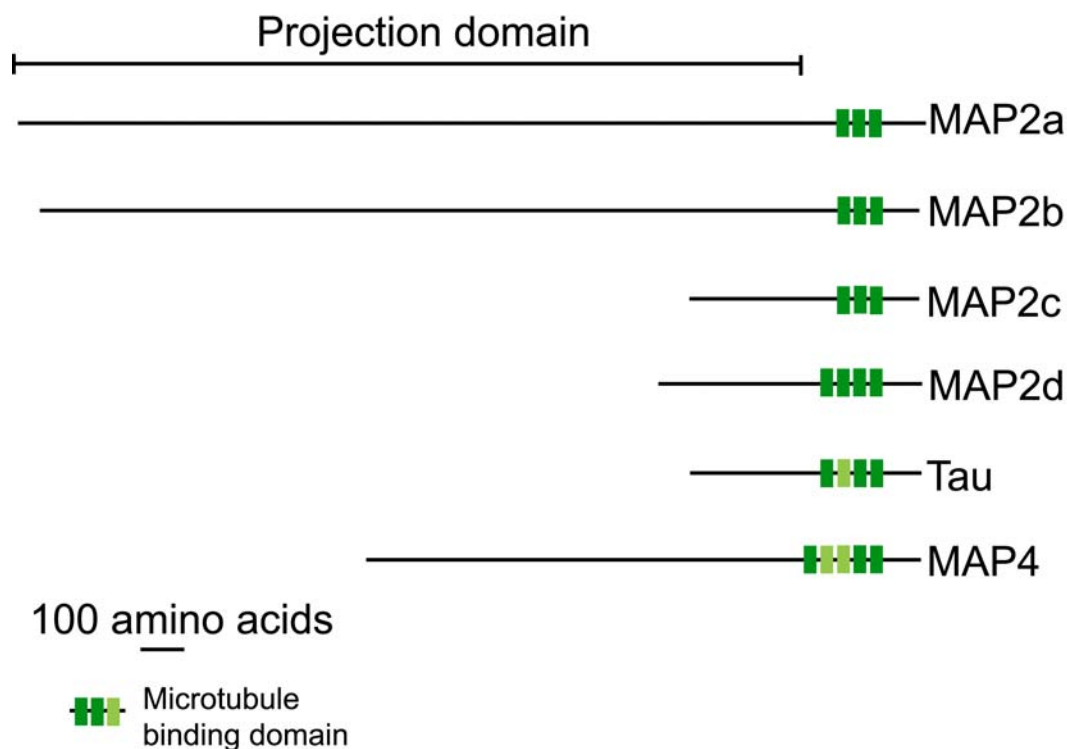
Abb. 6: Domänenorganisation der MAP2/Tau-Familie. Die einzelnen Vertreter zeigen unterschiedliche Anzahlen von C-terminalen „repeats" (grüne Kästen) und verschiedene Längen der „projection"-Domänen auf. „Repeats", die nicht in allen Isoformen vorkommen, sind heller gezeichnet (modifizierte Form von Dehmelt and Halpain, 2005).

MAP2c ist die juvenile Form von MAP2. Sie ist nur am Beginn der neuronalen Entwicklung vorhanden und wird später herunterreguliert. Während der weiteren Entwicklungsschritte wird im Gegenzug vermehrt MAP2a gebildet. MAP2b hingegen ist in allen Entwicklungsstadien der Neurone nachzuweisen. Im Gegensatz zu MAP2c können weder Tau noch ein Chimärenkonstrukt aus Tau mit der MT-bindenden Region von MAP2c Aktin binden (Chung et al., 1996; Garner et al., 1988). Die MAPs verringern durch Bindung an MTs – vorwiegend in ihrem dephosphorylierten Zustand – die Zahl der „Katastrophen" und erhöhen die Elongationsrate bzw. die Zahl der „Rettungen". Auf diese Weise wird MT-Assemblierung und -Stabilisierung gefördert.

Umgekehrt gibt es MAPs mit enzymatischer Aktivität, wie z.B. Op18 (Belmont et al., 1996). Op18 wird durch aufeinander folgende Phosphorylierungsschritte aktiviert und kann Tubulindimere binden sowie das Auftreten von „Katastrophen" verstärken (Cassimeris, 2004; Cassimeris and Spittle, 2001). Ein weiteres Protein dieser Gruppe ist Kar3p (Endow et al., 1994), welches den Abbau von MTs an ihrem (-)-Ende ermöglicht, was während der Mitose notwendig ist.

Beispiele für MAPs, die MTs schneiden können, sind Katanin (McNally and Thomas, 1998), p56 (Shiina et al., 1992) und der Elongationsfaktor 1α (Shiina et al., 1994). Die Regulation von Katanin ist noch unklar, da die cdc2-Kinase keinen direkten Einfluss auf Katanin zu haben scheint.

Bei allen MAPs scheint ihre jeweilige Lokalisierung in der Zelle auch eine Rolle zu spielen. Manche MAPs können am Zellkern gebunden sein und erst bei bestimmten Ereignissen in der Zelle, wie z.B. der Zellteilung, an den MTs detektiert werden. Diese heterogene Verteilung ist ein weiterer Steuermechanismus ihrer Funktionalität.

Zusätzlich zu den MAPs existieren sogenannte Motorproteine, die den Vesikel- und Organellentransport entlang der MTs ermöglichen. In Axonen ist eine lange Transportstrecke zurückzulegen, die ohne diese Klasse von Proteinen nicht zu überbrücken wäre. Die Transportrichtung wird durch die Polarität der MTs bestimmt, die derart beschaffen ist, dass das (+)-Ende zum Ende der Axone von dem Zellsoma wegweist. Der Transport in Richtung des (+)-Endes, demnach zu der Zellperipherie hin (anterograd), wird durch das Motorprotein Kinesin bewerkstelligt. Für den Transport in umgekehrter Richtung (retrograd), zum Soma hin, ist Dynein verantwortlich. Für beide Proteine gilt, dass ihre Aktivität an den Verbrauch von ATP gekoppelt ist. Durch Beeinflussung der Aktivität des jeweiligen Motorproteins, wie z.B. durch MAPs, ist es möglich, den Transport entsprechend den Bedürfnissen des Neurons

anzupassen. Tau konkurriert mit Kinesin um dieselben Bindungsstellen entlang der MTs und begünstigt auf diese Weise den retrograden Transport (Trinczek et al., 1999).

1.3   Das Tau- Protein

1.3.1   Allgemeines zum molekularen Aufbau und zur biologischen Funktion

Das Tau-Protein gehört zu der Klasse II der klassischen MAPs. Diese Klasse zeichnet sich dadurch aus, dass sie weitestgehend thermostabil, resistent gegen Säuren bzw. Detergenzien und stark hydrophil aufgrund zahlreicher ionischer und polarer Reste ist (Lee et al., 1988). Tau wird auf Chromosom 17 kodiert und besteht aus 16 Exons. Durch alternatives Spleißen können aus dem Tau-Gen sechs verschiedene Isoformen gebildet werden, wobei die längste (htau40 mit 441 Resten) beide „insert"-Regionen (I1 und I2) und alle vier „repeats" (R1 = Q^{244}-K^{274}, R2 = V^{275}-S^{305}, R3 = V^{306}-Q^{336}, R4 = V^{337}-N^{368}) besitzt, wohingegen die kürzeste (htau23 mit 352 Reste) keine „insert"-Regionen und nur drei „Repeats" enthält (R1, R3 und R4). Alle sechs Isoformen werden in Neuronen eines adulten Gehirns gefunden. Htau23 stellt die einzige Form dar, die schon während des fetalen Zustands im menschlichen Gehirn enthalten ist. In peripheren Nervenzellen gibt es zusätzliche Isoformen, die durch Hinzunahme weiterer Exons über ca. 300 zusätzliche Reste verfügen und auf diese Weise das sogenannte „big tau" darstellen (Mavilia et al., 1994) (**Abb. 7**). In Nervenzellen des adulten Gehirns beträgt das Mengenverhältnis zwischen Isoformen mit vier (4R) und drei (3R) „repeat"-Motiven ungefähr eins. Dieses Gleichgewicht zwischen 3R-und 4R-Formen kann in frontotemporalen Demenzen gestört sein. Die Anteile von Isoformen mit zwei, einem oder keinem Insert (2I, 1I und 0I) liegen in ZNS-Neuronen bei 9%, 54% und 37% (Goedert et al., 1989; Gong et al., 2005; Hong et al., 1998).
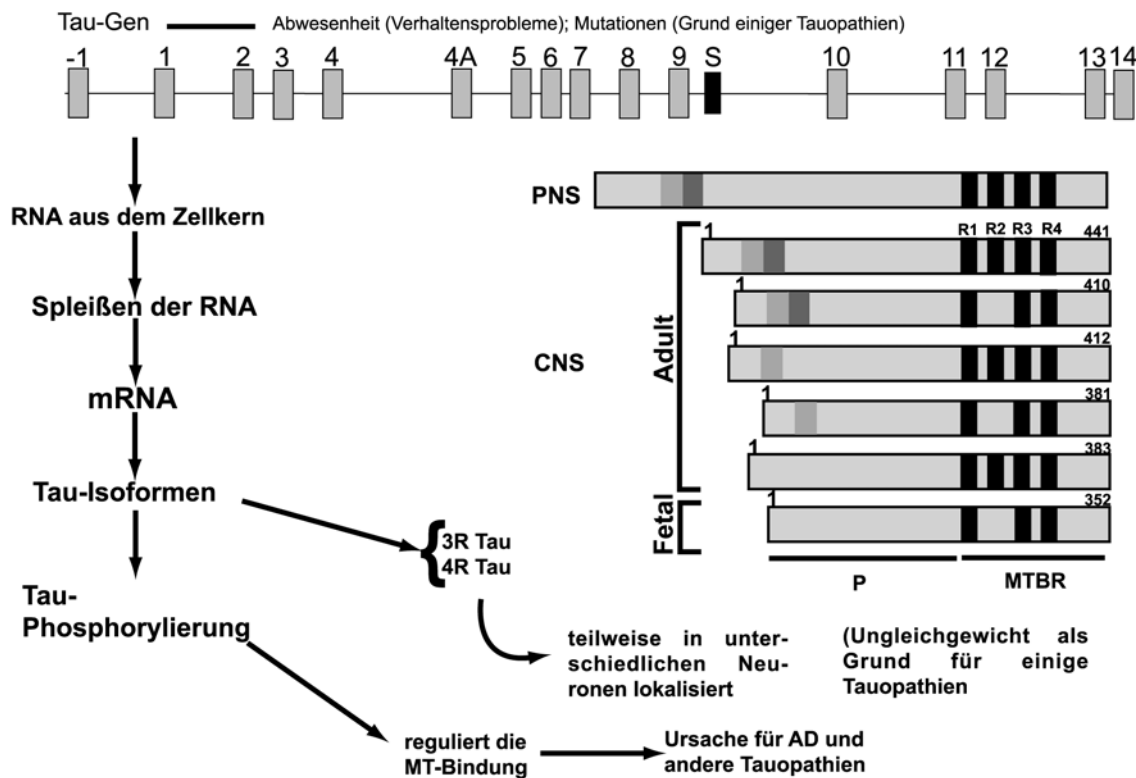
Abb. 7: Expression von Tau. Durch alternatives Spleißen entstehen aus dem Tau-Gen auf Chromosom 17 unterschiedliche Tau-mRNAs, aus welchen die verschiedenen Isoformen entstehen, wobei sechs im zentralen Nervensystem (CNS) enthalten sind und das sogenannte „big tau" im peripheren Nervensystem (PNS) lokalisiert ist. Die „projection"-Domäne (P) und die Mikrotubuli-bindende Region (MTBR) mit „repeats" (schwarze Rechtecke) sind eingezeichnet. S kodiert einen Abschnitt für das Protein Saithoin, über das wenig bekannt ist. Es erhöht wahrscheinlich die Tau-Pathogenität (entnommen aus Avila et al., 2004).

Der typische molekulare Aufbau dieser MAP-Klasse zeigt in der C-terminalen Hälfte des Proteins, welche auch Assemblierungsdomäne genannt wird, eine Region, welche aus drei bzw. vier imperfekten „repeat"-Sequenzen (R1-R4) mit einer Länge von jeweils ca. 31 Resten besteht und sehr viele kationische Reste, wie Lysine, Arginine und Histidine, aufweist. Die Region R1-R4 ist für die MT-Assemblierung notwendig. Sie selbst kann jedoch nur eine schwache Bindung an MTs ausüben. Um *in vivo* die notwendige Affinität für MTs zu gewährleisten, sind zwei Domänen, P2 und R' (**Abb. 1**), notwendig, die R1-R4 flankieren. P2 ist eine prolinreiche Region, die R1-R4 in der Sequenz vorangeht, während R' eine Art „Pseudorepeat" darstellt, der auf R1-R4 folgt. Diese beiden Regionen werden als „jaws"

bezeichnet (Gustke et al., 1994; Preuss et al., 1997), da sie gleich eines zuschnappenden Kiefers der R1-R4 Region eine feste Bindung an MTs verleihen. Goode et al. (1997) zeigten, dass insbesondere der hydrophobe Sequenzabschnitt ^{215}KKVAVVR^{221} in der Region P2 für die Affinität verantwortlich ist. Die übrigen Regionen des Tau-Proteins weisen keinerlei zusätzliche Affinität zu MTs auf. Die Bindungsstöchiometrie zwischen Tau und Tubulindimeren beträgt 1:2 (Gustke et al., 1994). Tau ist auch im gebundenen Zustand weitgehend ungefaltet, was in Cryo-EM-Experimenten beobachtet werden konnte (Santarella et al., 2004). Dennoch konnte mit Hilfe von Thioflavin-S-Färbung festgestellt werden, dass ein geringer Anteil von Tau auf der MT-Oberfläche eine PHF-artige Struktur annimmt (Ackmann et al., 2000; von Bergen et al., 2005). Die N-terminale Hälfte, die „projection"-Domäne von Tau, besteht vorwiegend aus aziden Sequenzen mit einem hohen Anteil an Glutamat- und Aspartatresten. Es wird vermutet, dass die „projection"-Domäne als „Abstandshalter" zwischen verschiedenen, mit Tau dekorierten MTs fungiert. Da die N-terminale Domäne entsprechend der jeweiligen Isoform in ihrer Länge variieren kann, könnte man hier eine Feinjustierung der MT-Abstände und somit eventuell auch der Durchmesser der Axone vermuten (Schoenfeld and Obar, 1994). Diese Hypothese wird dadurch unterstützt, dass MAP2 im Vergleich zu Tau größere Abstände zwischen den einzelnen MTs erzeugt, da es über eine längere „projection"-Domäne verfügt. Eine weitere mögliche Funktion dieser N-terminalen Domäne wäre die Kontaktaufnahme zu anderen Cytoskelettkomponenten, Zellorganellen oder Zellmembranen. Über eine genaue Strukturierung dieser Domäne ist nichts bekannt. Sie scheint über eine hohe strukturelle Flexibilität zu verfügen und weist keine markanten Anzeichen von Sekundärstruktur auf. Die C-terminale Domäne von ca. 50 Resten, die auf R' folgt, könnte ebenfalls die Funktion eines Abstandhalters für MTs haben (Schoenfeld and Obar, 1994). In ihr konnte die Tendenz zur Ausformung einer amphipatischen Helix gemessen werden (Esposito et al., 2000). Im Gegensatz zu MAP2, welches vorwiegend in den Dendriten gefunden werden kann, ist Tau im nicht-pathologischem Fall vorwiegend in den Axonen lokalisiert. Seine Aufgabe besteht in der Stabilisierung von MTs und der Kontrolle des Vesikeltransportes, den es in proximaler Richtung begünstigt. Wie bereits in Abschnitt 1.2.2 erwähnt, wirkt Tau jedoch nicht beschleunigend auf Dynein, welches diesen Transport bewerkstelligt, sondern es hemmt die Bindung dessen Gegenspielers Kinesin. Tau verringert die Affinität und auch die Laufstrecke von Kinesin entlang der MTs (Trinczek et al., 1999). Auf diese Weise wird der Transport von Vesikeln zum Zellsoma verstärkt.

Das Binden und Lösen von MAPs an Mikrotubuli wird durch ein komplexes Gleichgewicht von Phosphorylierung und Dephosphorylierung gesteuert. Das Tau-Protein enthält eine Reihe von Phosphorylierungsstellen, die von verschiedenen Kinasen angesteuert werden können.
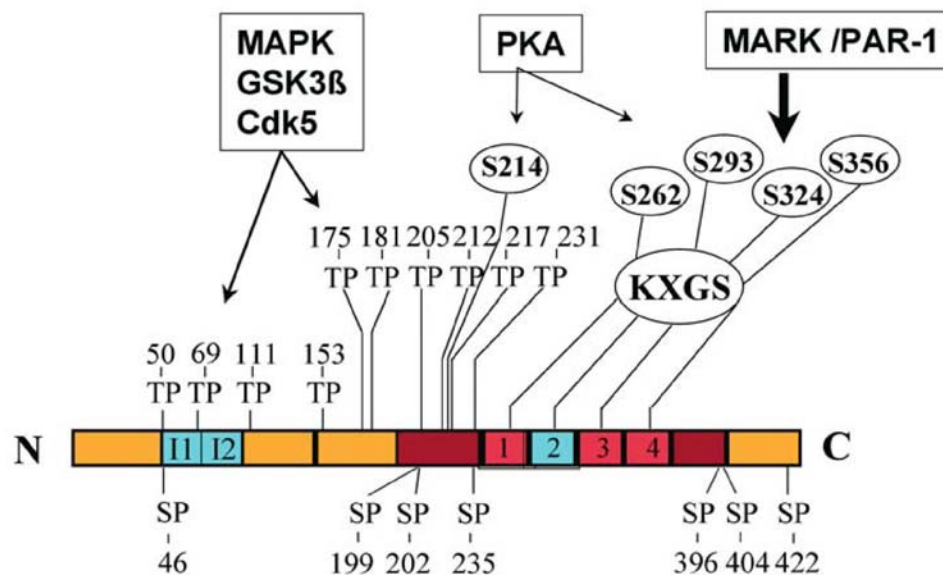
Abb. 8: Phosphorylierungsstellen in htau40. Die Kinasen, die die jeweiligen Serin- bzw. Threoninreste phosphorylieren sind ebenfalls aufgeführt. PKA und MARK/PAR-1 phosphorylieren alle KXGS-Motive innerhalb von R1-R4. PKA phosphoryliert zusätzlich S214. MAPK, GSK3β und cdk5 können alle eingezeichneten SP/TP-Motive phosphorylieren. (entnommen aus Jucker et al. – Alzheimer: 100 years and beyond - Springer Verlag Berlin Heidelberg 2006).

Viele der Phosphorylierungsstellen (**Abb. 8**) sind Teil eines SP- oder ST-Motivs (bis zu 17, abhängig von der jeweiligen Isoform) und werden von Prolin-„directed" Kinasen phosphoryliert, wie z.B. MAP Kinase (MAPK), Glykogen-Synthase-Kinase 3β (GSK-3β), Cyclin-dependent kinase 5 (cdk5) und cdc2. Andere relevante Kinasen sind: Protein Kinase A (PKA), Protein Kinase C (PKC), Ca^{2+}/Calmodulin-abhängige Kinase (CaMK) und „microtubule affinity regulating" Kinasen (MARK) (Stoothoff and Johnson, 2005). Die Phosphorylierung von S214 durch PKA, die während der Mitose hochreguliert wird, (Biernat et al., 1993; Brandt et al., 2005; Schneider et al., 1999) führt zu einem verstärkten Ablösen Taus von MTs. Dissoziation von MTs erfolgt auch, wenn MARK/Par-1 innerhalb von R1-R4 (Augustinack et al., 2001) die Sequenzmotive KIGS oder KCGS (**Abb. 8**) phosphoryliert. Phosphatgruppen an diesen Stellen inhibieren die Aggregation zu PHFs (Schneider et al., 1999). Phosphorylierung in den flankierenden Domänen führt ebenfalls zur Ablösung von

Tau; hingegen neigt Tau in diesem Phosphorylierungszustand verstärkt zur Aggregation (Augustinack et al., 2001; Avila et al., 2004; Gong et al., 2005; Wang et al., 2007). Weiterhin enthält Tau fünf verschiedene Tyrosinreste (Y18, Y29, Y197, Y310, Y394), von denen Y18 eine Phosphorylierungsstelle für die Tyr-Kinase Fyn darstellt (Gong et al., 2005).

Da Tau allgemein im phosporylierten Zustand schwächer an MTs bindet, ist es bei verstärkter Phosphorylierung vermehrt in ungebundener Form im Cytosol anzufinden, welche eventuell anfällig für PHF-Bildung ist. Der Phosphorylierungsgrad spielt im Zusammenhang mit PHFs, auf die im nächsten Abschnitt näher eingegangen wird, eine wichtige Rolle. Hyperphosphoryliertes Tau wird verstärkt im somatodendritischen Teil der Zelle gefunden, wohingegen sich die Menge in den Axonen verringert (Schoenfeld and Obar, 1994).

Mit Hilfe von FRET und Antikörperexperimenten konnte eine Rückfaltung der N- und C-terminalen Domänen auf R1-R4 beobachtet werden. Die Gruppe von E. Mandelkow (Jeganathan et al., 2006) postulierte aufgrund von FRET-Daten eine sogenannte „Paperclip"-Faltung, welche die N- und C-Termini in direkte räumliche Nähe zueinander bringt, so dass beide gleichzeitig in Kontakt zu der Repeatdomäne stehen (**Abb. 9**).
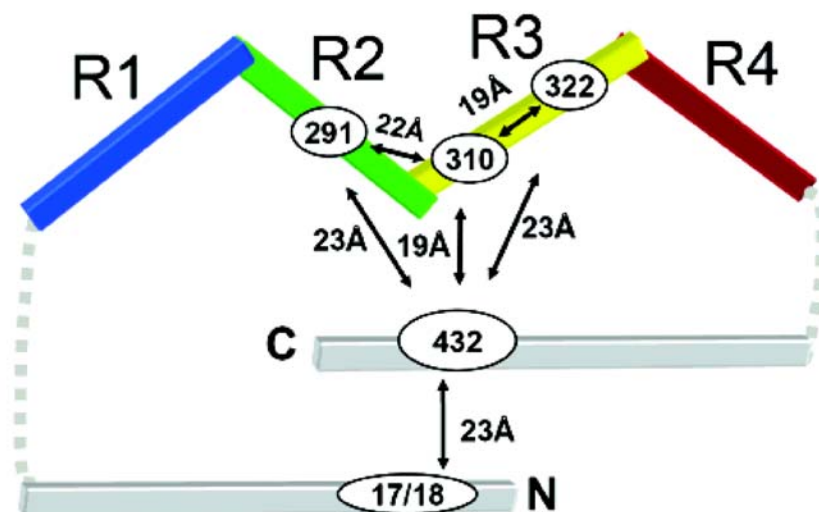
Abb. 9: Modell der mit FRET gemessenen intramolekularen Wechselwirkungen in htau40. Die Pfeile mit Distanzangaben in Å zeigen die FRET-Kontakte zwischen den jeweiligen Resten an (entnommen aus Jeganathan et al., 2006).

In Experimenten mit Antikörpern gegen Tau wie Alz50 und MC1 (Jicha et al., 1997a; Jicha et al., 1997b), welche sensitiv für bestimmte Konformationen ihrer Bindungsepitope

sind, konnte ebenfalls Rückfaltung bestimmter Taudomänen detektiert werden. Während des Übergangs von der monomeren Form zu NFTs durchläuft Tau mehrere Konformationen. Im Zusammenhang damit können Abspaltungen bestimmter Regionen im N- sowie C-terminalen Bereich, wie z.B. durch Caspasen (Proteasen, welche Apoptose einleiten können), Einfluss auf das Aggregationsverhalten und somit auf die Pathogenität Taus haben. Die Forschungsgruppe von Binder schlägt vor, dass Tau in einer vollkommen entfalteten Form vorliegt und erst bei Einleiten der PHF-Bildung eine langreichweitige Wechselwirkung (detektiert durch den Antikörper Alz50) zwischen Arg^5-Ala^{15} (Carmel et al., 1996; Horowitz et al., 2006) und den Resten ^{312}Pro-Cys^{322} aufweist, welche eine Vorbedingung für eine Aggregation zu sein scheint (s. **Abb. 11**). Bei Abwesenheit dieses Kontakts ist keine Fibrillenbildung möglich (Binder et al., 2005). Die FTDP-17-Mutation hingegen („frontotemporal dementia and Parkinsonism linked to Chromosom 17"), bei welcher Arg^5 in einen Leucinrest mutiert ist (R5L), verstärkt die Aggregationstendenz wahrscheinlich durch die erhöhte negative Netto-Ladung und die Verstärkung der Hydrophobizität des N-Terminus, der nun stärker mit der MTBR wechselwirken kann (Gamblin et al., 2003). Nach der ersten Fibrillenbildung kann es zu einer N-terminalen Abspaltung kommen, so dass eine neue Wechselwirkung (detektiert mit Antikörper Tau-66) zwischen der prolinreichen Region (Arg^{155}-Gln^{244}) und der Sequenz Ser^{305}-Asp^{314} innerhalb der MTBR entsteht. Im Gegensatz dazu steht die Bindung zwischen der R1-R4-Region und zwei N-und C-terminalen Sequenzen, Tyr^{18}-Gly^{42} und Ile^{392}-Asp^{421} (s. **Abb. 10**), welche einen inhibierenden Einfluss auf PHF-Bildung hat (Horowitz et al., 2006). Die Region Asp^{421}-Leu^{441} verlangsamt ebenfalls stark die Aggregation von Tau (Berry et al., 2003). Abspaltung dieses Peptids, welches die Tendenz zur Ausformung einer amphipatischen Helix besitzt (Esposito et al., 2000), löst diesen hemmenden Einfluss. Ein Grund hierfür könnte sein, dass es den aggregationsfördernden Kontakt des N-Terminus mit der MTBR verhindert, indem es dort an Aminosäuren einer überlappenden Region (Lys^{321}-Lys^{375}) bindet. Die Abtrennung von Asp^{421}-Leu^{441} stabilisiert PHFs und fördert so deren Wachstum, indem es die Rückreaktion hemmt (Berry et al., 2003; Gamblin et al., 2003).
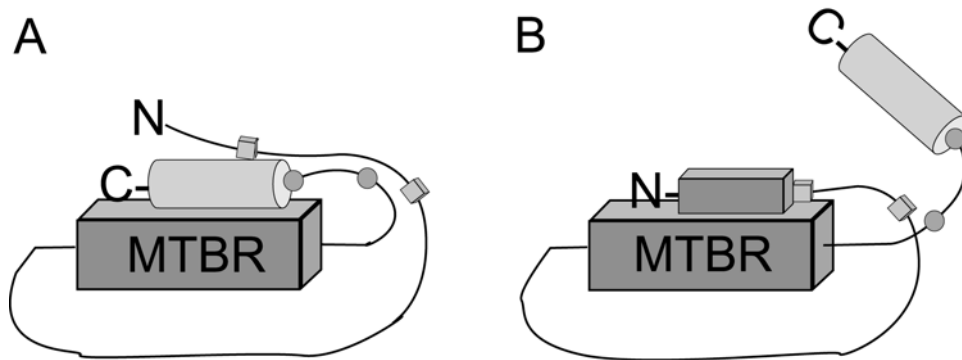
Abb. 10: Modell der Konformationsänderung Taus während des Übergangs von der löslichen zur aggregierenden Form. A: Tau-Aggregation wird durch die Bindung des C-Terminus an die MTBR verhindert. Diese Bindung wird durch die Wechselwirkung zwischen den Regionen 18-42 (Würfel) und 392-421 (Kreise) stabilisiert. **B**: Löst sich der C-Terminus ab, kann der äußere N-Terminus an die MTBR binden und so die Alz-50-Konformation einnehmen (Start der Aggregation) (entnommen aus Horowitz et al., 2006).
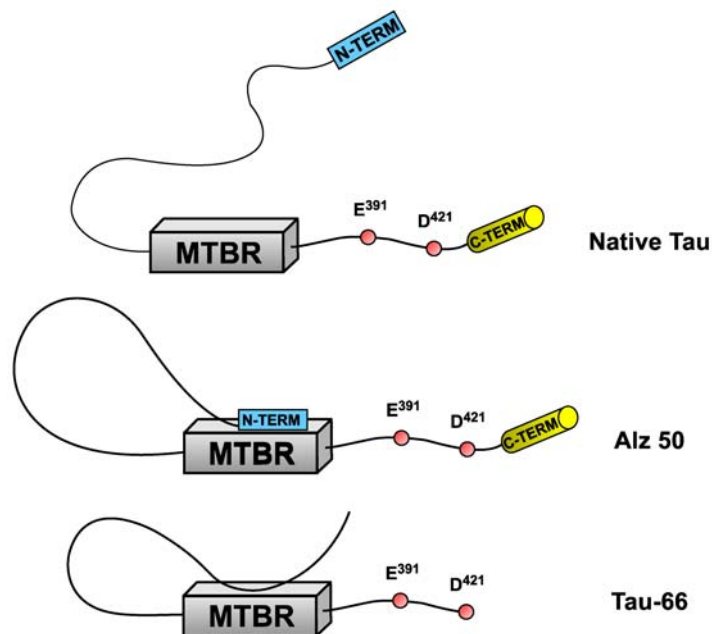
Abb. 11: Konformationeller Übergang von nativem Tau zu Fibrillen: Die Alz-50 – Konformation stellt den Beginn der Polymerisierung dar. Durch Caspasen – Proteasen, die Apoptose einleiten – wird an D421 der inhibierende C-terminale Teil abgespalten. Zusätzlich wird der äußere N-terminale Bereich abgetrennt. Die Tau-66-Konformation, die auch in PHFs beobachtbar ist, wird nun erreicht. (entnommen aus Binder et al., 2005).

1.3.2 Tau-Pathogenität – Aggregation zu „paired helical filaments" (PHFs) in Morbus Alzheimer und anderen Demenzen

Seit der Entdeckung von Morbus Alzheimer im Jahr 1907 ist bekannt, dass der Verlauf der Krankheit mit dem Auftreten zweier markanter Aggregate im Gehirn der Patienten einhergeht: Extrazelluläre Plaques und intrazelluläre neurofibrilläre Geflechte (NFT) (Haass and Selkoe, 2007). Im Zuge der Entwicklung immunbiologischer und biochemischer Methoden konnte in den 80ern des letzten Jahrhunderts von Glenner und Wong eindeutig nachgewiesen werden, dass die Plaques aus einem 40 bzw. 42 Aminosäure langen Peptid, dem Amyloid-β-Peptid (Aβ), bestehen (wobei Aβ-42 deutlich stärker aggregiert), welches ein Spaltprodukt aus dem größeren Membranprotein „Amyloid Protein Precursor" (APP) ist. 1987 wurde auf Chromosom 21 das Gen, welches APP kodiert, von Kang et al. identifiziert. 1991 konnte John Hardys Gruppe eine pathogene Mutation nachweisen, welche vererbbaren Morbus Alzheimer hervorrufen kann. Diese Erkenntnisse mündeten in einer sogenannten Kaskadenhypothese (Mullan et al., 1992), welche das Auftreten von Plaques als den zentralen Bestandteil im Verlauf von AD vorschlug und die Bedeutung und auch das Erscheinen von NFTs bei diesem Krankheitsbild als eher untergeordnete Komponente betrachtete. Dieses Schema wurde durch die Entdeckung von Mutationen an dem Enzym Presenilin unterstützt, welches Aβ von APP abspaltet. Aus diesem Grund konzentrierte man sich weitestgehend auf Aβ als Hauptangriffspunkt einer medikamentösen AD-Therapie. In den darauf folgenden Jahren traten jedoch Zweifel an diesem Alleinanspruch der Plaques auf. 1996 konnte gezeigt werden (Braak and Braak, 1996; Braak et al., 1996a; Braak et al., 1996b), dass es einen hohen Grad an Korrelation zwischen dem Krankheitsverlauf bei AD-Patienten und der Ausbreitung von NFTs in den Gehirnen der Patienten gibt. Es existiert ein stereotypes Schema, welches die zeitliche Abfolge beschreibt, in welcher NFTs in den unterschiedlichen Hirnarealen auftritt. Die Gruppen von Delacourte (Delacourte, 1999; Delacourte et al., 1999) teilt diesen Prozess in zehn Stadien (S1-S10) ein, in welchen angefangen beim Transenthorinalen Cortex (S1) bis zu Neokortikalen Arealen (S10) sukzessiv verschiedene Bereiche des Gehirns von der NFT-Bildung betroffen sind. Überdies sind ebenfalls Demenzen bekannt, wie z.B. Morbus Pick (PiD), Sporadische Kortikobasale Degeneration (CBD), progressive supranukleäre Blickparese (PSP), bei welchen in keinem Stadium Plaques beobachtbar sind und die man aus diesem Grund in die Gruppe der Tauopathien einordnet. Im Jahr 1997 wurden verschiedene Mutationen (Hutton et

al 1997, Foster et al 1997, Poorkaj et al 1998, Spillantini et al 1998) entdeckt, welche das Krankheitsbild FTDP-17 hervorrufen, das vererbbar sein kann (Ghetti et al., 1996; Hutton et al., 1998). Die Mutation V337M in der R3-Region von Tau führt zum Beispiel zu einer Taupathologie, die bezüglich ihrer strukturellen und biochemischen Beschaffenheit nicht von AD zu unterscheiden ist   (Spillantini et al., 1996). Durch diese Beobachtungen wurde offensichtlich, dass Tau neben Aβ, welches für sich allein genommen kein zuverlässiges Merkmal für eine Diagnose darstellt, eine entscheidende Rolle beim Auftreten von Demenzen und insbesondere Morbus Alzheimer spielt. NFTs scheinen den Verlauf von Demenzen bezüglich der Verluste von kognitiven Fähigkeiten bei Demenz- und insbesondere AD-Patienten besser widerzuspiegeln als Amyloid-β-Plaques (Armstrong, 2006; Braak and Braak, 1991; LaFerla and Oddo, 2005; Marx, 2007; Oddo et al., 2006). Werden phosphoryliertes und dephosphoryliertes, unlösliches Tau sowie lösliches Tau auf ein SDS-Polyacrylamidgel aufgetragen, erhält man nach der Auftrennung ein für die jeweilige Tauopathie spezifisches Bandenmuster (**Abb. 12**).
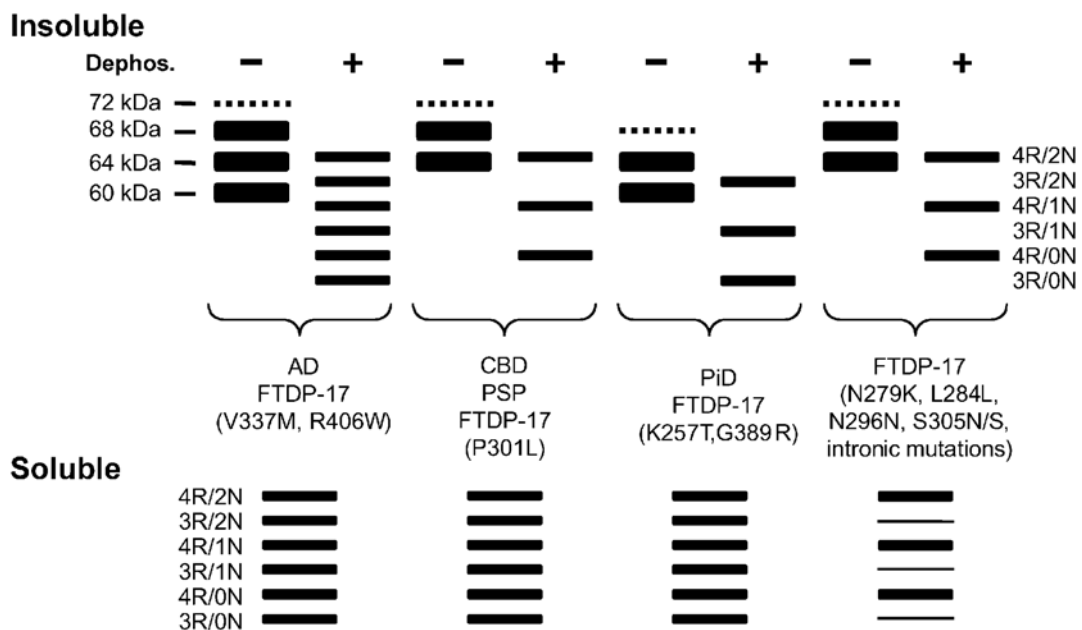
Abb. 12: Charakterisierung von Tauopathien: Anhand des Bandenmusters eines Western-Blots (von einer SDS-Polyacrylamid-Gelelektrophorese) von filamentösem Tau im dephosphoryliertem bzw. nicht-dephosphoryliertem Zustand sowie von löslichem Tau kann auf die Art der vorliegenden Tauopathie bzw. Mutation geschlossen werden (PiD = Morbus Pick, CBD = spontane kortikobasale Degeneration, PSP = progressive supranukleäre Blickparese) (entnommen aus Lee et al., 2001).

Die NFTs sind für alle Tauopathien das Hauptmerkmal, aber ihre genaue Beschaffenheit variiert in Abhängigkeit vom Typ der Demenz. Bei PiD z.B. werden die NFTs aus Fibrillen gebildet, die geradlinig verlaufen und sich so von den PHFs in AD deutlich unterscheiden. Zwischen dem Entdecken von Morbus Alzheimer (1907) und dem Identifizieren von PHFs (s. Abb. 15) (Kidd, 1963; Terry, 1963) liegt eine weite Zeitspanne. Hierzu bedurfte es der Fortschritte bei der Entwicklung der Elektronenmikroskopie und der Optimierung biochemischer Bedingungen zur Isolierung und Untersuchung der Fibrillen. Mit Hilfe der Entwicklung neuer spezifischer Antikörper (Brion et al., 1985; Grundkeiqbal et al., 1986a; Grundkeiqbal et al., 1986b; Grundkeiqbal et al., 1986c; Kosik et al., 1988a; Kosik et al., 1988b) konnte Tau als Hauptbestandteil dieser Fibrillen identifiziert werden. Im Gegensatz zu Amyloidfibrillen des Amyloid-β-Peptids oder des Prionenproteins mit einer „cross-β-Struktur", weisen PHFs kein eindeutiges Röntgenbeugungsmuster auf, bei welchem eine scharfe 0.47 nm-Reflektion auftritt. Der Grund hierfür ist der amorphe sogenannte „fuzzy coat", welcher den Kern der Fibrillen umgibt. Durch Behandlung mit Proteasen kann dieser Teil abgespalten werden. Verdeutlicht wird dieser Abbau durch Vergleich der Massen der PHFs vor (79 kDa/nm) und nach (65 kDa/nm) Behandlung mit dem Enzym (Crowther, 1991; Wischik et al., 1985). Mit Hilfe von „scanning transmission electron microscopy" (STEM) ergibt sich, dass auf einen Nanometer in der Fibrille 3.5-4.5 „repeat"-Domänenmoleküle kommen. Der Abstand zwischen zwei Taumolekülen in der Fibrille beträgt 0.47 nm (**Abb. 13**). Die Dimensionen der Fibrille betragen ~8 nm x ~20 nm (Inouye et al., 2006). Der proteasenresistente Fibrillenkern besteht demnach ausschließlich aus den „repeat"-Domänen R1-R4, wohingegen die „projection"- und die C-terminale Domäne den „fuzzy coat" bilden. Der C-terminale Teil muss stärker als der N-terminale an den Fibrillenkern gebunden sein, da er nicht im selben Maße zugänglich für den enzymatischen Abbau ist (von Bergen et al., 2006). Ebenfalls scheint R3 den rigidesten Teil der Fibrille zu bilden, da hier keine enzymatischen Spaltstellen bekannt sind, obwohl ausschließlich auf der Sequenz basierend Motive vorhanden wären, die einer Protease einen Abbau an dieser Stelle ermöglichen sollten (von Bergen et al., 2006). Diese erhöhte Rigidität in R3 wird ebenfalls in EPR (Elektronenspinresonanz)-Messungen (Margittai and Langen, 2004; Margittai and Langen, 2006) beobachtet.

Obwohl das Tau-Protein über eine hohe Löslichkeit verfügt, besitzt es die Fähigkeit zur Aggregation zu PHFs (**Abb. 15**), die sich zu toxischen NFTs zusammenlagern (Khlistunova et al., 2006). Es existieren keine deutlich hydrophoben Sequenzen, wie beim Amyloid-β-Peptid, oder Polyglutaminabschnitte, wie bei Huntington, die dazu führen

könnten, dass die Region R1-R4 den Kern der AD-Fibrillen (Novak et al., 1993; Wille et al., 1992) bildet, der gegen enzymatischen Verdau durch Proteasen weitgehend resistent ist. Bei der Tau-Aggregation sind zwei Sequenzmotive - ^{275}VQIINK^{280} und ^{306}VQIVYK^{311} - notwendig, die jeweils am Beginn der R2- bzw. R3-Regionen lokalisiert sind und über eine hohe Tendenz zur Ausbildung von β-Struktur verfügen (von Bergen et al., 2005; von Bergen et al., 2000). Mutationen in diesen Bereichen, wie z.B. der Austausch einer der Reste gegen Prolin, führen zu einer vollständigen Inhibierung der Aggregation. Umgekehrt kann die Bildung von PHFs beschleunigt werden durch die Mutationen P301L und ΔK280, welche beide in Exon 10 lokalisiert sind und zu einer deutlich geringeren Affinität zu MTs führen. Unter oxidativen Bedingungen können die Cysteine ^{291}Cys und ^{322}Cys Disulfidbrücken ausbilden. Im Falle von 4R-Tau bildet sich bevorzugt eine intramolekulare Disulfidbrücke aus, welche die Aggregation hemmt, wohingegen 3R-Tau nur intermolekulare Disulfidbrücken formen kann und es auf diese Weise zur Entstehung von kovalent gebundenen Dimeren (Wille et al., 1992) kommt. Diese Dimere bilden eine Art Aggregationsnukleus, welcher die weitere Fibrillisierung stark beschleunigt (Barghorn et al., 2004; Barghorn and Mandelkow, 2002; Barghorn et al., 2002; Friedhoff et al., 1998; Friedhoff et al., 2000). Für die *in vitro*-Analysen von Tau ist ebenfalls von großer Bedeutung, dass polyanionische Moleküle, wie z.B. RNA, Heparin, Polyglutamat und Arachidonsäuremicellen, ebenfalls stark dazu beitragen, die nur schwach ausgebildete Aggregationsneigung Taus zu verstärken und schließlich Fibrillenbildung einzuleiten (Goedert et al., 1996; Kampers et al., 1997; Perez et al., 1996).
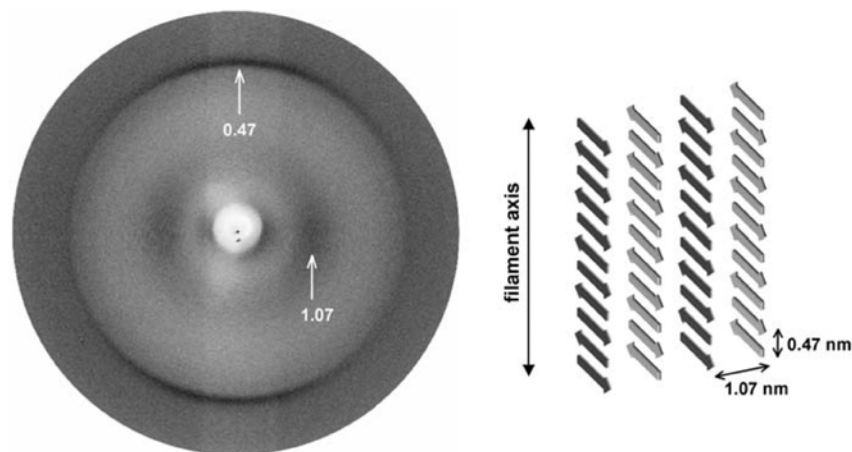
Abb. 13: Detektion von Cross-β-Struktur in PHFs. <u>Links:</u> Röntgenbeugungsbild von PHFs („repeat"-
Domänen von ΔK280-Tau). Meridionaler Reflex: Abstand zwischen den Strängen eines β-
Faltblattes beträgt 0.47 nm. Äquatorialer Reflex: Distanz zwischen den β-Faltblättern ist
1.07 nm. <u>Rechts:</u> Abstandsdaten wurden in ein Modell eingetragen (Jucker et al. –
Alzheimer: 100 years and beyond - Springer Verlag Berlin Heidelberg 2006).

Im Falle von Aggregation kann Tau seine Funktion als entscheidender Faktor bei der
Aufrechterhaltung der Zellpolarität und des Zellstoffwechsels nicht erfüllen (**Abb. 14**).
Überdies hindert hyperphosphoryliertes Tau andere MAPs wie MAP1, MAP2 oder
unphosphoryliertes Tau, MTs zu binden (Alonso et al 1994, 1996, 1997). Hierdurch
beeinflusst Tau auch MAPs, die eine Fehlfunktion kompensieren könnten, wodurch MTs eine
geringere Stabilität aufweisen und zelluläre Funktionen, wie Vesikel- oder
Organellentransport, nicht mehr erfüllt werden können, so dass eine erhöhte Sterblichkeit und
verminderte Funktionalität von Neuronen zu beobachten ist. Dies erklärt auch, warum die
Zerstörung von Synapsen im Hippocampus und der entorhinalen Hirnregion (Flood and
Coleman, 1990; Terry et al., 1991) der Ausbildung von Amyloid-β-Plaques und NFTs
vorangeht. Ebenfalls ist denkbar, dass „normales" Tau, wenn es überexprimiert wird oder
nicht von MTs gelöst werden kann, den Vesikeltransport in die Zellperipherie lähmt und auf
diese Weise eine Zellschädigung hervorruft (Stamer et al., 2002). Insbesondere gilt dies für
FTDP-17-Mutationen, die eine Überexprimierung von 4R-Tau, welches stärker als 3R-Tau an
MTs bindet, hervorrufen (Hutton et al., 1998; Lee et al., 2001).
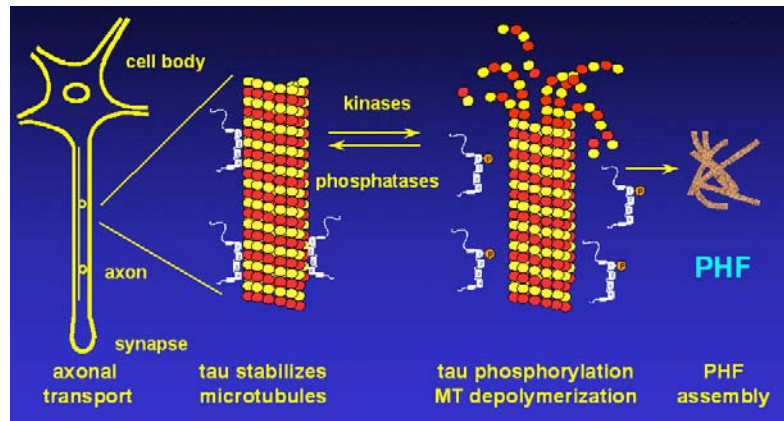
Abb. 14: Übergang von Taus biologischer Funktion zu pathogenen PHFs (Gruppe von Prof. Mandelkow/ https://www.MPASMB-HAMBURG.MPG.DE)
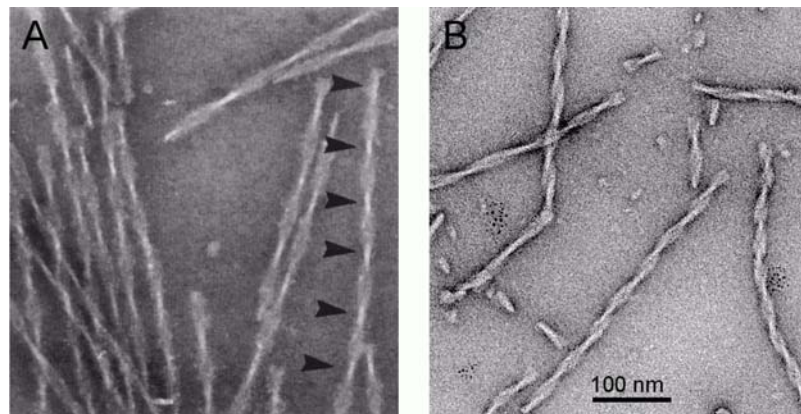
Abb. 15: EM-Bilder von PHFs. A: AD-Fibrillen aus dem Gehirn eines Patienten. B: *In-vitro* htau23-Fibrillen (Gruppe von Prof. Mandelkow/ https://www.MPASMB-HAMBURG.DE)

Pathogene FTDP-17-Mutationen Taus (FTDP-17) (Avila et al., 2004; Lee et al., 2001) verursachen entweder Veränderungen im Aggregationsverhalten oder im MT-Bindungsverhalten (**Abb. 16**). Exonische Mutationen können zur Expression von Isoformen führen, die eine stärkere Tendenz zur Aggregation zeigen und ebenfalls schwächer an MTs binden. Ausnahmen sind S305N und Q336R, die eine leichte Erhöhung der MT-Bindungsstärke bewirken. Insbesondere Mutationen auf Exon 10, welches R2 kodiert, beeinflussen stark das Bindungs- und Aggregationsverhalten von Tau. Beispiele hierfür sind ΔK280, ΔN296 und N296H, die sowohl Auswirkungen auf der RNA- als auch auf der Proteinebene aufweisen. Auch sogenannte „silence" Mutationen, bei denen der Aminosäuretyp beibehalten wird und nur das kodierende Basen-Triplett in der dritten Stelle mutiert (z.B. S305S), können ebenfalls pathogen sein. Die Mutationen N279K, L284L,

ΔN296, N296N, N296H, S305N und S305S führen zu einem verstärken Spleißen von Exon 10, wodurch vermehrt 4R-Isoformen exprimiert werden. 4R-Tau neigt stärker zur Fibrillenbildung als 3R-Tau, was eine höhere Schädlichkeit für Neuronen erklärt, wenn es verstärkt zur Expression jener Isoformen kommt (DeTure et al., 2000; D'Souza et al., 1999; D'Souza and Schellenberg, 2005; Hutton et al., 1998; Yoshida, 2006). Intronische Mutationen können ebenfalls das Verhältnis der einzelnen Isoformen zueinander beeinflussen (D'Souza and Schellenberg, 2005), indem sie spezifische Konformationen in der prä-mRNA verstärken, die wiederum zu einem veränderten Spleißschema führen (Goedert, 2005). Bezüglich des Phosphorylierungsgrades können Mutationen ebenfalls Veränderungen hervorrufen. Eine für die Dephosphorylierung von Tau wichtige Phosphatase, Phosphatase 2A, bindet schwächer an bestimmte Tau-Mutanten als an den Wildtyp (Goedert et al., 2000) und kann deshalb den Phosphorylierungsgrad nicht mehr regulieren. Es kommt zu verstärkter Phosphorylierung, welche die schon oben erwähnten Konsequenzen mit sich bringt. Die Morphologie der Fibrillen kann ebenfalls durch Mutationen beeinflusst werden. So fördern Mutationen, die ein verstärktes Spleißen von Exon 10 hervorrufen, die Ausbildung von PHFs mit einer weiten Windung, wohingegen Mutationen ohne einen Einfluss auf das Spleißverhalten von Exon 10 eher das Vorkommen eng gewundener Fibrillen begünstigen. In beiden Fällen jedoch bestehen die PHFs aus 4R-Tau. Die Entstehung von Fibrillen könnte als ein Schutzmechanismus (Lansbury, 1999) verstanden werden, der eventuell pathogene monomere (durch Caspasen geschnittenes Tau (Binder et al., 2005; Guillozet-Bongaarts et al., 2005) oder oligomere Formen (Neurodegeneration ohne Fibrillen in *Drosophila*-Modellen (Wittmann et al., 2001)) entfernt und in einer weitgehend inerten Form hält.

Mutation	Location	E10 Splicing	MT Assembly	Phenotype	Reference
K257T	E9, R1	No change	Reduced	PiD-like	Pickering-Brown et al (2000), Rizzini et al (2000)
1260V	E9, R1	ND	ND	NA	M Hutton, personal communication
G272V	E9, R1	No change	Reduced	FTDP-17	Hutton et al (1998)
N279K	E10, IR1-2	Increased	No effect	PSP-like	Clark et al (1998)
Δ280K	E10, IR1-2	Decreased	Reduced	FTDP-17	Rizzu et al (1999)
L284L	E10, IR1-2	Increased	No effect	AD-like	D'Souza et al (1999)
N296N	E10, R2	Increased	No effect	CBD-like	Spillantini et al (2000)
P301L	E10, R2	No change	Reduced	FTDP-17, CBD-like, PSP-like	Hutton et al (1998)
P301S	E10, R2	No change	Reduced	FTDP-17, CBD-like	Bugiani et al (1999), Sperfeld et al (1999)
S305N	E10, IR2-3	Increased	No effect	CBD-like	D'Souza et al (1999), Hasegawa et al (1999), Iijima et al (1999)
S305S	E10, IR2-3	Increased	No effect	PSP-like	Stanford et al (2000)
E10+3	I10	Increased	No effect	FTDP-17	Spillantini et al (1998c)
E10+12	I10	Increased	No effect	FTDP-17	Yasuda et al (2000)
E10+13	I10	Increased	No effect	NA	Hutton et al (1998)
E10+14	I10	Increased	No effect	FTDP-17, PSP-like	Hutton et al (1998)
E10+16	I10	Increased	No effect	FTDP-17, PSP-like CBD-like	Hutton et al (1998)
E9+33	I9	ND	ND	NA	Rizzu et al (1999)
V337M	E12, IR3-4	No change	Reduced	FTDP-17	Poorkaj et al (1998)
E342V	E12, IR3-4	ND	ND	FTDP-17	Lippa et al (2000)
G389R	E13	No change	Reduced	PiD-like	Murrell et al (1999)
R406W	E13	No change	Reduced	PSP-like	Hutton et al (1998)

Abb. 16: Tabelle mit Tau-Mutationen. Aufgelistet sind die jeweiligen Mutationen bezüglich Spleißen, MT-Assemblierung und Tauopathiekrankheitsbild (entnommen aus Lee et al., 2001).

1.4   NMR Spektroskopie als Werkzeug zur Erforschung des Tau Proteins

NMR Spektroskopie ist neben der Kristallographie die einzige biophysikalische Methode, die Strukturanalysen von Proteinen und anderen Biomakromolekülen in atomarer Auflösung liefern kann.   Beide Methoden haben ihre Vorzüge und Nachteile. Die Kristallographie ist in der Lage deutlich größere Moleküle als die NMR-Spektroskopie zu untersuchen. Allerdings wurde das Größenlimit der NMR-Spektroskopie z.B. durch die Entwicklung von 3D-Spektroskopie, Verwendung isotopenmarkierter Moleküle, TROSY- (Pervushin et al., 1997) und CRINEPT- (Riek et al., 1999) Sequenzen nach oben verschoben. Ein Vorteil der Kristallographie ist zudem, dass nach Lösen des Phasenproblems durch Röntgenbeugung im Idealfall eine dreidimensionale Elektronendichteverteilung sichtbar wird, die direkt in eine Struktur umgesetzt werden kann. Dies ist bei NMR nicht möglich. Hier werden in der klassischen Strukturanalyse Atomabstände mittels NOE-Daten ermittelt. Diese Information wird durch J-Kopplungen und durch residuale dipolare Kopplungen (RDCs) (Blackledge, 2005; Tjandra and Bax, 1997; Tolman et al., 1995) ergänzt. Diese Daten liefern sogenannte „restraints", mit welchen Strukturensembles errechnet werden können. Ein großer Nachteil der Kristallographie liegt in der Abhängigkeit von der Gewinnung von Kristallen, die über eine ausreichende Streuqualität verfügen. NMR-Spektroskopie hingegen kann bei Lösungen, halbkristallinen oder amorphen Proben durchgeführt werden. Diese Fähigkeit erweist sich insbesondere bei der Arbeit mit nativ ungefalteten Proteinen als positiv, da diese zumeist nicht kristallisieren und so nicht für hochauflösende Röntgenbeugung zugänglich sind. Überdies können IUPs aufgrund ihrer hohen konformationellen Dynamik nur durch Strukturensembles ausreichend beschrieben werden, weshalb wertvolle Informationen in Kristallen verloren gingen. Zwar ist es auch in den meisten Fällen von IUPs für NMR-Spektroskopie nicht möglich, eine klassische Strukturaufklärung mittels NOEs durchzuführen, da aufgrund der hohen konformationellen Flexibilität und der nur schwach bzw. nicht ausgeprägten Tertiärstruktur kaum NOE-Signale zu erwarten sind, die langreichweitige Wechselwirkungen anzeigen. Dennoch weist die NMR-Spektroskopie ein immenses methodisches Arsenal auf, um mit Proteinen wie Tau zu arbeiten, und wird auch in Zukunft über das größte Potential verfügen, um diese Proteinklasse, die gerade in vielen Krankheitsverläufen eine wichtige Rolle spielt, mit atomarer Auflösung zu beschreiben.

Die Grundlage der Erforschung von Proteinen mittels NMR ist die Zuordnung der Resonanzen in den Spektren zu den Atomen der jeweiligen Aminosäuren. Besonders nützlich sind hier Amidprotonen des Proteinrückgrats, die sich als wichtigstes Arbeitsmittel der vorliegenden Dissertation erwiesen. Mit der Einführung heteronuklearer 3D-NMR-Spektroskopie wurden Strategien entwickelt, die zu einer vollständigen Zuordnung der Resonanzen des Proteinrückgrats führen (z.B. die Kombination aus HNCACB, CBCA(CO)NH, HNCO und HN(CA)CO). Diese Strategie stammt jedoch weitestgehend aus der Arbeit mit gefalteten Proteinen, wohingegen diese Techniken im Falle des Tau-Proteins nur bedingt einsetzbar waren und ein alternatives Vorgehen gefunden werden musste. Allerdings liegt ein Vorteil der Arbeit an ungefalteten Proteinen gegenüber gefalteten Proteinen mittels NMR darin, dass die Größe des Proteins fast keine Auswirkungen auf das allgemeine Relaxationsverhalten des Moleküls hat. Aufgrund der hohen Proteinflexibilität sind die Korrelationszeiten von Aminosäuren in IUPs weitestgehend unabhängig vom Gesamtmolekül. Ebenfalls verfügen Protonen in IUPs im Vergleich zu Protonen in gefalteten Proteinen über weit weniger dipolare Kopplungspartner, über welche sie relaxieren können. Deshalb liegen die transversalen Relaxationszeiten dieser Proteine typischerweise im Bereich von ca. 200 ms, was dazu führt, dass die Linienbreite sehr scharf ist und auf TROSY-Sequenzen verzichtet werden kann. Demgegenüber stehen jedoch auch große Schwierigkeiten bei der Arbeit mit NMR-Spektren dieser Klasse von Proteinen, insbesondere von Tau. Die Signaldispersion in der Protonendimension ist stark verringert, von teilweise mehr als 6 ppm im Falle von gefalteten Proteinen auf weniger als 1 ppm für Tau (s. **Abb. 17**), was einen starken Resonanzüberlapp hervorruft. Außerdem ist ein hoher Grad an Frequenzentartung zu beobachten, was eine eindeutige Zuordnung sehr erschwert, da scheinbar für jede Aminosäuren mehrer Konnektivitätspartner denkbar sind. Zusätzlich weist das Tau-Protein einen Bereich (R1-R4) auf, der aus ca. 130 Aminosäuren besteht, dessen Sequenz einen stark monotonen und repetetiven Charakter zeigt, der zu weiterem Signalüberlapp führt. Es gibt einige Beispiele (z. B. Cys^{291}/Cys^{322}), bei denen Resonanzen zweier Reste in allen Dimensionen (^1H, ^{15}N, ^{13}C, ^{13}CO) vollständig identische Frequenzen besitzen. In zahlreichen Fällen sind die jeweiligen Frequenzunterschiede der Resonanzen so minimal, dass nur ein sehr genauer Vergleich der Konnektivitätsinformationen, aus unterschiedlichen Experimenten stammend, zum Ziel führte.
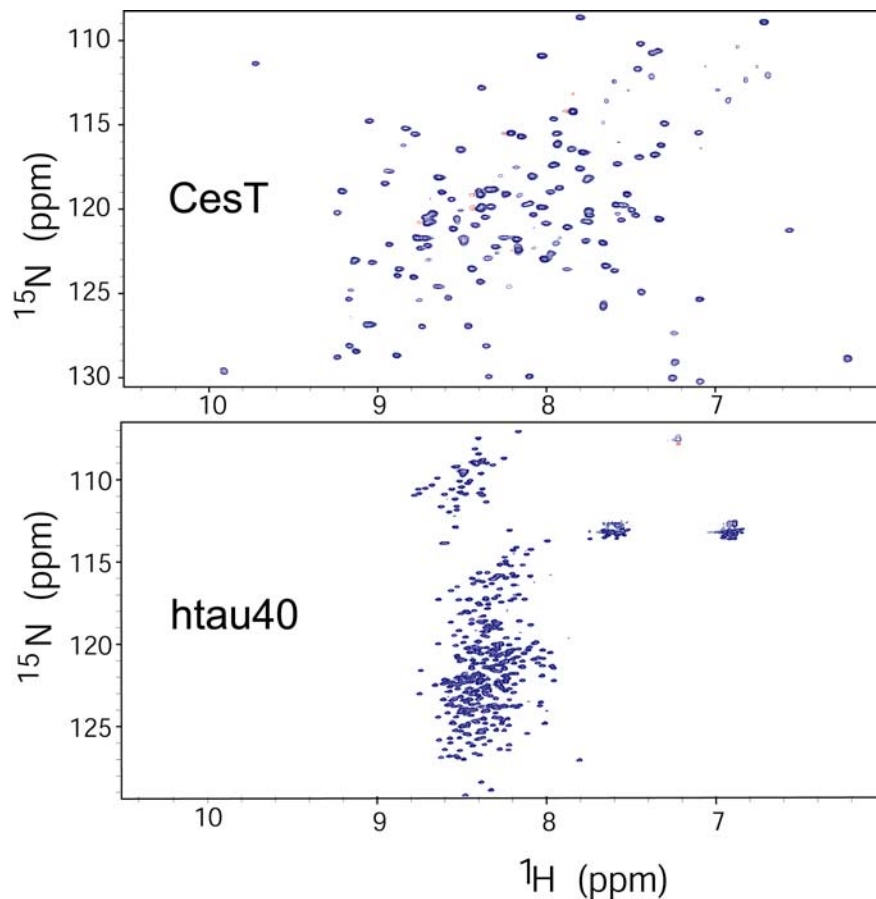
Abb. 17: Vergleich der ¹H, ¹⁵N-HSQC-Spektren eines gefalteten und eines ungefalteten Proteins.
<u>Oben:</u> CesT (bei 30°C) ist ein Homodimer mit 156 Resten pro Monomer und einem Molekulargewicht von 36 KDa. Das Spektrum wurde in der TROSY-Version aufgenommen. <u>Unten:</u> htau40 mit 441 Resten bei 5° C. Man erkennt deutlich die stark reduzierte Dispersion in der ¹H-Dimension für ungefaltete Proteine. Beide Spektren wurden an einem Bruker 900 Avance Spektrometer mit Cryo-Probenkopf gemessen.

Im Folgenden soll die Zuordnungsstrategie, die für Tau angewandt wurde, erläutert und die beiden 3D-NMR-Pulssequenzen, die schließlich zum Erfolg führten, aufgeführt werden. Obwohl die Zuordnung der Resonanzen bereits eine große Herausforderung darstellte, war sie hinsichtlich der Erörterung biologischer Fragestellungen nur der Ausgangspunkt. Sie stellte das Fundament für weitere Experimente dar, mit Hilfe derer Aussagen über strukturelle Eigenschaften und das Bindungsverhalten Taus gegenüber polyanionischen aggregationsfördernden Substanzen und MTs als physiologischer Interaktionspartner des Tau-Proteins gemacht werden konnten.

1.4.1 Resonanzzuordnung mit Hilfe der 3D-Sequenzen HNN und (HA)CANNH

Wie im vorherigen Abschnitt erwähnt, sind die Frequenzunterschiede von Resonanzen verschiedener Aminosäureresten in 3D-Spektren von Tau mit ^{13}C-Konnektivitätsinformationen sehr gering. Dies führt dazu, dass keine eindeutigen Konnektivitäten erhalten werden, sondern für jede Aminosäure zwei bis drei oder sogar mehrere Nachbarn in der Proteinsequenz möglich sind. Daher werden zu den ^{13}C-Daten komplementäre Konnektivitätsinformationen benötigt. Diese Informationen erbringt das HNN-Experiment (Panchal et al., 2001). Dies führt zwar häufig ebenfalls zu mehreren möglichen Konnektivitäten für den jeweiligen Rest, aber fast immer können mit Hilfe einer Kombination aus hochauflösendem (HA)CANNH-Spektrum (Zweckstetter and Bax, 2001b) mit dem HNN-Experiment eindeutige Zuordnungen der Aminosäurereste erzielt werden.
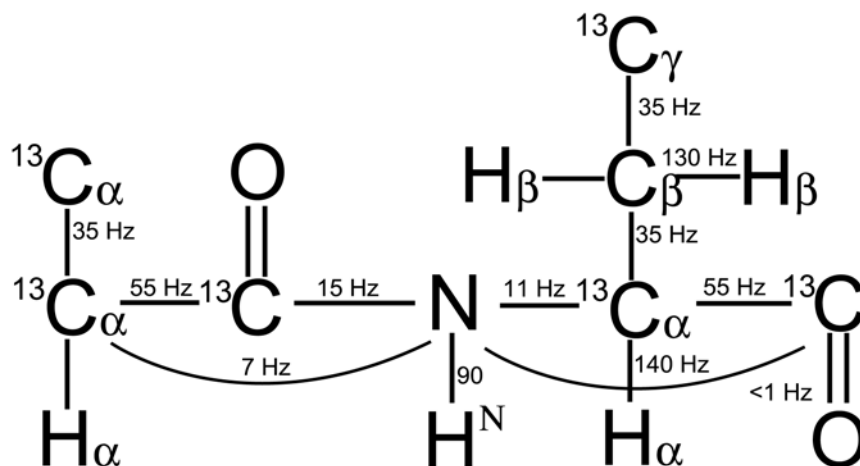
Abb. 18: Skalare Kopplungen in Proteinen (entnommen aus Sattler et al., 1999).

Beide 3D-Sequenzen nutzen ausschließlich skalare Kopplungen (s. **Abb. 18**) zwischen den jeweiligen Kernen, um den Magnetisierungstransfer zu bewerkstelligen.
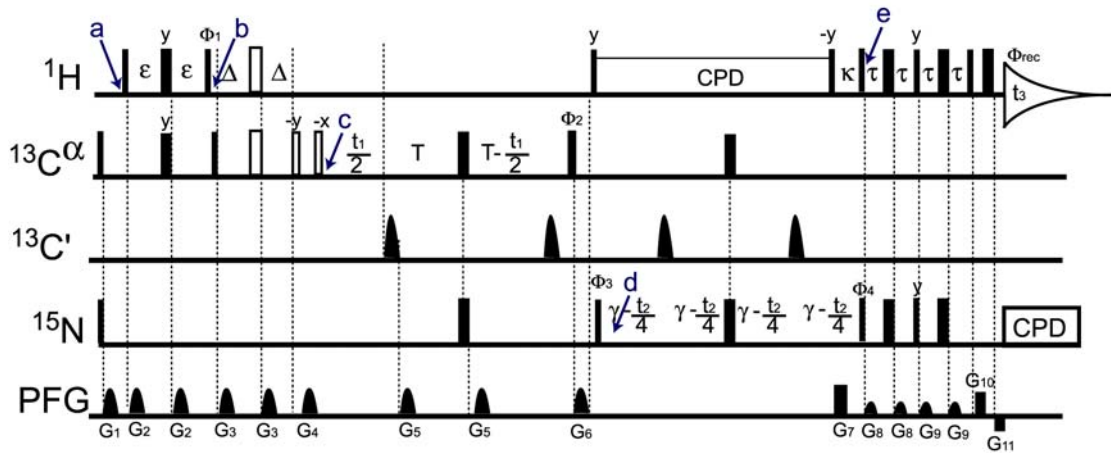
Abb. 19: (HA)CANNH-Pulssequenz. Schmale bzw. breite Rechtecke entsprechen Pulsen mit Flip-Winkeln von 90° bzw. 180°. Das IPAP-Element ist durch leere Rechtecke gekennzeichnet. Delays: ε = 1.4 ms; Δ = 1.7 ms; T = 14 ms; γ = 7 ms; κ = 5.35 ms; τ = 2.67 ms. Die selektiven ^{13}C'-Pulse haben ein (sinx)/x-Profil mit einer Länge von 150 μs. Phasenzyklus: ϕ_1 = y, -y; ϕ_2 = x; ϕ_3 = 2(x), 2(-x); ϕ_{rec} = x, 2(-x), x (Zweckstetter and Bax, 2001b).

Das (HA)CANNH-Experiment (Zweckstetter and Bax, 2001b) enthält für das C^{α}-Atom des jeweiligen Rests i die Konnektivität zur C^{α}-Resonanz der in der Sequenz vorangehenden Aminosäure i-1. Der Magnetisierungstransfer verläuft folgendermaßen:
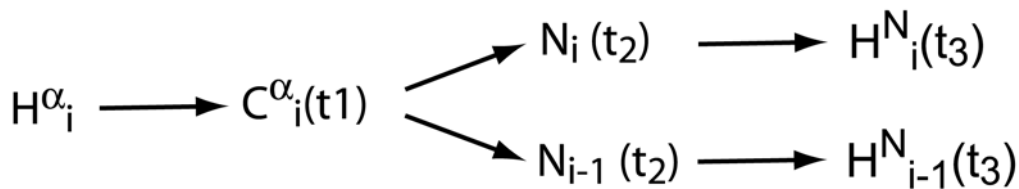
Abb. 20: Magnetisierungstransfer des (HA)CANNH-Experiments

a $\rightarrow$ b: Das Experiment beginnt mit der Anregung der H^{α}-Protonen (-H^{α}_Y), von denen die Magnetisierung über eine $^1J(C^{\alpha}H^{\alpha})$-Kopplung auf C^{α} übertragen wird ((-)2$H_Z C_Y$). Nun schließt sich in der Pulssequenz ein optionales IPAP-Element an, welches die Anti-Phasemagnetisierung (AP) in In-Phasemagnetisierung (IP) refokusiert. Ohne dieses Element bleibt Anti-Phasemagnetisierung erhalten. Demnach liegt die Magnetisierung in Form von 2$H_Z C_Y$ und C_Y vor.

b → d: Während t_1 kann die $^1J(H^\alpha C^\alpha)$-Kopplung evolvieren. Dies führt zu einem Dublett. Um im Spektrum eine durch diese Multiplettstruktur entstehende Resonanzüberlagerung zu vermeiden, wird das IPAP-Element in der t_1-Periode eingeführt und zwei Spektren für dasselbe t_1-Intervall in einer „interleaved"-Form gemessen, wobei eines ein Inphasedublett und das andere ein Antiphasedublett enthält. Die CT-Evolutionsperiode bietet den Vorteil, dass das Signal nicht durch Relaxation während t_1 moduliert wird und auf diese Weise eine hohe Auflösung durch eine hohe Zahl an komplexen Punkten erreicht werden kann. Da das Tau-Protein über sehr lange T_2-Relaxationszeiten verfügt, stellt die Länge des CT-Intervalls kein Problem dar, wohingegen im Falle von schnellrelaxierenden gefalteten Proteinen ein dramatischer Signalverlust eintreten könnte. Während der CT-Periode kommt es ebenfalls zum Magnetisierungstransfer von C^α_i auf N_i und N_{i-1} über $^1J(C^\alpha N)$- und $^2J(C^\alpha N)$-Kopplungen. Da die ^1J-Kopplung stärker als die ^2J-Kopplung ist, fällt die Intensität der interresidualen Komponente im Spektrum schwächer aus als die Intensität der intraresidualen Komponente. Dies ist ebenfalls ein nützlicher Hinweis in Bezug auf die Richtung der sequentiellen Verknüpfung. Vor Beginn der Evolutionszeit t_2 existieren folgende Komponenten: $(-)2C_Z N_Y$ (AP) bzw. $(-)4H_X C_Z N_Y$ (IP). Ein weiterer Vorteil des CT-Modus ist, dass sich homonukleare Kopplungen nicht während der Evolutionszeit entwickeln können und so eine Linienverbreiterung verhindert wird.

d → e: Die t_2-Zeit ist ebenfalls im CT-Modus. Bis auf die letzten 5.35 ms werden Protonen während der Evolutionsperiode entkoppelt und die Magnetisierung über $J(C^\alpha N)$-Kopplung zu $(-)2H_Z N_Y$ (AP) und $(-)N_Y$ (IP) refokusiert.

Die Magnetisierung beider Komponenten gelangt über einen „sensitivity enhancement"-Transferschritt auf die Amidprotonen (H_X) und wird hier detektiert.

Diese beiden Experimente aus IP und AP werden nun sowohl miteinander addiert als auch voneinander subtrahiert, wodurch letztendlich zwei Spektren entstehen, die jeweils eine der beiden Dublettkomponenten enthalten. Eine Auswertung der $^1J(H^\alpha C^\alpha)$-Kopplung ist möglich, indem der Abstand der beiden Komponenten gemessen wird. Diese Kopplungen enthalten Sekundärstrukturinformationen, da sie im Falle von α-Helices erhöht sind (> 145.5 Hz). Dementsprechend können α-Helices mit der beschriebenen Methode detektiert werden (Zweckstetter and Bax, 2001b).
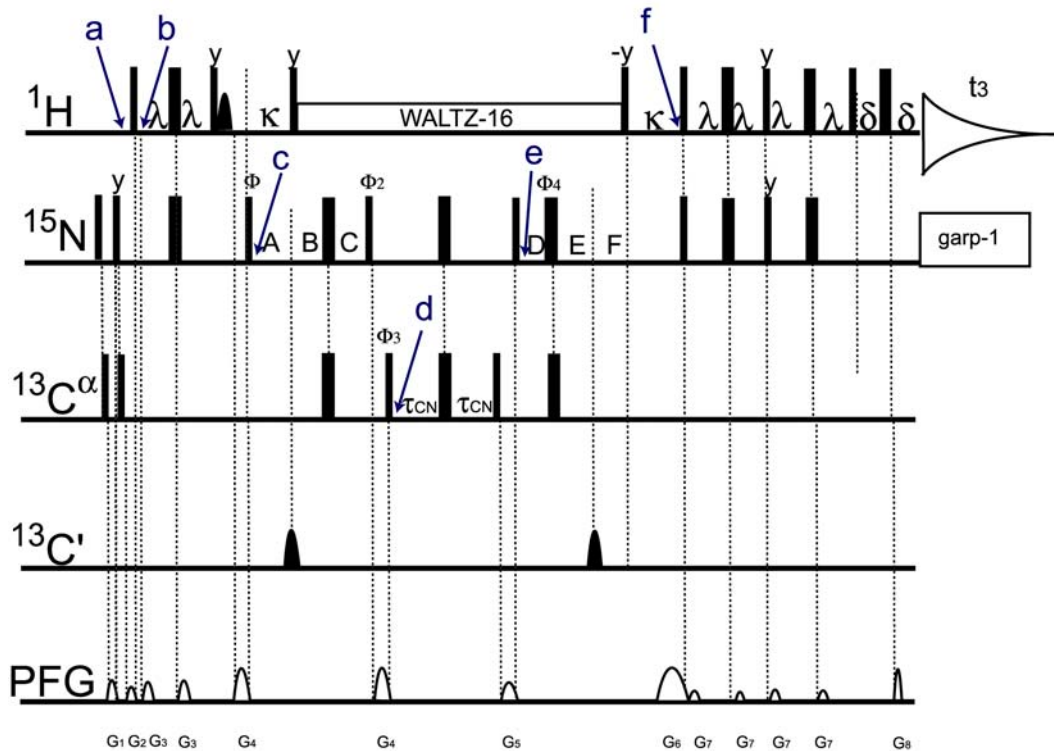
Abb. 21: Die HNN-Pulssequenz. Nicht-selektive 90°- und 180°-Pulse werden durch schmale und durch breite Rechtecke dargestellt. Alle Pulse ohne spezifische Angabe der Phase werden mit der Phase x angewendet. Der selektive 90°-Puls für den "Water Flip-Back" hat eine Länge von ca. 1 ms und wird durch eine sinc-Funktion beschrieben. Während der t_1 und t_2 Evolutionszeiten werden die Protonen mit Hilfe einer Waltz-16-Sequenz entkoppelt. ^{15}N-Entkopplung wird mit einer Garp-1-Sequenz durchgeführt. Zur Entkopplung der Carbonylatome werden selektive 180°-Pulse mit einem sinc-Profil verwendet. λ = 2.7 ms, κ = 5.4 ms and δ = 0.35 ms. τ_{CN} muss optimiert werden und liegt zwischen 12 und 16 ms. A=t_1/2, B = T_N, C = T_N - t_1/2, D = T_N-t_2/2, E = T_N und F =t_2/2. Phasenzyklus: ϕ_1 = 2(x), 2(-x); ϕ_2 = x, -x, x, -x; ϕ_3 = ϕ_2; ϕ_4 = x; ϕ_5 = 4(x), 4(-x), ϕ_{rec} = 2x), 2(-x) (Panchal et al., 2001).

Das HNN-Experiment (Panchal et al., 2001) bietet den Vorteil, dass es für einen Aminosäurerest sowohl den vorhergehenden als auch den nachfolgenden Konnektivitätspartner angibt. Dies ist sehr hilfreich, da es vorkommt, dass der Diagonalpeak und einer der beiden Kreuzpeaks überlagert sind und deshalb eine der beiden Informationskomponenten für einen Aminosäurerest fehlt. Der Magnetisierungstransfer der HNN-Sequenz wird in **Abb. 22** dargestellt.

$$H^N_i \longrightarrow N_i(t_1) \Big\langle {}^{C^\alpha_i}_{C^\alpha_{i-1}}$$

$$C^\alpha_i \Big\langle {}^{N_{i+1}(t_2) \longrightarrow H^N_{i+1}(t_3)}_{N_i(t_2) \longrightarrow H^N_i(t_3)}$$

$$C^\alpha_{i-1} \Big\langle {}^{N_i(t_2) \longrightarrow H^N_i(t_3)}_{N_{i-1}(t_2) \longrightarrow H^N_{i-1}(t_3)}$$
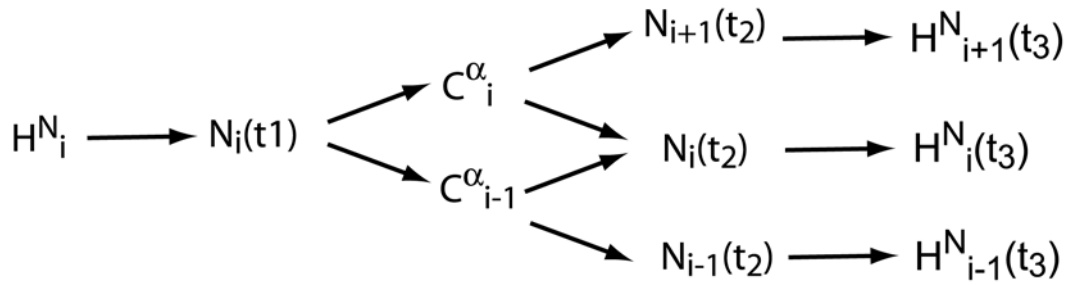
Abb. 22: Magnetisierungstransfer des HNN-Experiments (Panchal et al., 2001).

a → b → c: H_Z^i → - H_Y^i → $2H_Z^iN_Y^i$: Über ein INEPT-Element wird Magnetisierung von den angeregten Amidprotonen auf die ^{15}N-Atome übertragen.

c → d: 2 $H_Z^iN_Y^i$ → 2 $N_Z^iC_Y^i$ + 2 $N_Z^iC_Y^{i-1}$: Die ^1H-^{15}N-Anti-Phasemagnetisierung refokusiert während der CT-t_1-Periode. Protonen werden bis zum Ende von t_2 entkoppelt und spielen so keine Rolle. Über $^1J_{NC}^\alpha$ und $^2J_{NC}^\alpha$-Kopplungen wird Polarisation auf C^α_i und C^α_{i-1} transferiert, während sich die Magnetisierung mit der jeweiligen $^{15}N_i$ - Frequenz entwickeln kann.

d → e: 2 $N_Z^iC_Y^i$ + 2 $N_Z^iC_Y^{i-1}$ → -2 $N_Y^{i+1}C_Z^i$ + -2 $N_Y^{i-1}C_Z^{i-1}$. Via $^1J_{NC}^\alpha$ und $^2J_{NC}^\alpha$-Kopplungen wird die Magnetisierung der Kreuzsignale von C^α_i und C^α_{i-1} auf N_{i+1} und N_{i-1} übertragen.

e → f: -2 $N_Y^{i+1}C_Z^i$ + -2 $N_Y^{i-1}C_Z^{i-1}$ → $-N_X^{i+1}$ + $-N_X^{i-1}$ → -2 $H_Z^{i+1}N_Y^{i+1}$ + -2 $H_Z^{i-1}N_Y^{i-1}$

Im weiteren Verlauf wird die Magnetisierung auf die Amidprotonen übertragen und detektiert.
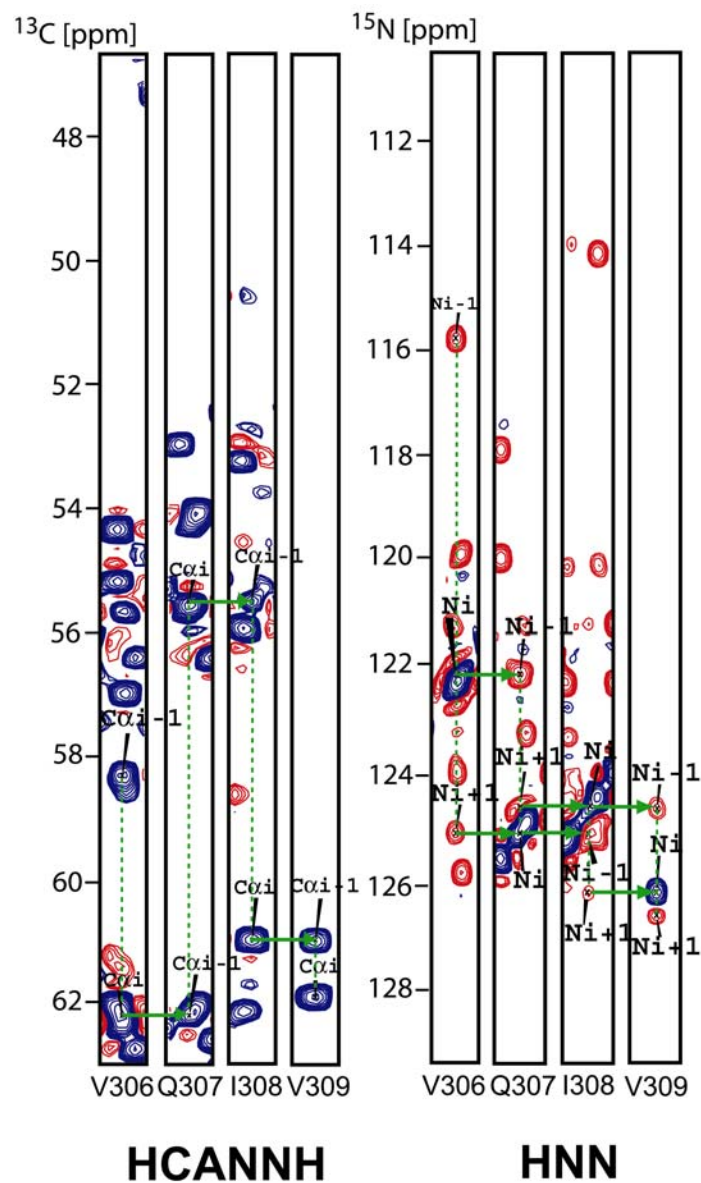
Abb. 23: Konnektivitätsinformationen in den 3D-Spektren von htau40. Zweidimensionale Streifen aus den 3D-(HA)CANNH und HNN Spektren für die Reste Val[306] (^{1}H:8.243 ppm ^{15}N: 122.2 ppm ^{13}C$^{\alpha}$: 62.21 ppm), Gln[307] (^{1}H: 8.505 ppm ^{15}N: 125.243 ppm ^{13}C$^{\alpha}$: 55.41 ppm), Ile[308] (^{1}H: 8.361 ppm ^{15}N: 124.765 ^{13}C$^{\alpha}$: 60.91 ppm) und Val[309] (^{1}H: 8.276 ppm ^{15}N: 126.338 ppm ^{13}C$^{\alpha}$: 61.84 ppm) werden dargestellt. Sequentielle Konnektivitäten sind durch grüne Pfeile gekennzeichnet

1.4.2 Analyse residualer Strukturelemente mit Hilfe von sekundärchemischen Verschiebungen, ^{3}J(H^{N}H$^\alpha$)-Kopplungen und RDCs

C$^\alpha$-Frequenzen sind von den Dihedralwinkeln ϕ/ψ des Proteinrückgrats abhängig, welche wiederum von der jeweiligen Art der Sekundärstruktur (α-Helix, β-Faltblatt) bestimmt werden. Charakteristisch für eine α-Helix ist eine Tieffeldverschiebung und für β-Faltblatt eine Hochfeldverschiebung in der ^{13}C-Dimension gegenüber sogenannten „random-coil" (RC)-Werten, die von Proteinen bzw. Peptiden in Gegenwart denaturierender Reagenzien gemessen wurden. Die Abweichungen der gemessenen C$^\alpha$-Werte von diesen RC-Werten geben Aufschluss über die jeweilige Sekundärstruktur (Schwarzinger et al., 2001; Schwarzinger et al., 2000; Wishart and Sykes, 1994a; Wishart and Sykes, 1994c; Wishart et al., 1992). Auf diese Weise konnten mit Hilfe des (HA)CANNH-Spektrums residuale Strukturelemente identifiziert werden.

Ein anderer Parameter, der Informationen über Rückgrat-Dihedralwinkel und damit Sekundärstruktur liefern kann, sind ^{3}J(H^{N}H$^\alpha$)-Kopplungen, die vom Winkel ϕ abhängig sind. Die Kopplungen nehmen für β-Strukturbereiche Werte von bis zu ca. 8-11 Hz an, wohingegen sie für α-Helices bis auf 4-6 Hz zurückgehen können (Karplus, 1959; Permi et al., 2000).

Es ist möglich, die ^{3}J-Kopplungen über ein intensitätsmoduliertes HSQC-Spektrum zu messen. Hierbei werden zwei Spektren in „interleaved"-Form aufgenommen. Bei dem einen kann sich die ^{3}J(H^{N}H$^\alpha$)-Kopplung entwickeln, wohingegen bei dem anderen entkoppelt wird. Die Kreuzpeaks der beiden Spektren stehen so in der folgenden Beziehung zueinander:

$$\mathbf{I_{kop.}}/\mathbf{I_{entkopp.}} = \cos(\pi\,^3J(H^NH^\alpha)\,2\tau)$$

Hierbei ist 2τ das Zeitintervall während dessen sich die ^{3}J(H^{N}H$^\alpha$)-Kopplung entwickelt. Die Pulssequenz ist in **Abb. 24** angegeben.

Die Komponente, bei welcher die ^{3}J-Kopplung evolvieren kann, entwickelt sich folgendermaßen:

$a \rightarrow b:\ H_Z \rightarrow -H_Y$

$b \rightarrow c:\ -H_Y \rightarrow -H_X N_Z \cos(\pi\ ^3J(H^N H^\alpha)\ 2\tau\ )$

Der Magnetisierungstransfer der Komponente, bei welcher während 2τ keine $^3J(H^N H^\alpha)$- Kopplung aktiv ist, verläuft folgendermaßen:

$b \rightarrow c:\ -H_Y \rightarrow -H_X N_Z$
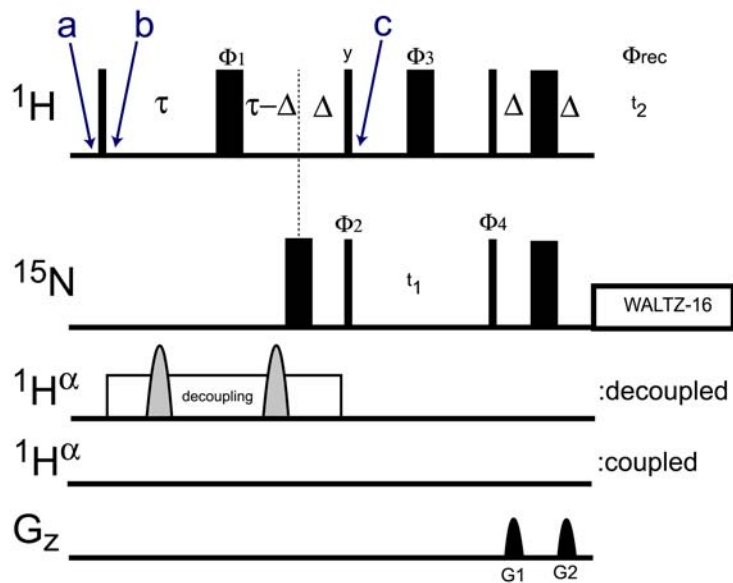
Abb. 24: Pulssequenz des intensitätsmodulierten HSQCs. Delays: $\Delta = 1/4J_{HN}$, $2\tau < 1/2\,^3J_{HN}H^\alpha_{max}$. Phasenzyklus: $\phi 1$ = x,x, y, y, -x, -x, -y, -y; $\phi 2$ = x, -x; $\phi 3$ = x; $\phi 4$ = 8(x), 8(-x). Das Spektrum wurde mit und ohne H^α-Entkopplung (REBURP oder G3-Pulskaskade) aufgenommen. Eine Wasserunterdrückung erfolgte durch eine WET-Sequenz. Die ^{15}N-Entkopplung wurde während der Akquisition mit einer WALTZ-16-Sequenz erzielt (Permi et al., 2000).

Die beiden bisher genannten Parameter, sekundärchemische Verschiebungen und ^{3}J-Kopplungen, ergeben weitestgehend nur lokale Strukturinformationen. Residuale dipolare Kopplungen (RDCs) sind hingegen in der Lage, globale Informationen über das vorliegende Protein zugänglich zu machen, da sie sensitiv für die Orientierung der internuklearen Bindungsvektoren (wie z.B. des ^{1}H-^{15}N-Bindungsvektors) zum B$_0$-Magnetfeld sind und darüber hinaus auch Dynamikinformationen enthalten, die Rückschlüsse auf die Rigidität von Molekülregionen zulassen. Da RDCs das Integral über alle Orientierungen eines ^{1}H-^{15}N-Bindungsvektors darstellen, sind sie in einem Medium mit einer isotropen Ausrichtung des Proteins zum Magnetfeld nicht messbar, da sie sich gegenseitig ausmitteln. Aus diesem Grund ist es notwendig, das Protein in ein anisotropes Medium zu überführen, in dem es eine Vorzugsausrichtung gegenüber dem B$_0$-Feld einnehmen kann. Das führt dazu, dass sich dipolare Kopplungen durch isotrope Bewegungen nicht mehr gegenseitig aufheben. Beispiele für solche Medien sind:

- Bicellen (Tjandra and Bax, 1997); Ottiger and Bax, 1998; Ottiger and Bax, 1999; Ottiger et al., 1998b)

- Pf1 Bakteriophagen (Hansen et al., 1998; Zweckstetter and Bax, 2001a)

- Komprimierte Polyacrylamid-Gele (s. Diplomarbeit von N. Lakomek bzw. (Tycko et al., 2000))

Die Größe der dipolaren Kopplungen ist gegeben durch (Blackledge, 2005; Tolman and Ruan, 2006):

$$D_{NH} = D_{NH}^{max} < (3\cos^2\theta - 1) / 2 >$$

Hierbei ist θ der Winkel zwischen dem internuklearen Bindungsvektor und dem B$_0$-Feld. Die Klammern zeigen an, dass es sich um den Durchschnitt aus Zeit und Ensemble handelt. Die maximale dipolare Kopplung für Amidbindungen ist gegeben durch:

$$D_{NH}^{max} = - \mu_0 (h/2\pi) \gamma_N \gamma_H / (4\pi^2 r_{NH}^3)$$
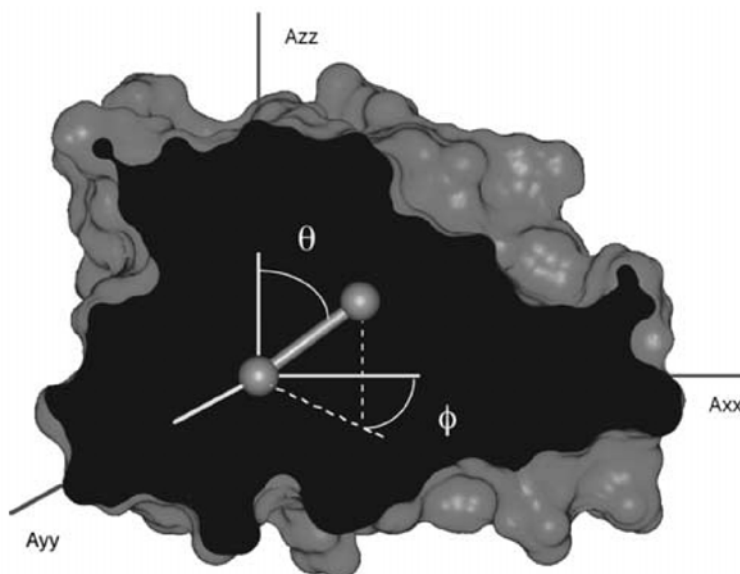
Abb. 25: ^{1}H, ^{15}N-Bindungsvektor in der Polarkoordinatendarstellung. Der ^{1}H, ^{15}N-Bindungsvektor und das B_0-Magnetfeld entlang A_{zz} schließen den Winkel θ ein, aus dem die RDC-Werte resultieren (entnommen aus Blackledge, 2005)

Hierbei ist μ_0 die magnetische Suszeptibilität im Vakuum, h das Plancksche Wirkungsquantum, γ_N und γ_H die gyromagnetischen Verhältnisse von ^{15}N und ^{1}H Nuklei und r_{NH} die Länge des Amidbindungsvektors. Der maximale Wert von D_{NH} beträgt 21 kHz und kann in Festkörperproben beobachtet werden. In schwach orientierten Medien, wie sie in der Flüssig-NMR-Spektroskopie verwendet werden, liegen die Kopplungswerte typischerweise für D_{NH} im ein- bzw. zweistelligen Hertzbereich. RDCs führen zu einer Aufspaltung von Signalen, die zusätzlich zu der aus J-Kopplungen resultierenden Signalaufspaltung beobachtbar ist. Aufgrund dessen ist es notwendig, eine Probe in isotroper und anisotroper Phase zu messen, um die RDCs von den J-Kopplungen zu trennen. Es werden IPAP-HSQC-Experimente gemessen, die in einer „interleaved"-Form aufgenommen werden und ähnlich dem (HA)CANNH-Experiment aus der Kombination einer In-Phase- und einer Anti-Phase-Komponente bestehen. Die Pulssequenz ist in **Abb. 26** angegeben.
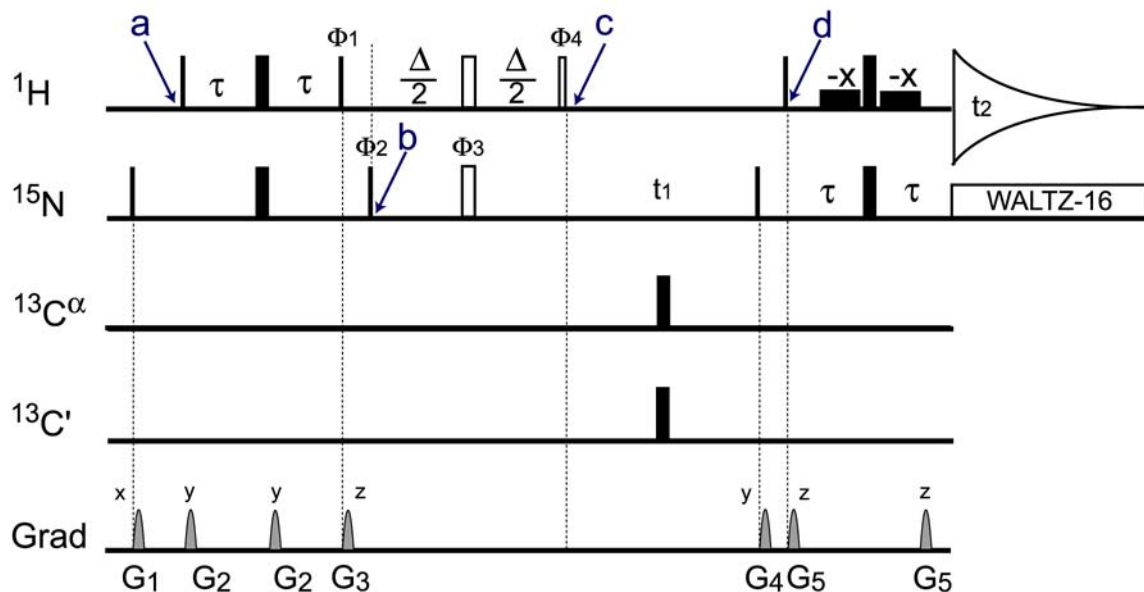
Abb. 26: Pulssequenz des IPAP-[^{1}H, ^{15}N]-HSQC-Experiments. Schmale und breite Rechtecke entsprechen Pulsen mit Flipwinkeln von 90° bzw. 180°. Das IPAP-Element ist in offenen Rechtecken dargestellt. Die selektiven Pulse, die den letzten ^{1}H-180° - Puls umgeben, gehören zu dem WATERGATE-Wasserunterdrückungsschema (Piotto et al., 1992). ^{13}C' und ^{13}C$^\alpha$ 180°-Pulse entkoppeln ^{13}C von ^{15}N während t_1. Delays: τ = 2.5 ms; Δ = 5.3 ms. Phasenzyklus: ϕ_1 = -y, y; ϕ_2 = 2(x), 2(-x) für IP; ϕ_2 = 2(-y), 2(y) for AP; ϕ_3 = 4(x), 4(y), 4(-x), 4(-y), 4(-y); ϕ_4 = 8(x), 8(-x); ϕ_{rec} = x, 2(-x), x for IP; ϕ_{rec} = x, 2(-x), x, -x, 2(x), -x für AP (Ottiger et al., 1998a).

a → c: H_Z → $-H_Y$ → $2 I_Z S_Y$. Protonen werden durch einen 90°-Puls angeregt und der Polarisationstransfer durch ein INEPT-Element bewerkstelligt. Anti-Phase-Magnetisierung liegt nun vor, die entweder direkt die Evolutionsperiode t_1 durchläuft oder durch das optionale IPAP-Element (b → c) in In-Phase-Magnetisierung $-I_Y$ refokusiert wird.

c → d: AP: $2 I_Z S_Y$ → $- I_Y S_Z$. IP: $- S_Y$ → $- I_Y S_Z$. Während t_1 wird ^{13}C durch 180°-Pulse entkoppelt. Die J-Kopplung und dipolare Kopplungen zwischen ^{1}H und ^{15}N können sich jedoch entwickeln und führen zu einer Signalaufspaltung in der ^{15}N-Dimension, die im anisotropen Medium aus ^{1}J(^{1}H^{15}N) + D_{HN} und im isotropen Medium nur aus ^{1}J(^{1}H^{15}N) besteht.

$-I_Y S_Z$ wird anschließend vor der Detektion zu I_X refokusiert.

Das Ergebnis der Kombination von IP- und AP-Komponenten führt zu zwei Spektren, von denen Ausschnitte beispielhaft für zwei Reste in **Abb. 27** übereinander gelegt sind. Zusätzliche spektrale Überlagerung wird durch die Verteilung der beiden Kopplungskomponenten einer Aminosäure auf zwei Spektren vermieden. Der Abstand der beiden Dublettkomponenten enthält die Summe der Kopplungen.
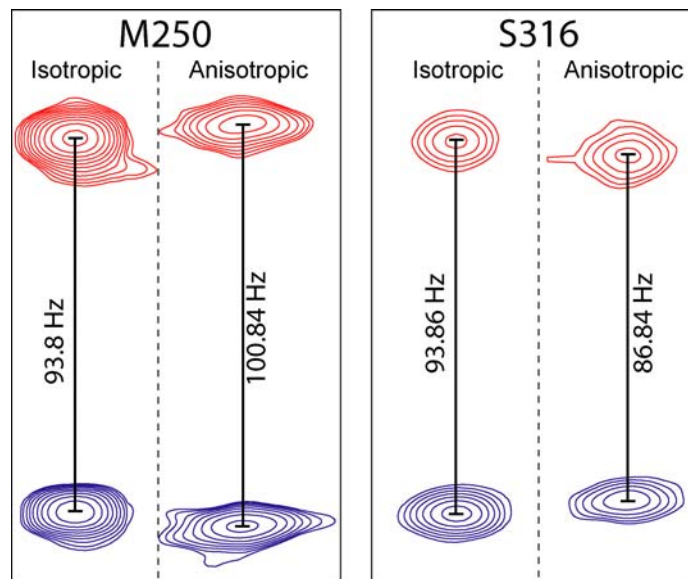
Abb. 27: Analyse der IPAP-Experimente in isotroper und anisotroper Phase am Beispiel von Met[250] und Ser[316]. Die Abstände zwischen den Signalen (rot/blau) geben die $^1J_{HN}$-Kopplungen (isotrop) bzw. die Summe aus $^1J_{HN}$-Kopplungen und RDCs (anisotrop) in Hz an (aus Mukrasch et al., 2007a).

1.4.3 Charakterisierung von Bindungsstellen

NMR-Spektroskopie bietet die Möglichkeit, mit Hilfe von „chemical shift perturbation mapping" Regionen in einem Protein zu lokalisieren, die mit einem Bindungspartner wechselwirken (Craik and Wilce, 1997). Amidprotonenresonanzen sind empfindliche Indikatoren für eine lokale Änderung der chemischen Umgebung. Hierbei können

unterschiedliche Effekte, die vom jeweiligen Liganden hervorgerufen werden, eine Rolle spielen: Elektrostatische Wechselwirkung, Ringstromeffekte bei aromatischen Gruppen, veränderte Protonenaustauschraten und konformationeller Austausch. Die Einflüsse des Bindungspartners können anhand der veränderten chemischen Verschiebung bzw. Intensität der Resonanz des Restes, der in der Bindungsstelle vorkommt, abgelesen werden. Hierzu werden [^{1}H,^{15}N]-HSQC-Spektren des Proteins in Anwesenheit und Abwesenheit des jeweiligen Liganden gemessen (**Abb. 28**). Die Veränderungen der Signale in den Spektren in Gegenwart des Liganden gegenüber dem Ausgangsspektrum des Proteins können nun quantifiziert werden. Bindungsstellen sind nun daran zu erkennen, dass die betroffenen Reste Resonanzen mit einer chemischen Verschiebungsänderung bzw. einer veränderten Signalintensität aufweisen.
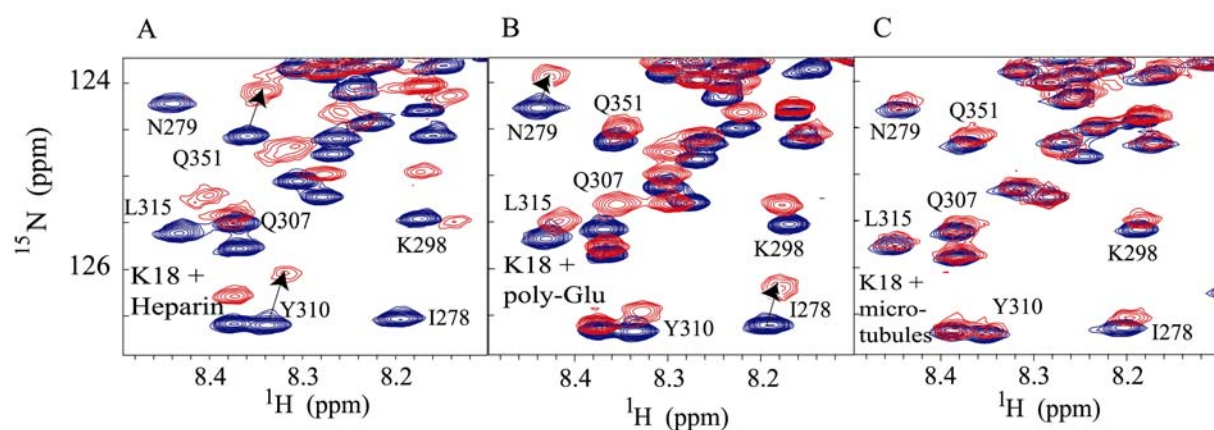
Abb. 28: Übereinandergelegte [^{1}H, ^{15}N]-HSQC-Spektren aus Titrationen des Konstruktes K18 (0.2 mM) mit Heparin, Polyglutamat und Mikrotubuli. Das Spektrum ohne Ligand ist in blau eingezeichnet und das in Anwesenheit des Liganden in rot. Chemische Verschiebungsänderungen sind am Beispiel einiger Aminosäuren mit Pfeilen hervorgehoben. A: mit 0.15 mM Heparin B: mit 1.3 mM Polyglutamat C: mit 0.8 mM MTs (entnommen aus Mukrasch et al., 2005).

1.5   Referenzen

Ackmann, M., Wiech, H., and Mandelkow, E. (2000). Nonsaturable binding indicates clustering of Tau on the microtubule surface in a paired helical filament-like conformation. J. Biol. Chem. *275*, 30335-30343.

Aravin, A., and Tuschl, T. (2005). Identification and characterization of small RNAs involved in RNA silencing. FEBS Lett. *579*, 5830-5840.

Arawaka, S., Saito, Y., Murayama, S., and Mori, H. (1998). Lewy body in neurodegeneration with brain iron accumulation type 1 is immunoreactive for alpha-synuclein. Neurology *51*, 887-889.

Arima, K., Ueda, K., Sunohara, N., Arakawa, K., Hirai, S., Nakamura, M., Tonozuka-Uehara, H., and Kawai, M. (1998a). NACP/alpha-synuclein immunoreactivity in fibrillary components of neuronal and oligodendroglial cytoplasmic inclusions in the pontine nuclei in multiple system atrophy. Acta Neuropathol. (Berl.) *96*, 439-444.

Arima, K., Ueda, K., Sunohara, N., Hirai, S., Izumiyama, Y., Tonozuka-Uehara, H., and Kawai, M. (1998b). Immunoelectron-microscopic demonstration of NACP/alpha-synuclein-epitopes on the filamentous component of Lewy bodies in Parkinson's disease and in dementia with Lewy bodies. Brain. Res. *808*, 93-100.

Armstrong, R. A. (2006). Plaques and tangles and the pathogenesis of Alzheimer's disease. Folia Neuropathol. *44*, 1-11.

Augustinack, J. C., Schneider, A., Mandelkow, E. M., and Hyman, B. T. (2001). Specific tau phosphorylation sites correlate with severity of neuronal cytopathology in Alzheimer's disease. Soc. Neurosc. Abstracts *27*.

Avila, J., Lucas, J. L., Perez, M., and Hernandez, F. (2004). Role of tau protein in both physiological and pathological conditions. Physiol. Rev. *84*, 361-384.

Aviles, F. J., Chapman, G. E., Kneale, G. G., Crane-Robinson, C., and Bradbury, E. M. (1978). The conformation of histone H5. Isolation and characterisation of the globular segment. Eur. J. Biochem. *88*, 363-371.

Balbach, J. J., Yang, J., Weliky, D. P., Steinbach, P. J., Tugarinov, V., Anglister, J., and Tycko, R. (2000). Probing hydrogen bonds in the antibody-bound HIV-1 gp120 V3 loop by solid state NMR REDOR measurements. J. Biomol. NMR *16*, 313-327.

Barghorn, S., Davies, P., and Mandelkow, E. (2004). Tau paired helical filaments from Alzheimer's disease brain and assembled in vitro are based on beta-structure in the core domain. Biochemistry *43*, 1694-1703.

Barghorn, S., and Mandelkow, E. (2002). Toward a unified scheme for the aggregation of tau into Alzheimer paired helical filaments. Biochemistry *41*, 14885-14896.

Barghorn, S., von Bergen, M., Li, L., Biernat, J., Mandelkow, E. M., and Mandelkow, E. (2002). Some mutations of tau protein in frontotemporal dementia (FTDP-17) promote aggregation of paired helical filaments by enhancing, local beta structure. Neurobiol. Aging *23*, S528-S528.

Barghorn, S., Zheng-Fischhofer, Q., Ackmann, M., Biernat, J., von Bergen, M., Mandelkow, E. M., and Mandelkow, E. (2000). Structure, microtubule interactions, and paired helical filament aggregation by tau mutants of frontotemporal dementias. Biochemistry *39*, 11714-11721.

Belmont, L., Mitchison, T., and Deacon, H. W. (1996). Catastrophic revelations about Op18/stathmin. Trends Biochem. Sci. *21*, 197-198.

Bennett, W. S., and Steitz, T. A. (1978). Glucose-Induced Conformational Change in Yeast Hexokinase. Proc. Natl. Acad. Sci. U. S. A. *75*, 4848-4852.

Bernado, P., Bertoncini, C. W., Griesinger, C., Zweckstetter, M., and Blackledge, M. (2005a). Defining long-range order and local disorder in native alpha-synuclein using residual dipolar couplings. J. Am. Chem. Soc. *127*, 17968-17969.

Bernado, P., Blanchard, L., Timmins, P., Marion, D., Ruigrok, R. W. H., and Blackledge, M. (2005b). A structural model for unfolded proteins from residual dipolar couplings and small-angle x-ray scattering. Proc. Natl. Acad. Sci. U. S. A. *102*, 17002-17007.

Berry, R. W., Abraha, A., Lagalwar, S., LaPointe, N., Gamblin, T. C., Cryns, V. L., and Binder, L. I. (2003). Inhibition of tau polymerization by its carboxy-terminal caspase cleavage fragment. Biochemistry *42*, 8325-8331.

Biernat, J., Gustke, N., Drewes, G., Mandelkow, E. M., and Mandelkow, E. (1993). Phosphorylation of Ser(262) Strongly Reduces Binding of Tau-Protein to Microtubules - Distinction between Phf-Like Immunoreactivity and Microtubule-Binding. Neuron *11*, 153-163.

Binder, L. I., Guillozet-Bongaarts, A. L., Garcia-Sierra, F., and Berry, R. W. (2005). Tau, tangles, and Alzheimer's disease. Biochim. Biophys. Acta *1739*, 216-223.

Blackledge, M. (2005). Recent progress in the study of biomolecular structure and dynamics in solution from residual dipolar couplings. Prog. Nucl. Magn. Res. Spectrosc. *46*, 23-61.

Booth, D. R., Sunde, M., Bellotti, V., Robinson, C. V., Hutchinson, W. L., Fraser, P. E., Hawkins, P. N., Dobson, C. M., Radford, S. E., Blake, C. C., and Pepys, M. B. (1997). Instability, unfolding and aggregation of human lysozyme variants underlying amyloid fibrillogenesis. Nature *385*, 787-793.

Braak, H., and Braak, E. (1991). Neuropathological Staging of Alzheimer-Related Changes. Acta Neuropathol. *82*, 239-259.

Braak, H., and Braak, E. (1996). Development of Alzheimer-related neurofibrillary changes in the neocortex inversely recapitulates cortical myelogenesis. Acta Neuropathol. (Berl.) *92*, 197-201.

Braak, H., Braak, E., Bohl, J., and Reintjes, R. (1996a). Age, neurofibrillary changes, A beta-amyloid and the onset of Alzheimer's disease. Neurosci. Lett. *210*, 87-90.

Braak, H., Braak, E., Yilmazer, D., de Vos, R. A., Jansen, E. N., and Bohl, J. (1996b). Pattern of brain destruction in Parkinson's and Alzheimer's diseases. J. Neural. Transm. *103*, 455-490.

Brandt, R., Hundelt, M., and Shahani, N. (2005). Tau alteration and neuronal degeneration in tauopathies: mechanisms and models. Biochim. Biophys. Acta *1739*, 331-354.

Bretscher, A. (1999). Regulation of cortical structure by the ezrin-radixin-moesin protein family. Curr. Opin. Cell Biol. *11*, 109-116.

Brion, J. P., Couck, A. M., Passareiro, E., and Flamentdurand, J. (1985). Neurofibrillary Tangles of Alzheimers-Disease - an Immunohistochemical Study. J. Submicroscopic Cyt. Pathol. *17*, 89-96.

Bukau, B., and Horwich, A. L. (1998). The Hsp70 and Hsp60 chaperone machines. Cell *92*, 351-366.

Bukau, B., Weissman, J., and Horwich, A. (2006). Molecular chaperones and protein quality control. Cell *125*, 443-451.

Carmel, G., Mager, E. M., Binder, L. I., and Kuret, J. (1996). The structural basis of monoclonal antibody Alz50's selectivity for Alzheimer's disease pathology. J. Biol. Chem. *271*, 32789-32795.

Cassimeris, L. (1999). Accessory protein regulation of microtubule dynamics throughout the cell cycle. Curr. Op. Cell Biol. *11*, 134-141.

Cassimeris, L. (2004). Cell division: eg'ing on microtubule flux. Curr. Biol. *14*, R1000-1002.

Cassimeris, L., and Spittle, C. (2001). Regulation of microtubule-associated proteins. Int. Rev. Cyt., Vol 210 *210*, 163-226.

Chamberlain, A. K., MacPhee, C. E., Zurdo, J., Morozova-Roche, L. A., Hill, H. A., Dobson, C. M., and Davis, J. J. (2000). Ultrastructural organization of amyloid fibrils by atomic force microscopy. Biophys. J. *79*, 3282-3293.

Chen, X., Li, N., and Ellington, A. D. (2007). Ribozyme catalysis of metabolism in the RNA world. Chem. Biodivers. *4*, 633-655.

Chiti, F., Webster, P., Taddei, N., Clark, A., Stefani, M., Ramponi, G., and Dobson, C. M. (1999). Designing conditions for in vitro formation of amyloid protofilaments and fibrils. Proc. Natl. Acad. Sci. U. S. A. *96*, 3590-3594.

Chung, W. J., Kindler, S., Seidenbecher, C., and Garner, C. C. (1996). MAP2a, an alternatively spliced variant of microtubule-associated protein 2. J. Neurochem. *66*, 1273-1281.

Crowther, R. A. (1991). Straight and Paired Helical Filaments in Alzheimer-Disease Have a Common Structural Unit. Proc. Natl. Acad. Sci. U. S. A. *88*, 2288-2292.

Dehmelt, L., and Halpain, S. (2004). Actin and microtubules in neurite initiation: Are MAPs the missing link? J. Neurobiol. *58*, 18-33.

Dehmelt, L., and Halpain, S. (2005). The MAP2/Tau family of microtubule-associated proteins. Genome Biol. *6*, 204.

Delacourte, A. (1999). Biochemical and molecular characterization of neurofibrillary degeneration in frontotemporal dementias. Dement. Geriatr. Cogn. Disord. *10 Suppl 1*, 75-79.

Delacourte, A., David, J. P., Sergeant, N., Buee, L., Wattez, A., Vermersch, P., Ghozali, F., Fallet-Bianco, C., Pasquier, F., Lebert, F.*, et al.* (1999). The biochemical pathway of neurofibrillary degeneration in aging and Alzheimer's disease. Neurology *52*, 1158-1165.

Desai, A., and Mitchison, T. J. (1997). Microtubule polymerization dynamics. Annu. Rev. Cell Dev. Biol. *13*, 83-117.

DeTure, M., Ko, L. W., Yen, S., Nacharaju, P., Easson, C., Lewis, J., van Slegtenhorst, M., Hutton, M., and Yen, S. H. (2000). Missense tau mutations identified in FTDP-17 have a small effect on tau-microtubule interactions. Brain Res. *853*, 5-14.

Dobson, C. M. (2003). Protein folding and misfolding. Nature *426*, 884-890.

D'Souza, I., Poorkaj, P., Hong, M., Nochlin, D., Lee, V. M. Y., Bird, T. D., and Schellenberg, G. D. (1999). Missense and silent tau gene mutations cause frontotemporal dementia with parkinsonism-chromosome 17 type, by affecting multiple alternative RNA splicing regulatory elements. Proc. Natl. Acad. Sci. U. S. A. *96*, 5598-5603.

D'Souza, I., and Schellenberg, G. D. (2005). Regulation of tau isoform expression and dementia. Biochim. Biophys. Acta *1739*, 104-115.

Dunker, A. K., Brown, C. J., Lawson, J. D., Iakoucheva, L. M., and Obradovic, Z. (2002a). Intrinsic disorder and protein function. Biochemistry *41*, 6573-6582.

Dunker, A. K., Brown, C. J., Lawson, J. D., Iakoucheva-Sebat, L. M., Vucetic, S., and Obradovic, Z. (2002b). The protein trinity: Structure/function relationships that include intrinsic disorder. Biophys. J. *82*, 460a-460a.

Dunker, A. K., Lawson, J. D., Brown, C. J., Williams, R. M., Romero, P., Oh, J. S., Oldfield, C. J., Campen, A. M., Ratliff, C. R., Hipps, K. W.*, et al.* (2001). Intrinsically disordered protein. J. Mol. Graphics & Modelling *19*, 26-59.

Dunker, A. K., and Obradovic, Z. (2001). The protein trinity - linking function and disorder. Nature Biotech. *19*, 805-806.

Dunker, K., and Obradovic, Z. (2002). The protein trinity: Importance of intrinsic disorder for protein function. Human Genome News *12*, 13-14.

Dyson, H. J., and Wright, P. E. (2005). Elucidation of the protein folding landscape by NMR. Methods Enzymol. *394*, 299-321.

Endow, S. A., Kang, S. J., Satterwhite, L. L., Rose, M. D., Skeen, V. P., and Salmon, E. D. (1994). Yeast Kar3 Is a Minus-End Microtubule Motor Protein That Destabilizes Microtubules Preferentially at the Minus Ends. EMBO J. *13*, 2708-2713.

Esposito, G., Viglino, P., Novak, M., and Cattaneo, A. (2000). The solution structure of the C-terminal segment of tau protein. J. Pept. Sci. *6*, 550-559.

Fiebig, K. M., Schwalbe, H., Buck, M., Smith, L. J., and Dobson, C. M. (1996). Toward a description of the conformations of denatured states of proteins. Comparison of a random coil model with NMR measurements. J. Phys. Chem. *100*, 2661-2666.

Fischer, D., Mukrasch, M. D., Bergen, M. V., Klos-Witkowska, A., Biernat, J., Griesinger, C., Mandelkow, E., and Zweckstetter, M. (2007). Structural and Microtubule Binding Properties of Tau Mutants of Frontotemporal Dementias. Biochemistry *46*, 2574-2582.

Flood, D. G., and Coleman, P. D. (1990). Hippocampal Plasticity in Normal Aging and Decreased Plasticity in Alzheimers-Disease. Prog. Brain Res. *83*, 435-443.

Friedhoff, P., Schneider, A., Mandelkow, E. M., and Mandelkow, E. (1998). Rapid assembly of Alzheimer-like paired helical filaments from microtubule-associated protein tau monitored by fluorescence in solution. Biochemistry *37*, 10223-10230.

Friedhoff, P., von Bergen, M., Mandelkow, E. M., and Mandelkow, E. (2000). Structure of tau protein and assembly into paired helical filaments. Biochim. Biophys. Acta *1502*, 122-132.

Fuchs, E. (1996). The cytoskeleton and disease: genetic disorders of intermediate filaments. Annu. Rev. Genet. *30*, 197-231.

Fuchs, E., and Weber, K. (1994). Intermediate filaments: structure, dynamics, function, and disease. Annu. Rev. Biochem. *63*, 345-382.

Furukawa, R., and Fechheimer, M. (1997). The structure, function, and assembly of actin filament bundles. Int. Rev. Cytol. *175*, 29-90.

Galvin, J. E., Lee, V. M., Schmidt, M. L., Tu, P. H., Iwatsubo, T., and Trojanowski, J. Q. (1999a). Pathobiology of the Lewy body. Adv. Neurol. *80*, 313-324.

Galvin, J. E., Uryu, K., Lee, V. M., and Trojanowski, J. Q. (1999b). Axon pathology in Parkinson's disease and Lewy body dementia hippocampus contains alpha-, beta-, and gamma-synuclein. Proc. Natl. Acad. Sci. U. S. A. *96*, 13450-13455.

Gamblin, T. C., Berry, R. W., and Binder, L. I. (2003). Tau polymerization: Role of the amino terminus. Biochemistry *42*, 2252-2257.

Garcia, M. L., and Cleveland, D. V. (2001). Going new places using an old MAP: tau, microtubules and human neurodegenerative disease. Curr. Op. Cell Biol. *13*, 41-48.

Garner, C. C., Brugg, B., and Matus, A. (1988). A 70-Kilodalton Microtubule-Associated Protein (Map2c), Related to Map2. J. Neurochem. *50*, 609-615.

Gast, K., Damaschun, H., Eckert, K., Schulze-Forster, K., Maurer, H. R., Muller-Frohne, M., Zirwer, D., Czarnecki, J., and Damaschun, G. (1995). Prothymosin alpha: a biologically active protein with random coil conformation. Biochemistry *34*, 13211-13218.

Geschwind, D. H. (2003). Tau phosphorylation, tangles, and neurodegeneration: The chicken or the egg? Neuron *40*, 457-460.

Ghetti, B., Farlow, M. R., Crowther, R. A., Goedert, M., and Spillantini, M. G. (1996). Hereditary multiple system degeneration with presenile dementia: Tau (tau) abnormalities in nerve cells and oligodendroglia. J. Neuropath. Exp. Neurol. *55*, 12-12.

Goedert, M. (2005). Tau gene mutations and their effects. Movement Disorders *20*, S45-S52.

Goedert, M., Jakes, R., Crowther, R. A., Hasegawa, M., Smith, M. J., and Spilantini, M. G. (1998). Intraneuronal filamentous tau protein and alpha-synuclein deposits in neurodegenerative diseases. Biochem. Soc. Trans. *26*, 463-471.

Goedert, M., Jakes, R., Spillantini, M. G., Hasegawa, M., Smith, M. J., and Crowther, R. A. (1996). Assembly of microtubule-associated protein tau into Alzheimer-like filaments induced by sulphated glycosaminoglycans. Nature *383*, 550-553.

Goedert, M., Satumtira, S., Jakes, R., Smith, M. J., Kamibayashi, C., White, C. L., and Sontag, E. (2000). Reduced binding of protein phosphatase 2A to tau protein with frontotemporal dementia and parkinsonism linked to chromosome 17 mutations. J. Neurochem. *75*, 2155-2162.

Goedert, M., Spillantini, M. G., Jakes, R., Rutherford, D., and Crowther, R. A. (1989). Multiple Isoforms of Human Microtubule-Associated Protein-Tau - Sequences and Localization in Neurofibrillary Tangles of Alzheimers-Disease. Neuron *3*, 519-526.

Gong, C. X., Liu, F., Grundke-Iqbal, I., and Iqbal, K. (2005). Post-translational modifications of tau protein in Alzheimer's disease. J. Neural Transmission *112*, 813-838.

Goode, B. L., Denis, P. E., Panda, D., Radeke, M. J., Miller, H. P., Wilson, L., and Feinstein, S. C. (1997). Functional interactions between the proline-rich and repeat regions of tau enhance microtubule binding and assembly. Mol. Biol. Cell *8*, 353-365.

Griffith, J., Manning, M., and Dunn, K. (1981). Filamentous bacteriophage contract into hollow spherical particles upon exposure to a chloroform-water interface. Cell *23*, 747-753.

Grundkeiqbal, I., Iqbal, K., Quinlan, M., Tung, Y. C., Zaidi, M. S., and Wisniewski, H. M. (1986a). Microtubule-Associated Protein-Tau - a Component of Alzheimer Paired Helical Filaments. J. Biol. Chem. *261*, 6084-6089.

Grundkeiqbal, I., Iqbal, K., Tung, Y. C., Quinlan, M., Wisniewski, H. M., and Binder, L. I. (1986b). Abnormal Phosphorylation of the Microtubule-Associated Protein-Tau (Tau) in Alzheimer Cytoskeletal Pathology. Proc. Natl. Acad. Sci. U. S. A. *83*, 4913-4917.

Grundkeiqbal, I., Iqbal, K., and Wisniewski, H. M. (1986c). Microtubule Associated Protein, Tau Is Abnormally Phosphorylated in Alzheimer Brain. J. Neuropath. Exp. Neurol. *45*, 379-379.

Guillozet-Bongaarts, A. L., Garcia-Sierra, F., Reynolds, M. R., Horowitz, P. M., Fu, Y. F., Wang, T. Y., Cahill, M. E., Bigio, E. H., Berry, R. W., and Binder, L. I. (2005). Tau truncation during neurofibrillary tangle evolution in Alzheimer's disease. Neurobiol. Aging. *26*, 1015-1022.

Gustke, N., Trinczek, B., Biernat, J., Mandelkow, E. M., and Mandelkow, E. (1994). Domains of Tau-Protein and Interactions with Microtubules. Biochemistry *33*, 9511-9522.

Haass, C., and Selkoe, D. J. (2007). Soluble protein oligomers in neurodegeneration: lessons from the Alzheimer's amyloid beta-peptide. Nat. Rev. Mol. Cell Biol. *8*, 101-112.

Hammond, C., and Helenius, A. (1995). Quality control in the secretory pathway. Curr. Opin. Cell Biol. *7*, 523-529.

Hansen, M. R., Mueller, L., and Pardi, A. (1998). Tunable alignment of macromolecules by filamentous phage yields dipolar coupling interactions. Nat. Struct. Biol. *5*, 1065-1074.

Hartl, F. U., and Hayer-Hartl, M. (2002). Molecular chaperones in the cytosol: from nascent chain to folded protein. Science *295*, 1852-1858.

Hong, M., Zhukareva, V., Vogelsberg-Ragaglia, V., Wszolek, Z., Reed, L., Miller, B. I., Geschwind, D. H., Bird, T. D., McKeel, D., Goate, A.*, et al.* (1998). Mutation-specific functional impairments in distinct Tau isoforms of hereditary FTDP-17. Science *282*, 1914-1917.

Horowitz, P. M., LaPointe, N., Guillozet-Bongaarts, A. L., Berry, R. W., and Binder, L. I. (2006). N-terminal fragments of tau inhibit full-length tau polymerization in vitro. Biochemistry *45*, 12859-12866.

Hutton, M., Lendon, C. L., Rizzu, P., Baker, M., Froelich, S., Houlden, H., Pickering-Brown, S., Chakraverty, S., Isaacs, A., Grover, A.*, et al.* (1998). Association of missense and 5 '-splice-site mutations in tau with the inherited dementia FTDP-17. Nature *393*, 702-705.

Inouye, H., Sharma, D., Goux, W. J., and Kirschner, D. A. (2006). Structure of core domain of fibril-forming PHF/Tau fragments. Biophys. J. *90*, 1774-1789.

Jeganathan, S., von Bergen, M., Brutlach, H., Steinhoff, H. J., and Mandelkow, E. (2006). Global hairpin folding of tau in solution. Biochemistry *45*, 2283-2293.

Ji, X., Oh, J., Dunker, A. K., and Hipps, K. W. (1998). Effects of relative humidity and applied force on atomic force microscopy images of the filamentous phage fd. Ultramicroscopy *72*, 165-176.

Jicha, G. A., Berenfeld, B., and Davies, P. (1999). Sequence requirements for formation of conformational variants of tau similar to those found in Alzheimer's disease. J. Neurosci. Res. *55*, 713-723.

Jicha, G. A., Bowser, R., Kazam, I. G., and Davies, P. (1997a). Alz-50 and MC-1, a new monoclonal antibody raised to paired helical filaments, recognize conformational epitopes on recombinant tau. J. Neurosci. Res. *48*, 128-132.

Jicha, G. A., Lane, E., Vincent, I., Otvos, L., Hoffmann, R., and Davies, P. (1997b). A conformation- and phosphorylation-dependent antibody recognizing the paired helical filaments of Alzheimer's disease. J. Neurochem. *69*, 2087-2095.

Kahle, P. J., Haass, C., Kretzschmar, H. A., and Neumann, M. (2002). Structure/function of alpha-synuclein in health and disease: rational development of animal models for Parkinson's and related diseases. J. Neurochem. *82*, 449-457.

Kampers, T., Friedhoff, P., Biernat, J., Mandelkow, E. M., and Mandelkow, E. (1997). RNA stimulates the aggregation of microtubule-associated protein tau into Alzheimer-like paired helical filaments. Mol. Biol. Cell *8*, 1528-1528.

Karplus, M. (1959). Contact Electron-Spin Coupling of Nuclear Magnetic Moments. J. Chem. Phys. *30*, 11-15.

Karush, F. (1950a). The Competitive Interaction of Organic Anions with Bovine Serum Albumin. J. Am. Chem. Soc. *72*, 2714-2718.

Karush, F. (1950b). Heterogeneity of the Binding Sites of Bovine Serum Albumin. J. Am. Chem. Soc. *72*, 2705-2713.

Kaufman, R. J. (2002). Orchestrating the unfolded protein response in health and disease. J. Clin. Invest. *110*, 1389-1398.

Khlistunova, I., Biernat, J., Wang, Y. P., Pickhardt, M., von Bergen, M., Gazova, Z., Mandelkow, E., and Mandelkow, M. (2006). Inducible expression of tau repeat domain in cell models of tauopathy - Aggregation is toxic to cells but can be reversed by inhibitor drugs. J. Biol. Chem. *281*, 1205-1214.

Kidd, M. (1963). Paired Helical Filaments in Electron Microscopy of Alzheimers Disease. Nature *197*, 192-&.

Klein-Seetharaman, J., Oikawa, M., Grimshaw, S. B., Wirmer, J., Duchardt, E., Ueda, T., Imoto, T., Smith, L. J., Dobson, C. M., and Schwalbe, H. (2002). Long-range interactions within a nonnative protein. Science *295*, 1719-1722.

Koshland, D. E. (1953). Stereochemistry and the Mechanism of Enzymatic Reactions. Biol. Rev. Camb. Phil. Soc. *28*, 416-436.

Koshland, D. E. (1954). General Mechanisms for Enzyme Action. Science *120*, 782-783.

Kosik, K. S., Orecchio, L. D., Bakalis, S., Duffy, L., and Neve, R. L. (1988a). Partial Sequence of Map2 in the Region of a Shared Epitope with Alzheimer Neurofibrillary Tangles. J. Neurochem. *51*, 587-598.

Kosik, K. S., Orecchio, L. D., Trojanowski, J. Q., and Lee, V. M. Y. (1988b). Well-Defined Tau Epitopes and Their Antigenic Accessibility within the Neurofibrillary Tangle. J. Neuropath. Exp. Neurol. *47*, 320-320.

Krause, K. H., Milos, M., Luan-Rilliet, Y., Lew, D. P., and Cox, J. A. (1991). Thermodynamics of cation binding to rabbit skeletal muscle calsequestrin. Evidence for distinct Ca(2+)- and Mg(2+)-binding sites. J. Biol. Chem. *266*, 9453-9459.

Kriwacki, R. W., Hengst, L., Tennant, L., Reed, S. I., and Wright, P. E. (1996). Structural studies of p21Waf1/Cip1/Sdi1 in the free and Cdk2-bound state: conformational disorder mediates binding diversity. Proc. Natl. Acad. Sci. U. S. A. *93*, 11504-11509.

LaFerla, F. M., and Oddo, S. (2005). Alzheimer's disease: A beta, tau and synaptic dysfunction. Trends Mol. Med. *11*, 170-176.

Landrieu, I., Lacosse, L., Leroy, A., Wieruszeski, J. M., Trivelli, X., Sillen, A., Sibille, N., Schwalbe, H., Saxena, K., Langer, T., and Lippens, G. (2006). NMR analysis of a Tau phosphorylation pattern. J. Am. Chem. Soc. *128*, 3575-3583.

Lansbury, P. T., Jr. (1999). Evolution of amyloid: what normal protein folding may tell us about fibrillogenesis and disease. Proc. Natl. Acad. Sci. U. S. A. *96*, 3342-3344.

Lee, G., Cowan, N., and Kirschner, M. (1988). The primary structure and heterogeneity of tau protein from mouse brain. Science *239*, 285-288.

Lee, V. M. Y., Goedert, M., and Trojanowski, J. Q. (2001). Neurodegenerative tauopathies. Ann. Rev. Neurosci. *24*, 1121-1159.

Levinthal.C (1968). Are There Pathways for Protein Folding. J. Chim. Phys. Phys.-Chim. Biol. *65*, 44-&.

Lippens, G., Sillen, A., Smet, C., Wieruszeski, J. M., Leroy, A., Buee, L., and Landrieu, I. (2006). Studying the natively unfolded neuronal Tau protein by solution NMR spectroscopy. Protein Pept. Lett. *13*, 235-246.

Mandelkow, E. M. (2004). Tau and tauopathy: Physiological role and pathological dysfunction. Neurobiol. Aging *25*, S24-S24.

Margittai, M., and Langen, R. (2004). Template-assisted filament growth by parallel stacking of tau. Proc. Natl. Acad. Sci. U. S. A. *101*, 10278-10283.

Margittai, M., and Langen, R. (2006). Spin labeling analysis of amyloids and other protein aggregates. Amyloid, Prions, and Other Protein Aggregates, Pt .C. *413*, 122-139.

Marx, J. (2007). Alzheimer's disease. A new take on tau. Science *316*, 1416-1417.

Mavilia, C., Couchie, D., and Nunez, J. (1994). Diversity of High-Molecular-Weight Tau-Proteins in Different Regions of the Nervous-System. J. Neurochem. *63*, 2300-2306.

Mayor, U., Guydosh, N. R., Johnson, C. M., Grossmann, J. G., Sato, S., Jas, G. S., Freund, S. M., Alonso, D. O., Daggett, V., and Fersht, A. R. (2003). The complete folding pathway of a protein from nanoseconds to microseconds. Nature *421*, 863-867.

McNally, F. J., and Thomas, S. (1998). Katanin is responsible for the M-phase microtubule-severing activity in Xenopus eggs. Mol. Biol. Cell *9*, 1847-1861.

Mirsky, A. E., and Pauling, L. (1936). On the Structure of Native, Denatured, and Coagulated Proteins. Proc. Natl. Acad. Sci. U. S. A. *22*, 439-447.

Mitchison, T. J., and Salmon, E. D. (1992). Poleward kinetochore fiber movement occurs during both metaphase and anaphase-A in newt lung cell mitosis. J. Cell Biol. *119*, 569-582.

Mukrasch, M. D., Biernat, J., von Bergen, M., Griesinger, C., Mandelkow, E., and Zweckstetter, M. (2005). Sites of tau important for aggregation populate beta-structure and bind to microtubules and polyanions. J. Biol. Chem. *280*, 24978-24986.

Mukrasch, M. D., Markwick, P., Biernat, J., Bergen, M., Bernado, P., Griesinger, C., Mandelkow, E., Zweckstetter, M., and Blackledge, M. (2007a). Highly populated turn conformations in natively unfolded tau protein identified from residual dipolar couplings and molecular simulation. J. Am. Chem. Soc. *129*, 5235-5243.

Mukrasch, M. D., von Bergen, M., Biernat, J., Fischer, D., Griesinger, C., Mandelkow, E., and Zweckstetter, M. (2007b). The "jaws" of the tau-microtubule interaction. J. Biol. Chem. *282*, 12230-12239.

Mullan, M., Crawford, F., Axelman, K., Houlden, H., Lilius, L., Winblad, B., and Lannfelt, L. (1992). A pathogenic mutation for probable Alzheimer's disease in the APP gene at the N-terminus of beta-amyloid. Nat. Genet. *1*, 345-347.

Novak, M., Kabat, J., and Wischik, C. M. (1993). Molecular Characterization of the Minimal Protease Resistant Tau-Unit of the Alzheimers-Disease Paired Helical Filament. EMBO J. *12*, 365-370.

Oddo, S., Caccamo, A., Tran, L., Lambert, M. P., Glabe, C. G., Klein, W. L., and LaFerla, F. M. (2006). Temporal profile of amyloid-beta (A beta) oligomerization in an in vivo model of Alzheimer disease - A link between A beta and tau pathology. J. Biol. Chem. *281*, 1599-1604.

Oliva, R., Bazett-Jones, D. P., Locklear, L., and Dixon, G. H. (1990). Histone hyperacetylation can induce unfolding of the nucleosome core particle. Nucleic Acids Res. *18*, 2739-2747.

Omary, M. B., Coulombe, P. A., and McLean, W. H. (2004). Intermediate filament proteins and their associated diseases. N. Engl. J. Med. *351*, 2087-2100.

Omary, M. B., Ku, N. O., Tao, G. Z., Toivola, D. M., and Liao, J. (2006). "Heads and tails" of intermediate filament phosphorylation: multiple sites and functional insights. Trends Biochem. Sci. *31*, 383-394.

Ottiger, M., and Bax, A. (1998). Characterization of magnetically oriented phospholipid micelles for measurement of dipolar couplings in macromolecules. J. Biomol. NMR *12*, 361-372.

Ottiger, M., and Bax, A. (1999). Bicelle-based liquid crystals for NMR-measurement of dipolar couplings at acidic and basic pH values. J. Biomol. NMR *13*, 187-191.

Ottiger, M., Delaglio, F., and Bax, A. (1998a). Measurement of J and dipolar couplings from simplified two-dimensional NMR spectra. J. Magn. Res. *131*, 373-378.

Ottiger, M., Delaglio, F., Marquardt, J. L., Tjandra, N., and Bax, A. (1998b). Measurement of dipolar couplings for methylene and methyl sites in weakly oriented macromolecules and their use in structure determination. J. Magn. Res. *134*, 365-369.

Palmer, A. G., Kroenke, C. D., and Loria, J. P. (2001). Nuclear magnetic resonance methods for quantifying microsecond-to-millisecond motions in biological macromolecules. Nucl. Magn. Res. Biol. Macromol., Pt. B. *339*, 204-238.

Panchal, S. C., Bhavesh, N. S., and Hosur, R. V. (2001). Improved 3D triple resonance experiments, HNN and HN(C)N, for H-N and N-15 sequential correlations in (C-13, N-15) labeled proteins: Application to unfolded proteins. J. Biomol. NMR *20*, 135-147.

Paramio, J. M., and Jorcano, J. L. (2002). Beyond structure: do intermediate filaments modulate cell signalling? Bioessays *24*, 836-844.

Parry, D. A., and Steinert, P. M. (1999). Intermediate filaments: molecular architecture, assembly, dynamics and polymorphism. Q. Rev. Biophys. *32*, 99-187.

Perez, M., Valpuesta, J. M., Medina, M., deGarcini, E. M., and Avila, J. (1996). Polymerization of tau into filaments in the presence of heparin: The minimal sequence required for tau-tau interaction. J. Neurochem. *67*, 1183-1190.

Permi, P., Kilpelainen, I., Annila, A., and Heikkinen, S. (2000). Intensity modulated HSQC and HMQC: two simple methods to measure 3J(HNH)alpha in proteins. J. Biomol. NMR *16*, 29-37.

Pervushin, K., Riek, R., Wider, G., and Wuthrich, K. (1997). Attenuated T-2 relaxation by mutual cancellation of dipole-dipole coupling and chemical shift anisotropy indicates an avenue to NMR structures of very large biological macromolecules in solution. Proc. Natl. Acad. Sci. U. S. A. *94*, 12366-12371.

Pettit, E. J., and Fay, F. S. (1998). Cytosolic free calcium and the cytoskeleton in the control of leukocyte chemotaxis. Physiol. Rev. *78*, 949-967.

Piotto, M., Saudek, V., and Sklenar, V. (1992). Gradient-tailored excitation for single-quantum NMR spectroscopy of aqueous solutions. J. Biomol. NMR *2*, 661-665.

Plaxco, K. W., and Gross, M. (1997). Cell biology - The importance of being unfolded. Nature *386*, 657-&.

Preuss, U., Biernat, J., Mandelkow, E. M., and Mandelkow, E. (1997). The 'jaws' model of tau-microtubule interaction examined in CHO cells. J. Cell Sci. *110*, 789-800.

Radivojac, P., Obradovic, Z., Smith, D. K., Zhu, G., Vucetic, S., Brown, C. J., Lawson, J. D., and Dunker, A. K. (2004). Protein flexibility and intrinsic disorder. Protein Sci. *13*, 71-80.

Riek, R., Wider, G., Pervushin, K., and Wuthrich, K. (1999). Polarization transfer by cross-correlated relaxation in solution NMR with very large molecules. Proc. Natl. Acad. Sci. U. S. A. *96*, 4918-4923.

Rodriguez, O. C., Schaefer, A. W., Mandato, C. A., Forscher, P., Bement, W. M., and Waterman-Storer, C. M. (2003). Conserved microtubule-actin interactions in cell movement and morphogenesis. Nat. Cell Biol. *5*, 599-609.

Santarella, R. A., Skiniotis, G., Goldie, K. N., Tittmann, P., Gross, H., Mandelkow, E. M., Mandelkow, E., and Hoenger, A. (2004). Surface-decoration of microtubules by human Tau. J. Mol. Biol. *339*, 539-553.

Sattler, M., Schleucher, J., and Griesinger, C. (1999). Heteronuclear multidimensional NMR experiments for the structure determination of proteins in solution employing pulsed field gradients. Prog. Nucl. Magn. Res. Spec. *34*, 93-158.

Sawaya, M. R., Sambashivan, S., Nelson, R., Ivanova, M. I., Sievers, S. A., Apostol, M. I., Thompson, M. J., Balbirnie, M., Wiltzius, J. J., McFarlane, H. T.*, et al.* (2007). Atomic structures of amyloid cross-beta spines reveal varied steric zippers. Nature *447*, 453-457.

Schneider, A., Biernat, J., von Bergen, M., Mandelkow, E., and Mandelkow, E. M. (1999). Phosphorylation that detaches tau protein from microtubules (Ser262, Ser214) also protects it against aggregation into Alzheimer paired helical filaments. Biochemistry *38*, 3549-3558.

Schoenfeld, T. A., and Obar, R. A. (1994). Diverse Distribution and Function of Fibrous Microtubule-Associated Proteins in the Nervous-System. Internat. Rev. Cyt., Vol 151, pp. 67-137.

Schroder, M., and Kaufman, R. J. (2005). The mammalian unfolded protein response. Annual Rev. Biochem. *74*, 739-789.

Schwarzinger, S., Kroon, G. J. A., Foss, T. R., Chung, J., Wright, P. E., and Dyson, H. J. (2001). Sequence-dependent correction of random coil NMR chemical shifts. J. Am. Chem. Soc. *123*, 2970-2978.

Schwarzinger, S., Kroon, G. J. A., Foss, T. R., Wright, P. E., and Dyson, H. J. (2000). Random coil chemical shifts in acidic 8 M urea: Implementation of random coil shift data in NMRView. J. Biomol. NMR *18*, 43-48.

Sheterline, P., Clayton, J., and Sparrow, J. (1995). Actin. Protein Profile *2*, 1-103.

Shiina, N., Gotoh, Y., Kubomura, N., Iwamatsu, A., and Nishida, E. (1994). Microtubule Severing by Elongation-Factor 1-Alpha. Science *266*, 282-285.

Shiina, N., Gotoh, Y., and Nishida, E. (1992). A Novel Homooligomeric Protein Responsible for an Mpf-Dependent Microtubule-Severing Activity. EMBO J. *11*, 4723-4731.

Sibille, N., Sillen, A., Leroy, A., Wieruszeski, J. M., Mulloy, B., Landrieu, I., and Lippens, G. (2006). Structural impact of heparin binding to full-length Tau as studied by NMR spectroscopy. Biochemistry *45*, 12560-12572.

Sillen, A., Barbier, P., Landrieu, I., Lefebvre, S., Wieruszeski, J. M., Leroy, A., Peyrot, V., and Lippens, G. (2007). NMR investigation of the interaction between the neuronal protein Tau and the microtubules. Biochemistry *46*, 3055-3064.

Sillen, A., Leroy, A., Wieruszeski, J. M., Loyens, A., Beauvillain, J. C., Buee, L., Landrieu, I., and Lippens, G. (2005a). Regions of tau implicated in the paired helical fragment core as defined by NMR. Chembiochem *6*, 1849-1856.

Sillen, A., Wieruszeski, J. M., Leroy, A., Ben Younes, A., Landrieu, I., and Lippens, G. (2005b). High-resolution magic angle spinning NMR of the neuronal tau protein integrated in Alzheimer's-like paired helical fragments. J. Am. Chem. Soc. *127*, 10138-10139.

Snow, C. D., Nguyen, H., Pande, V. S., and Gruebele, M. (2002). Absolute comparison of simulated and experimental protein-folding dynamics. Nature *420*, 102-106.

Spillantini, M. G., Crowther, R. A., and Goedert, M. (1996). Comparison of the neurofibrillary pathology in Alzheimer's disease and familial presenile dementia with tangles. Acta Neuropath. *92*, 42-48.

Stamer, K., Vogel, R., Thies, E., Mandelkow, E., and Mandelkow, E. M. (2002). Tau blocks traffic of organelles, neurofilaments, and APP vesicles in neurons and enhances oxidative stress. J. Cell Biol. *156*, 1051-1063.

Stanfield, R., Cabezas, E., Satterthwait, A., Stura, E., Profy, A., and Wilson, I. (1999). Dual conformations for the HIV-1 gp120 V3 loop in complexes with different neutralizing fabs. Structure *7*, 131-142.

Stoothoff, W. H., and Johnson, G. V. W. (2005). Tau phosphorylation: physiological and pathological consequences. Biochim. Biophys. Acta *1739*, 280-297.

Terry, R. D. (1963). Fine Structure of Neurofibrillary Tangles in Alzheimers Disease. J. Neuropath. Exp. Neurol. *22*, 350-&.

Terry, R. D., Masliah, E., Salmon, D. P., Butters, N., Deteresa, R., Hill, R., Hansen, L. A., and Katzman, R. (1991). Physical Basis of Cognitive Alterations in Alzheimers-Disease - Synapse Loss Is the Major Correlate of Cognitive Impairment. Ann. Neurol. *30*, 572-580.

Theriot, J. A. (1997). Accelerating on a treadmill: ADF/cofilin promotes rapid actin filament turnover in the dynamic cytoskeleton. J. Cell. Biol. *136*, 1165-1168.

Tissieres, A., Mitchell, H. K., and Tracy, U. M. (1974). Protein synthesis in salivary glands of Drosophila melanogaster: Relation to chromosome puffs. J. Mol. Biol. *85*, 389-398.

Tjandra, N., and Bax, A. (1997). Direct measurement of distances and angles in biomolecules by NMR in a dilute liquid crystalline medium. Science *278*, 1111-1114.

Toivola, D. M., Tao, G. Z., Habtezion, A., Liao, J., and Omary, M. B. (2005). Cellular integrity plus: organelle-related and protein-targeting functions of intermediate filaments. Trends Cell. Biol. *15*, 608-617.

Tolman, J. R., Flanagan, J. M., Kennedy, M. A., and Prestegard, J. H. (1995). Nuclear Magnetic Dipole Interactions in Field-Oriented Proteins - Information for Structure Determination in Solution. Proc. Natl. Acad. Sci. U. S. A. *92*, 9279-9283.

Tolman, J. R., and Ruan, K. (2006). NMR residual dipolar couplings as probes of biomolecular dynamics. Chem. Rev. *106*, 1720-1736.

Trinczek, B., Ebneth, A., Mandelkow, E., and Mandelkow, E. (1999). Tau regulates the attachment/detachment but not the speed of motors in microtubule-dependent transport of single vesicles and organelles. J. Cell Sci. *112*, 2355-2367.

Tu, P. H., Galvin, J. E., Baba, M., Giasson, B., Tomita, T., Leight, S., Nakajo, S., Iwatsubo, T., Trojanowski, J. Q., and Lee, V. M. (1998). Glial cytoplasmic inclusions in white matter oligodendrocytes of multiple system atrophy brains contain insoluble alpha-synuclein. Ann. Neurol. *44*, 415-422.

Tycko, R., Blanco, F. J., and Ishii, Y. (2000). Alignment of biopolymers in strained gels: A new way to create detectable dipole-dipole couplings in high-resolution biomolecular NMR. J. Am. Chem. Soc. *122*, 9340-9341.

Uversky, V. N. (2002). What does it mean to be natively unfolded? Eur. J. Biochem. *269*, 2-12.

Uversky, V. N., Oldfield, C. J., and Dunker, A. K. (2005). Showing your ID: intrinsic disorder as an ID for recognition, regulation and cell signaling. J. Mol. Recog. *18*, 343-384.

Vaughn, K. C., and Harper, J. D. (1998). Microtubule-organizing centers and nucleating sites in land plants. Int. Rev. Cytol. *181*, 75-149.

von Bergen, M., Barghorn, S., Biernat, J., Mandelkow, E. M., and Mandelkow, E. (2005). Tau aggregation is driven by a transition from random coil to beta sheet structure. Biochim. Biophys. Acta *1739*, 158-166.

von Bergen, M., Barghorn, S., Li, L., Marx, A., Biernat, J., Mandelkow, E. M., and Mandelkow, E. (2001). Mutations of tau protein in frontotemporal dementia promote aggregation of paired helical filaments by enhancing local beta-structure. J. Biol. Chem. *276*, 48165-48174.

von Bergen, M., Barghorn, S., Muller, S. A., Pickhardt, M., Biernat, J., Mandelkow, E. M., Davies, P., Aebi, U., and Mandelkow, E. (2006). The core of tau-paired helical filaments studied by scanning transmission electron microscopy and limited proteolysis. Biochemistry *45*, 6446-6457.

von Bergen, M., Friedhoff, P., Biernat, J., Heberle, J., Mandelkow, E. M., and Mandelkow, E. (2000). Assembly of tau protein into Alzheimer paired helical filaments depends on a local sequence motif (306-VQIVYK-311) forming beta structure. Mol. Biol. Cell *11*, 363A-363A.

Wakabayashi, K., Hayashi, S., Kakita, A., Yamada, M., Toyoshima, Y., Yoshimoto, M., and Takahashi, H. (1998a). Accumulation of alpha-synuclein/NACP is a cytopathological feature common to Lewy body disease and multiple system atrophy. Acta Neuropathol. (Berl) *96*, 445-452.

Wakabayashi, K., Yoshimoto, M., Tsuji, S., and Takahashi, H. (1998b). Alpha-synuclein immunoreactivity in glial cytoplasmic inclusions in multiple system atrophy. Neurosci. Lett. *249*, 180-182.

Wang, J. Z., Grundke-Iqbal, I., and Iqbal, K. (2007). Kinases and phosphatases and tau sites involved in Alzheimer neurofibrillary degeneration. Eur. J. Neurosci. *25*, 59-68.

WatermanStorer, C. M., and Salmon, E. D. (1997). Microtubule dynamics: Treadmilling comes around again. Curr. Biol. *7*, R369-R372.

Weinberg, R. L., Freund, S. M. V., Veprintsev, D. B., Bycroft, M., and Fersht, A. R. (2004). Regulation of DNA binding of p53 by its C-terminal domain. J. Mol. Biol. *342*, 801-811.

Weinreb, P. H., Zhen, W. G., Poon, A. W., Conway, K. A., and Lansbury, P. T. (1996). NACP, a protein implicated in Alzheimer's disease and learning, is natively unfolded. Biochemistry *35*, 13709-13715.

Welch, M. D., Mallavarapu, A., Rosenblatt, J., and Mitchison, T. J. (1997). Actin dynamics in vivo. Curr. Opin. Cell Biol. *9*, 54-61.

Wille, H., Drewes, G., Biernat, J., Mandelkow, E. M., and Mandelkow, E. (1992). Alzheimer-Like Paired Helical Filaments and Antiparallel Dimers Formed from Microtubule-Associated Protein-Tau Invitro. J. Cell Biol. *118*, 573-584.

Winkler, W. C., and Breaker, R. R. (2005). Regulation of bacterial gene expression by riboswitches. Annu. Rev. Microbiol. *59*, 487-517.

Wirmer, J., Schlorb, C., Klein-Seetharaman, J., Hirano, R., Ueda, T., Imoto, T., and Schwalbe, H. (2004). Modulation of compactness and long-range interactions of unfolded lysozyme by single point mutations. Angew. Chem. *43*, 5780-5785.

Wischik, C. M., Crowther, R. A., Stewart, M., and Roth, M. (1985). Subunit Structure of Paired Helical Filaments in Alzheimers-Disease. J. Cell Biol. *100*, 1905-1912.

Wishart, D. S., and Sykes, B. D. (1994a). The C-13 Chemical-Shift Index - a Simple Method for the Identification of Protein Secondary Structure Using C-13 Chemical-Shift Data. J. Biomol. NMR *4*, 171-180.

Wishart, D. S., and Sykes, B. D. (1994b). Chemical shifts as a tool for structure determination. Methods Enzymol. *239*, 363-392.

Wishart, D. S., and Sykes, B. D. (1994c). Chemical-Shifts as a Tool for Structure Determination. Nucl. Magn. Res., Pt C *239*, 363-392.

Wishart, D. S., Sykes, B. D., and Richards, F. M. (1992). The chemical shift index: a fast and simple method for the assignment of protein secondary structure through NMR spectroscopy. Biochemistry *31*, 1647-1651.

Wittmann, C. W., Wszolek, M. F., Shulman, J. M., Salvaterra, P. M., Lewis, J., Hutton, M., and Feany, M. B. (2001). Tauopathy in Drosophila: neurodegeneration without neurofibrillary tangles. Science *293*, 711-714.

Wright, P. E., and Dyson, H. J. (1999). Intrinsically unstructured proteins: Re-assessing the protein structure-function paradigm. J. Mol. Biol. *293*, 321-331.

Yang, W. Y., and Gruebele, M. (2003). Folding at the speed limit. Nature *423*, 193-197.

Yoshida, M. (2006). Cellular tau pathology and immunohistochemical study of tau isoforms in sporadic tauopathies. Neuropath.. *26*, 457-470.

Zerovnik, E. (2002). Amyloid-fibril formation - Proposed mechanisms and relevance to conformational disease. European J. Biochem. *269*, 3362-3371.

Zweckstetter, M., and Bax, A. (2001a). Characterization of molecular alignment in aqueous suspensions of Pf1 bacteriophage. J. Biomol. NMR *20*, 365-377.

Zweckstetter, M., and Bax, A. (2001b). Single-step determination of protein substructures using dipolar couplings: Aid to structural genomics. J. Am. Chem. Soc. *123*, 9490-9491.

2 Sites of tau important for aggregation populate β-structure and bind to microtubules and polyanions

Marco D. Mukrasch[§], Jacek Biernat[*], Martin von Bergen[*],

Christian Griesinger[§], Eckhard Mandelkow[*] and Markus Zweckstetter[§]

From the [§] Department for NMR-based Structural Biology, Max Planck Institute for Biophysical Chemistry, Am Fassberg 11, 37077 Göttingen, Germany, and the [*] Max Planck Unit for Structural Molecular Biology c/o DESY, Notkestrasse 85, 22607 Hamburg, Germany

ABSTRACT

The aggregation of the microtubule-associated tau protein and formation of 'neurofibrillary tangles' is one of the hallmarks of Alzheimer's disease. The mechanisms underlying the structural transition of innocuous, natively unfolded tau to neurotoxic forms and the detailed mechanisms of binding to microtubules are largely unknown. Here we report the high-resolution characterization of the repeat domain of soluble tau using multidimensional NMR spectroscopy. NMR secondary chemical shifts detect residual β-structure for 8-10 residues at the beginning of repeats R2-R4. The regions correspond to sequence motifs known to form the core of the cross-β structure of tau paired helical filaments. Chemical shift perturbation studies show that polyanions, which promote PHF aggregation, as well as microtubules interact with tau through positive charges near the ends of the repeats, and through the β-forming motifs at the beginning of repeats 2 and 3. The high degree of similarity between the binding of polyanions and microtubules supports the hypothesis that stable microtubules prevent PHF formation by blocking the tau:polyanions interaction sites which are crucial for PHF formation.

Alzheimer's disease is characterized by abnormal protein deposits in the brain, such as amyloid plaques or neurofibrillary tangles, formed by fibrous assemblies of the Aβ peptide (1) or of the microtubule (MT)-associated tau protein. (2). These aggregates are thought to be toxic to neurons, either by causing some toxic signalling defect or by obstructing the cell interior. Therefore, one of the top priorities in Alzheimer research is to understand the reasons for the pathological aggregation and to find methods to prevent it. Whereas the structural principles governing Aβ aggregation are known in some detail, little is known for the tau protein.

Tau is a microtubule-associated protein that regulates MT stability, neurite outgrowth, and other MT-dependent functions. The three or four repeats in the C-terminal half of the protein and the flanking proline-rich basic domains are known to be involved in MT-binding (3). The affinity is regulated by phosphorylation, particularly at KXGS-motifs in the repeats (4). Interestingly the same phosphorylation sites have an inhibitory influence on aggregation (5). Unbound tau can assemble into Alzheimer-like paired helical filaments (PHFs) whose

polymerization can be enhanced by oxidation of SH groups and by polyanions (e.g. heparin, poly-Glu, (6)). On the other hand, tau has a hydrophilic character, is highly soluble and belongs to the class of natively unfolded proteins with no apparent ordered secondary structure detectable by far-UV CD or FTIR (7,8). Therefore, it is unclear why tau should aggregate in a specific manner and what structural principles could be responsible for this.
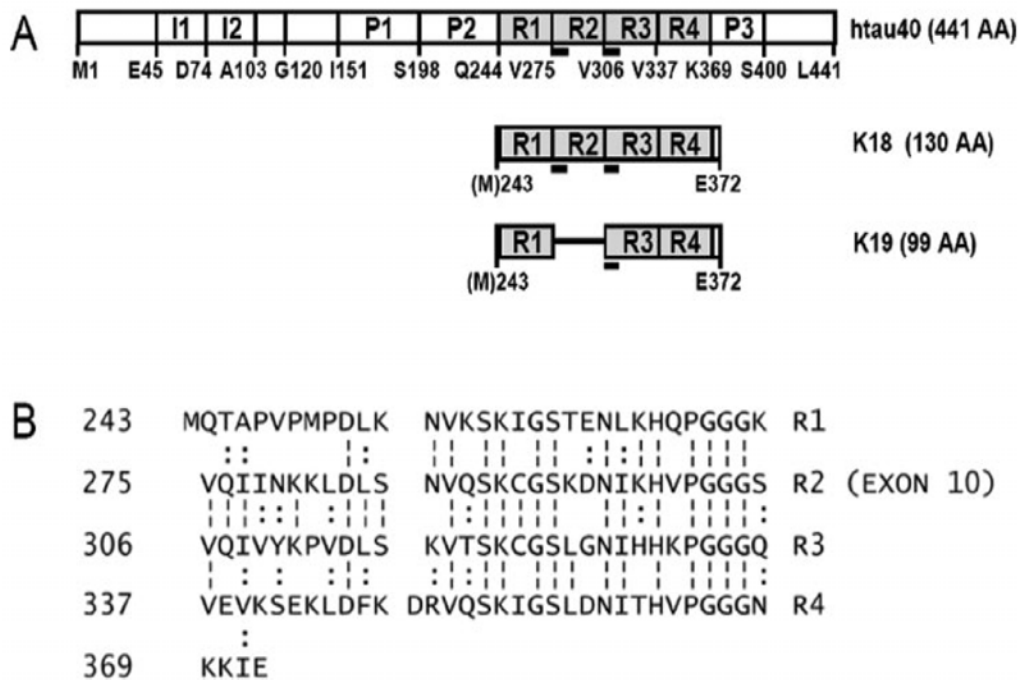
Fig. 1. (A) Tau isoforms and tau-derived constructs. The bars show the tau isoform htau40 and the constructs K18 and K19. The isoform htau40 is the largest one in the human CNS (441 residues). According to the isoform the C-terminal half contains three or four pseudo-repeats (~31 residues each, R1-R4, gray shade) which are involved in MT binding and form the core of PHFs. The constructs K18 and K19 represent the repeat domains of htau40, comprising 4 repeats or 3 repeats, respectively. The positions of the hexapeptides ^{275}VQIINK^{280} and ^{306}VQIVYK^{311} in R2 and R3 are underlined. Domain boundaries are labelled by the residue numbers. (B) Amino acid sequence of the repeat domain of tau. The sequence shows the 4-repeat construct K18, repeat R2 (275-305) is absent in K19, corresponding to the alternative splicing of exon 10. The overall character of the protein is hydrophilic and basic. Each repeat terminates with a characteristic PGGG motif. Identical amino acids in all repeats are marked by a dashed line; similar amino acids are indicated by a double dot.

Tau can aggregate as an intact protein, 352-441 residues in length (depending on isoform), so that all six tau isoforms are found in Alzheimer PHFs (9). The isoforms differ by two inserts near the N-terminal end and the presence of either four or three imperfect repeat

sequences in the C-terminal half of the protein (Fig. 1). The region comprising the repeat sequences forms the core of PHFs (10) and also promotes PHF assembly *in vitro* (11,12). For PHF aggregation two hexapeptides at the beginning of the second and third repeats (^{275}VQIINK^{280} and ^{306}VQIVYK^{311}) are crucial . These are able to initiate the aggregation of tau into bona fide paired helical filaments with cross-β structure and thereby represent minimal tau-tau interaction motifs (13,14).

Since tau is a highly flexible protein it has resisted all attempts of crystallization for a high resolution X-ray structure. X-ray analyses exist only in the form of solution scattering (confirming the unfolded nature of the protein, (7)) and fiber diffraction (confirming the cross-β structure of PHFs, (13)). We have now applied NMR spectroscopy as an alternative approach to structural studies. Here we report the high-resolution characterization of the repeat domain of tau, in which either all four repeats are present (K18) or repeat two has been deleted (K19), corresponding to the adult and fetal tau isoforms htau40 and htau23 (Fig. 1). Our findings show that the repeat domain of soluble tau contains regions of residual β-structure that have the potential to serve as seeds for aggregation of tau into PHFs, and we identify residues involved in the interaction with MTs and with polyanions that promote PHF-aggregation.

EXPERIMENTAL PROCEDURES

Expression of recombinant tau constructs and isotope labeling - Human tau constructs were expressed in the vector pNG2 (a derivative of pET-3a, Merck-Novagen, Darmstadt) in E.coli strain BL21(DE3) as described (Gustke et al., 1994) (see Fig. 1). K18 comprises all four repeats of the largest tau isoform (residues Q244 – E372 plus initial M243), K19 is similar but lacks the second repeat, corresponding to fetal tau (residues M243 + Q244-K274, V337-E372, without R2 = V275-S305). The expressed proteins were purified from bacterial extracts by making use of the heat stability of the protein and by FPLC SP-Sepharose chromatography (Amersham Biosciences). In order to label the tau proteins with ^{15}N and ^{13}C stable isotopes, the E.coli culture expressing K18 protein was grown in a M9 minimal medium with ^{15}NH$_4$Cl (1g L^{-1}) and ^{13}C glucose (4 g L^{-1}) (Campro Scientific, Berlin), and the E.coli culture expressing K19 protein was grown on rich growth medium based on chemolithoautotrophic bacteria labeled with ^{13}C and ^{15}N isotopes (Silantes, Munich). Protein

samples uniformly enriched in ^{15}N were prepared by growing E.coli bacteria in minimal medium containing 1g L^{-1} of ^{15}NH$_4$Cl .

The cell pellets were resuspended in boiling-extraction buffer (50 mM MES, 500 mM NaCl, 1 mM MgCl$_2$, 1 mM EGTA, 5 mM DTT, pH 6.8) complemented with a protease inhibitor cocktail. The cells were disrupted with a French pressure cell and subsequently boiled for 20 min. The soluble extract was isolated by centrifugation, the supernatant was dialyzed against two changes of cation exchange chromatography buffer A (20 mM MES, 50 mM NaCl, 1 mM EGTA, 1 mM MgCl$_2$, 2 mM DTT, 0.1 mM PMSF, pH 6.8) and loaded on an FPLC SP-Sepharose column. The proteins were eluted by a linear gradient of cation exchange chromatography buffer B (20 mM MES, 1 M NaCl, 1 mM EGTA, 1 mM MgCl$_2$, 2 mM DTT, 0.1 mM PMSF, pH 6.8). NMR samples contained 0.9 to 1.5 mM ^{15}N- or ^{15}N/^{13}C-labeled protein in 95% H$_2$O/5% D$_2$O, 50 mM phosphate buffer pH 6.8 with 1 mM DTT.

NMR spectroscopy - NMR spectra were acquired at 5 °C on Bruker DRX 800, Avance 600 and DRX 600 NMR spectrometers. Aggregation did not occur under these conditions of low temperature. NMR data were processed and analysed using nmrPipe (16) and Sparky 3 (www.cgl.ucsf.edu/home/sparky/). 3D triple-resonance experiments were collected to obtain sequence specific assignments for the backbone of K18 and K19 (Supplemental Table S1). Secondary shift values were calculated as the differences between the measured C$^\alpha$/C' chemical shifts and the empirical random coil value for the appropriate amino acid type at pH 3.0 (17). Random coil values for histidines, glutamates and aspartates were taken from Wishart et al. as the chemical shifts of these residues are particularly sensitive to pH and the pH in the studies by Wishart et al. (pH 5.0) is more similar to the one used here (pH 6.9). (18). To estimate the β-sheet propensity in contiguous segments of tau, the observed C$^\alpha$ secondary shifts were normalized by the empirically determined secondary shift expected for that residue type in a fully β-sheet conformation (18), summed, and normalized by the number of residues in the segment.

Tau-polyanion titrations were carried out with uniformly ^{15}N-labelled protein containing 0.2 mM (heparin titration) and 0.3 mM (poly-Glu titration) K18, and 0.12 mM (heparin titration) and 0.14 mM (poly-Glu titration) K19 at pH 6.8. Heparin (average mol. wt. 3000, about 5.8 disaccharide subunits, charge per subunit ~2.5, ~0.31 z/Å) and poly-Glu (average mol. wt. 10000, 7-8 Glu residues, 7-8 negative net charge, in extended conformation 0.33 z/Å) were from Sigma. Complex formation was monitored by recording 2D ^{1}H-^{15}N-HSQC spectra for increasing polyanion concentrations (mM): 0.03, 0.06, 0.15, 0.3, 0.58, 1.37

and 2.53 (K18 with heparin), 0.008, 0.015, 0.03, 0.072, 0.142, 0.28, 0.68, 1.3, 2.4 and 4.3 (K18 with poly-Glu), 0.008, 0.015, 0.03, 0.07, 0.14, 0.28, 0.67 and 1.3 (K19 with heparin) and 0.015, 0.03, 0.074, 0.146, 0.29, 0.70, 1.35, 2.49 (K19 with poly-Glu). For tau-MT titrations NMR samples contained 0.13 and 0.14 mM uniformly ^{15}N-labelled K18 and K19, respectively. Complex formation was monitored at 5 and 20 °C for MT concentrations (αβ-tubulin dimers) of 26.5, 79.5 and 159.0 μM in the K18 titrations, and 2.8, 5.4, 20.0, 35.0 and 84.3 μM in the K19 titration. Normalized weighted average chemical shift differences for amide ^{1}H and ^{15}N chemical shifts upon polyanion/MT binding were calculated using $\Delta_{av}(NH)$ = $[(\Delta H^2 + (\Delta N/5)^2)/2]^{1/2}$, where ΔH and ΔN are the differences between the free and bound chemical shifts.

Preparation of MTs - Porcine brain tubulin was purified as described (15) and incubated at concentrations higher than 200 μM in MT assembly buffer (100 mM Pipes pH 6.9, 1 mM EDTA, 1 mM MgSO$_4$, 1 mM DTT) in the presence of 1 mM GTP at 37° C for 5 minutes. After addition of 100 μM Paclitaxel (Sigma-Aldrich Chemie, Munich, Germany) the polymerisation was performed for 20 min at 37° C. *Electron microscopy* - Proteins were diluted to a concentration of about 0.1 mg/ml, placed on 600-mesh carbon-coated copper grids for 1 min, washed with two drops of H$_2$O and negatively stained with 2% uranyl acetate for 45 s. The specimen were examined in a Philipps 12M electron microscope at 100 kV.

RESULTS

Backbone resonance assignment of K18 and K19 – NMR resonances in ^{1}H-^{15}N HSQC spectra of the tau repeat domain constructs K18 and K19, uniformly labeled with ^{15}N, were recorded at 5°C and pH 6.9. The resonances were sharp, showed only a limited dispersion of chemical shifts, reflecting a high degree of backbone mobility and unfolded nature, in agreement with CD and FTIR measurements (7,13). In order to enable a study of the structure and dynamics of tau with atomic resolution, the assignment of the NMR resonances was required. Assignment of globular proteins with a molecular mass below 15 kDa is straightforward nowadays using multidimensional NMR techniques. Backbone assignment of K18 (130 residues) and K19 (99 residues) was however complicated by the limited dispersion of NMR resonances due to the absence of well-defined secondary and tertiary structure elements. In addition, only five amino acid types make up more than 50% of

the primary sequence and these amino acids are arranged in sequence motifs that occur repetitively, further increasing NMR signal overlap. Therefore, an unambiguous assignment was not possible just relying on the conventional 3D spectra HNCO, HN(CA)CO, HNCACB and CBCA(CO)NH (19). A high-resolution (HA)CANNH (20) together with three-dimensional HNN and HN(C)N experiments were required (21). With these NMR spectra the backbone resonance assignment of K18 and K19 could be achieved in an iterative fashion based on automatic assignment using the program MARS (22) and manual assignment mainly relying on the HNN experiment. The sequence motif PGGG, which is located characteristically at the C-terminal end of each of the four repeats, caused the biggest problems. Due to severe chemical shift overlap, it was only possible to assign G273, G304 and G335. The resonances of the remaining glycines within these motifs could be identified in the spectra, but not unambiguously assigned to one of the repeats. Otherwise, all ^{1}H, ^{15}N, ^{13}C$^\alpha$, ^{13}C$^\beta$ and ^{13}C' chemical shifts were assigned in both K18 and K19.

Soluble tau contains residual β-structure − NMR chemical shifts, in particular of C$^\alpha$ and C' atoms, are very sensitive probes of secondary structure both in globular and unfolded proteins (23);Wishart, 1994 #31}. These shifts show small but distinct deviations from random coil values for both K18 and K19 (Fig. 2). In the case of K18, continuous stretches (containinig more than six amino acids) of negative C$^\alpha$ secondary chemical shifts were found for residues K274-L284, S305-L315 and Q336-D345 (numbering according to the longest isoform htau40), indicative of nascent β-structure (Fig. 2A). These stretches lie at the beginning of repeats R2, R3, and R4, downstream from PGGG motifs and encompass the hexapeptide motifs VQIINK and VQIVYK known to be important for tau's abnormal aggregation into PHFs (8). In case of C', negative secondary chemical shifts were detected for a similar range of residues, G273-L282, G304-D314 and G335-D345 (Supplemental Fig. S1). It is notable that the preponderance of negative secondary chemical shifts persists even at the beginning of the less homologous repeats R1 (residues A246-L253) and R5 (N368-I371). In the case of R1 this is likely not due to a propensity to form β-structure but rather due to the occurrence of three prolines (P247, P249, P251). Indeed, the C' secondary chemical shifts alternated in this region consistent with the fact that C$^\alpha$ atoms of residues preceeding prolines show unusual chemical shifts due to the absence of an amide proton in the proline. In the case of R5 the results must be viewed with caution due to the presence of only three residues of R5 (not counting the C-terminal residue). A remarkably similar pattern is observed for K19, even though repeat R2 (exon 10) is absent (Fig. 2C)**,** suggesting that the repeats represent

independent structural units. A quantitative analysis of the averaged C^{α} and C' secondary chemical shifts (Fig. 2B) indicates that β-structure like conformations are populated approximately 16%, 24% and 13% of the time for residues K274-D283, S305-D314 and Q336-D345, respectively. Besides the regions in the beginning of each repeat, residues ^{295}KDNIK^{298} and ^{357}LDNIT^{361} in repeats R2 and R4 show a stretch of negative C^{α}/C' secondary shifts, indicating β-structure propensity. Note that no β-structure propensity is present in the corresponding region of repeat 3 (^{325}LGNIH^{329}), possibly due to the presence of a glycine (Fig. 2B).

The regions of high propensity for β-structure are limited upstream by PGGG motifs, where the three glycines show positive C^{α} and C' secondary chemical shifts in all four repeats. This indicates either a helical propensity or a turn, in agreement with the fact that GGK and GGS sequences (present in R1 or R2) are the most common motifs in classic γ-turns. Alternatively, the PGGG motif is also common in type II β-turns. The downstream ends of the regions of high β-structure propensity are most prominently identified by positive C^{α}/C' secondary chemical shifts of the 10th and/or 11th residue in repeat 2-4 (S285, S316, F346) (Fig. 2B). Taking further into account that sequence dyads such as ^{285}SN^{286} and ^{316}SK^{317} (the motifs following high β-propensity regions in R2 and R3) are common in type I β-turns, the C^{α} and C' secondary chemical shifts suggest a β-turn at the C-terminal end of the regions of high β-structure propensity.
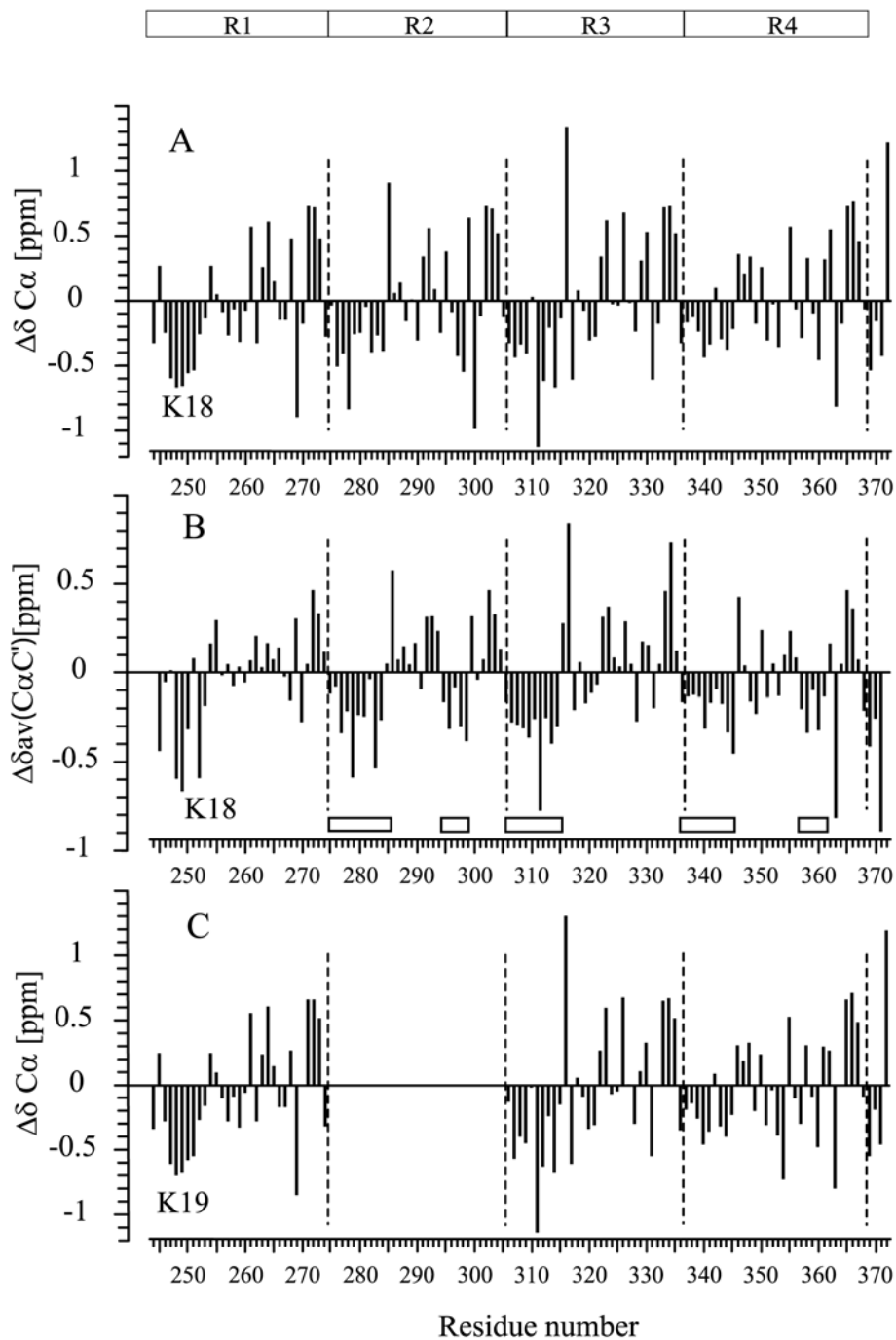
Fig. 2. <u>Secondary</u> chemical shifts of tau constructs in solution. Secondary chemical shifts for C^α (A) and averaged for C^α and C' (B) in K18, and C^α in K19 (C) recorded at 5 °C in 50 mM sodium phosphate buffer, pH 6.9, protein concentration 1 mM. The average shifts in (B) were calculated as $[3\Delta\delta(C^\alpha) + 4\Delta\delta(C')]/7$. Regions of β-structure propensity are identified by negative values of $\Delta_{av}(C^\alpha C')$ extending over several residues and are highlighted by boxes in (B). Repeat boundaries are indicated by vertical dashed lines. All glycines at position two and three in the PGGG motifs exhibited identical secondary chemical shifts.

In conclusion, 8-10 residues at the beginning of repeats 2-4 show residual β-structure sandwiched between regions with a high turn propensity. The most pronounced β-structure

propensity is present at the N-terminus of the third repeat, whereas in the second and fourth repeat it is about a factor of 1.5 to 2 lower. These β-conformations in K18 and K19 are presumably in rapid exchange with random-like structures. The C^α secondary chemical pattern observed for K19 is almost identical to that in K18. This indicates that removal of the second repeat does not affect the local β-structure propensity in the remaining part of the repeat domain of tau.
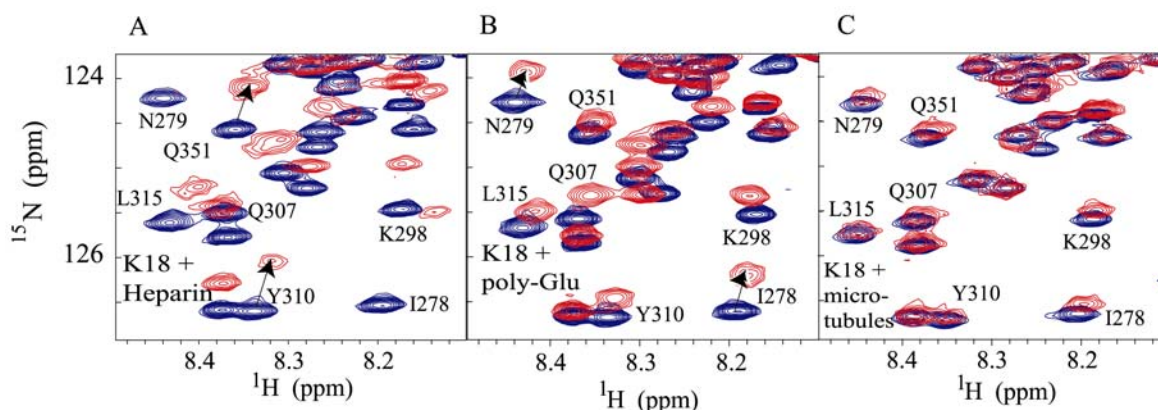
Fig. 3. NMR titration of K18 with polyanions and MTs. Overlay of the ^{1}H-^{15}N HSQC spectra of (A) 0.20 mM K18 (blue) with 0.15 mM heparin (red), (B) 0.30 mM K18 (blue) with 1.3 mM poly-Glu (red) and (C) 0.13 mM K18 (blue) with 0.80 mM MTs (red). Spectra were recorded at 5 °C in 50 mM sodium phosphate buffer, pH 6.9. Some particularly strong shifts are indicated by arrows. In (A) the signal of N279 was already attenuated below detection, indicating chemical shift exchange intermediate on the NMR time scale

Characterization of K18 and K19 and its polyanion complexes − NMR signals of backbone amides constitute excellent probes of complex formation, providing maps of the interaction interfaces and binding constants (24). The binding of the polyanions heparin and poly-Glu to K18 and K19 was monitored by ^{1}H-^{15}N HSQC spectra. The size of the chemical shift changes for increasing polyanion concentrations depends on the binding strength to the corresponding residues. At high polyanion concentrations chemical shift changes of some residues was accompanied by a decrease of the intensity of their signals, indicating chemical shift exchange intermediate on the NMR time scale (Fig. 3).

In the case of heparin the residues exhibiting the largest displacements in the amide resonances of K18 were V275-L284 at the beginning of the second repeat (Fig. 4A). In addition, strong chemical shift changes were observed in the environment of selected lysine and histidine residues: L253-K254, H268-Q269, K298-V300, H329-K331 and H362. The

importance of lysine and histidine residues suggests that the binding to polyanions is electrostatically driven. Upon titration of K18 with poly-Glu, a similar pattern of chemical shift changes was observed (Fig. 4B), indicating that the overall binding behaviour for the two types of polyanions is similar. In K19, repeat 2 is missing and can therefore not contribute to the interaction with polyanions. However, the same lysine and histidine residues as in K18 were strongly affected. In addition, slightly more pronounced chemical shift changes were observed for V306-K311, the six residues in the third repeat that are important for tau aggregation to PHFs (Fig. 4C and 4D).
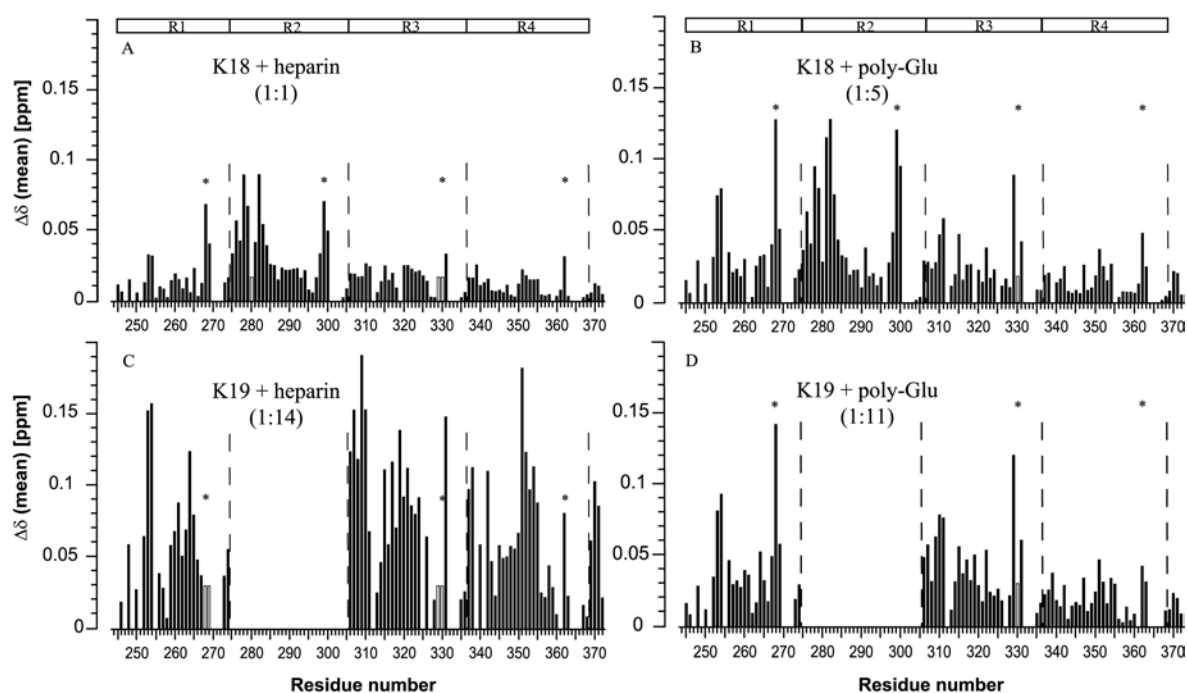
Fig. 4. Binding of polyanions to tau. Mean weighted ^{1}H–^{15}N chemical shifts between the ^{1}H–^{15}N HSQC spectra of free tau and tau in the presence of polyanions. (A) 0.2 mM K18 with 0.15 mM Heparin (~1:1), (B) 0.25 mM K18 with 1.3 mM poly-Glu (~1:5), (C) 0.09 mM K19 with 1.3 mM Heparin (~1:14) and (D) 0.12 mM K19 with 1.35 mM poly-Glu (~1:11). Resonances that were attenuated below detection by addition of polyanions are indicated by open bars. Gaps are due to overlap or the presence of prolines. The average molecular weight of heparin and poly-Glu was 3000 and 1000, respectively. Repeat boundaries are indicated by vertical dashed lines. * indicate histidine-lysine dyads downstream of PGGG motifs.

Concomitant with the chemical shift changes and the disappearance of some resonances at high polyanion concentrations (caused by ligand binding), the overall signal intensity in the ^{1}H-^{15}N HSQC spectra decreased with increasing polyanion concentration

(after correction for dilution effects). The latter effect is likely due to partial aggregation since biochemical analysis indicated that at the end of the polyanion titration 50% of K18 was polymerized, as analyzed by pelleting and SDS-PAGE. A similar behavior was observed in the K19-poly-Glu titration.

In order to investigate the effect of aggregation further, we performed a series of ^{1}H-^{15}N HSQC spectra, in which the ratio of concentration between heparin and K18 (1:4) was held constant and the sample was kept for variable times at 50 °C, in order to induce and accelerate aggregation. After measurement of initial ^{1}H-^{15}N HSQCs without heparin and with a heparin to K18 ratio of 1:4at 5 °C, the sample was heated to 50 °C and kept at this temperature for two hours. After the two hours the sample was cooled down to 5 °C and an HSQC spectrum was recorded. This procedure was repeated five times, such that the protein was kept at 50 °C for ten hours in total. Addition of heparin induced the chemical shift changes that were reported in Fig. 4. The peak intensities for most residues were reduced by less than 15% upon addition of heparin with the exception of those residues showing very strong chemical shift changes. After the first two hours at 50 °C the intensities of almost all peaks were reduced to 72% compared to the starting spectrum without heparin. There was no area in the protein that was affected particularly strongly, rather an overall loss of signal intensity was observed. At the same time, the chemical shift changes that were initially induced by addition of heparin were largely lost, i.e. the spectrum after two hours at 50 °C with a heparin:K18 ratio of 1:4 was highly similar to the one of K18 before addition of heparin (shown in Fig. 3). After four, six, eight and ten hours at 50 °C the overall signal intensity in ^{1}H-^{15}N HSQC spectra continuously decreased to 68%, 65%, 64% and 61% compared to the starting spectrum without heparin, respectively. No large chemical shifts differences relative to the spectrum after two hours at 50 °C were observed. In addition, the average transverse ^{15}N relaxation time did not change compared to free K18 upon addition of heparin or after keeping the protein up to ten hours at 50 °C (data not shown). At the end of the temperature titration biochemical analysis indicated that about 50 % of K18 was polymerised. These data indicate that the observed chemical shift changes, were due to the binding of the polyanion to the protein and not due to aggregation. When the protein was exposed to high levels of heparin for prolonged times or to high temperature at a constant heparin:K18 ratio of 1:4, part of the protein aggregated. As the chemical shift changes, which were induced by addition of heparin, were largely removed upon aggregation, heparin may became bound to the aggregates, thereby reducing the effective concentration of heparin in solution.

The binding mode of MTs and polyanions to tau is similar – The binding of K18 and K19 to MTs was characterized using the NMR chemical shift perturbation method (24), in which two-dimensional ^{1}H-^{15}N HSQC spectra of K18 and K19 were recorded in the presence of increasing amounts of taxol-stabilized MTs. The influence of temperature was probed by performing the NMR titrations at 5 °C and 20 °C. In order to ascertain the stability of the taxol-stabilized MTs at these temperatures, aliquots from the reactions of tau with MTs were characterized by sedimentation, SDS-PAGE, and electron microscopy (Fig. 5). After assembly at 37 °C the MTs exhibit the typical morphological features of protofilaments spaced ~5 nm apart. During the NMR-analysis the sample is incubated for more than one hour at 5 °C, but this does not lead to the disintegration of MTs in the presence of taxol (Figs. 5A, 5B). In the presence of tau the surface features of MTs become somewhat fuzzier, but without a change in subunit arrangement (see Santarella et al., 2004) (Fig. 5C). For a quantitative analysis the samples were centrifuged and supernatants and pellets were checked by SDS-PAGE (Figs. 5D, 5E). After MT assembly with taxol and incubation at 20 °C or 5 °C tubulin is found mostly in the pellet fraction (Fig. 5D). When increasing amounts of MTs were added to K18, the binding resulted in increasing amounts of K18 in the pellet fraction (Fig. 5D). The same was true for K19. These experiments show that the taxol-stabilized MTs persist over the time course of the NMR measurement and that binding parameters of both K19 and K18 are in good agreement with earlier results (3).

Continuous chemical shift changes of selected residues followed by the disappearance of the most strongly shifting resonances, especially at 20 °C, were observed. In addition, the signal-to-noise ratio rapidly decreased at high MT concentrations, indicative of an increasing amount of K18 or K19 bound to MTs. When bound to MTs, the NMR signals of K18 or K19 are not observable due to very fast relaxation.

Fig. 5. **Analysis of MT stability and interaction with tau by electron microscopy and SDS-PAGE**.
(A) The morphology of MTs after assembly at 37° C exhibit the typical features of MTs with
a width of about 25-28 nm and 6-7 visible protofilaments. After incubation at 4° C the
morphology is not altered (B). In the presence of tau (C) the surface of the MTs appears
fuzzier than in the absence of tau. Bar = 100 nm. The stability of MTs at different
concentrations and the interaction with K18 (130 µM) was further analyzed by
centrifugation (100.000xg for 1 hour at 4° C) and subsequent SDS-PAGE on 17% SDS-
gels. (D) MTs pelleted after incubation at 20° C and 5° C (#2-7). Samples of the interaction
studies were directly centrifuged after the NMR-analysis (#8-11). (E) Similar analysis of the
interaction between K19 and MT s. K19 at a fixed concentration (140 µM) was incubated
with increasing concentrations of MTs and after centrifugation supernatants and pellets
were applied to a 17% SDS-PAGE.

At 5 °C the most strongly shifting resonances in K18 were found mainly in the
environment of lysine and histidine residues: L253-K254, H268-Q269, K298-V300, H329-
K331 and H362 (Fig. 6A). This indicates that each repeat contains a binding site for
anchoring K18 to MTs. In agreement with the repetitive nature of the repeat region, these
anchors are primarily located at equivalent positions in each repeat, just N-terminal to the
PGGG motif. The same lysine and histidines resonances were affected at 20 °C, although to a
lesser extent. At 20 °C the most pronounced chemical shift changes were observed for
residues K274-L284 at the beginning of the second repeat (Fig. 6B). Within this region I278

and N279, together with K281 and L282 displayed the strongest chemical shift changes, whereas K280 was only weakly affected by addition of MTs.
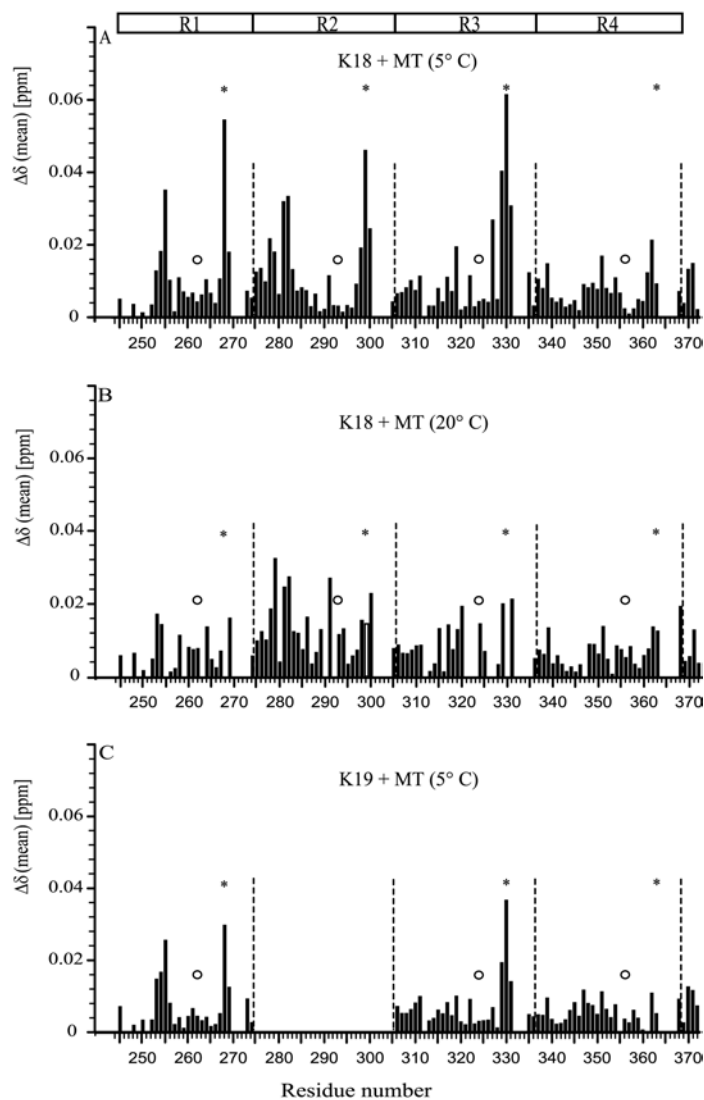
Fig. 6. **Binding of tau to preassembled MTs**. Mean weighted [1]H–[15]N chemical shifts between the ^{1}H–^{15}N HSQC spectra of free tau and tau in the presence of MTs. (A) 0.13 mM K18 with 79 μM of MTs at 5 °C, (B) 0.13 mM K18 with 79 μM of MTs at 20 °C and (C) 0.14 mM K19 with 35 μM of MTs at 5 °C. Resonances that were attenuated beyond detection by addition of MTs are indicated by open bars. Gaps are due to overlap or the presence of prolines. Repeat boundaries are marked by vertical dashed lines. * and ° indicate histidine-lysine dyads downstream of PGGG motifs and Serines known to be phosphorylated, respectively.

In the K18-MT titration, only minor chemical shift changes were observed for resonances located in the beginning of repeat 3. Addition of heparin to K19, on the other

hand, had a pronounced effect on residues V306-K311. In addition, slightly stronger chemical shift changes were observed for these residues in the K19-MT titration (Fig. 6B and Supplemental Fig. S2). Further evidence for the involvement of the N-terminal part of the third repeat into binding to MTs comes from the decrease of the signal intensity for increasing MT concentrations: the signal intensity for residues V306-K311 decreased as quickly as that of the interacting part of the second repeat, i.e. the site that showed the strongest chemical shift changes upon addition of MTs to K18, and decreased more rapidly than the intensity for other residues in the K19-MT titration (Supplemental Fig. S3). Overall, the pattern of chemical shift changes induced by addition of MTs was very similar for K18 and K19 (Figs. 6A and 6C).

We conclude that repeats R1 – R4 of 4-repeat tau are attached to MTs mainly via the positive charges just upstream of the PGGG motif. The attachment of repeat one is further stabilized by electrostatic interactions involving the positive charge of K254. In addition, the region K274-L284 is important for binding to MTs. An additional MT-binding site is located in the beginning of the third repeat, which it is particularly important for binding of 3-repat tau to MTs.

DISCUSSION

Tau is an interesting protein from several different perspectives: First, tau is one of the major microtubule-associated proteins in the brain, it plays a prominent role in the formation of axons and is therefore important for understanding neuronal cell biology and brain development. Secondly, tau is a prototype of the emerging class of "natively unfolded" or "intrinsically unstructured" proteins whose properties are not accessible by X-ray crystallography. Thirdly, from a medical perspective tau represents one of the hallmarks of Alzheimer's disease, the most common form of dementia, where it forms pathological protein aggregates that are toxic to the neurons. These reasons prompted us to apply state-of-the-art, multidimensional NMR spectroscopy, with the aim of identifying the structural features of tau that are responsible for its physiological and pathological roles. In the present study we focus on the repeat domain of tau which forms the core of the MT -binding domain as well as the core of Alzheimer paired helical filaments (PHFs). We have used NMR spectroscopy to detect structural motifs and potential seeds of aggregation in the repeat region of tau, and to

characterize its interaction with MTs and certain polyanions that are known to promote the aggregation into PHFs.
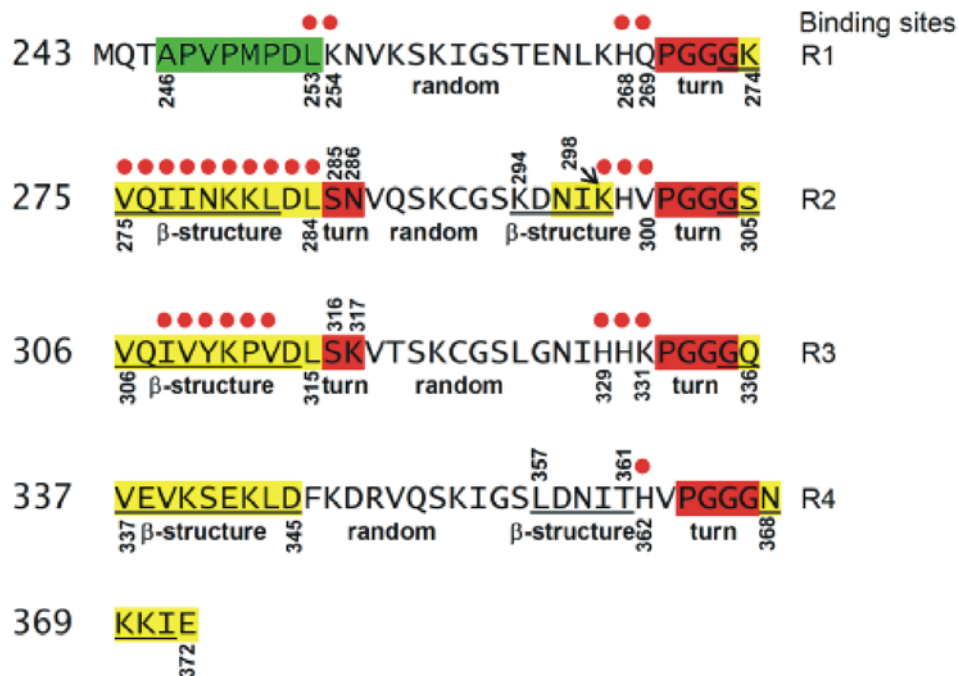
Fig. 7. Summary of results. The sequence of the four repeats of K18 plus the adjacent four amino acid is shown ordered by the repeat structure. The residues of special significance are highlighted. Green amino acids show negative secondary shifts but are not proposed to exhibit β-structure because this part of the sequence contains several prolines (in R1). Red amino acids are likely involved in turn structures, e.g. the PGGG motifs at the end of each repeat. Yellow amino acids show a negative secondary C^{α} shift, underlined residues exhibit a negative secondary C' chemical shift. At the beginning of R2, R3 and R4 there are regions of 8-10 residues with negative secondary C^{α} chemical shifts and negative secondary C` chemical shifts, indicating residual β-structure. The middle of R2 and R4 contain a further short stretch with negative secondary C'-shifts. The binding sites for polyanions (heparin, poly-Glu and MTs) are marked by red circles above the sequence.

The major results can be summarized as follows:

- The beginning of each repeat is characterized by a stretch of 8-10 residues with negative secondary chemical shift values. For the case of R2-R4 this indicates a high propensity of β-structure. These regions coincide with sequence motifs known to be involved in the abnormal aggregation of tau. The β-forming motifs are sandwiched between motifs that have a high propensity for turns and therefore interrupt the β-conformation (e.g. the

PGGG motifs). Additional stretches of β-propensity occur upstream of the PGGG motifs in repeats R2 and R4.

- The conformational preferences are the same in different variants of tau with 3 or 4 repeats (corresponding to fetal or adult tau). This suggests that the repeats behave like independent folding units.

- MTs and other polyanionic binding partners of tau show similar preferred regions of interaction. They include the beginning of repeats R2 and R3 (coincident with the PHF-forming hexapeptide motifs), and spots of high positive charge upstream of the PGGG motifs. This supports the view that the abnormal aggregation (caused by polyanionic cofactors) is based on the same structural features as the physiological interaction with MTs.

Soluble tau contains residual β-structure providing seeds of aggregation − In order to allow a high-resolution characterization by NMR, it was necessary to assign the backbone resonances of all residues. Previously, the NMR resonances of single residues, at most dipeptides, were assigned unambiguously covering only 12 % of the repeat domain of tau. These isolated assignments did not provide any indication for residual structure (25). Despite the high degree of overlap caused by the absence of a well-defined secondary and three-dimensional structure, we were able to fully assign the backbone resonances of K18 and K19. NMR chemical shifts are sensitive probes for the environments of nuclei. Comparison of the assigned backbone resonances showed that signals of V275 and Q276 at the beginning of R2 in K18 were exactly coincident with the signals of V306 and Q307 at the beginning of R3 in K19. Either the chemical shifts are dominated by the local sequence composition, or any potentially present residual structure is very similar in K18 and K19.

At the beginning of repeats R2, R3 and R4 a significant propensity for β-structure within continuous stretches of eight to ten residues could be identified (16%, 24% and 13%, respectively). These β-regions terminate on both ends by motifs with a high propensity for turns, such as the PGGG motifs or the SN or SK dyads. The β-structure propensity is most pronounced (~23%) for residues S305-D314 in the beginning of R3. Note, that this is an average value calculated for all residues within this regions and it does not necessarily indicate that all residues populate β-structure at the same time. In addition, negative secondary chemical shifts for residues [295]KDNIK[298] and [357]LDNIT[361] suggest a weak propensity for β-structure in the C-terminal half of repeats R2 and R4. These findings are in

agreement with other data (X-ray scattering, CD, gel filtration, secondary structure predictions etc) indicating that tau has a very low content of secondary structure (Schweers et al., 1994).

While this manuscript was in preparation an NMR study of K19 was published (26). Similar to our results, these authors observed a tendency to form β-structure in the beginning of R3. No tendency to form β-structure is reported for R4. In addition, as only K19 was studied, neither the structural properties of R2 nor any isoform-specific differences between 3- and 4-repeat tau could be addressed. Most strikingly, however, Eliezer et al. concluded that much of K19, comprising residues 253-267, 315-328 and 346-361, preferentially populates helical conformations. This conclusion was mainly based on long stretches of positive C^α secondary chemical shifts. We were not able to observe such positive C^α secondary chemical shifts (Fig. 2A), despite the fact that our pattern of C' secondary chemical shifts is very similar to that reported by Eliezer et al. (Supplemental Fig. S1). Our data are in agreement with earlier results obtained by CD and FTIR spectroscopy, in which no helical propensities were detected for monomeric K18 or K19 (13). In addition, we have characterized the interaction of K18 and K19 with polyanions and microtubules and the high degree of similarity between the binding of polyanions and microtubules suggests that stable microtubules prevent PHF formation by blocking the tau:polyanions interaction sites, which are crucial for PHF formation (see below).

The partially populated β-structure at the beginning of R2 and R3 is also consistent with the essential role of two hexapeptide motifs, [275]VQIINK[280] and [306]VQIVYK[311], for the assembly of tau into PHFs. [306]VQIVYK[311] represents the minimal hexapeptide motif for tau-tau interaction and is capable of inducing tau aggregation. In addition, a 43-residue fragment of K19, which contains the third repeat of tau and some flanking residues, acquires a pronounced β-structure in conditions of selfassembly (8). The key role of the hexapeptide [306]VQIVYK[311] in R3 for PHF aggregation and its pronounced β-structure propensity is also in agreement with data on peptide fragments comprising a single repeat: Trifluoroethanol at low concentrations only induced α-helical structure in the hexapeptide in R2 but not in [306]VQIVYK[311] in R3 (27,28). Furthermore, the isolated hexapeptides [275]VQIINK[280] and [306]VQIVYK[311] are able to polymerize with formation of β-structure (13,14).

Several mutations in the tau gene have been linked to frontotemporal dementias and parkinsonism (FTDP-17,(29)). Their mode of action may not be uniform, but some of them appear to enhance aggregation by increasing the β-structure propensity within the repeat

domain. This holds particularly for the mutations ΔK280 and P301L which are located in or near the regions with high β-structure propensity in the wild-type protein (13). A higher β-structure propensity leads to more molecules that preferentially adopt β-structure thereby increasing the rate of aggregation. Conversely, proline mutants introduced into these regions disrupt the β-propensity and thus render the molecule largely incapable of PHF formation (8). The repeat region of 4-repeat tau contains two cysteines whose cross-linking strongly attenuates aggregation by formation of an inactive monomer (6). These two cysteines are just C-terminal of the regions of high β-propensity. This suggest that cross-linking of these cysteines brings together the regions of high β-propensity in repeats R2 and R3 forming a partially populated intramolecular β-sheet. Such an intramolecular β-sheet would reduce the tendency to form PHFs, as PHF assembly requires the formation of intermolecular H-bonds within these regions. On the other hand, cross-linking of tau molecules into dimers by intermolecular disulphide bonds can bring regions of high β-propensity close together. This would favour formation of intermolecular β-sheets in agreement with a strong enhancement of aggregation by dimerization (12).

Regions with β-structure propensity coincide with binding sites to polyanions – PHFs isolated from the brains of patients with Alzheimer's disease are not only composed of tau molecules, but contain other nonprotein components, including heparan, a glycosaminoglycan, the more extensively sulphated form of which is heparin. *In vitro*, heparin and other polyanions, such as poly-Glu and RNA, greatly improve polymerizability of tau. This is thought to be due to a neutralization of positive residues as the enhancement is not restricted to a specific polyanion (30-32). Our results show that the binding of polyanions is concentrated around positively charged patches, including the KK motif (280-281) at the beginning of repeat R2, and the KH (267-268, 298-299) or HHK (329-331) motifs near the end of R1, R2 and R3. By comparison, single positive charges in equivalent locations have a much weaker effect on binding (e.g. K311 at the beginning of R3, or H362 near the end of R4). The patterns of the altered backbone chemical shifts mapped onto the primary sequence (Figs. 4A and 4B) were very similar for heparin and poly-Glu, suggesting a common mode of binding dictated largely by electrostatic interactions.

The binding of polyanions to the positively charged amino acids reduces the net charge and therefore decreases the propensity for random coil (33). Additionally the binding to the sites of residual β-structure might help to stabilize the β-conformation and might thereby allow interaction of the β-strand with other tau molecules. Thus, polyanions enhance

aggregation by directly stabilizing the regions which are essential for aggregation. This is opposite to the interaction of α-synuclein with polyamines, which bind to the C-terminal domain of α-synuclein, cause a release of an autoinhibitory residual structure and render the hydrophobic patches of the NAC (Non-Aβ component of Alzheimer's disease amyloid) region accessible, such that α-synuclein is able to adopt β-sheet conformations conductive of aggregation (34).

MTs prevent PHF formation by blocking the tau:polyanion interaction sites that are crucial for PHF formation – Tau is a microtubule-associated protein that regulates diverse and essential MT functions, including polymerisation and stabilization of MT and modulation of MT dynamics. Mutations in tau associated with frontotemporal dementia with parkinsonism linked to chromosome 17 (FDTP-17) weaken the interaction between tau and MTs and cause a decrease in MT stabilization (35). Therefore, knowledge of the detailed mechanism by which tau binds to MTs is highly important. In the study presented herein we have characterized the reversible binding of tau to preassembeld, taxol-stabilized MTs on the level of individual tau residues. Since it has been demonstrated previously that the repeat domain of tau is important for MT binding activity, we targeted our high-resolution study to this region of the protein.

The NMR titrations identified residues K274-L284 as an important region of tau for binding to MTs. This is in agreement with truncation analyses by Goode and Feinstein (36,37). A 2.3 and 3.1 fold reduction of MT binding affinity, which was observed when mutating K274 or K281 to alanine, correlates well with the strong chemical shift changes observed for I278 and K281 upon addition of MTs. In addition, K280 showed only small chemical shift changes, consistent with a smaller contribution to binding affinity as indicated by site-directed mutagenesis. Besides these strong electrostatic interactions involving the N-terminal part of R2, the NMR data show that the tau-MT interaction is further enhanced by discrete interaction clusters of positive charges upstream of the PGGG motifs.

To investigate isoform specific differences in MT binding affinity, we also studied the interaction of K19 with MTs. Previously, it was shown that the carboxyl-terminal sequences downstream of the repeat region make a strong but indirect contribution to MT binding affinity in 3-repeat tau, whereas in 4-repeat they almost have no effect. The K19 construct does not include these carboxyl-terminal sequences. However, the K19-MT NMR data give insight on a residue basis and can be used to probe for local changes in the MT interaction.

The highly similar pattern of chemical shift changes in K18 and K19 upon addition of MTs suggests that the lysine-histidine binding sites upstream of the PGGG motifs, contribute independently to the interaction.

Our study does not directly address the nature of the tau binding sites on tubulin and MTs. It is commonly accepted that tau interacts with the C-terminus of tubulin that is believed to be exposed on the surface of MTs (38). Comparison of chemical shift changes observed for K18 and K19 upon addition of MTs with those observed upon addition of polyanions indicate a very similar binding mode. Considering that poly-Glu resembles the Glu-rich C-terminal sequence of tubulin, the NMR data suggest that the positively charged clusters described above bind to the carboxy-terminus of tubulin. The similar binding mode of tau to MTs and polyanions also supports the hypothesis that stable MTs prevent PHF formation by blocking the tau:polyanion interaction sites which are crucial for PHF formation.

It is known that phosphorylation at KXGS motifs regulate affinity of tau to MTs (4). We have shown that the repeat domain of tau binds to MTs through spots of high positive charge comprising the beginning of R2 and R3, as well as histidine-lysine regions upstream of the PGGG motifs. Serine 262, 293, 324 and 356 are separated by only four residues from these histidine-lysine regions carrying two to three positive charges at the C-terminal end of each repeat. Thus the effect of phosphorylation can be achieved because the introduction of the negative charge of the phosphate group partially neutralizes the positive spots required for MT-binding. This intramolecular charge neutralization might be favoured by the high flexibility of the protein backbone of tau, which allows the spots of positive and negative charges to come close together. Even more, the high flexibility of tau might actually be required to allow a detailed control of the tau-MT interaction by phosphorylation. In addition, the attraction between the phosphate and the positively charged lysine-histidine region might force a turn, reducing the propensity for β-structure, which was observed for residues ^{295}KDNIK^{298} and ^{357}LDNIT^{361}, and might alter the distances between the distributed weak interaction sites in a way that they do not longer fit to their interaction sites on the MT surface.

The investigations featured above provide a detailed novel view of the native state of the repeat region of the microtubule-associated protein tau and its interaction with polyanions and MTs. The presence of seeds of aggregation at the beginning of repeats R2 and R3 (hexapeptide motifs) which coincide with the observed propensity for β-structure and the binding regions of tau to MTs and polyanions stresses the importance of these regions for

their normal MT regulating function, as well as for their involvement in the neurodegenerative process in which tau is assembled into Alzheimer paired helical filaments. The results presented in this study will be important when assessing factors or drugs designed to suppress the aggregation of tau in neurons, and thus to prevent one of the crucial steps in Alzheimer's disease.

REFERENCES

1.   Selkoe, D. J., and Schenk, D. (2003) *Annu. Rev. Pharmacol. Toxicol.* **43**, 545-584

2.   Mandelkow, E. M., and Mandelkow, E. (1998) *Trends Cell. Biol.* **8**, 425-427

3.   Gustke, N., Trinczek, B., Biernat, J., Mandelkow, E. M., and Mandelkow, E. (1994) *Biochemistry* **33**, 9511-9522

4.   Biernat, J., Gustke, N., Drewes, G., Mandelkow, E. M., and Mandelkow, E. (1993) *Neuron* **11**, 153-163

5.   Schneider, A., Biernat, J., von Bergen, M., Mandelkow, E., and Mandelkow, E. M. (1999) *Biochemistry* **38**, 3549-3558

6.   Barghorn, S., and Mandelkow, E. (2002) *Biochemistry* **41**, 14885-14896

7.   Schweers, O., Schonbrunn-Hanebeck, E., Marx, A., and Mandelkow, E. (1994) *J. Biol. Chem.* **269**, 24290-24297

8.   von Bergen, M., Friedhoff, P., Biernat, J., Heberle, J., Mandelkow, E. M., and Mandelkow, E. (2000) *Mol. Biol. Cell* **11**, 363A-363A

9.   Buee, L., Hamdane, M., Delobel, P., Sambo, A. V., Begard, S., Ghestem, A., Sergeant, N., and Delacourte, A. (2002) *J. Soc. Biol.* **196**, 103-108

10.   Wischik, C. M., Novak, M., Thogersen, H. C., Edwards, P. C., Runswick, M. J., Jakes, R., Walker, J. E., Milstein, C., Roth, M., and Klug, A. (1988) *Proc. Natl. Acad. Sci. U. S. A.* **85**, 4506-4510

11.   Wille, H., Drewes, G., Biernat, J., Mandelkow, E. M., and Mandelkow, E. (1992) *J. Cell. Biol.* **118**, 573-584

12.   Friedhoff, P., von Bergen, M., Mandelkow, E. M., Davies, P., and Mandelkow, E. (1998) *Proc. Natl. Acad. Sci. U. S. A.* **95**, 15712-15717

13.   von Bergen, M., Barghorn, S., Li, L., Marx, A., Biernat, J., Mandelkow, E. M., and Mandelkow, E. (2001) *J. Biol. Chem.* **276**, 48165-48174

14.   Goux, W. J., Kopplin, L., Nguyen, A. D., Leak, K., Rutkofsky, M., Shanmuganandam, V. D., Sharma, D., Inouye, H., and Kirschner, D. A. (2004) *J. Biol. Chem.* **279**, 26868-26875

15.   Mandelkow, E. M., Herrmann, M., and Ruhl, U. (1985) *J. Mol. Biol.* **185**, 311-327

16.   Delaglio, F., Grzesiek, S., Vuister, G. W., Zhu, G., Pfeifer, J., and Bax, A. (1995) *J. Biomol. NMR.* **6**, 277-293

17.   Schwarzinger, S., Kroon, G. J. A., Foss, T. R., Chung, J., Wright, P. E., and Dyson, H. J. (2001) *J. Am. Chem. Soc.* **123**, 2970-2978

18.   Wishart, D. S., and Sykes, B. D. (1994) *Nuclear Magnetic Resonance, Pt C* **239**, 363-392

19.   Bax, A., and Grzesiek, S. (1993) *Acc. Chem. Res.* **26**, 131-138

20.   Zweckstetter, M., and Bax, A. (2001) *J. Am. Chem. Soc.* **123**, 9490-9491

21.   Panchal, S. C., Bhavesh, N. S., and Hosur, R. V. (2001) *J. Biomol. NMR* **20**, 135-147

22.   Jung, Y. S., and Zweckstetter, M. (2004) *J. Biomol. NMR.* **30**, 11-23

23.   Dyson, H. J., and Wright, P. E. (1998) *Nat. Struct. Biol.* **5 Suppl**, 499-503

24.   Craik, D. J., and Wilce, J. A. (1997) *Methods Mol. Biol.* **60**, 195-232

25.   Smet, C., Leroy, A., Sillen, A., Wieruszeski, J. M., Landrieu, I., and Lippens, G. (2004) *Chembiochem* **5**, 1639-1646

26.   Eliezer, D., Barre, P., Kobaslija, M., Chan, D., Li, X., and Heend, L. (2005) *Biochemistry* **44**, 1026-1036

27.   Hiraoka, S., Yao, T. M., Minoura, K., Tomoo, K., Sumida, M., Taniguchi, T., and Ishida, T. (2004) *Biochem. Biophys. Res. Commun.* **315**, 659-663

28.   Minoura, K., Yao, T. M., Tomoo, K., Sumida, M., Sasaki, M., Taniguchi, T., and Ishida, T. (2004) *Eur. J. Biochem.* **271**, 545-552

29.   Higuchi, M., Lee, V. M., and Trojanowski, J. Q. (2002) *Neuromolecular Med.* **2**, 131-150

30.   Goedert, M., Jakes, R., Spillantini, M. G., Hasegawa, M., Smith, M. J., and Crowther, R. A. (1996) *Nature* **383**, 550-553

31.   Kampers, T., Friedhoff, P., Biernat, J., Mandelkow, E. M., and Mandelkow, E. (1996) *FEBS Lett.* **399**, 344-349

32.   Perez, M., Valpuesta, J. M., Medina, M., Montejo de Garcini, E., and Avila, J. (1996) *J. Neurochem.* **67**, 1183-1190

33.   Uversky, V. N., Gillespie, J. R., and Fink, A. L. (2000) *Proteins* **41**, 415-427.

34.   Bertoncini, C. W., Jung, Y. S., Fernandez, C. O., Hoyer, W., Griesinger, C., Jovin, T. M., and Zweckstetter, M. (2005) *Proc. Natl. Acad. Sci. U. S. A.* **102**, 1430-1435

35.   Hasegawa, M., Smith, M. J., and Goedert, M. (1998) *FEBS Lett.* **437**, 207-210

36.   Goode, B. L., Chau, M., Denis, P. E., and Feinstein, S. C. (2000) *J. Biol. Chem.* **275**, 38182-38189

37.   Goode, B. L., and Feinstein, S. C. (1994) *J. Cell. Biol.* **124**, 769-782

38.   Downing, K. H., and Nogales, E. (1999) *Cell. Struct. Funct.* **24**, 269-275

FOOTNOTES

The on-line version of this article (available at http://www.jbc.org) contains Supplemental Figs. S1, S2 and S3, and Supplemental Tables S1.

SUPPLEMENTARY MATERIAL

Tau polyanion and tau-MT NMR titrations

Tau-polyanion titrations were carried out with uniformly ^{15}N-labelled protein containing 0.2 mM (heparin titration) and 0.3 mM (poly-Glu titration) K18, and 0.12 mM (heparin titration) and 0.14 mM (poly-Glu titration) K19 at pH 6.8. Heparin (average mol. wt. 3000, about 5.8 disaccharide subunits, charge per subunit ~2.5, ~0.31 z/Å) and poly-Glu (average mol. wt. 1000, 7-8 Glu residues, 7-8 negative net charge, in extended conformation 0.33 z/Å) were from Sigma. Complex formation was monitored by recording 2D ^{1}H-^{15}N-HSQC spectra for increasing polyanion concentrations (mM): 0.03, 0.06, 0.15, 0.3, 0.58, 1.37 and 2.53 (K18 with heparin), 0.008, 0.015, 0.03, 0.072, 0.142, 0.28, 0.68, 1.3, 2.4 and 4.3 (K18 with poly-Glu), 0.008, 0.015, 0.03, 0.07, 0.14, 0.28, 0.67 and 1.3 (K19 with heparin) and 0.015, 0.03, 0.074, 0.146, 0.29, 0.70, 1.35, 2.49 (K19 with poly-Glu). For tau-MT titrations NMR samples contained 0.13 and 0.14 mM uniformly ^{15}N-labelled K18 and K19, respectively. Complex formation was monitored at 5 and 20 °C for MT concentrations (αβ-tubulin dimers) of 26.5, 79.5 and 159.0 µM in the K18 titrations, and 2.8, 5.4, 20.0, 35.0 and 84.3 µM in the K19 titration. Normalized weighted average chemical shift differences for amide ^{1}H and ^{15}N chemical shifts upon polyanion/MT binding were calculated using av(NH) = $[(\Delta H^2 + (\Delta N/5)^2)/2]^{1/2}$, where H and N are the differences between the free and bound chemical shifts.
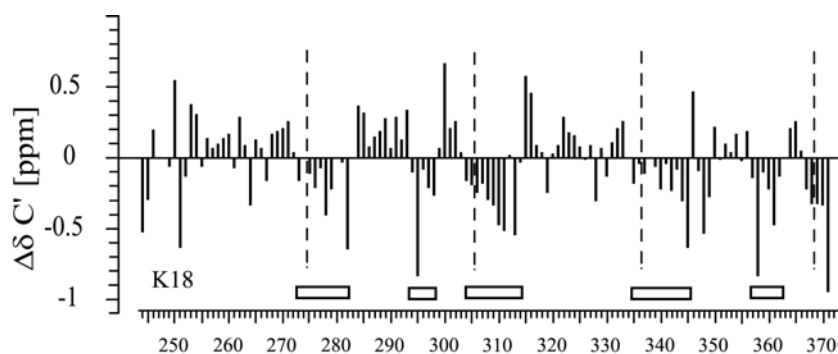
Figure S1 Secondary chemical shifts for C' in K18 recorded at 5 °C in 50 mM sodium phosphate buffer, pH 6.9. Regions of β-structure propensity are indicated by negative values extending over several residues.
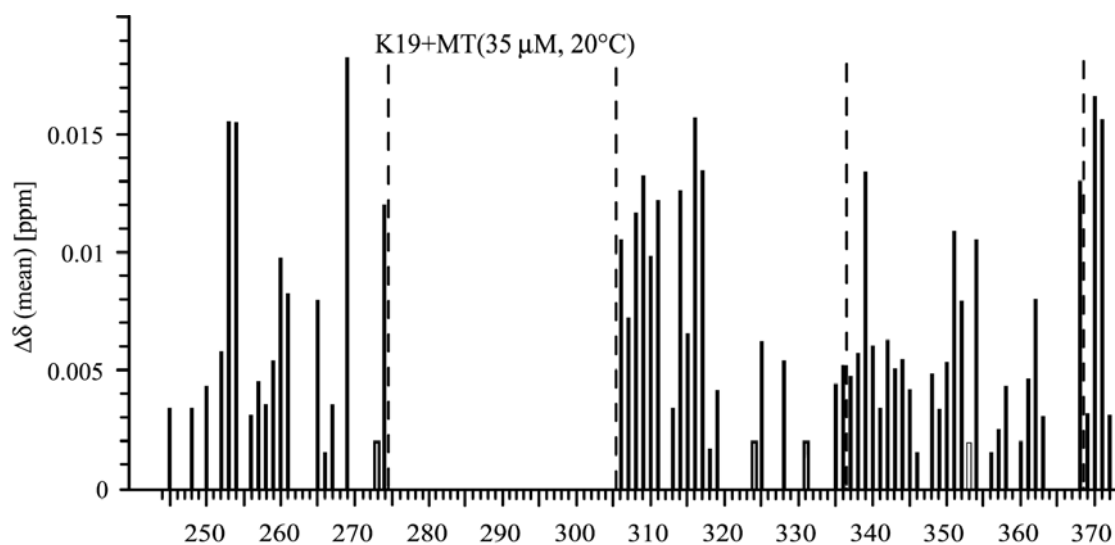
Figure S2 Mean weighted [1]H–[15]N chemical shifts between the ^{1}H–^{15}N HSQC spectra of free K19 (140 μM) and K19 in the presence of 35 μM microtubules at 20 °C. Resonances that were attenuated beyond detection by addition of MTs are indicated by open bars. Gaps are due to overlap or the presence of prolines
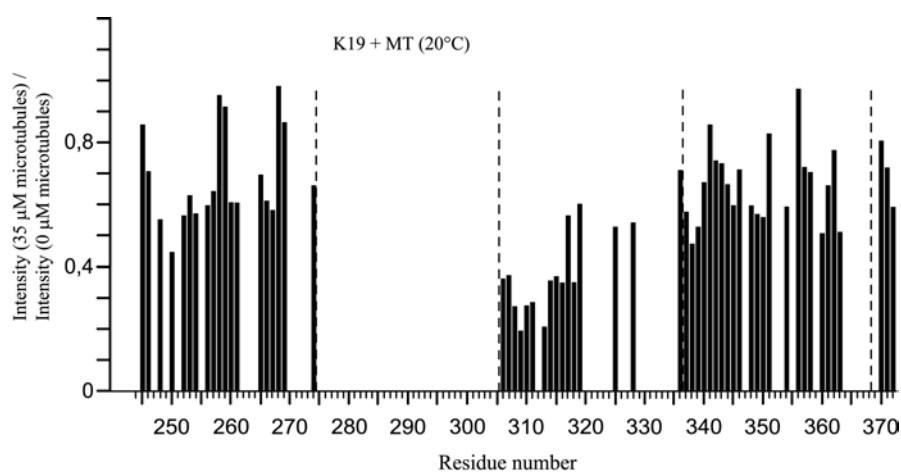
Figure S3 S/N ratio between the ^{1}H–^{15}N HSQC spectra of free K19 (140 μM) and K19 in the presence of 35 μM microtubules at 20 °

Table S1. Dissociation constants Kd (mM) for binding of the repeat domain of tau to polyanions. The table shows residues that were well resolved over the entire polyanion concentration range and did not disappear towards the end of the titrations.

K18 + heparin	K18 + poly-Glu	K19 + heparin	K19 + poly-Glu
I278: 0.11 +/- 0.06	K254: 0.40 +/- 0.09	L253: 0.069 +/- 0.01	L253: 0.30 +/- 0.04
L282: 0.21 +/- 0.07	H268: 0.41 +/- 0.13	K254: 0.049 +/- 0.01	K254: 0.31 +/- 0.05
D283: 0.21 +/- 0.07	I278: 0.39 +/- 0.14	Q307: 0.045 +/- 0.01	H299: 0.28 +/- 0.04
V300: 0.11 +/- 0.08	K281: 0.38 +/- 0.09	V309: 0.034 +/- 0.01	H329: 0.30 +/- 0.05
K331: 0.22 +/- 0.06	H299: 0.43 +/- 0.15	K331: 0.059 +/- 0.01	K331: 0.21 +/- 0.04
Q351: 0.23 +/- 0.12	H329: 0.36 +/- 0.10		

Table S2. NMR experiment parameters.

experiment (spectrometer)	complex data points (F3, F2, F1)	spectral width [Hz]	Recovery delay [s]	number of scans
HNCACB (DRX800)	1024 x 128 x 160	F3: 8012.821 F2: 1904.762 F1: 13157.895	1.05	8
CBCA(CO)NH (DRX600)	1024 x 76 x 128	F3: 6613.757 F2: 1428.571 F1: 9861.933	1.1	16
(HA)CANNH (DRX800)	1024 x 76 x 128	F3: 6613.757 F2: 1428.571 F1: 9861.933	1.1	16
HNCO (DRX600)	1024 x 128 x 88	F3: 6613.757 F2: 1428.57 F1: 1428.571	1.0	4
HN(CA)CO (Avance 700)	1024 x 36 x 72	F3: 7716.049 F2: 1666.667 F1: 2000	1.0	48
HNN and HN(C)N (DRX800)	1024 x 140 x 140	F3: 9259.259 F2: 1904.762 F1: 1904.762	1.2	4
^{1}H-^{15}N HSQC titration (DRX600)	2048 x 600 (F2 x F1)	F2: 6009.615 F1: 1428.571	1.0	4

3   Structural and Microtubule-binding Properties of Tau Mutants of Frontotemporal Dementias

Daniela Fischer[1], Marco Mukrasch[1], Martin von Bergen[4], Aleksandra Klos-Witkowska[1,3], Jacek Biernat[4], Christian Griesinger[1], Eckhard Mandelkow[4], Markus Zweckstetter[1,2,*]

[1] *Department for NMR-based Structural Biology, Max Planck Institute for Biophysical Chemistry, Am Fassberg 11, 37077 Göttingen, Germany*

[2] *DFG Research Center for the Molecular Physiology of the Brain (CMPB)*

[3] *Department of Medical Physics, University of Silesia, Uniwersytecka 4, 40007 Katowice, Poland*

[4] *Max Planck Unit for Structural Molecular Biology c/o DESY, Notkestrasse 85, 22607 Hamburg, Germany*
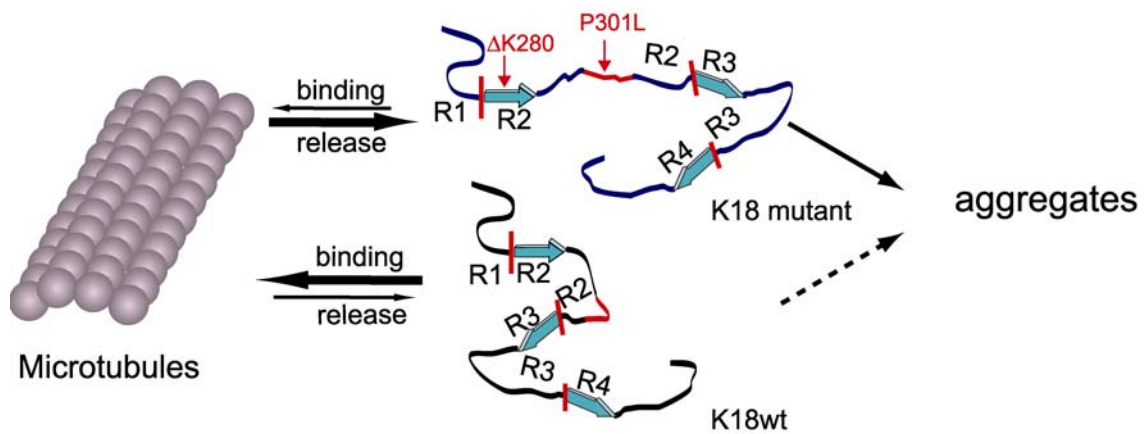
ABSTRACT

Several mutations in the gene coding for the microtubule-associated protein tau are responsible for the formation of neurofibrillary inclusions in frontotemporal dementia with Parkinsonism linked to chromosome 17 (FTDP-17). Here we present the high-resolution characterization of the conformational properties of two FTDP-17 mutants of the 4-repeat domain of tau, P301L and ΔK280, and their binding properties to polyanions and microtubules. Multidimensional NMR spectroscopy shows that the mutations do no lead to a significant increase in β-structure in their monomeric state, even though the mutations strongly promote β-structure during aggregation. However, local structural changes are induced in the second repeat. These changes only weakly affect the binding to the polyanion heparin, which promotes paired helical filament formation. The binding to microtubules, however, is strongly decreased. Our results demonstrate that the reversible binding of tau to microtubules involves specific interactions, which are not essential for binding to polyanions.

INTRODUCTION

Several neurological disorders such as Alzheimer's disease, Parkinson's disease, Pick's disease and frontotemporal dementia with Parkinsonism linked to chromosome 17 (FTDP-17) are accompanied by the formation of filamentous inclusions in neurons. These consist mainly of the microtubule (MT)-associated protein tau (*1-7*).

Tau can aggregate into Alzheimer-like paired helical filaments (PHFs) as an intact protein, 352–441 residues in length (depending on isoform), so that all six tau isoforms are found in Alzheimer PHFs (*8, 9*). The isoforms differ by two inserts near the N-terminal end and the presence of either four or three imperfect repeat sequences in the C-terminal half of the protein (Figure 1). The region comprising the repeat sequences forms the core of PHFs (*10*) and also promotes PHF assembly in vitro (*11, 12*). For PHF aggregation two hexapeptides at the beginning of the second and third repeats (275-VQIINK-280 and 306-VQIVYK-311) are crucial. These are able to initiate the aggregation of tau into bona fide

PHFs with their specific β-sheet based molecular architecture termed cross-β-structure and thereby represent minimal tau-tau interaction motifs (*3, 13*).
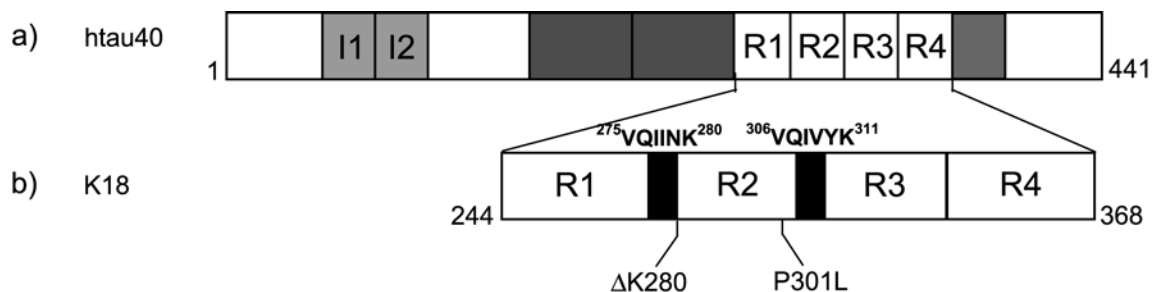
Figure 1

Figure 1: Tau isoforms, the repeat domain and FTDP-17 mutations. (a) htau40 is the largest isoform in the human CNS (441 residues). The C-terminal half contains 3 or 4 pseudo-repeats (~ 31 residues each, R1 to R4). Repeat 2 and the two near-N-terminal inserts (I1, I2) may be absent due to alternative splicing. Most FTDP-17 mutations are located in the repeat domain. (b) Construct K18 (130 residues, (M)Q244-E372) comprises only the 4 repeats. The positions of the aggregation-prone hexapeptide motifs 275-VQIINK-280 and 306-VQIVYK-311 in R2 and R3 are highlighted. The mutations ΔK280 and P301L lie near the hexapeptide motifs and increase the tendency for aggregation. Numbering of residues follows that of the longest isoform.

The physiological function of tau is the regulation of MT stability, neurite outgrowth, and other MT-dependent functions. The three or four repeats in the C-terminal half of the protein and the flanking proline-rich basic domains are known to be involved in MT binding (*14, 15*). The affinity is regulated by phosphorylation particularly at KXGS-motifs in the repeats (*16*).

In hereditary FTDP-17, several mutations within the tau gene are known which give rise to neurofibrillary deposits (*2-4, 6*). They include missense mutations (e.g. G272V, N279K, P301L, R406W), deletion (ΔK280), silent (L284L) and intronic mutations which do not change the protein sequence but affect the ratio of 3-repeat/4-repeat tau isoforms (*13, 17*). The missense and deletion mutants are concentrated in the repeat domain of tau (*14, 18, 19*). *In vitro* and in cell culture experiments some of the mutations weaken the binding of tau to MTs (*20-22*), affect the assembly of MTs and enhance PHF aggregation (*4*). In particular, the two mutants P301L and ΔK280 have a much stronger tendency to aggregate (*4, 23*). Some mutations, including P301L, also make tau more prone to hyperphosphorylation in cells (*24*).

Tau has a hydrophilic character, is highly soluble, and belongs to the class of natively unfolded proteins with no apparent ordered secondary structure detectable by far-UV CD or

Fourier transform infrared spectroscopy (*3, 13, 19*). Because of its high flexibility, it cannot be studied by high-resolution x-ray crystallography. X-ray analyses exist only in the form of solution scattering and fiber diffraction. Recently we and others have shown that the repeat domain of tau contains regions of residual β-structure, which have the potential to serve as seeds for aggregation of tau into PHFs (*25, 26*). The same regions were involved in binding to MTs and polyanions (*25*), supporting the hypothesis that stable MTs prevent PHF formation by blocking the tau-polyanion interaction sites, which are crucial for paired helical filament formation (*11, 27*).

Here we report the high-resolution characterization of the conformational properties of two FTDP-17 mutants of the 4-repeat domain of tau (K18), P301L and ΔK280, and their binding properties to the polyanion heparin and to MTs. The mutations do not change the secondary structure propensity of the repeat domain of tau, even though they strongly promote β-structure during aggregation. However, the mutations induce conformational changes in repeat 2 and they strongly attenuate the binding to microtubules whereas the interaction with heparin is only slightly affected.

MATERIALS AND METHODS

Expression of recombinant tau constructs and isotope labeling. P301L and ΔK280 mutations in the construct K18 (residues Q244 – E372 of the longest tau isoform in the human brain plus initial M243, 130 residues*)* were created by site-directed mutagenesis using the Quick-change kit (Stratagene, Amsterdam, The Netherlands). The introduced modifications were verified by DNA sequencing. Expression, purification and isotope labeling was performed as described previously (*25*). NMR samples contained 0.9 to 1.5 mM ^{15}N- or ^{15}N/^{13}C-labeled protein in 95% H_2O/5% D_2O, 50 mM phosphate buffer pH 6.8 with 1 mM dithiothreitol.

Preparation of MTs. Porcine brain tubulin was purified as described (*14*) and incubated at concentrations higher than 200 μM in MT assembly buffer (100 mM Pipes, pH 6.9, 1 mM EGTA, 1 mM $MgSO_4$, 1 mM DTT) in the presence of 1 mM GTP at 37 °C for 5 minutes. After the addition of 100 μM Paclitaxel (Sigma-Aldrich Chemie, Munich, Germany) the polymerization was performed for 20 min at 37 °C.

CD Spectroscopy. All measurements were carried out with a Jasco J-715 CD spectrometer (Jasco, Groß-Umstadt, Germany) in a cuvette with a path length of 0.1 cm. The spectra were recorded between 190-240 nm at a scanning speed of 100 nm/min, a bandwidth of 1.0 nm and with a response time of 0.5 s. In each experiment 3 spectra were summed and averaged. For calculation of the mean residue ellipticity, the protein concentration was obtained by using the second channel of the CD spectrometer measuring the absorption of the protein sample at 214 nm (where absorption is dominated by the peptide bonds). Calibration at 214 nm was done with a BSA standard.

NMR Spectroscopy. NMR spectra were acquired at 5 °C on Bruker DRX 800, Avance 700, Avance 600 and DRX 600 spectrometers. Aggregation did not occur at 5 °C in the absence of polyanions. NMR data were processed and analyzed using nmrPipe (*28*) and Sparky 3 (www.cgl.ucsf.edu/home/sparky/). 3D triple-resonance experiments were collected to obtain sequence specific assignments for the backbone of K18P301L and K18ΔK280. Secondary chemical shifts were calculated using NMRView (*29*) as the difference between the measured Cα/C' chemical shifts and the empirical, sequence-corrected random coil values (*30, 31*) for the appropriate amino acid type at pH 2.3. Random coil values for the pH sensitive residues histidine, glutamate and aspartate were taken from Wishart et al. (*32*) for a better accordance of the pH value and our experimental conditions. Random coil values for residues preceding Pro were taken from Wishart et al. (*33*). The averaged value for Cα and C' was defined as $\Delta\delta av \, (C\alpha C') = (3*\Delta C\alpha + 4*\Delta C')/7$. To clarify the effect of the chosen random coil values, we also calculated the secondary Cα chemical shifts using for all amino acid types the random coil values as determined by Wishart et al. (*33*).

Tau-heparin titrations were carried out at pH 6.8 using uniformly ^{15}N,^{13}C-labeled protein containing 150 μM K18P301L in MT assembly buffer and K18ΔK280 in 50 mM phosphate buffer, respectively. Heparin (average molecular weight 3350, 5.8 disaccharide subunits, charge/subunit -2.5, -0.31 z/Å) was purchased from Sigma. The formation of the tau-heparin complex was tracked by 2D ^{1}H-^{15}N Heteronuclear Single Quantum Coherence (HSQC) spectra for increasing heparin concentrations (mM): 0.015, 0.074, 0.146, 0.284 and 1.17 (K18P301L) and 0.015, 0.029, 0.071, 0.271 and 1.13 (K18ΔK280). For tau-MT titrations the samples contained 150 μM uniformly ^{15}N,^{13}C-labeled K18P301L and K18ΔK280, respectively, in MT assembly buffer. Complex formation was monitored at 5 °C for MT concentrations (αβ-tubulin dimers) of 10.5, 42.0 and 58.0 μM for K18P301L, and 42.0, 84.0 and 122.0 μM for K18ΔK280, respectively. NaCl was added to one K18ΔK280/MT sample

(tau:MT=5) to yield a final concentration of 150 and 300 mM, respectively. Again ^{1}H-^{15}N HSQC spectra were recorded at 5 °C. Normalized weighted average chemical shift differences for amide ^{1}H and ^{15}N chemical shifts upon heparin or MT binding were calculated using $\Delta\delta av(NH)= [(\Delta H^2+(\Delta N/5)^2)]^{1/2}$, in which ΔH and ΔN are the difference between chemical shifts of the free and bound form.

The aggregation behavior of K18ΔK280 was investigated during a measurement period of three days at 5° C. The signal intensity was monitored by the integration of signals of ^{1}H-^{15}N HSQC spectra and the relaxation behavior was probed with $T_{1\rho}$ relaxation time measurements. Neither a loss in the monomeric species, detectable via decreased signal intensity, nor an increase in the oligomeric species, causing a change in the relaxation, was identified. Aggregation does therefore not take place under the experimental conditions used here (at 5 °C without polyanions and without agitation).

RESULTS

Backbone Resonance Assignment of K18P301L and K18ΔK280. The ^{1}H-^{15}N HSQC spectra of construct K18, equivalent to the four microtubule binding repeats of full-length tau (Figure 1), and the spectra of both mutants, exhibited sharp resonances with a congestion of signals due to the protein's unfolded nature (Figure 2a) (*34*). Starting from the assignment of wild type (wt) K18, which was previously determined by us (*25*), it was possible to assign the mutant proteins by three-dimensional HNCO and high-resolution (HA)CANNH spectra. The sequence motifs PGGG could not be assigned unambiguously due to a strong signal overlap in the glycine region similar to the assignment of the *wt* protein (this accounts for the gaps in Figure 2b, c and following). The degeneracy of the glycines in the ^{301}PGGG^{304} motif was partially lifted by the P301L mutation enabling unambiguous assignment of Leu301 and Gly302. However, the effect of the mutation on Gly303 and Gly304 was not sufficient to resolve the assignment degeneracy of these residues, in agreement with the fact that the mutation primarily influences the upstream residues (see below). For all other residues of K18ΔK280 and K18P301L the ^{1}H, ^{15}N, ^{13}Cα and ^{13}C' chemical shifts were assigned. Changes in the ^{15}N and ^{1}H chemical shifts are pronounced in the vicinity of the mutations, i.e. at residues 281-284 (in C-terminal direction) in the case of K18ΔK280 (Figure 2b), and at residues 298-300 (in the N-terminal direction) in the case of K18P301L (Figure 2c).

Residual secondary structure. NMR chemical shifts of Cα and C' atoms are sensitive indicators for secondary structure both in globular and unfolded proteins (*35*). These shifts show small but distinct deviations from random coil values. The deviations, called secondary chemical shifts, are shown in Figure 3. For both mutant proteins, continuous stretches of negative secondary chemical shifts were found for residues 274-284, 295-298, 305-315, 336-345 and 357-361, indicative of a propensity to form β-structure. These stretches encompass the hexapeptide motifs VQIINK and VQIVYK at the beginning of the second and the third repeat, known to be important for the abnormal aggregation of tau into Paired Helical Filamentes (PHFs) (*13*). The secondary chemical shifts of the mutants are nearly identical to those in the wild-type protein (Figure 3). The strongest deviations from K18wt were found for histidine residues, most likely due to slight changes in the buffer conditions (the experimental pH is close to the pKa value of histidines).
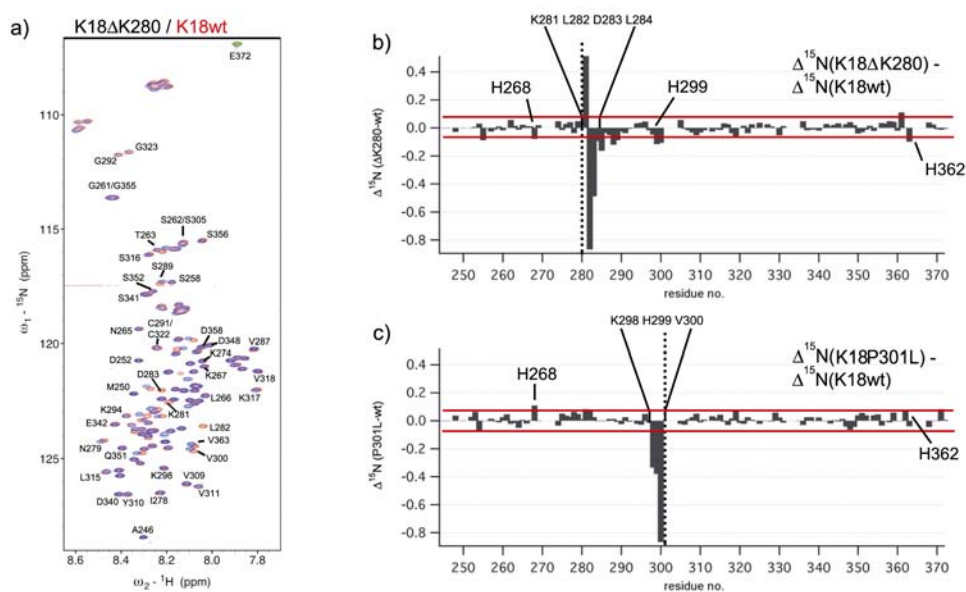
Figure 2

Figure 2: Changes in chemical environment induced by FTDP-17 mutations. (a) Overlay of HSQC spectra for K18ΔK280 (blue) and K18wt (red). Selected sequence-specific assignments are marked. (b) Difference in ^{15}N chemical shifts between K18ΔK280 and K18wt extracted from Figure 2a. (b) Difference in ^{15}N chemical shifts between K18P301L and K18wt. Horizontal lines indicate the average variation of chemical shifts observed for K18wt from sample to sample due to slightly different buffer conditions. Shift changes that exceed the red lines are regarded as significant and are located downstream of ΔK280 and upstream of P301L. Gaps are due to unassigned residues.

The secondary chemical shifts shown in Figure 2 were calculated on the basis of sequence-corrected random coil chemical shifts obtained on G-G-X-G-G peptides (*31*). For comparison, the ΔCα secondary chemical shifts for K18ΔK280 were also calculated using non sequence-corrected random coil values obtained on G-G-X-A-G-G peptides (*33*). The resulting Cα secondary chemical shift pattern indicated β-structure propensity for the two hexapeptides in the beginning of repeat 2 and 3, similar to what is seen in Figure 2. However, due to the non-sequence-corrected random coil values the Cα secondary chemical shifts were shifted by about 0.36 ppm towards more positive values (except Asp, Glu and Cys), such that several continuous stretches of positive secondary chemical shifts appeared. These stretches were previously interpreted as an indication that most of K19 (the construct comprising only three repeats), preferentially populate helical conformations (*26*). Currently, it cannot unambiguously be judged, which of the two sets of Cα random coil values is more appropriate. However, secondary chemical shift patterns obtained separately for Cα and C' were more consistent, when the sequence-corrected random coil values were used (as is done here). In addition, no helical propensities were detected for monomeric K18 or K19 by CD and FTIR spectroscopy (*3*)(also see below).
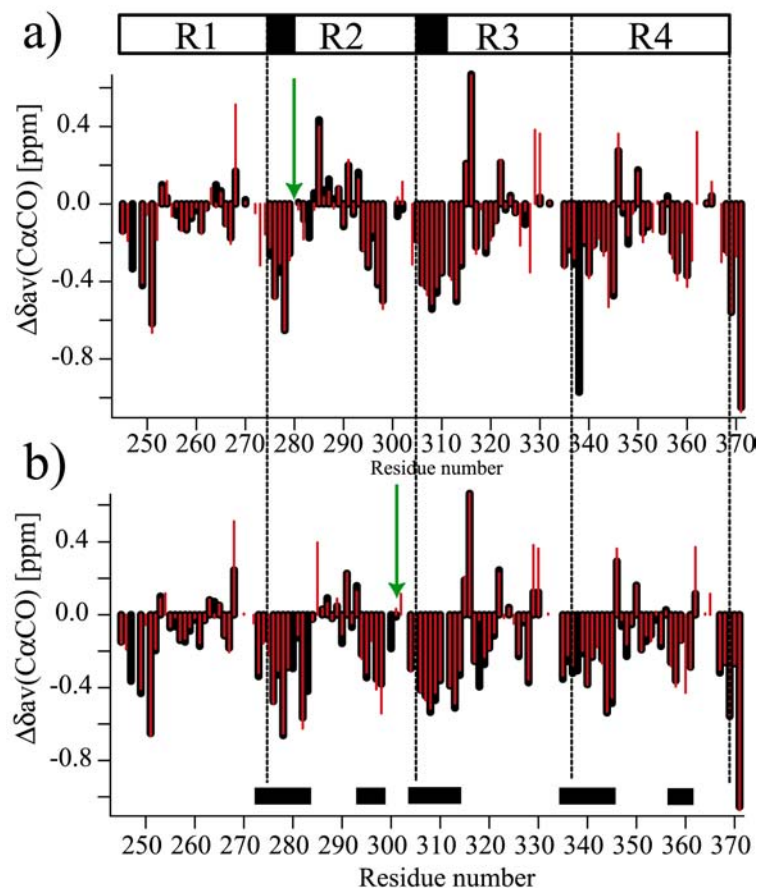
Figure 3

Figure 3: Secondary structure propensity of K18ΔK280 and K18P301L. Averaged secondary chemical shift, Δδav, in K18ΔK280 (a) and in K18P301L (b) in comparison to K18wt (red bars) at 5 °C, in 50 mM phosphate buffer, pH 6.9. The averaged shifts were calculated as [3Δδ(Cα) + 4Δδ(C')]/7. Five regions of enhanced β-structure propensity (274-284, 295-298, 305-315, 336-345 and 357-361) are indicated by grey boxes. They are characterized by contiguous blocks of negative secondary chemical shifts. Residues 246-253 most likely do not have an enhanced β-structure propensity due to the presence of three prolines (P247, P249, P251). The positions of the mutations are indicated by arrows. All glycines at position two and three in the PGGG motifs exhibited identical secondary chemical shifts.

Since the mutants K18ΔK280 and K18P301L have a higher tendency to aggregate we considered the possibility of a higher tendency of the monomer to form β-structure. We therefore used CD spectroscopy to check the conditions of the NMR experiments at different temperatures, because earlier experiments were performed at room temperature, whereas the NMR experiments were performed at 5° C. The CD spectra show for both K18wt (solid lines) and for K18ΔK280 a clear minimum at 200 nm at both 5 and 20°C (Figure 4; note that the slight differences in the spectra are within the error of the method). The minimum at 200 nm

indicates a mostly random coil structure (*36*), and in these monomeric fractions no increase of β-sheet structure in K18ΔK280 could be observed by CD.
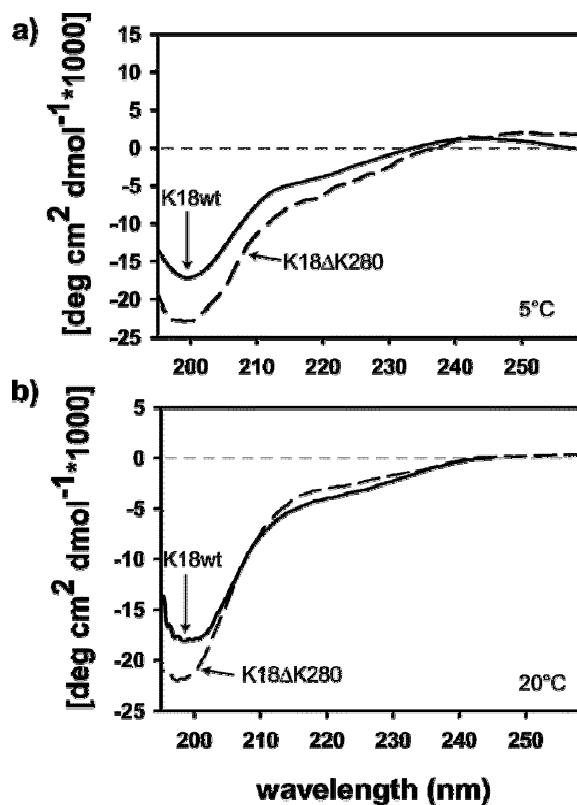
Figure 4: Circular dichroism of K18 wt and K18ΔK280. The secondary structure content of K18wt (solid line) and K18ΔK280 (dashed line) was measured at 5°C (a) and at 20°C (b). The molecular ellipticity was plotted versus the wavelength

Characterization of the complexes between tau mutants and polyanions. Polyanions such as heparin are often used to accelerate the assembly of tau into PHFs (*37-39*). To observe the complex formation between tau and polyanions, the shifts of the backbone amide protons can be followed providing information about the interacting regions and strength of binding. The binding of heparin was monitored by ^{1}H-^{15}N HSQC spectra. This allows one to identify the residues which are important for the binding to polyanions. At higher polyanion concentrations the change in chemical shift can be accompanied by a decrease in signal intensity, indicating chemical shift exchange intermediate on the NMR time scale.
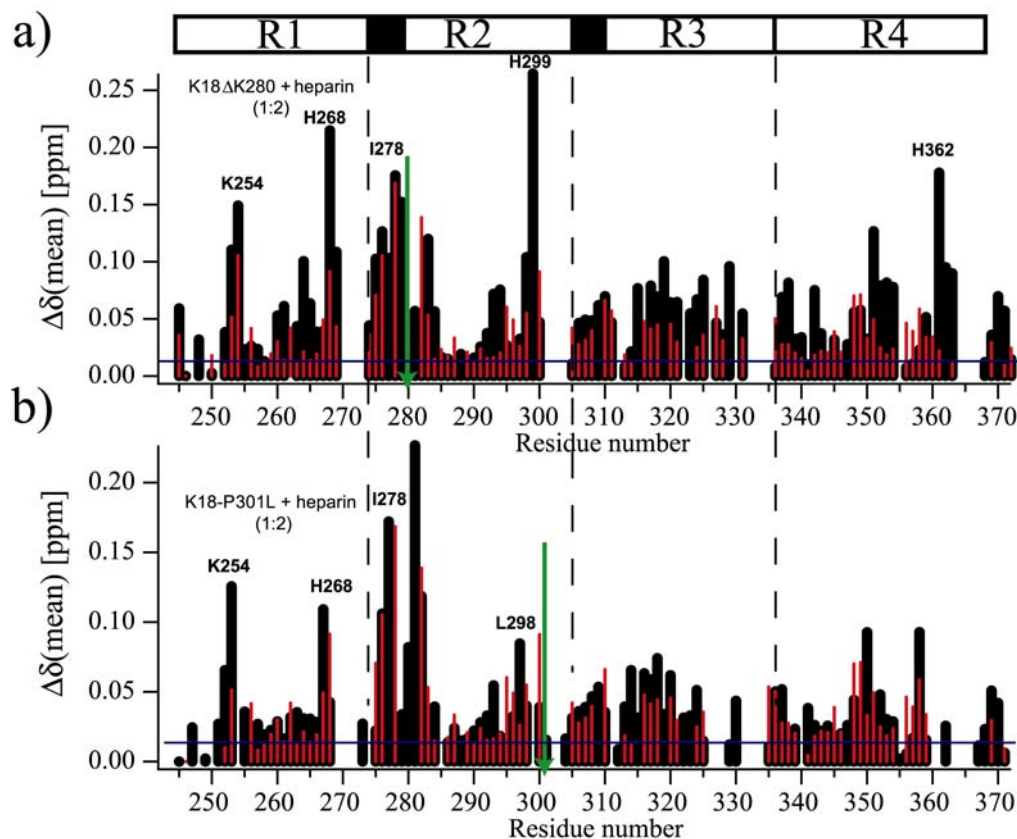
Figure 5

Figure 5: Binding of tau mutants to the polyanion heparin. Mean weighted ^{1}H-^{15}N chemical shift changes, Δδ(mean), induced by binding of heparin to K18ΔK280 (a) and K18P301L (b) and in comparison to K18wt (red bars). The concentration of the tau constructs was 150 μM, the molar tau:heparin ratio was ~1:2 for K18P301L and K18ΔK280, and ~1:1.5 for K18wt. Horizontal lines indicate the average variation of chemical shifts observed between different samples all containing K18:heparin (4:1) due to slightly different buffer conditions. Arrows mark the mutation sites. Gaps are due to overlap or the presence of prolines.

For both mutants, large chemical shift changes were present for residues V275–L284, the hexapeptide motif in the beginning of repeat 2 (black bars in Figure 5). In addition, the chemical shifts of selected lysine and histidine residues (L253-K254, H268-N269, L298-H299 and H362) were strongly affected by the addition of heparin. Overall, the patterns of chemical shift changes induced in the mutant proteins were similar to those previously observed for K18wt (red bars in Figure 5). The magnitude of chemical shift changes at K18mutant-to-heparin ratios of 1:2 were comparable to those measured for a K18wt:heparin ratio of 1:1.5.
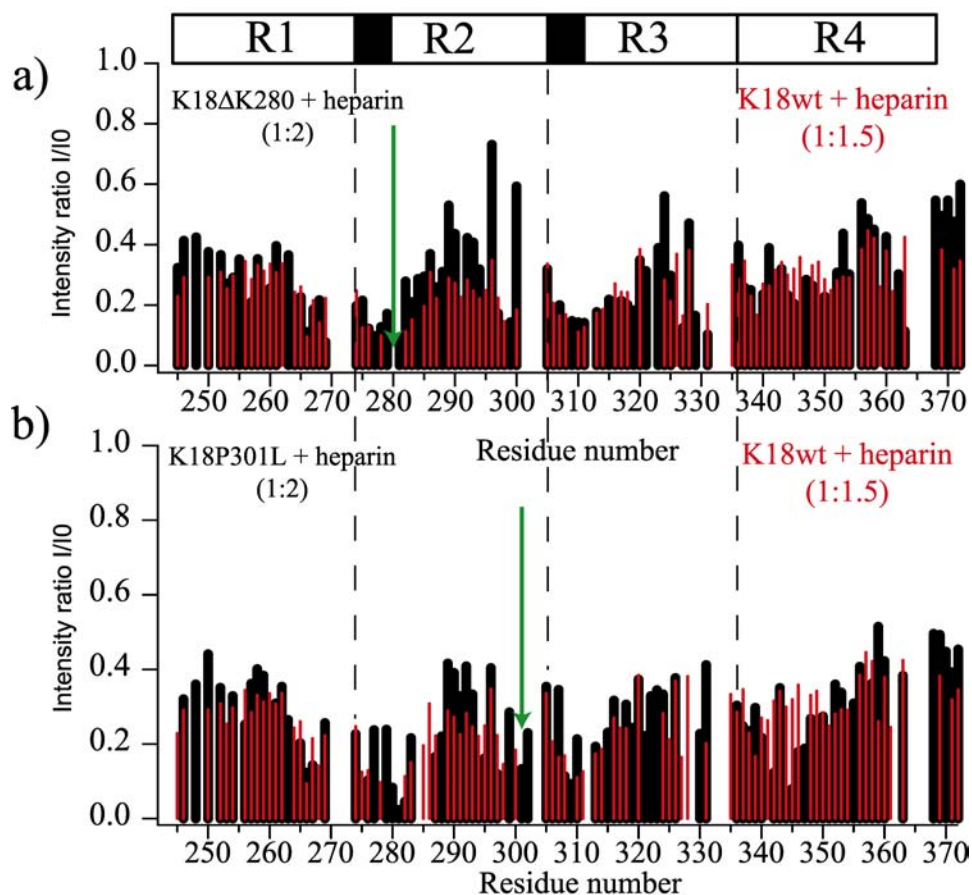
Figure 6

Figure 6: *^{1}H/^{15}N signal intensity changes upon addition of heparin*. (a) Binding of heparin to K18ΔK280. (b) Binding of heparin to K18P301L. The intensity ratio is calculated as the signal intensity I for a sample with heparin divided by the signal intensity I0 for a sample without heparin. The tau concentration was 150 µM, the tau:heparin ratio was ~1:2 for K18P301L and K18ΔK280, and ~1:1.5 for K18wt. For comparison K18 wt is also shown (red bars). Arrows mark the mutation sites. Global intensity changes due to partial aggregation are accompanied by intensity reductions in certain regions (V275–L282 and V306–T319), which are caused by chemical exchange intermediate on the NMR time scale and report on the binding of polyanions to tau.

In the presence of heparin, K18ΔK280 and K18P301L gradually begin to aggregate similar to K18wt as evidenced by a decrease in the overall signal intensity in the ^{1}H-^{15}N HSQC spectra (Figure 6). Besides this overall decrease in signal intensity, resonances of some residues were further broadened by chemical exchange intermediate on the NMR time scale. In particular, residues in the two hexapeptide motifs (V275–L282 and V306–T319) were attenuated, consistent with their involvement in the binding process. In comparison to the wild-type protein, however, the signal intensities of residues S289-S293 appeared enhanced in

particular for K18ΔK280, suggesting a reduced contribution from chemical exchange. The reduced influence of chemical exchange for residues S289-S293 together with the overall slightly lower magnitude of chemical shift changes for the mutant proteins may be interpreted as a reduced affinity for heparin caused by the mutations, potentially due to a less efficient binding of heparin to repeat 2.

Binding of the repeat domain of tau to microtubules. The binding of K18ΔK280 and K18P301L to MTs was characterized using the NMR chemical shift perturbation method (*40*), in which ^{1}H-^{15}N HSQC spectra were recorded in the presence of increasing amounts of taxol-stabilized MTs. Previous experiments including sedimentation, SDS-PAGE and electron microscopy on K18 and K19 wild-type protein had already shown that MTs in the taxol-stabilized form are stable at low temperature (5 °C) during the time course of the NMR measurements (*25*). In general, the shifts observed for the mutants were much weaker than those detected for K18wt (Figures 7a and 7c). In particular for K18P301L, only very small chemical shift changes were observed (Figure 7c). In case of K18ΔK280 and similar to the wt protein, the most strongly shifting residues were histidines and the corresponding hot spot regions, K267–H268, H299–V300 and H329, and in addition E264 (Figure 7a). On the other hand, the resonance positions of residues L253-256 and V275-L284 stayed almost unchanged upon addition of MTs in clear contrast to the wt protein (Figure 7a).

Tau binds to MTs in a biphasic manner. After a first tight and specific binding phase at low tau concentrations, a weak and unspecific binding takes place resulting in an accumulation of tau on the MT surface (*23*). From an NMR perspective, tau in the MT-bound state is invisible due to the very fast relaxation of the NMR signals. Accordingly, the signal-to-noise ratio in the ^{1}H-^{15}N HSQC spectra decreased rapidly at higher MT concentrations. Comparison with the wild-type construct (red bars in Figures 7b and 7d) shows that the intensity decrease is less pronounced for the mutant proteins, with K18ΔK280 even less affected than K18P301L. Despite the smaller reduction in overall signal intensity, however, resonances of residues V306-T319 showed a strong attenuation similar to what had been observed for K18wt. The signal intensity in this region is about a factor of 1.5-2 lower than the average signal intensity for all residues of K18. In summary, chemical shift changes and average signal intensities indicate that the MT-binding contribution of the hexapeptide motif in the beginning of repeat 2 was strongly reduced by the ΔK280 mutation, whereas no effect

of either the ΔK280 or the P301L mutation on the hexapeptide in the beginning of repeat 3 could be detected.
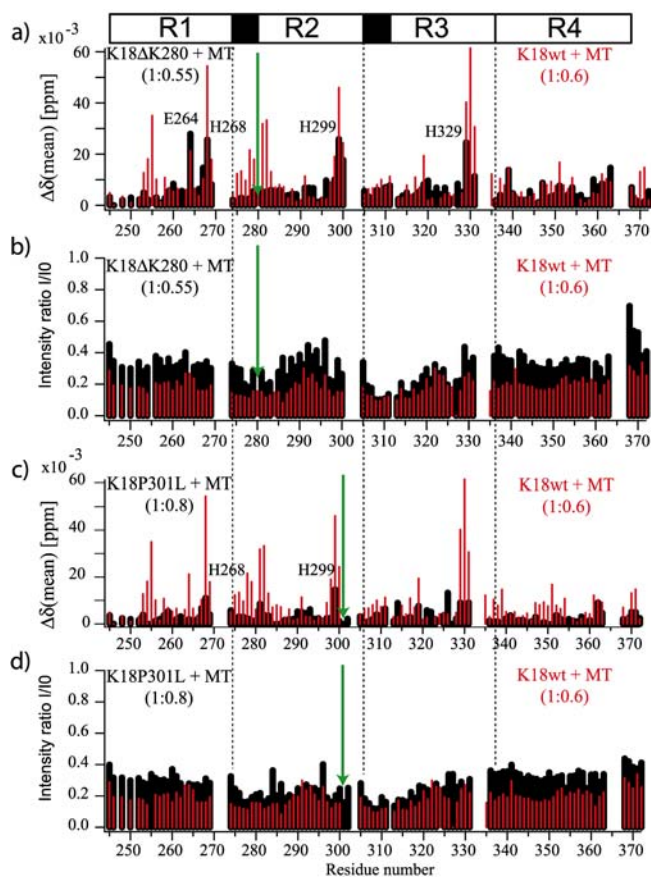
Figure 7

Figure 7: Identification of microtubule-binding hot spots in FTDP-17 mutations carrying tau. Mean weighted ^{1}H-^{15}N chemical shift changes of K18ΔK280 (a) and K18P301L (c) and signal intensity ratios in K18ΔK280 (b) and K18P301L (d) between the ^{1}H-^{15}N HSQC spectra of free tau (I0) and tau in the presence of MTs (I) at 5 °C. Values for K18wt are shown as red bars, arrows mark the mutation sites and gaps are due to overlap or the presence of prolines. The tau:MT ratio was 1:0.55 for K18ΔK280, 1:0.80 for K18P301L and 1:0.60 for K18wt. Binding sites were identified on the basis of large chemical shift changes and local intensity reductions due to chemical exchange. Previous experiments on K18 wild-type protein had already shown that MTs in the taxol-stabilized form are stable at low temperature (5 °C) during the time course of the NMR measurements (25).

Effect of NaCl on the binding affinity to microtubules. To remove weak unspecific binding and weaken the strong specific binding of tau to MTs such that it is observable by NMR, NaCl was added in two steps (final concentration 150 and 300 mM, respectively) to a sample with a K18ΔK280:MT ratio of 5:1 (absolute concentration of tau 150 μM). At 150 mM NaCl, the overall signal intensity was increased to an average value of 0.71 (Figure 8a). Moreover, the signal intensity was quite uniform across all residues of K18ΔK280. Especially

the region around the two hexapeptide motifs, residues K274–L284 and V306–T319, showed a pronounced regain of signal intensity. The regain in NMR signal intensity demonstrates that at 150 mM NaCl the binding of K18ΔK280 to MTs is weakened and many more K18ΔK280 molecules contribute to the observable NMR signal. Nevertheless, strong chemical shift changes were induced by the presence of MTs (green bars in Figure 8b). The strongest shifting residues were 260, 264, 267-268 and 299, 329-331 and 360-361, although the magnitude of these chemical shift changes was reduced in the presence of NaCl. In addition, significantly smaller chemical shift changes were observed for residues 283-289 and 316-323 when the MT-titration was performed at 150 mM instead of 0 mM NaCl. This indicates that electrostatic interactions play an important role in binding of K18 to MTs. Importantly, however, the chemical shift changes induced by addition of MTs in the absence of NaCl (when a significant fraction of tau molecules strongly binds to MTs and is therefore invisible to liquid-state NMR spectroscopy) and those at 150 mM NaCl (when most K18ΔK280 molecules contribute to the NMR signal) identify the same regions as being important for MT-binding.
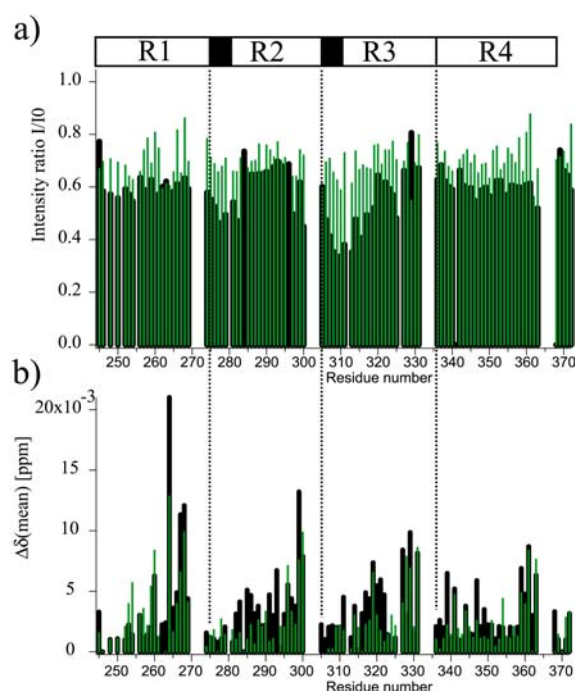
Figure 8

Figure 8: Influence of ionic strength on interaction of K18ΔK280 with preassembled microtubules. Signal intensity ratios (a) and mean weighted ^{1}H-^{15}N chemical shift changes (b) between the ^{1}H-^{15}N HSQC spectra of free tau and tau in the presence of MTs without NaCl (black bars) and with 150 mM NaCl (green bars) (both at 5 °C). The tau:MT ratio was 5:1. For all signal intensity ratio calculations the reference signal intensity I_0 was obtained from a sample containing K18ΔK280 and the appropriate amount of NaCl, but no MTs.

DISCUSSION

Tau is one of the major microtubule-associated proteins in the brain. It occurs predominantly in the axons of neurons and promotes the assembly and stability of microtubules. Pathological tau aggregation in the form of filaments, on the other hand, represents one of the hallmarks of a variety of dementias called tauopathies, including Alzheimer's disease, Pick's disease and FTDP-17. From a biophysial view, tau is an interesting research object as it belongs to the class of "intrinsically disordered" proteins, which can perform a specific function despite the lack of a well-defined three-dimensional structure. Here we have characterized the secondary structure propensity and the binding properties to polyanions and microtubules of the repeat region of tau (K18), when it carries two mutations that co-segregate with inherited FTDP-17 disease. Knowing the molecular mechanisms that underly the reduced binding affinity of the ΔK280 and P301L mutations to MTs and for their increased propensity to aggregate might help to understand the progression of dementia in FTDP-17 patients. Multidimensional NMR spectroscopy is one of the few methods that allow investigation of such dynamic proteins as tau with high-resolution.

The major results can be summarized as follows: 1) Both mutations do not significantly influence the secondary structure propensity of K18 in its monomeric state in solution. However, they induce local structural changes in the second repeat. 2) The interaction with the polyanion heparin is slightly weakened by the FTDP-17 associated mutations. 3) The mutations significantly attenuate the binding to microtubules. The more pronounced effect of the mutations on binding to microtubules indicates that the interaction of the repeat domain of tau with microtubules is more specific than the binding to polyanions.

Mutations induce local structural changes in repeat 2. NMR chemical shifts of backbone resonances allow a sensitive detection of structural changes, as induced for example by binding of a ligand or by mutations. Even changes in ^1H and ^{15}N chemical shifts, which are readily available from two-dimensional correlation spectra, are valuable reporters on the extent of changes induced by mutations. In particular, changes that affect only the immediate vicinity of the site of mutation can be distinguished from those having more global effects. The FTDP-17 mutations ΔK280 and P301L induce the largest changes in the ^1H and ^{15}N chemical shifts in repeat 2, i.e. for K18P301L upstream of the mutation site (K298–V300) and for K18ΔK280 downstream (K281–S285). The directionality of the chemical changes caused

by the P301L mutation is in agreement with the proposal that the PGGG motif which normally adopts a turn structure is straightened out into a more extended structure which includes even the preceding residues K298-V300 (*3*). K18ΔK280, on the other hand, is at the center of a region that preferentially populates β-structure in K18wt. Therefore, the pronounced effect on the upstream residues is not clear.

NMR chemical shifts of backbone atoms, such as Cα and CO, are strongly influenced by secondary structure. In particular, the comparison of secondary chemical shifts in two different states, for example free and bound to a ligand or wild-type and mutant protein, enables the detection of even small changes in secondary structure propensity. The secondary chemical shifts of K18ΔK280 and K18P301L were highly similar to values observed for K18wt. No strong increase in the propensity to form secondary structure (β or α) was observed for the mutants in solution.

Previous studies had revealed that peptides derived from the repeat domain and containing the K18ΔK280 or P301L mutations had an increased tendency to aggregate with formation of beta-structure, as judged by FTIR and CD (*3, 4*). However, when the protein was freshly prepared by gel filtration, the monomeric fraction did not show a different content of β-structure (Figure 4). This suggests that the higher rate of aggregation of the two K18 mutants *in vitro* is not due to increased content of β-structure in their monomeric, soluble state. Rather, intermolecular interactions become more favorable: The deletion mutation ΔK280 results in a pattern of alternating polar and non-polar residues, which favors aggregation (*3, 41*). The missense mutation P301L removes a proline residue from the core of the repeat domain, enabling longer β-strands and a better stacking between strands within the fibril (*3*).

We mention in this context that a predominantly α-helical content has been reported for certain FTDP-17 mutants of tau (*42*). We have not been able to confirm this in experiments using CD and FTIR spectroscopy (*3, 43*), in agreement with other investigators showing that tau has a mostly random-coil conformation in solution (*44-47*). The discrepancy could possibly be explained by the fact that Jicha et al. (1999) (*42*) used tau proteins expressed with poly-histidine tags.

ΔK280 and P301L mutations only weakly affect the interaction of K18 with heparin. It is not clear at present how PHF aggregation is initiated in neuronal cells. However, the fact that *in vitro*, heparin can greatly improve polymerizability of tau (*38, 39*) points to a possible

role of cytosolic polyanions (examples are RNAs or acidic peptides such as the C-terminal tail of tubulin (*37*)). Our results show that the binding of heparin to K18ΔK280 and K18P301L is slightly weakened, and it is likely that this holds for other polyanions as well since our previous results showed that the same residues are important for microtubule and heparin binding (*25*). Despite the deletion of K280 in K18ΔK280, the NMR signals of V275-L284 were strongly influenced by the addition of heparin. On the other hand, signal intensities of residues S289-S293 appeared enhanced and mutations only affected ^{1}H/^{15}N chemical shifts of residues in repeat 2 of the free protein. Therefore, we attribute the slightly reduced affinity for heparin to a combination of altered electrostatic properties and conformational changes.

The interaction of the repeat domain of tau with microtubules is more specific than the binding to polyanions. Tau is a microtubule-associated protein that regulates diverse and essential MT functions, including polymerization and stabilization of MTs and modulation of MT dynamics (*14*). The domains flanking the repeat region bind strongly to MTs, even in the absence of the repeats, whereas the repeat motifs are essential for MT assembly (*48*). Notably there are hotspots of MT binding, such as the KK motif (residues 280-281) in repeat R2 (*15*). FTDP-17 associated mutations, which cluster in the repeat region of tau, are known to weaken the interaction of tau with MTs and cause a decrease in MT stabilization (*3*), whereas mutations which increase the concentration of 4Rtau lead to a decrease of dynamic microtubules (*49*). Therefore, knowledge of the detailed mechanism by which the disease-associated mutations affect the ability of tau to bind to MTs is important. Here, we have characterized the binding of the repeat domain of tau, containing the two FTDP-17 linked mutations K18ΔK280 and K18P301L, to preassembled, taxol-stabilized MTs on the level of individual residues.

Previously, we have shown that the binding of the repeat domain of tau to polyanions and taxol-stabilized microtubules involves similar residues (*25*). K18 interacts with microtubules and heparin/ poly-Glu through positive charges upstream of the PGGG motifs (K267–H268, H299 and H329) and through the hexapeptides at the beginning of repeat 2 and 3. In particular, I278 and K281 played an important role, in agreement with results obtained by site-directed mutagenesis (*15*). As poly-Glu resembles the Glu-rich C-terminal sequence of tubulin, the NMR data suggested that the positively charged clusters in the repeat domain bind to the C-terminus of tubulin. This is in agreement with biochemical studies showing an interaction between tau and the tubulin tail (*50, 51*). The data presented here show that the binding of the two FTDP-17 linked mutations K18ΔK280 and K18P301L to microtubules

differs from the binding to heparin. The disease-associated mutations reduce strongly the binding to MTs, whereas heparin binding is only slightly affected. In particular, the contribution of residues K274-L284 to MT-binding is almost absent. This demonstrates that the binding to microtubules is more specific than a simple, electrostatically driven binding to polyanions. The directionality of changes in the ^{1}H/^{15}N chemical shifts induced by the mutations (see above) suggests that the detrimental effect of the mutations is due to an altered conformation centered around repeat 2 or a lack of ability to form such a conformation upon binding, involving in particular the hexapeptide V275-K280 (note that the ΔK280 mutation strongly perturbs one of the MT-binding hotspots (*15*), Goode & Feinstein 1994). Binding to heparin, on the other hand, does not require a specific conformational arrangement in the repeat domain of tau or heparin can more easily adjust to a mutation-induced conformational change.

In interpreting the results reported here, one should recall that different binding modes of tau to MT have been described in the literature. The predominant one, observed in most *in vitro* experiments and in cell-based experiments, shows tau as a molecule binding to the surface of microtubules rapidly and reversibly. At high concentrations of tau:tubulin ratios, this primary interaction can be complemented by a weak secondary interaction which has the hallmarks of unspecific "overloading" of the MT surface and can be avoided by increasing the ionic strength (see Figure 8; note that a high salt step is typically included in the preparation of tubulin in order to eliminate MAPs). Another type of binding can occur when tau is co-polymerized with tubulin; in this case, a fraction of tau appears to be trapped in the tubulin lattice in a fashion that is not readily reversible (*52*). This latter mode of binding does not apply here since the experiments were done with pre-polymerized microtubules.

In summary, the two FTDP-17 associated mutations ΔK280 and P301L in the repeat domain of tau, which cause rapid aggregation *in vitro*, do not show significant changes in the secondary structure propensity of the soluble, monomeric protein. However, local structural changes in the second repeat are induced. The FTDP-17 associated mutations only slightly affect the binding to the polyanion heparin, but significantly attenuate the binding to microtubules. This suggests that binding of 4-repeat tau to microtubules involves specific interactions. Due to the reduced MT-affinity of 4-repeat tau carrying the FTDP-17 mutations ΔK280 and P301L, more tau protein will be free in solution, increasing the effective concentration and thereby the tendency to aggregate. Aggregation nuclei formed by mutant tau could be elongated even from the pool of normal tau and thus poison the entire tau population in a cell.

Abbreviations: CD, circular dichroism spectroscopy; FTDP-17, frontotemporal dementia with Parkinsonism linked to chromosome 17; HSQC, Heteronuclear Single Quantum Coherence; K18, 4 repeat domain of tau; MT, microtubule; PHF, Paired Helical Filament; wt, wild type

REFERENCES

1.   D'Souza, I., Poorkaj, P., Hong, M., Nochlin, D., Lee, V. M., Bird, T. D., and Schellenberg, G. D. (1999) Missense and silent tau gene mutations cause frontotemporal dementia with parkinsonism-chromosome 17 type, by affecting multiple alternative RNA splicing regulatory elements, *Proc. Natl. Acad. Sci. U S A 96*, 5598-5603.

2.   Nacharaju, P., Lewis, J., Easson, C., Yen, S., Hackett, J., Hutton, M., and Yen, S. H. (1999) Accelerated filament formation from tau protein with specific FTDP-17 missense mutations, *FEBS Lett. 447*, 195-199.

3.   von Bergen, M., Barghorn, S., Li, L., Marx, A., Biernat, J., Mandelkow, E. M., and Mandelkow, E. (2001) Mutations of tau protein in frontotemporal dementia promote aggregation of paired helical filaments by enhancing local beta-structure, *J. Biol. Chem. 276*, 48165-48174.

4.   Barghorn, S., Zheng-Fischhofer, Q., Ackmann, M., Biernat, J., von Bergen, M., Mandelkow, E. M., and Mandelkow, E. (2000) Structure, microtubule interactions, and paired helical filament aggregation by tau mutants of frontotemporal dementias, *Biochemistry 39*, 11714-11721.

5.   Goedert, M., Jakes, R., Crowther, R. A., Hasegawa, M., Smith, M. J., and Spillantini, M. G. (1998) Intraneuronal filamentous tau protein and alpha-synuclein deposits in neurodegenerative diseases, *Biochem. Soc. Trans. 26*, 463-471.

6.   Goedert, M., and Spillantini, M. G. (2000) Tau mutations in frontotemporal dementia FTDP-17 and their relevance for Alzheimer's disease, *Biochim. Biophys. Acta 1502*, 110-121.

7.   Hutton, M., Lendon, C. L., Rizzu, P., Baker, M., Froelich, S., Houlden, H., Pickering-Brown, S., Chakraverty, S., Isaacs, A., Grover, A., Hackett, J., Adamson, J., Lincoln, S., Dickson, D., Davies, P., Petersen, R. C., Stevens, M., de Graaff, E., Wauters, E., van Baren, J., Hillebrand, M., Joosse, M., Kwon, J. M., Nowotny, P., Che, L. K., Norton, J., Morris, J. C., Reed, L. A., Trojanowski, J., Basun, H., Lannfelt, L., Neystat, M., Fahn, S., Dark, F., Tannenberg, T., Dodd, P. R., Hayward, N., Kwok, J. B., Schofield, P. R., Andreadis, A., Snowden, J., Craufurd, D., Neary, D., Owen, F., Oostra, B. A., Hardy, J., Goate, A., van Swieten, J., Mann, D., Lynch, T., and Heutink,

P. (1998) Association of missense and 5'-splice-site mutations in tau with the inherited dementia FTDP-17, *Nature 393*, 702-705.

8. Goedert, M., Spillantini, M. G., Jakes, R., Rutherford, D., and Crowther, R. A. (1989) Multiple isoforms of human microtubule-associated protein tau: sequences and localization in neurofibrillary tangles of Alzheimer's disease, *Neuron 3*, 519-526.

9. Buee, L., Laine, A., Delacourte, A., Flament, S., and Han, K. K. (1989) Qualitative and quantitative comparison of brain proteins in Alzheimer's disease, *Biol. Chem. Hoppe Seyler 370*, 1229-1234.

10. Wischik, C. M., Novak, M., Edwards, P. C., Klug, A., Tichelaar, W., and Crowther, R. A. (1988) Structural characterization of the core of the paired helical filament of Alzheimer disease, *Proc. Natl. Acad. Sci. U S A 85*, 4884-4888.

11. Wille, H., Drewes, G., Biernat, J., Mandelkow, E. M., and Mandelkow, E. (1992) Alzheimer-like paired helical filaments and antiparallel dimers formed from microtubule-associated protein tau in vitro, *J. Cell Biol. 118*, 573-584.

12. Friedhoff, P., Schneider, A., Mandelkow, E. M., and Mandelkow, E. (1998) Rapid assembly of Alzheimer-like paired helical filaments from microtubule-associated protein tau monitored by fluorescence in solution, *Biochemistry 37*, 10223-10230.

13. von Bergen, M., Friedhoff, P., Biernat, J., Heberle, J., Mandelkow, E. M., and Mandelkow, E. (2000) Assembly of tau protein into Alzheimer paired helical filaments depends on a local sequence motif ((306)VQIVYK(311)) forming beta structure, *Proc. Natl. Acad. Sci. U S A 97*, 5129-5134.

14. Gustke, N., Trinczek, B., Biernat, J., Mandelkow, E. M., and Mandelkow, E. (1994) Domains of tau protein and interactions with microtubules, *Biochemistry 33*, 9511-9522.

15. Goode, B. L., and Feinstein, S. C. (1994) Identification of a novel microtubule binding and assembly domain in the developmentally regulated inter-repeat region of tau, *J. Cell Biol. 124*, 769-782.

16. Biernat, J., Gustke, N., Drewes, G., Mandelkow, E. M., and Mandelkow, E. (1993) Phosphorylation of Ser262 strongly reduces binding of tau to microtubules: distinction between PHF-like immunoreactivity and microtubule binding, *Neuron 11*, 153-163.

17.   Minoura, K., Yao, T. M., Tomoo, K., Sumida, M., Sasaki, M., Taniguchi, T., and Ishida, T. (2004) Different associational and conformational behaviors between the second and third repeat fragments in the tau microtubule-binding domain, *Eur. J. Biochem. 271*, 545-552.

18.   DeTure, M., Ko, L. W., Yen, S., Nacharaju, P., Easson, C., Lewis, J., van Slegtenhorst, M., Hutton, M., and Yen, S. H. (2000) Missense tau mutations identified in FTDP-17 have a small effect on tau-microtubule interactions, *Brain Res. 853*, 5-14.

19.   Schweers, O., Schonbrunn-Hanebeck, E., Marx, A., and Mandelkow, E. (1994) Structural studies of tau protein and Alzheimer paired helical filaments show no evidence for beta-structure, *J. Biol. Chem. 269*, 24290-24297.

20.   Goedert, M. (2005) Tau gene mutations and their effects, *Mov. Disord. 20 Suppl. 12*, S45-52.

21.   Bunker, J. M., Kamath, K., Wilson, L., Jordan, M. A., and Feinstein, S. C. (2006) FTDP-17 mutations compromise the ability of tau to regulate microtubule dynamics in cells, *J. Biol. Chem. 281*, 11856-11863.

22.   Lu, M., and Kosik, K. S. (2001) Competition for microtubule-binding with dual expression of tau missense and splice isoforms, *Mol. Biol. Cell 12*, 171-184.

23.   Ackmann, M., Wiech, H., and Mandelkow, E. (2000) Nonsaturable binding indicates clustering of tau on the microtubule surface in a paired helical filament-like conformation, *J. Biol. Chem. 275*, 30335-30343.

24.   Avila, J., Lucas, J. J., Perez, M., and Hernandez, F. (2004) Role of tau protein in both physiological and pathological conditions, *Physiol. Rev. 84*, 361-384.

25.   Mukrasch, M. D., Biernat, J., von Bergen, M., Griesinger, C., Mandelkow, E., and Zweckstetter, M. (2005) Sites of tau important for aggregation populate {beta}-structure and bind to microtubules and polyanions, *J. Biol. Chem. 280*, 24978-24986.

26.   Eliezer, D., Barre, P., Kobaslija, M., Chan, D., Li, X., and Heend, L. (2005) Residual structure in the repeat domain of tau: echoes of microtubule binding and paired helical filament formation, *Biochemistry 44*, 1026-1036.

27.   Wischik, C. M., Novak, M., Thogersen, H. C., Edwards, P. C., Runswick, M. J., Jakes, R., Walker, J. E., Milstein, C., Roth, M., and Klug, A. (1988) Isolation of a fragment

of tau derived from the core of the paired helical filament of Alzheimer disease, *Proc. Natl. Acad. Sci. U S A 85*, 4506-4510.

28.   Delaglio, F., Grzesiek, S., Vuister, G. W., Zhu, G., Pfeifer, J., and Bax, A. (1995) NMRPipe: a multidimensional spectral processing system based on UNIX pipes, *J. Biomol. NMR 6*, 277-293.

29.   Johnson, B. A., and Blevins, R. A. (1994) Nmr View - a Computer-Program for the Visualization and Analysis of Nmr Data, *J. Biomol. NMR 4*, 603-614.

30.   Schwarzinger, S., Kroon, G. J., Foss, T. R., Wright, P. E., and Dyson, H. J. (2000) Random coil chemical shifts in acidic 8 M urea: implementation of random coil shift data in NMRView, *J. Biomol. NMR 18*, 43-48.

31.   Schwarzinger, S., Kroon, G. J., Foss, T. R., Chung, J., Wright, P. E., and Dyson, H. J. (2001) Sequence-dependent correction of random coil NMR chemical shifts, *J. Am. Chem. Soc. 123*, 2970-2978.

32.   Wishart, D. S., and Sykes, B. D. (1994) Chemical shifts as a tool for structure determination, *Methods Enzymol. 239*, 363-392.

33.   Wishart, D. S., Bigam, C. G., Holm, A., Hodges, R. S., and Sykes, B. D. (1995) 1H, 13C and 15N random coil NMR chemical shifts of the common amino acids. I. Investigations of nearest-neighbor effects, *J. Biomol. NMR 5*, 67-81.

34.   Lippens, G., Sillen, A., Smet, C., Wieruszeski, J. M., Leroy, A., Buee, L., and Landrieu, I. (2006) Studying the natively unfolded neuronal Tau protein by solution NMR spectroscopy, *Protein Pept. Lett. 13*, 235-246.

35.   Dyson, H. J., and Wright, P. E. (2004) Unfolded proteins and protein folding studied by NMR, *Chem. Rev. 104*, 3607-3622.

36.   Fasman, G. D. (1989) Protein conformational prediction, *Trends Biochem. Sci. 14*, 295-299.

37.   Kampers, T., Friedhoff, P., Biernat, J., Mandelkow, E. M., and Mandelkow, E. (1996) RNA stimulates aggregation of microtubule-associated protein tau into Alzheimer-like paired helical filaments, *FEBS Lett. 399*, 344-349.

38.   Goedert, M. (1996) Tau protein and the neurofibrillary pathology of Alzheimer's disease, *Ann. N Y Acad. Sci. 777*, 121-131.

39. Perez, M., Valpuesta, J. M., Medina, M., Montejo de Garcini, E., and Avila, J. (1996) Polymerization of tau into filaments in the presence of heparin: the minimal sequence required for tau-tau interaction, *J. Neurochem. 67*, 1183-1190.

40. Craik, D. J., and Wilce, J. A. (1997) Studies of protein-ligand interactions by NMR, *Methods Mol. Biol. 60*, 195-232.

41. Pawar, A. P., Dubay, K. F., Zurdo, J., Chiti, F., Vendruscolo, M., and Dobson, C. M. (2005 Prediction of "aggregation-prone" and "aggregation-susceptible" regions in proteins associated with neurodegenerative diseases, *J. Mol. Biol. 350*, 379-392.

42. Jicha, G. A., Rockwood, J. M., Berenfeld, B., Hutton, M., and Davies, P. (1999) Altered conformation of recombinant frontotemporal dementia-17 mutant tau proteins, *Neurosci. Lett. 260*, 153-156.

43. Barghorn, S., Davies, P., and Mandelkow, E. (2004) Tau paired helical filaments from Alzheimer's disease brain and assembled in vitro are based on beta-structure in the core domain, *Biochemistry 43*, 1694-1703.

44. Cleveland, D. W., Kirschner, M. W., and Cowan, N. J. (1978) Isolation of separate mRNAs for alpha- and beta-tubulin and characterization of the corresponding in vitro translation products, *Cell 15*, 1021-1031.

45. Goux, W. J. (2002) The conformations of filamentous and soluble tau associated with Alzheimer paired helical filaments, *Biochemistry 41*, 13798-13806.

46. Sadqi, M., Hernandez, F., Pan, U., Perez, M., Schaeberle, M. D., Avila, J., and Munoz, V. (2002) Alpha-helix structure in Alzheimer's disease aggregates of tau-protein, *Biochemistry 41*, 7150-7155.

47. Berriman, J., Serpell, L. C., Oberg, K. A., Fink, A. L., Goedert, M., and Crowther, R. A. (2003) Tau filaments from human brain and from in vitro assembly of recombinant protein show cross-beta structure, *Proc. Natl. Acad. Sci. U S A 100*, 9034-9038.

48. Preuss, U., Biernat, J., Mandelkow, E. M., and Mandelkow, E. (1997) The 'jaws' model of tau-microtubule interaction examined in CHO cell, *J. Cell Sci. 110*, 789-800.

49. Bunker, J. M., Wilson, L., Jordan, M. A., and Feinstein, S. C. (2004) Modulation of microtubule dynamics by tau in living cells: implications for development and neurodegeneration, *Mol. Biol. Cell 15*, 2720-2728.

50.   Littauer, U. Z., Giveon, D., Thierauf, M., Ginzburg, I., and Ponstingl, H. (1986)
       Common and distinct tubulin binding sites for microtubule-associated proteins, *Proc.
       Natl. Acad. Sci. U S A 83*, 7162-7166.

51.   Serrano, L., Montejo de Garcini, E., Hernandez, M. A., and Avila, J. (1985)
       Localization of the tubulin binding site for tau protein, *Eur. J. Biochem. 153*, 595-600.

52.   Makrides, V., Massie, M. R., Feinstein, S. C., and Lew, J. (2004) Evidence for two
       distinct binding sites for tau on microtubules, *Proc. Natl. Acad. Sci. U S A 101*, 6746-
       6751.

4   The 'Jaws' of the Tau-Microtubule Interaction

Marco D. Mukrasch‡, Martin von Bergen¶, Jacek Biernat¶, Daniela Fischer‡, Christian Griesinger‡, Eckhard Mandelkow¶, Markus Zweckstetter‡

From the ‡Department for NMR-based Structural Biology, Max Planck Institute for Biophysical Chemistry, Am Fassberg 11, 37077 Göttingen, Germany and the ¶Max Planck Unit for Structural Molecular Biology, c/o DESY, Notkestrasse 85, 22607 Hamburg, Germany

ABSTRACT

Tau is the major microtubule-associated protein in neuronal axons. It aggregates into "neurofibrillary tangles" during the course of Alzheimer's disease. Binding to microtubules and microtubule-assembly requires the "repeat domain" in the C-terminal half of Tau, as well as the two regions flanking the repeats. Here we report the NMR characterization of a 198-residue tau fragment composed of the four tandem repeats and the flanking domains and containing the full microtubule-binding and assembly activity of tau. NMR secondary chemical shifts and dipolar couplings detect the highest propensity for β-structure within the four-repeat region, whereas the flanking domains are largely random coil, with an increased rigidity in the proline-rich region. Chemical shift perturbation experiments identify two motifs in the upstream flanking domain, ^{225}KVAVVRT^{231} and ^{243}LQTA^{246}, and one downstream of the repeats, ^{370}KIETHKTFREN^{380}, which strongly contribute to the binding to the acidic outside of microtubules, as well as to the binding of other polyanions such as heparin. This is consistent with the "jaws"-model of tau-microtubule interactions and highlights the importance of the regions flanking the repeats for both microtubule-binding and pathological tau aggregation.

INTRODUCTION

Tau, the major MAP of neurons, is localized predominantly in axons. Tau stabilizes MTs and is necessary for neurite outgrowth (1,2). Tau occurs in six main isoforms in the human brain (ranging between 352 and 441 amino acid residues), obtained by alternative splicing and differ by having 3 or 4 semi-conserved repeats of ~31 residues in the MT-assembly domain and 0-2 insertions in the N-terminal projection domain (Fig. 1) (3,4). The repeat domain is important for promoting microtubule assembly, but it binds to microtubules only with low affinity. However, strong MT binding and efficient assembly is achieved when the repeat domain is combined with the flanking domains, while the flanking domains alone

bind to microtubules but do not promote MT assembly. This lead to the proposition of the 'jaws' model of tau whereby the flanking regions are considered as targetting domains, responsible for positioning tau on the MT surface, and the repeats are considered as catalytic domains for MT assembly (5,6).

In Alzheimer's disease (AD), tau aggregates into neurofibrillary tangles which consist of "paired helical filaments" (PHFs) (7,8). The repeat domain coincides with the core of PHFs (9-11) and promotes PHF assembly in vitro (12). For PHF aggregation two hexapeptides at the beginning of the second and third repeats (^{275}VQIINK^{280} and ^{306}VQIVYK^{311}) are crucial (13,14). The role of the repeat domain both in MT assembly and PHF aggregation illustrates a remarkable overlap between physiological and pathological functions of tau. Both functions are regulated by phosphorylation, whereby the phosphorylation of the repeat domain (KXGS motifs) efficiently detaches tau from microtubules and prevents PHF aggregation while phosphorylation in the flanking domains has a modulating effect (15).
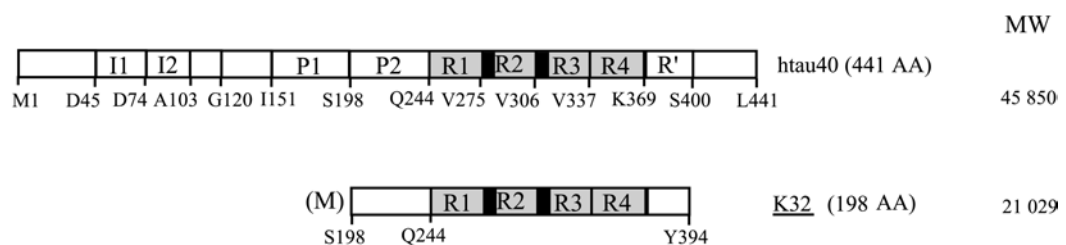
Fig. 1. Bar diagrams of full-length tau and the fragment K32. Full-length adult tau (htau40) contains 441 residues and can be subdivided into several domains (5). The N-terminal "projection domain" comprises residues 1-197 and does not contribute to MT binding. The C-terminal "assembly domain" contains the residues important for microtubule nucleation and stabilization. The four repeats (31 or 32 residues) are denoted as R1-R4. R2 (encoded by exon 10) is absent in 3-repeat isoforms due to alternative splicing. The basic and proline-rich region preceding the repeats is subdivided into P1 and P2, separated by the chymotryptic cleavage site behind Y197 which divides the projection domain and assembly domain. Fragment K32 comprises residues S198-Y394 with a preceding methionine (198 residues), i.e. domains P2, R1-R4, and R'. P2 contributes a major part of the microtubule-binding affinity and contains many of the proline-directed phosphorylation sites (e.g. AT8 site = S202^P+T205^P, AT100 site = T210^P+S212^P which represents the binding site of the Pin1 proline isomerase (16), and the AT180 site = S231^P+T235^P which contributes to a conformational change upon proline isomerization). The C-terminal flanking region is denoted R' because it shows weak sequence homology to the other repeats ("5th repeat"). The two hexapeptide motives ^{275}VQIINK^{280} and ^{306}VQIVYK^{311} in R2 and R3, which are necessary for PHF formation (13), are indicated by black filled rectangles.

In order to gain a structural understanding of the MT-binding and PHF-aggregation activities we performed a detailed NMR characterization of a 198-residue fragment (construct K32), containing the repeat domain and the two flanking domains. Tau is a natively unfolded protein so that X-ray crystallography cannot be applied, leaving NMR spectroscopy as almost the only method that allows detailed structure information. The results presented here provide a view of the jaws in tau that are essential for efficient binding of tau to microtubules.

EXPERIMENTAL PROCEDURES

Expression and isotopic labeling of recombinant tau constructs: Human tau constructs were expressed in the vector pNG2 (a derivative of pET-3a, Merck-Novagen, Darmstadt) in E.coli strain BL21(DE3) as described (5) (see Fig. 1). K32 comprises residues (M)S198-Y394, equivalent to the 4 repeats and the two flanking regions (198 residues). The expressed proteins were purified from bacterial extracts by making use of the heat stability of the protein and by FPLC SP-Sepharose chromatography (Amersham Biosciences). In order to label the tau proteins with ^{15}N and ^{13}C stable isotopes, the E. coli culture expressing K32 protein was grown on rich growth medium based on chemolithoautotrophic bacteria labeled with ^{13}C and ^{15}N isotopes (Silantes, Munich). Protein samples uniformly enriched in ^{15}N were prepared by growing E. coli bacteria in minimal medium containing 1g L^{-1} of $^{15}NH_4Cl$.

The cell pellets were resuspended in boiling-extraction buffer (50 mM MES, 500 mM NaCl, 1 mM $MgCl_2$, 1 mM EGTA, 5 mM DTT, pH 6.8) complemented with a protease inhibitor cocktail. The cells were disrupted with a French pressure cell and subsequently boiled for 20 min. The soluble extract was isolated by centrifugation, the supernatant was dialyzed against two changes of cation exchange chromatography buffer A (20 mM MES, 50 mM NaCl, 1 mM EGTA, 1 mM $MgCl_2$, 2 mM DTT, 0.1 mM PMSF, pH 6.8) and loaded on an FPLC SP-Sepharose column. The proteins were eluted by a linear gradient of cation exchange chromatography buffer B (20 mM MES, 1 M NaCl, 1 mM EGTA, 1 mM $MgCl_2$, 2 mM DTT, 0.1 mM PMSF, pH 6.8). In the second purification step, the K32 breakdown products were removed by applying the gel filtration column Superdex G75 with PBS buffer (137 mM NaCl, 3 mM KCI, 10 mM Na_2HPO_4, 2 mM KH_2PO_4, pH 7.4 with 1 mM DTT).

NMR samples contained 0.9 to 1.5 mM [15]N- or ^{15}N/^{13}C-labeled protein in 95% H_2O/5% D_2O, 50 mM phosphate buffer pH 6.8 with 1 mM DTT.

Microtubule preparation: Porcine brain tubulin was purified as described (5,17) and incubated at concentrations higher than 200 µM in microtubule assembly buffer (100 mM Pipes pH 6.9, 1 mM EDTA, 1 mM $MgSO_4$, 1 mM DTT) in the presence of 1 mM GTP at 37° C for 5 minutes. After addition of 100 µM Paclitaxel (Sigma-Aldrich Chemie, Munich, Germany) the polymerisation was performed for 20 min at 37° C. The integrity of microtubules was checked by standard negative stain electron microscopy.

NMR Spectroscopy: NMR spectra were acquired at 5°C on a Bruker Avance 900 spectrometer equipped with a cryo-probe. Aggregation did not occur under these low temperature conditions. Three-dimensional (HA)CANNH and HNN experiments (4 scans, 1.2 s recovery delay) were collected to obtain sequence-specific assignments for the backbone of K32. NMR data were processed and analysed using NMRPipe (18) and Sparky 3 (T. D. Goddard and D. G. Kneller, SPARKY 3, University of California, San Francisco). Secondary shift values were calculated as the differences between measured C^α or C' (as obtained from a 3D HNCO experiment) chemical shifts and the empirical random coil value for the appropriate amino acid type (19,20). Using the program NMRView Version 5 (21), random-coil values for the primary sequence of K32 were generated. Random coil values for histidines, glutamates and aspartates were taken from Wishart et al. (22), as the chemical shifts of these residues are particularly sensitive to pH and the pH in the studies by Wishart et al. (23) (pH 5) is more similar to the one used here (pH 6.9). Furthermore, correction factors for residues occurring in the sequence before a proline residue were also taken from Wishart et al. (21)(24). To estimate the β-sheet propensity in contiguous segments of tau, the observed C^α and C' chemical shifts were normalized by the empirically determined secondary shift expected for that residue type in a fully β-sheet conformation (23), summed and normalized by the number of residues in the segment (25). To probe the structural consequences of binding of heparin to K32, C^α chemical shifts were measured using a 3D (HA)CANNH with a K32:heparin ratio of 4:1.

Titration of K32 with heparin was carried out with uniformly ^{15}N-labeled protein containing 0.15 mM K32 at pH 6.9 (100 mM Pipes, 1 mM EDTA, 1 mM MgSO$_4$, 1 mM dithiothreitol). Heparin (average molecular weight 3350, 5.8 dissaccharide subunits, charge/subunit -2.5, -0.31 z/Å) was from Sigma. Complex formation was monitored by recording two-dimensional ^{1}H-^{15}N HSQC spectra for increasing heparin concentrations (in mM): 0.0075, 0.015, 0.030, 0.074, 0.148, 0.291, 0.698, 1.304, and 2.308. As a control, an additional, single titration point was measured with a K32 solution of 67 μM with 17 μM heparin (heparin : K32 ratio of 1:4).

For tau-MT titrations NMR samples contained 136 μM (MT titration without sodium chloride) uniformly ^{15}N, ^{13}C-labeled and 200 μM uniformly ^{15}N-labeled K32 (titration with salt). The complex formation without salt was monitored at 5 °C for MT concentrations (αβ-tubulin dimers) of 15, 37.5 and 75 μM. The salt titration was performed at a MT concentration of 100 μM at 5 and 20 °C with salt concentrations 50, 100, 150, 200 and 300 mM sodium chloride.

One-bond N-H RDCs (D$_{NH}$) were determined by using the 2D inphase-antiphase (IPAP)-HSQC sequence (26) in 300 mM sodium chloride. D$_{NH}$ values were calculated as the difference between splittings measured in the isotropic phase and in a sample, in which K32 had been aligned in 8 mg/ml Pf1 bacteriophage (Asla, Riga, Latvia) (deuterium splitting 4.4 Hz). RDCs were not corrected for the negative gyromagnetic ratio of ^{15}N.

^{15}N R$_2$ and R$_{1\rho}$ relaxation rates were measured with pulse sequences based on Farrow et al. (27) at 5°C on a Bruker Avance 700 MHz spectrometer. For T$_{1\rho}$, where the expected range of values is small, only two relaxation periods with 20 and 320 ms were used (28). The spinlock frequency was 1.5 kHz. For R$_2$ measurements, the relaxation delays were set to 20, 100, 200 and 260 ms. Relaxation times were calculated from the ratio of the signal integrals (R$_{1\rho}$) or by fitting a exponential function to the decaying signal integrals (R$_2$). Heteronuclear NOE values are reported as the ratio of peak heights in paired spectra collected with and without an initial period (4 s) of proton saturation during the 5-s recycle delay. Errors were calculated on the basis of the S/N ratio for each residue.

RESULTS

Backbone assignment of K32 – NMR resonances in ^{1}H, ^{15}N-HSQC spectra of the construct K32, consisting of all four repeat motifs (R1-R4) of tau and the two flanking regions P2 and R' (Fig. 1), were recorded at 5 °C and pH 6.9. The resonances were sharp and showed only a limited dispersion of chemical shifts (supplemental Fig. S1), reflecting a high degree of backbone mobility and the lack of well-defined secondary and tertiary structure, in agreement with circular dichroism and Fourier transform-infrared spectroscopy measurements.

To enable the study of the structure and dynamics of tau, the assignment of the NMR resonances was required. K32 comprises 198 residues with a calculated mass of 21029 Da. Assignment of an intrinsically disordered protein of this size is not a trivial task due to the very limited chemical shift dispersion. Because of the strongly repetitive primary sequence (5 types of amino acids make up more than 50 % of the protein), resonances from residues located in the repeat domain were particularly affected by overlap. Moreover, the presence of 11 prolines, out of a total of 46 residues (almost 25 %) in the basic region P2, further complicated the assignment. These complications could be overcome by the use of high-resolution 3D (HA)CANNH and 3D HNN experiments (supplemental Fig. S2), in combination with the previously determined assignment of the isolated four repeats (further on referred to as construct K18) (29). No resonances for Ser^{198} and Ser^{199} were detectable. This could be due to enzymatic cleavage of these N-terminal residues or line broadening caused by the conformational flexibility of the N-terminus. In addition, residues Gly^{272}, Gly^{303}, Gly^{334}, Gly^{366} (surrounded by two glycines in the sequence motif PGGG, which occurs at the C-terminal end of each repeat region) and Gly^{304}/Gly^{335} could be identified in the spectra, but their unambiguous assignment was not possible due to high resonance overlap. In total, about 95% of K32 residues were assigned unambiguously (prolines excluded). The achieved assignment constitutes approximately 45% of the sequence of htau40, the longest tau isoform in the human brain (441 residues).

Comparison with the assignment of K18 showed that the positions of peaks belonging to the four repeats remained largely unaffected by the presence of additional flanking regions (data not shown). Moreover, with the exception of the ten N-terminal residues of K18, signal

intensities within the repeat domain were not significantly altered. This underlines the character of tau as an intrinsically disordered protein.
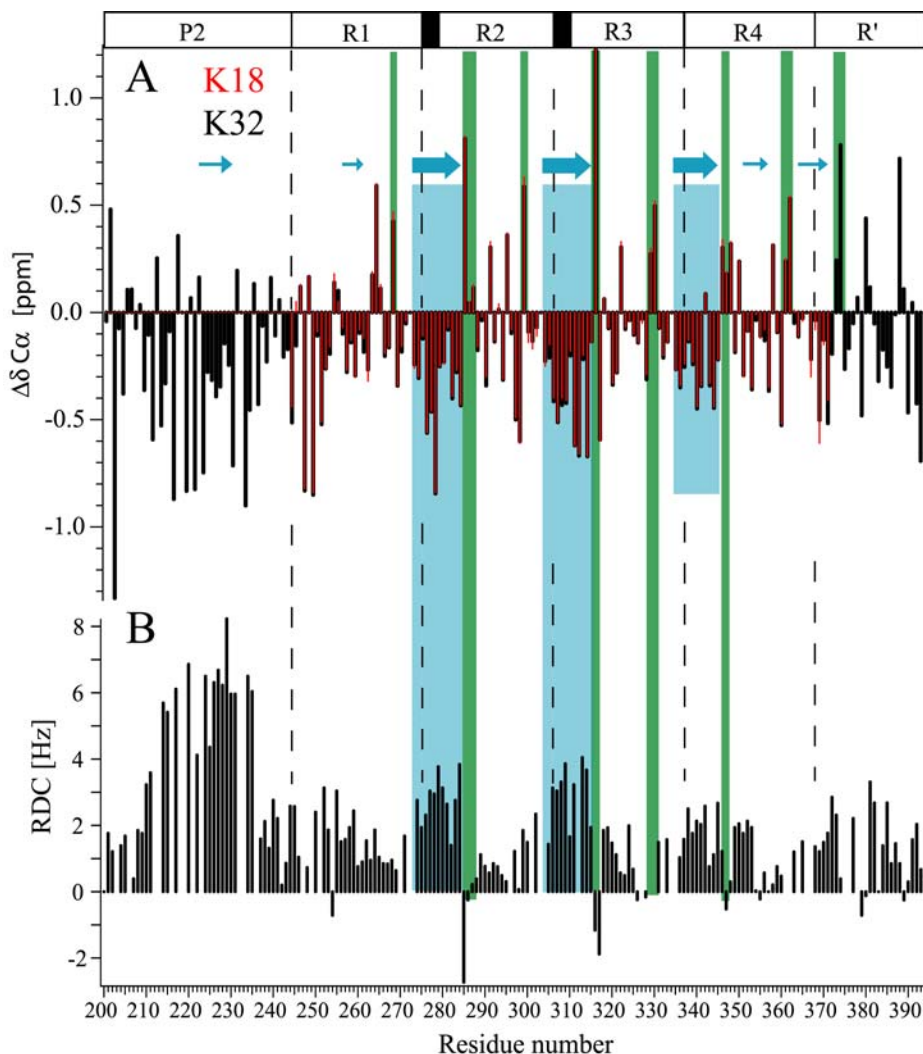
Figure 2

Fig. 2. Secondary structure propensity in K32. (A) Secondary chemical shifts of K32 (black) in comparison to K18 (red). (B) One-bond N-H RDCs. Regions of β-structure propensity (marked by arrows; bigger ones for stronger β-structure propensity) are identified by negative values extending over several residues, which are also highlighted by blue boxes. Green boxes indicate residues with turn character as suggested by positive secondary chemical shifts and negative RDCs. Repeat boundaries are indicated by vertical dashed lines.

Secondary structure propensity in K32 – NMR chemical shifts, in particular of C^α atoms, are very sensitive probes of secondary structure both in globular and intrinsically disordered proteins (23,30). These shifts show small but distinct deviations from random coil

values for K32 (Fig. 2). Several continuous stretches (containing 7-11 residues) with negative secondary chemical shifts were observed, in particular ^{274}Lys-Leu^{284} (R1/R2), ^{305}Ser-Asp^{315} (R2/R3) and ^{336}Gln-Asp^{345} (R3/R4). Continuous stretches of negative secondary chemical shifts indicate a propensity for β-structure. According to a quantitative analysis of the C$^{\alpha}$ secondary chemical shifts, the β-structure-like conformations are populated 22%, 25% and 19% of the time for residues ^{273}Gly-Leu^{284}, ^{304}Gly-Leu^{315} and ^{333}Gly-Asp^{345}, respectively. These elements of β-structure are located at the beginning of R2, R3 and R4. The corresponding region in repeat 1 does not show a strong propensity for β-structure, most likely due to the presence of proline residues Pro^{247} and Pro^{251}. Residual β-structure was also observed for residues ^{256}Val-Ser^{262} and ^{351}Gln-Leu^{357}, which are located roughly in the center of repeats R1 and R3. In R', the region downstream of the repeat motifs which shows only a weak sequence homology to the repeats, no strong tendency to populate either helical or β-structure was detected. On the other hand, quite large negative secondary chemical shifts were present in the proline-rich region P2, with ^{223}Pro-Arg^{230} forming a continuous stretch. The pattern of C' secondary chemical shifts was very similar to that observed for C$^{\alpha}$ (supplemental Fig. S3) indicating that either C$^{\alpha}$ or C' chemical shifts can be used for detection of transient structure in unfolded proteins. Comparison of K32 with K18, i.e. the construct in which the two flanking domains are missing, shows an almost identical pattern of secondary chemical shifts for residues Ala^{246}-Ile^{371} demonstrating that the flanking regions do not significantly affect the secondary structure propensity in the repeat domain of tau.

To obtain further insight into the secondary structure propensity, we measured one-bond N-H residual dipolar couplings (RDCs) in K32, which had been partially oriented in a Pf1 bacteriophage alignment medium. In an anisotropic environment, like magnetically oriented Pf1 phage, the large one-bond internuclear dipolar interactions no longer average to zero. In contrast to the bell-like smooth distribution of dipolar couplings, which is expected for random flight chains (31), a very specific distribution of positive and negative couplings was observed for K32 (Fig. 2B). In the region R1-R4 two stretches of high positive RDC values were evident: ^{274}KVQIINKKLDL^{284} and ^{306}VQIVYKPVD^{314}. These regions correlate well with the elements of high β-structure propensity at the beginning of R2 and R3, as identified by NMR secondary chemical shifts (Fig. 2). Note that the β-regions at the beginning of R2 and R3 encompass the two PHF-promoting hexapeptide motifs (*13*), whereas the β-region in R4 overlaps with the "module B" motif that determines the packing of tau into

twisted PHFs (32). The regions with large RDCs end with residues displaying negative RDCs: Lys[254], Ser[285], Asn[286], Ser[316], Lys[317], Gly[326], Ile[328], Lys[347], Gly[355], Arg[379], Glu[380] and Gly[389]. The same residues show positive secondary chemical shifts and we previously proposed that they are involved in turn structures (29). In the proline rich region P2, particularly large positive RDC values were found. The RDC magnitude for residues [214]Ser-Ser[235], a region in which 8 prolines are located, is about twice the size than in the rest of the protein.

In contrast to RDCs, which are influenced by both structure and dynamics, ^{15}N spin relaxation times can directly probe the motion of the protein backbone in a site-specific manner (33). ^{15}N $R_{1\rho}$ and R_2 spin relaxation rates are sensitive to motions of the backbone occurring on the pico- to nanosecond as well as micro- to millisecond time scale. The ^{15}N on-resonance $R_{1\rho}$ rates observed in K32 at 5 °C follow a smooth bell-like distribution with an average value of 3.7 Hz, underlining the character of tau as a natively unfolded protein. At the termini the relaxation rates are reduced, in agreement with an increased flexibility. Some residues such as ^{308}I-K^{317} show slightly higher $R_{1\rho}$ values, reporting on motional restrictions in these regions. On the other hand, heteronuclear steady-state ^{15}N NOE values were all close to zero (supplemental Fig. S4), indicating that abundant pico- to nanosecond dynamics occur along the polypeptide chain of K32 and fully formed regular secondary structure elements are not present. In contrast to $R_{1\rho}$ rates, R_2 spin relaxation times are also affected by chemical exchange. Thus, a difference plot between R_2 and $R_{1\rho}$ rates identifies residues that exchange between multiple conformations in solution. In K32, above average chemical exchange contributions are most evident for residues ^{201}Gly-Ser^{210}, Ser^{237}-Ser^{241}, Gly^{271}, ^{290}Lys-Gly^{292}, Lys^{298}, Gly^{302}, ^{309}Val-Lys^{321}, Gly^{323}, Gly^{333}, Asn^{368} and Phe^{378}.
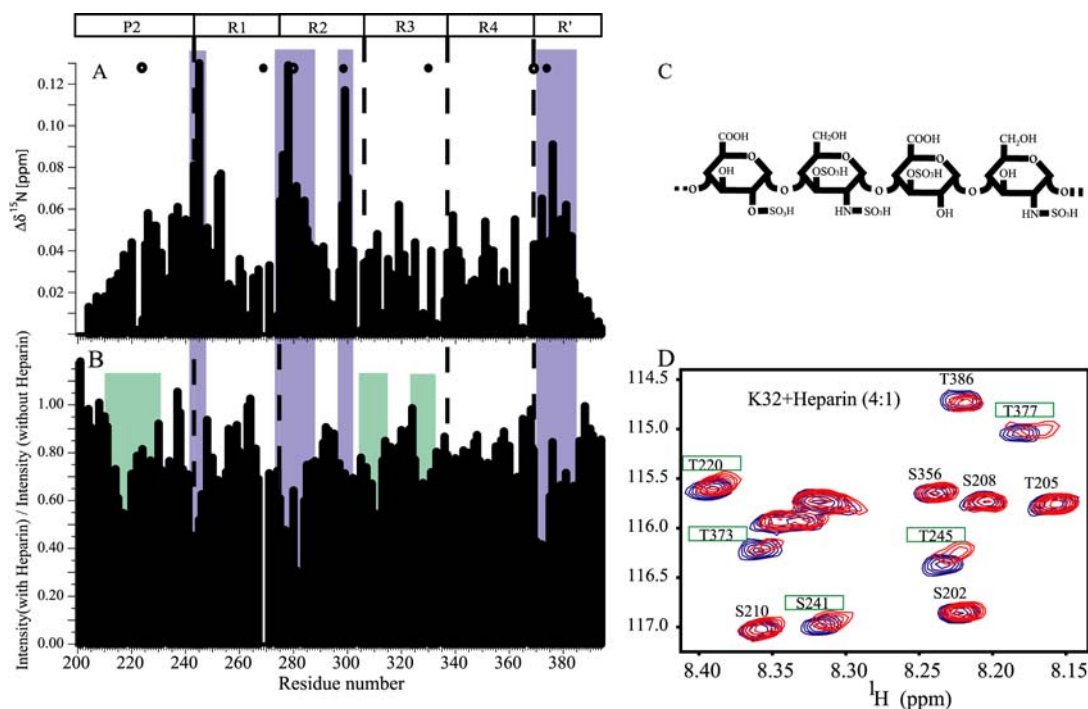
Figure 3

Fig.3. Tau- heparin interaction. (A) ^{15}N chemical shift differences, (B) Ratio of signal intensity of the protein in the heparin bound state and in solution without heparin. K32 (67 µM) with heparin (17 µM) at 5°C and pH 6.9. Blue boxes indicate the strongest binding sites identified on the basis of chemical shift differences. Green boxes highlight binding sites only visible by comparison of intensities. Lys-Lys dyads are indicated by open circles and Lys-His dyads by filled circles. (C) Structure of heparin. (D) Overlay of the [^{1}H, ^{15}N]-HSQC spectra of K32 without (blue) and with heparin (red). Some strongly shifting residues are highlighted with green boxes.

Interaction of tau-K32 with the PHF-inducer heparin – NMR signals of backbone amides constitute excellent probes of complex formation (34), providing maps of interaction interfaces. We were particularly interested in the interaction of tau with its physiological target microtubules, and with the polyanion heparin which induces the formation of Alzheimer-like PHFs. The binding of heparin to K32 was monitored by 2D ^{1}H-^{15}N HSQC spectra. This allows one to identify the residues which are important for the binding to polyanions. At high heparin concentrations chemical shift changes of some residues were accompanied by a decrease of the intensity of their signals, indicating chemical shift exchange intermediate on the NMR time scale. The chemical shift perturbation experiments showed the strongest shifts in the following regions (Fig. 3A): ^{217}T-L^{253} (most pronounced for ^{243}LQTA^{246}), ^{275}VQIINKKLDLSN^{286}, ^{298}KHV^{300}, ^{372}ETHKLTFRENAK^{383}. The chemical shift differences correlate very well with the signal intensity ratios (residue intensity of

spectrum with ligand: residue intensity of the unperturbed spectrum of unbound protein) of these spots (Fig. 3B). For strongly shifting residues the intensity ratios were generally below 70% of their original values. In the regions around K^{225}, T^{244}, N^{279} and T^{373} the signal intensity was reduced even down to about 40%, indicating that these residues are strongly involved in exchange processes intermediate on the NMR time scale. Besides the binding sites deduced from the chemical shift changes, ^{212}TPSLP^{216}, ^{306}VQIVYKPV^{313} and ^{325}LGNIHHK^{331} were identified as being important for the heparin-binding by exchange broadening (Fig. 3B). In most regions of K32 strongly affected by heparin, positively charged residues are present: Arg^{211}, Arg^{242}, Lys^{280}, Lys^{281}, Lys^{298}, His^{299}, Lys^{311}, His^{329}, His^{330}, Lys^{331}, His^{374}, Lys^{375} and Arg^{379}. This indicates that the binding to heparin is of electrostatic nature. Due to the presence of two lysine residues and one arginine, charge-charge interactions might also occur with the stretch ^{224}KKVAVVR^{230}, but in this case a hydrophobic contribution is possible as well.

To probe the structural impact of binding of heparin to tau, we determined the C^{α} secondary chemical shifts of tau in presence of heparin (tau:heparin 4:1). NMR chemical shifts can be measured with high accuracy such that even minute changes in secondary structure can be detected. However, the C^{α} chemical shifts of K32 with and without heparin were virtually identical (supplemental Fig. S5), indicating that heparin binding does not induce a significant increase in β-structure under these conditions.

Tau-microtubule interactions and the "jaws" model – The binding of K32 to MTs was characterized using NMR chemical shift perturbation as described (29), where two-dimensional ^{1}H-^{15}N HSQC spectra of K32 were recorded in the presence of increasing amounts of taxol-stabilized MTs. The influence of temperature was probed by performing NMR titrations at 5 and 20 °C. As shown previously, taxol stabilized microtubules are stable at 5°C for several hours, sufficient for the time-course of the NMR experiment, and that tau binds to them (29). The overall signal intensity in 2D ^{1}H-^{15}N HSQC experiments decreases rapidly at high MT concentrations, indicative of an increasing amount of K32 strongly bound to MTs. Due to very fast relaxation, the NMR signals of MT-bound K32 are no longer observable. Nevertheless, continuous chemical shift changes and additional exchange-induced broadening of specific regions of K32 were observed with increasing MT concentrations. It is immediately apparent from Fig. 4 that both the P2 and the R' flanking regions, as well as the

repeat domain itself strongly contribute to the interaction with microtubules. The strongest chemical shift changes, pointing to a strong involvement into the MT-binding process, were observed for residues ^{225}KVAVVRT^{231} in domain P2, ^{240}KSRLQTAPV^{248} in domain R1, ^{275}VQIINKKLDLS^{285}, ^{297}IKHV^{300} in R2, and ^{370}KIETHK^{375} in R'. The strong contribution of the flanking domains is consistent with their role as microtubule-targetting domains (jaws). In addition, however, other isolated residues were strongly perturbed in the presence of MTs. The location of the jaws of MT-binding became clearer, when the reduction in ^{1}H-^{15}N HSQC signal intensities caused by addition of MTs was taken into account (Fig. 4B). For most of the residues from L^{215} to K^{331}, the intensity was reduced to below 40% at a K32:MT ratio of ~2:1. Particular low signal intensities were observed for residues ^{222}EKKVAVVRT^{231}, ^{275}VQIINKKLDLSNVQSK^{290}, ^{306}VQIVYKPVDLSKVTSK^{321} and ^{377}TFREN^{381}. Both signal intensity ratios and chemical shift changes indicate that repeat R4 and the outermost residues in K32, ^{200}Gly-Ala^{209} and ^{386}Thr-Tyr^{394}, do not significantly bind to MTs.

At 20 °C, the overall magnitude of chemical shift changes induced by the presence of MTs was decreased (Fig. 4A). In particular, the chemical shift changes of residues ^{240}KSRLQTAPV^{248}, ^{275}VQIINKKLDLS^{285} and ^{370}KIETHK^{375} were less pronounced. In comparison to the results at 5 °C, large chemical shift changes remained for ^{225}KVAVVRT^{231} and ^{297}IKHV^{300}. Signal intensity ratios between the free and the MT-bound state of K32 were less informative than at 5 °C. Overall the reduction in signal intensity in the MT-bound state was lower than at 5 °C and signal intensities were more uniform along the whole K32 sequence (data not shown).
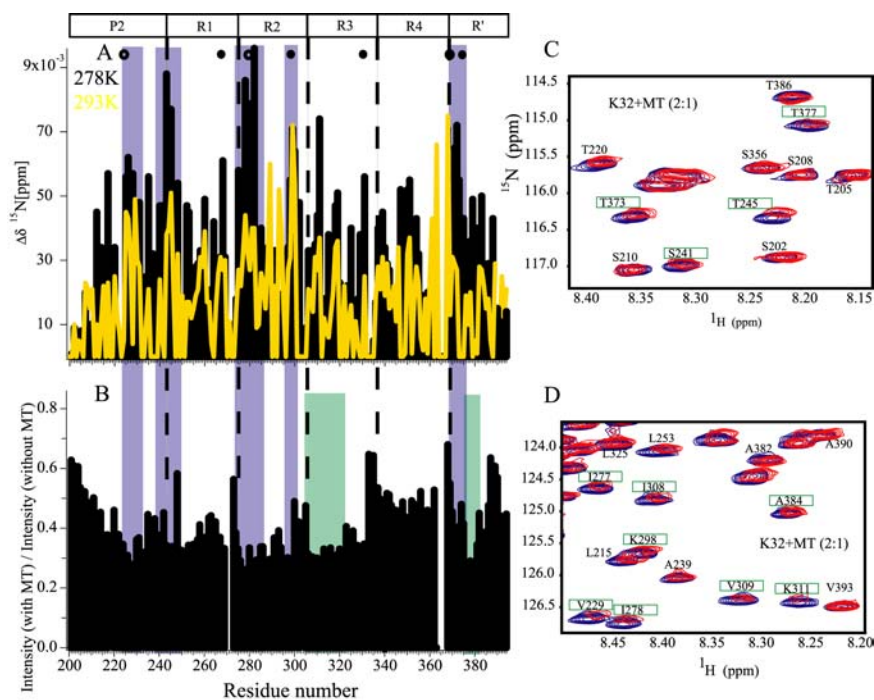
Figure 4

Fig.4. Binding of tau to microtubules. (A) ^{15}N chemical shift differences. K32 (136 µM) with MT (75 µM) at 5 °C (black bars) and K32 (200 µM) with MT (100 µM) at 20 °C (yellow curve). Lys-Lys dyads are indicated by open circles and Lys-His dyads by filled circles. (B) Ratio of intensities of signals of the protein in the MT-bound state and in the free state. Binding sites identified by reduced intensities are indicated by green boxes.(C) and (D) Overlay of the [^{1}H, ^{15}N]-HSQC spectra of K32 without (blue) and with MT (red). Some residues that experience a strong change in chemical shift or have a significantly reduced signal intensity are highlighted with green boxes.

The binding of tau to MTs occurs in two structurally and kinetically distinct steps, comprising a first binding phase with low stoichiometry but tight binding (K_d ~0.1 µM) and a second phase of weaker affinity but higher and nonsaturable stoichiometry (35). Solution NMR spectroscopy cannot detect tau molecules that are fully bound to MTs due to the large molecular weight of the complex and the accompanying fast signal decay. To test if the binding sites identified by the NMR titrations of K32 with MT are characteristic also for the strong primary binding of tau to MTs, we repeated the K32-MT titration at increased ionic strengths. Previous studies have shown that in the presence of sodium chloride the MT-binding strength of tau is reduced and the weaker, nonsaturable binding is strongly attenuated (36). In agreement with these results, the addition of 100 mM NaCl to the tau-MT solution (K32:MT = 2:1) increased the average ratio of signal intensities to about 80% (data not shown). A further increase to 300 and 600 mM NaCl raised the average signal intensity ratio

to a maximum value of 85%. This indicates that at 300 mM NaCl the off-rate is sufficiently increased, such that most K32 molecules now contribute to the NMR signal. Fig. 5A shows the chemical shift changes induced in K32 upon addition of MTs at 5 °C in the presence of 300 mM NaCl. The same residues that show large chemical shift changes without NaCl were also strongly affected at 300 mM NaCl. Due to the higher ionic strength, the interactions with the positively charged binding hot spots of K32 were weakened. The most strongly shifting resonances were now located in the stretch ^{225}KVAVVRT^{231} in the upstream flanking domain, suggesting that there is a hydrophobic MT-binding contribution originating from this region. In addition, signals from residues ^{337}VEVK^{340} and ^{350}VQSKI^{354} were more strongly affected than in the absence of sodium chloride. Taken together, the high-salt titration of K32 with MTs demonstrates that the binding profile identified by our NMR studies reports on the primary, strong binding of tau to microtubules. Note, that at 20 °C and in the presence of 300 mM NaCl no MT-binding was detected anymore, as judged by NMR chemical shifts and signal intensity ratios (data not shown).
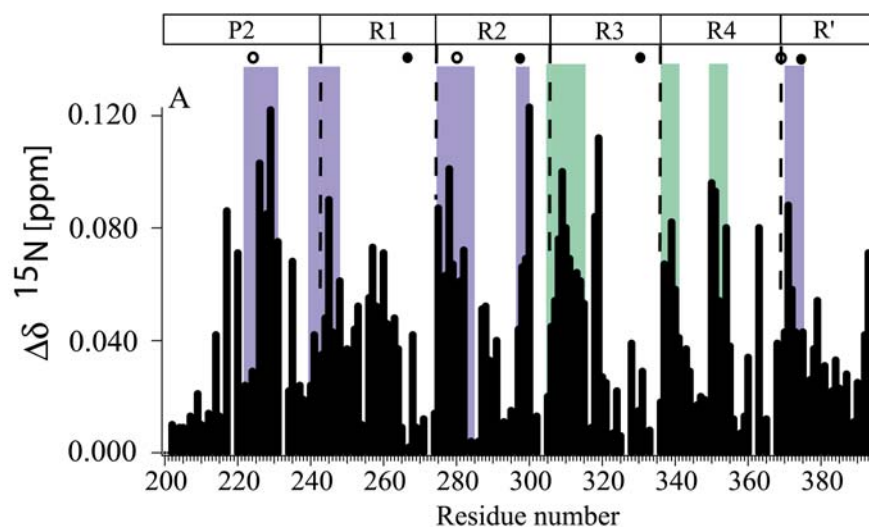
Figure 5

Fig. 5. Influence of ionic strength on tau-MT interaction.^{15}N chemical shift differences in K32 (200 μM) in the presence of 100 μM MT and 300 mM sodium chloride at 5 °C, pH 6.9. Binding sites observed in absence of salt are highlighted by blue boxes, whereas spots with stronger shifts in presence of sodium chloride are indicated by green boxes. Lys-Lys dyads are indicated by open circles and Lys-His by filled circles.

DISCUSSION

Tau is an interesting protein in several respects. As an intrinsically disordered protein it challenges the paradigm that a folded structure is necessary for function. Tau is a major microtubule-associated protein involved in the formation of axons and stabilization of microtubules as tracks for axonal transport. In the form of paired helical filaments, tau constitutes one of the hallmarks of Alzheimer's disease. Therefore, key questions concerning the structure and function of tau protein include the following: What are the binding sites and of tau to microtubules? How is the aggregation of tau into PHFs facilitated? To address some of these questions we investigated a 198-residue fragment (K32), comprising the four repeat motifs and the two flanking basic domains P2 and R' (Fig. 1). The repeat domain forms the core of the microtubule-binding domain and also the core of PHFs (3,9). However, maximal binding of tau to microtubules requires the two flanking regions P2 and R'. This was interpreted in terms of "jaws" of the tau-microtubule interaction (37).

Residual β-structure in repeat domain, random coil structure in flanking domains – Backbone resonance assignment of K32 is challenging, due to the small chemical shift dispersion, the repetitive nature of the repeat domain and the large number of prolines in domain P2. We were able to assign 95% of non-proline residues of K32, equivalent to 40% of all residues of full-length tau. This extends and is complementary to recent work of Lippens and coworkers who reported a partial assignment of tau (38). In this work, the unambiguously assigned residues (~30-40%) were mainly located in the acidic N-terminal header domain (residues 1-120) and in the C-terminal tail domain (residues 390-441), whereas only a few residues in the K32 region could be assigned unambiguously. Thus, our assignment of K32 was essential for the investigations reported here and will be useful for future studies of tau, such as the structural consequences of phosphorylation or the influence of FTDP-17 mutations.

Assignment of backbone chemical shifts in proteins gives access to detailed information on secondary structure. The difference between experimental chemical shifts and random coil values, which are specific for the sequence of the protein under investigation, allows site-specific detection of even small propensities for helical or β-structure. In K32, the

initial stretches of R2, R3, and R4 have the most pronounced β-sheet propensity, with average values of 22%, 24% and 19% for residues ^{273}Gly-Leu^{284}, ^{304}Gly-Leu^{315} and ^{333}Gly-Asp^{345}, respectively. This agrees well with other biochemical and structural studies showing that these regions are involved in the assembly of PHFs and their molecular packing (13,32). In addition, residues ^{224}Lys-Arg^{230}, ^{256}Val-Ser^{262}, ^{351}Gln-Leu^{357} and ^{363}Val-Glu^{372} preferentially populate extended structures (Fig. 2 and Fig. 7). No α-helical structure was detected in the repeat domain in the current study. This is contrary to other NMR studies of tau-derived fragments which were however performed in the presence of helix-inducing agents such as trifluoroethanol or SDS (39), (40), (41). In addition, no strong tendency to populate α-helical or β-structure was detected in the regions flanking the repeat domain. In the N-terminal P2 domain (S198-L243) this is most likely due to the large number of proline residues. This feature, combined with the presence of many residues with comparably large negative secondary chemical shifts (Fig. 2A), hints to a tendency for formation of a poly-proline helix in this region. Indeed, phosphorylation at residues ^{231}Thr, ^{235}Ser and ^{237}Ser seems to induce poly-proline helix conformations for residues ^{229}Val-Ser^{238} (42).

Residual dipolar couplings can be measured in a weakly aligned macromolecule, for which the large one-bond internuclear dipolar interactions no longer average to zero (43,44). RDCs are exquisitely sensitive to bond vector orientation and offer many new opportunities in NMR studies of proteins in solution. In highly dynamic systems, such as intrinsically disordered proteins, RDCs define local conformational behaviour as well as long-range order (45). In the repeat domain of tau, large RDCs correlate with regions that preferentially populate β-structure as indicated by NMR chemical shifts. In particular, in the two hexapeptide motifs at the beginning of repeats R2 and R3, which are crucial for aggregation of tau into PHFs, RDCs are about twice the size than in the rest of the repeat domain (Fig. 2B). The C-terminal ends of these regions are characterized by positive secondary chemical shifts and negative RDCs. This suggests the formation of turns at these sites. The largest positive RDCs were however observed for residues S214-S235 in the center of the proline-rich domain P2. For the analogous case of α-synuclein (the protein which irreversibly aggregates in the course of Parkinson's disease) we have shown previously that large RDCs in the C-terminal domain were due to an increased rigidity of the protein backbone, which was induced by long-range interactions (46). Thus, long-range interactions within K32 might be responsible for the increased magnitude of RDCs in the P2 domain. Alternatively, the

increased RDC magnitude of ^{214}Ser-Ser^{235} might be due to the large number of prolines in this region, which make the backbone more rigid. Comparison of chemical shifts and signal intensity ratios between K32 and K18 (the construct lacking the flanking P2 and R' domains), steady-state NOE values and ^{15}N transverse relaxation rates do not provide any evidence for a folding back of P2 or R' on the repeat region. This, however, does not exclude very transient interactions. To probe for transient long-range interactions several single-cysteine mutants of K32 would be required, to which a paramagnetic nitroxide radical can be specifically attached. This work is in progress. Noteworthy, the strongly increased RDC magnitude of ^{214}Ser-Ser^{235} is not accompanied by above average ^{15}N R$_{1\rho}$ rates or steady-state NOE values, indicating that motions in the nano- to microsecond time scale (toward which R$_{1\rho}$ rates are not sensitive) are reduced in this region.

To probe the intrinsic dynamics of tau, we measured ^{15}N transverse spin relaxation rates. Especially the glycine residues Gly^{201}, Gly^{271}, Gly^{292}, Gly^{302} Gly^{323} and Gly^{333} were strongly affected by chemical exchange (Fig. 6), suggesting that they function as flexible linkers between more rigid parts of the molecule. Gly^{271}, Gly^{302} and Gly^{333} are part of the PGGG motifs just upstream of the hexapeptides in the repeats. On the basis of secondary chemical shifts, we previously suggested that these residues form turns. In addition, pronounced chemical exchange was observed for the stretch ^{309}V-K^{321}, which encompasses the hexapeptide motif of R3. This region has the strongest propensity to form β-structure according to secondary chemical shifts, suggesting that the hexapeptide motif of R3 exchanges between a random coil conformation and β-structure in solution.
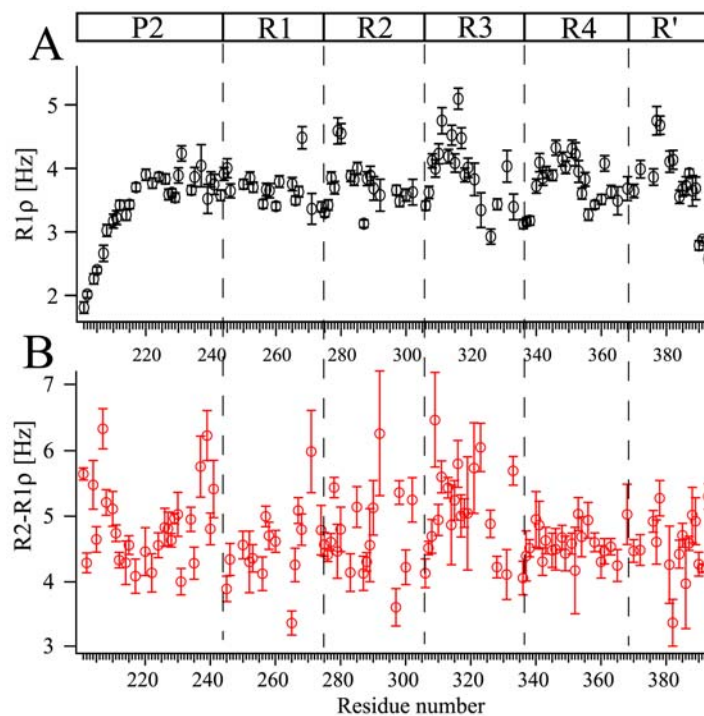
Figure 6

Fig. 6. Intrinsic dynamics of K32. (A) [15]N R2 (red) and R1ρ (black) spin relaxation rates of K32 (300 μM) at 5 °C.(B) Difference between R2 and R1ρ rates, which probes chemical exchange occurring on the micro- to millisecond time scale.

In the fibrillar state, the repeat domain of tau assumes the characteristic cross-β structure with a high content of β-strands (47-49). By NMR secondary chemical shifts we could clearly identify several regions in K32, primarily located in the repeat domain, with a pronounced tendency to populate β-structure. Therefore, it is tempting to speculate that these regions serve as seeds of aggregation. Dimer formation as the initial step of aggregation might be initiated be intermolecular contacts between the regions of high β-structure propensity. The intermolecular interaction will stabilize the β-structure and ultimately convert these parts into β-sheets in PHFs. This idea is supported by the prediction of aggregation hot spots using the program Zyggregator (50). It predicts three hot spots of aggregation for the tau peptide [265]N-E[338]: residues [280]K-V[287], [305]V-K[311], and [335]G-K[340]. In addition, based on experimental aggregation propensities derived from tau-related peptides, the two hexapeptides in the beginning of repeats R2 and R3 ([275]VQIINK[280] and [306]VQIVYK[311]), [226]VAVVR[230] and [392]IVYK[395] are predicted to have high aggregation propensities (51). These stretches correlate well with the regions of experimentally determined β-structure propensity.

Regions flanking the repeat domain are involved in binding to PHF-inducing polyanions –

Since tau is a highly soluble protein it normally resists aggregation; however, aggregation can be enhanced by different polyanions, presumably because they overcome the charge repulsion of the cationic tau molecules. Examples are sulfated glycosaminoglycans, heparin, RNA, and acidic peptides resembling the C-terminal domain of tubulin (52-54). It was therefore of interest to determine which residues in tau are involved in the interaction with microtubules and polyanions such as heparin.

Previously, we have shown that heparin binds to the hexapeptide motifs in the repeat domain, as well as to positively charged patches such as the KK motif at the beginning of R2 (^{280}KK^{281}), and the KH (^{267}KH^{268}, ^{298}KH^{299}) or HHK (^{329}HHK^{331}) motifs near the end of the repeats R1, R2 and R3. These studies were performed on K18, a 130-residue fragment of tau which just comprised the repeat domain (29). The present studies show that heparin binds to the same positively charged patches in the repeat domain, even when the two flanking regions P2 and R' are present. In particular, the fact that the hexapeptide VQIINK in the beginning of repeat 2, which is important for aggregation of tau into PHFs, preferentially populates β-structure and binds to the polyanion heparin also in K32, underlines the hypothesis that polyanions enhance aggregation of tau by reducing electrostatic repulsion between different tau molecules. In contrast to a recent study (55), we could not detect any increase in β-structure in tau upon addition of heparin. Our measurements were performed with a 4:1 ratio of tau:heparin, which was described as optimum for induction of tau aggregation by heparin (56). Besides a different tau:heparin ratio, Sibille et al. (53) used full-length tau and a specific low-molecular weight version of heparin.

Here we show that both flanking domains, P2 and R', are also involved in the interaction with heparin (Fig. 3). Most notably, ^{224}Lys-Arg^{230}, the only region outside of the repeat domain for which NMR secondary chemical shifts indicated a propensity to form β-structure, binds to heparin. Similar to the hot spot of aggregation in the beginning of repeat 2 (^{274}KVQINNK^{280}), the ^{224}KKVAVVR^{230} sequence contains two adjacent lysine residues separated from a third positively charged residue (R^{230}) by several uncharged amino acids. Therefore, the mechanism of interaction with heparin might be similar and regions outside of the repeat domain may play a role in aggregation of tau into PHFs.

The 'jaws' of the tau-microtubule interaction – The microtubule-associated protein tau is a critical regulator of diverse microtubule functions (5,57,58). The repeat domain with its four repeats is essential for microtubule assembly, however, in the absence of the two flanking regions P2 and R', the repeat domain binds only weakly to microtubules. The flanking domains, on the other hand, bind to microtubules even in the absence of the repeats. This has led to the proposition of the 'jaws' model of tau whereby the regions flanking the repeats are considered as targeting domains, responsible for positioning tau on the microtubule surface, and the repeats which act as catalytic domains for microtubule assembly (5,6). The aim of the current study was to provide a structural view of the residues located in the flanking regions, which are important for binding of tau to microtubules. The 198-residue fragment K32, which consists of the repeats and the flanking domains P2 and R', is well suited for this aim, as it captures the full microtubule-binding and assembly activity of the longest tau isoform, htau40, in the human brain.

We used solution-state NMR to identify which residues contribute to the 'jaws' of the tau-microtubule interaction. Solution-state NMR can only observe molecules that are rapidly tumbling in solution, excluding the direct observation of tau molecules completely bound to MTs. Nevertheless, information about the residues important for binding to microtubules can be obtained when the exchange between the fully bound form and the free state is sufficiently fast, such that conformational characteristics of the bound state are transferred to the soluble, unbound protein. Here, we investigated changes in NMR chemical shifts and signal intensity ratios for increasing amounts of MTs. The observed signal is an average of the resonances originating from the unbound and bound forms of tau. The magnitude of chemical shift changes will depend on the chemical environment in the bound state and the concentration of the bound species. The latter depends on the rates with which tau binds and detaches from MTs. In addition, residues that are involved in the binding process will be affected by conformational exchange, potentially affecting the NMR signal intensity of these residues. Therefore, we have two tools available, NMR chemical shift and signal intensity changes that allow identification of the binding sites of tau to MTs. These two tools show that the binding behaviour of tau to heparin and taxol-stabilized MTs is similar (Fig. 4 and Fig. 7). Within the repeats the same residues that were identified as binding sites on the basis of a NMR-titration of K18 (the construct comprising only the repeats) with MTs (29) are important for binding of

K32 to MTs. In particular, residues ^{275}VQIINKKLDLS^{285} (comprising the hexapeptide in the beginning of repeat 2) show large chemical shift changes, in agreement with biochemical analyses which reported a strong reduction of MT binding affinity upon mutation of K^{274} or K^{281} to alanine (59). In addition, clusters of positive charges upstream of the PGGG motifs at the end of repeats 1, 2 and 3 contribute to the MT-binding, thereby providing attachment points for these repeats to tubulin. Repeat 4, on the other hand, does not significantly contribute to MT-binding (Fig. 4).

For high-affinity binding of tau to MTs, the regions flanking the repeats are required (5). Our NMR studies show that ^{225}KVAVVRT^{231} and ^{240}KSRLQTAPV^{248} in the proline-rich domain, and ^{370}KIETHKLTFREN^{381} in the region downstream of the repeats are binding sites for both heparin and microtubules (Fig. 7). In the proline-rich domain the most strongly affected residues are ^{226}VAV^{228} and ^{243}LQT^{245}. In agreement with the NMR data, deletion analysis mapped the microtubule-binding activity of the proline-rich region to residues K^{224}-N^{255} and in particular to the stretch ^{225}KVAVVRT^{231}. Moreover, site-directed mutagenesis indicated that K^{224}, K^{225} and R^{230} are important for MT-binding and –assembly (60). It is noteworthy that the region ^{225}KVAVVRT^{231} is conserved between tau and two other microtubule-associated proteins MAP-2 and MAP-4 (60). Interestingly, the two motifs 225-231 and 240-248 flank the motif ^{231}TPPKSP^{236} which contains two major phosphorylation sites (by GSK3β and/or cdk5) and the residue P^{232} whose isomerization by Pin-1 is important for the accessibility to phosphatases (16).
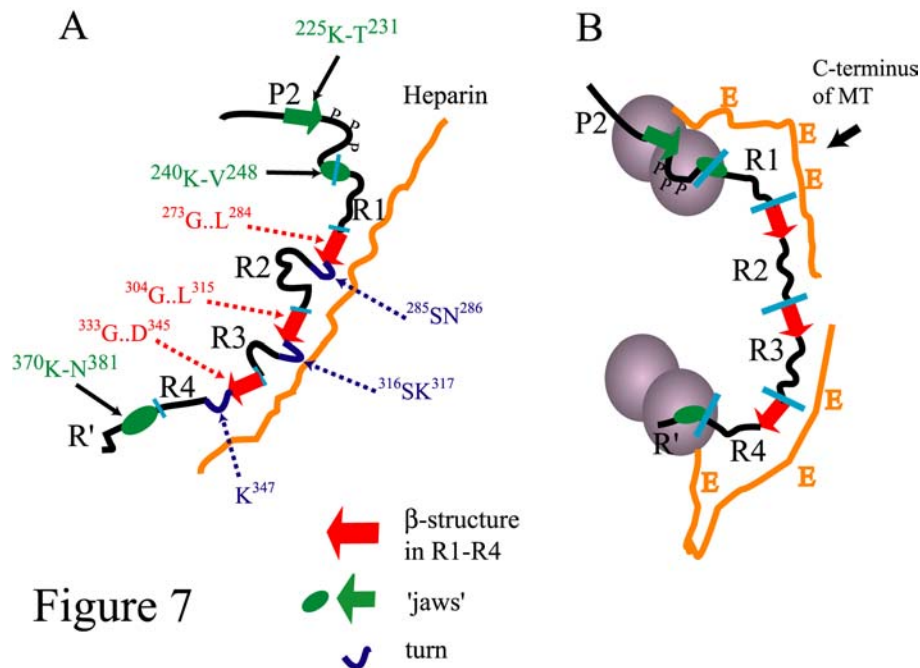
Fig.7. Transient structure and microtubules and polyanion-binding properties of K32. (A) Regions that transiently populate β-structure are indicated by red (within the repeat region) and green (in the flanking domains) arrows. Turns are highlighted in blue. Domain boundaries are marked by light blue bars. The interaction with heparin is depicted schematically. (B) Tau binds to the Glu rich C-terminus of MTs via specific (green ellipses and green arrow) regions located in the P2 and R' regions of tau. The negative charges of the Glu residues function like polyanions and shield repulsive positive charges.

Over 30 phosphorylation sites have been identified in tau, for many of which the level of modification is elevated in Alzheimer's disease (61-63). Prominent sites are located in the flanking domains, e.g. Ser^{199}, Ser^{202}, Thr^{205}, Thr^{212}, Ser^{214}, Thr^{231}, Ser^{235} before the repeats, Ser^{396}, Ser^{404} and others after the repeats (not contained in K32). The major sites within the repeats are located in the KXGS motifs, i.e. Ser^{262}, Ser^{293}, Ser^{324} and Ser^{356}. These sites are phosphorylated by the kinase MARK which results in the detachment of tau from microtubules (64). Ser^{262}, Ser^{293} and Ser^{324} are separated by only four residues from the charged patches at the C-terminal end of repeat 1, 2 and 3, and Thr^{231} is right in the middle of the MT-binding region in the proline-rich domain. Thus, phosphorylation might lead to intramolecular charge neutralization of the positive spots required for MT-binding. The required bending in the backbone would easily be possible due to the high conformational flexibility of tau. Alternatively or in combination, phosphorylation can induce other conformational changes, such as the stabilization of a polyproline II helix. Indeed, CD and NMR data on peptides derived from the proline-rich region of tau suggest that phosphorylation induces a polyproline II helix for residues Val^{229}-Ser^{238} (42). Residues

Val^{229}-Ser^{238} are located between the two MT-binding elements of the proline-rich domain (^{225}KVAVVRT^{231} and ^{240}KSRLQTAPV^{248}) and include the Pin1 target site of proline isomerization that is a major regulator of tau's conformation. Thus, stabilization of a polyproline II helix in this region would increase the distance between the two MT-binding sites, such that they no longer fit to their interaction sites on the MT surface.

In conclusion, we have provided a detailed view of the structural properties and of the sites of interaction with microtubules and polyanions of a fragment of tau, which contains the full microtubule-binding and assembly activity of the longest tau isoform, htau40, in the human brain. It will be interesting to see how genetic mutations and phosphorylation affect the hot spots of aggregation and the 'jaws' of the tau-microtubule interaction. These studies are currently in progress.

FOOTNOTES

The abbreviations used are: AD = Alzheimer's disease; MT = microtubule; PHF = paired helical filament; MAP = microtubule-associated protein;

REFERENCES

1.   Garcia, M. L., and Cleveland, D. V. (2001) *Curr. Opin. Cell Biol.* 13, 41-48

2.   Cassimeris, L., and Spittle, C. (2001) *Int. Rev. Cyt., Vol 210* 210, 163-226

3.   Lee, G., Cowan, N., and Kirschner, M. (1988) *Science* 239, 285-288

4.   Goedert, M., Spillantini, M. G., Jakes, R., Rutherford, D., and Crowther, R. A. (1989) *Neuron* 3, 519-526

5.   Gustke, N., Trinczek, B., Biernat, J., Mandelkow, E. M., and Mandelkow, E. (1994) *Biochemistry* 33, 9511-9522

6.   Preuss, U., Biernat, J., Mandelkow, E. M., and Mandelkow, E. (1997) *J. Cell Sci.* 110, 789-800

7.   Lee, V. M. Y., Goedert, M., and Trojanowski, J. Q. (2001) *Ann. Rev. Neurosci.* 24, 1121-1159

8.   Delacourte, A., and Buee, L. (2000) *Curr. Opin. Neurol.* 13, 371-376

9.   Wischik, C. M., Novak, M., Thogersen, H. C., Edwards, P. C., Runswick, M. J., Jakes, R., Walker, J. E., Milstein, C., Roth, M., and Klug, A. (1988) *Proc. Natl. Acad. Sci. U.S.A.* 85, 4506-4510

10.   Jakes, R., Novak, M., Davison, M., and Wischik, C. M. (1991) *EMBO J.* 10, 2725-2729

11.   von Bergen, M., Barghorn, S., Muller, S. A., Pickhardt, M., Biernat, J., Mandelkow, E. M., Davies, P., Aebi, U., and Mandelkow, E. (2006) *Biochemistry* 45, 6446-6457

12.   Wille, H., Drewes, G., Biernat, J., Mandelkow, E. M., and Mandelkow, E. (1992) *J. Cell Biol.* 118, 573-584

13.   von Bergen, M., Friedhoff, P., Biernat, J., Heberle, J., Mandelkow, E. M., and Mandelkow, E. (2000) *Mol. Biol. Cell* 11, 363A-363A

14.   von Bergen, M., Barghorn, S., Li, L., Marx, A., Biernat, J., Mandelkow, E. M., and Mandelkow, E. (2001) *J. Biol. Chem.* 276, 48165-48174

15.   Biernat, J., Gustke, N., Drewes, G., Mandelkow, E. M., and Mandelkow, E. (1993) *Neuron* 11, 153-163

16.   Mandelkow, E. M., Herrmann, M., and Ruhl, U. (1985) *J. Mol. Biol.* 185, 311-327

17.   Delaglio, F., Grzesiek, S., Vuister, G. W., Zhu, G., Pfeifer, J., and Bax, A. (1995) *J. Biomol. NMR* 6, 277-293

18.   Schwarzinger, S., Kroon, G. J. A., Foss, T. R., Wright, P. E., and Dyson, H. J. (2000) *J. Biomol. NMR* 18, 43-48

19.   Schwarzinger, S., Kroon, G. J. A., Foss, T. R., Chung, J., Wright, P. E., and Dyson, H. J. (2001) *J. Am. Chem. Soc.* 123, 2970-2978

20.   Johnson, B. A., and Blevins, R. A. (1994) *J. Biomol. NMR* 4, 603-614

21. Wishart, D. S., and Sykes, B. D. (1994) *Nucl. Magn. Reson., Pt C* 239, 363-392

22. Wishart, D. S., and Sykes, B. D. (1994) *Methods Enzymol.* 239, 363-392

23. Bussell, R., and Eliezer, D. (2001) *J. Biol. Chem.* 276, 45996-46003

24. Ottiger, M., Delaglio, F., and Bax, A. (1998) *J. Magn. Reson.* 131, 373-378

25. Farrow, N. A., Muhandiram, R., Singer, A. U., Pascal, S. M., Kay, C. M., Gish, G., Shoelson, S. E., Pawson, T., Formankay, J. D., and Kay, L. E. (1994) *Biochemistry* 33, 5984-6003

26. Jones, J. A., Hodgkinson, P., Barker, A.L., and Hore, P.J. (1996) *J. Magn. Reson.* 113, 25-34

27. Mukrasch, M. D., Biernat, J., von Bergen, M., Griesinger, C., Mandelkow, E., and Zweckstetter, M. (2005) *J. Biol. Chem.* 280, 24978-24986

28. Eliezer, D., Yao, J., Dyson, H. J., and Wright, P. E. (1998) *Nat. Struct. Biol.* 5, 148-155

29. Louhivuori, M., Paakkonen, K., Fredriksson, K., Permi, P., Lounila, J., and Annila, A. (2003) *J. Am. Chem. Soc.* 125, 15647-15650

30. DeTure, M. A., Di Noto, L., and Purich, D. L. (2002) *J. Biol. Chem.* 277, 34755-34759

31. Palmer, A. G., 3rd, Kroenke, C. D., and Loria, J. P. (2001) *Methods Enzymol.* 339, 204-238

32. Craik, D. J., and Wilce, J. A. (1997) *Methods Mol. Biol.* 60, 195-232

33. Ackmann, M., Wiech, H., and Mandelkow, E. (2000) *J. Biol. Chem.* 275, 30335-30343

34. Fischer, D., Mukrasch, D. M., von Bergen, M., Klos-Witkowska, A., Biernat, J., Griesinger, C., Mandelkow, E., Zweckstetter, M. (2006) *Biochemistry*

35. Preuss, U., Biernat, J., Mandelkow, E. M., and Mandelkow, E. (1997) *J. Cell. Sci.* 110 (Pt 6), 789-800

36. Smet, C., Leroy, A., Sillen, A., Wieruszeski, J. M., Landrieu, I., and Lippens, G. (2004) *Chembiochem* 5, 1639-1646

37. Eliezer, D., Barre, P., Kobaslija, M., Chan, D., Li, X. H., and Heend, L. (2005) *Biochemistry* 44, 1026-1036

38. Tokimasa, M., Minoura, K., Hiraoka, S., Tomoo, K., Sumida, M., Taniguchi, T., and Ishida, T. (2005) *FEBS Lett.* 579, 3481-3486

39. Barre, P., and Eliezer, D. (2006) *J. Mol. Biol.* 362, 312-326

40. Bielska, A. A., and Zondlo, N. J. (2006) *Biochemistry* 45, 5527-5537

41. Tjandra, N., and Bax, A. (1997) *Science* 278, 1111-1114

42. Tolman, J. R., Flanagan, J. M., Kennedy, M. A., and Prestegard, J. H. (1995) *Proc. Natl. Acad. Sci. U.S.A.* 92, 9279-9283

43. Bertoncini, C. W., Jung, Y. S., Fernandez, C. O., Hoyer, W., Griesinger, C., Jovin, T. M., and Zweckstetter, M. (2005) *Proc. Natl. Acad. Sci. U.S.A.* 102, 1430-1435

44.   Bernado, P., Bertoncini, C. W., Griesinger, C., Zweckstetter, M., and Blackledge, M. (2005) *J. Am. Chem. Soc.* 127, 17968-17969

45.   von Bergen, M., Barghorn, S., Biernat, J., Mandelkow, E. M., and Mandelkow, E. (2005) *Biochim. Biophys. Acta* 1739, 158-166

46.   Inouye, H., Sharma, D., Goux, W. J., and Kirschner, D. A. (2006) *Biophys. J.* 90, 1774-1789

47.   Berriman, J., Serpell, L. C., Oberg, K. A., Fink, A. L., Goedert, M., and Crowther, R. A. (2003) *Proc. Natl. Acad. Sci. U. S. A.* 100, 9034-9038

48.   Pawar, A. P., DuBay, K. F., Zurdo, J., Chiti, F., Vendruscolo, M., and Dobson, C. M. (2005) *J. Mol. Biol.* 350, 379-392

49.   Rojas Quijano, F. A., Morrow, D., Wise, B. M., Brancia, F. L., and Goux, W. J. (2006) *Biochemistry* 45, 4638-4652

50.   Goedert, M., Jakes, R., Spillantini, M. G., Hasegawa, M., Smith, M. J., and Crowther, R. A. (1996) *Nature* 383, 550-553

51.   Perez, M., Valpuesta, J. M., Medina, M., deGarcini, E. M., and Avila, J. (1996) *J. Neurochem.* 67, 1183-1190

52.   Kampers, T., Friedhoff, P., Biernat, J., and Mandelkow, E. M. (1996) FEBS *Lett.* 399, 344-349

53.   Sibille, N., Sillen, A., Leroy, A., Wieruszeski, J. M., Mulloy, B., Landrieu, I., and Lippens, G. (2006) *Biochemistry* 45, 12560-12572

54.   Barghorn, S., Davies, P., and Mandelkow, E. (2004) *Biochemistry* 43, 1694-1703

55.   Butner, K. A., and Kirschner, M. W. (1991) *J. Cell Biol.* 115, 717-730

56.   Goode, B. L., and Feinstein, S. C. (1994) *J. Cell Biol.* 124, 769-782

57.   Panda, D., Goode, B. L., Feinstein, S. C., and Wilson, L. (1995) *Biochemistry* 34, 11117-11127

58.   Goode, B. L., Denis, P. E., Panda, D., Radeke, M. J., Miller, H. P., Wilson, L., and Feinstein, S. C. (1997) *Mol. Biol. Cell* 8, 353-365

59.   Smet, C., Sambo, A. V., Wieruszeski, J. M., Leroy, A., Landrieu, I., Buee, L., and Lippens, G. (2004) *Biochemistry* 43, 2032-2040

60.   Landrieu, I., Lacosse, L., Leroy, A., Wieruszeski, J. M., Trivelli, X., Sillen, A., Sibille, N., Schwalbe, H., Saxena, K., Langer, T., and Lippens, G. (2006) *J. Am. Chem. Soc.* 128, 3575-3583

61.   Hanger, D. P., Betts, J. C., Loviny, T. L. F., Blackstock, W. P., and Anderton, B. H. (1998) *J. Neurochem.* 71, 2465-2476

62.   Morishimakawashima, M., Hasegawa, M., Takio, K., Suzuki, M., Yoshida, H., Titani, K., and Ihara, Y. (1995) *J. Biol. Chem.* 270, 823-829

63.   Drewes, G., Ebneth, A., Preuss, U., Mandelkow, E. M., and Mandelkow, E. (1997) *Cell* 89, 297-308

SUPPLEMENTARY MATERIAL
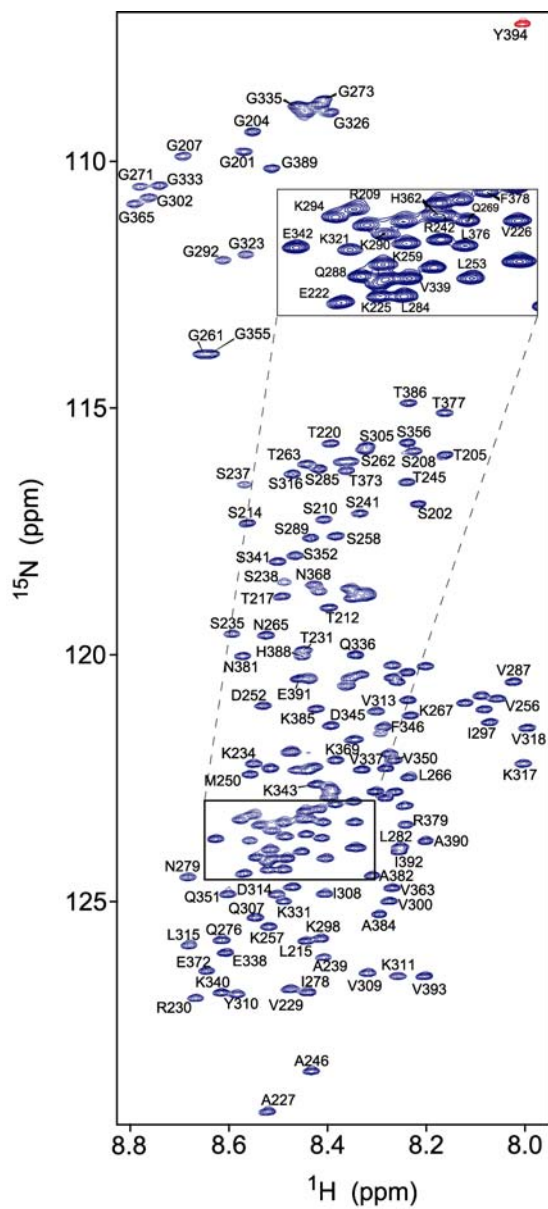
Figure 1 (suppl.)

Fig. S1. 900 MHz [^{1}H, ^{15}N]-HSQC spectrum of K32. Resonance assignments are indicated with residue numbers. One region with particularly strongly overlapping resonances was magnified and is shown in a separate box.
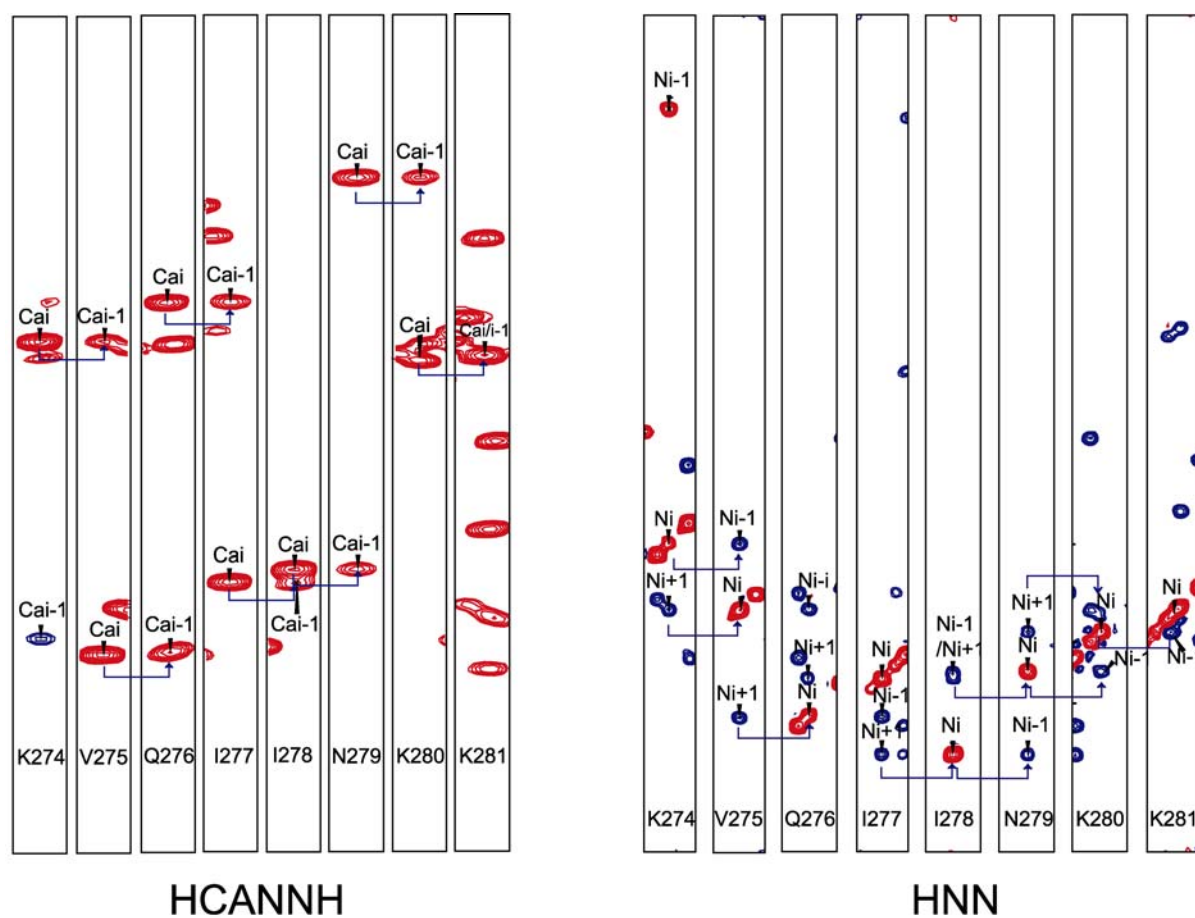
Figure 2 (suppl.)

Fig. S2. Selected strips of the 3D HCANNH and 3D HNN spectra highlighting the sequential connectivities observed in the region K274-K281. Intra- and interresidual C^{α} and N resonances are indicated.
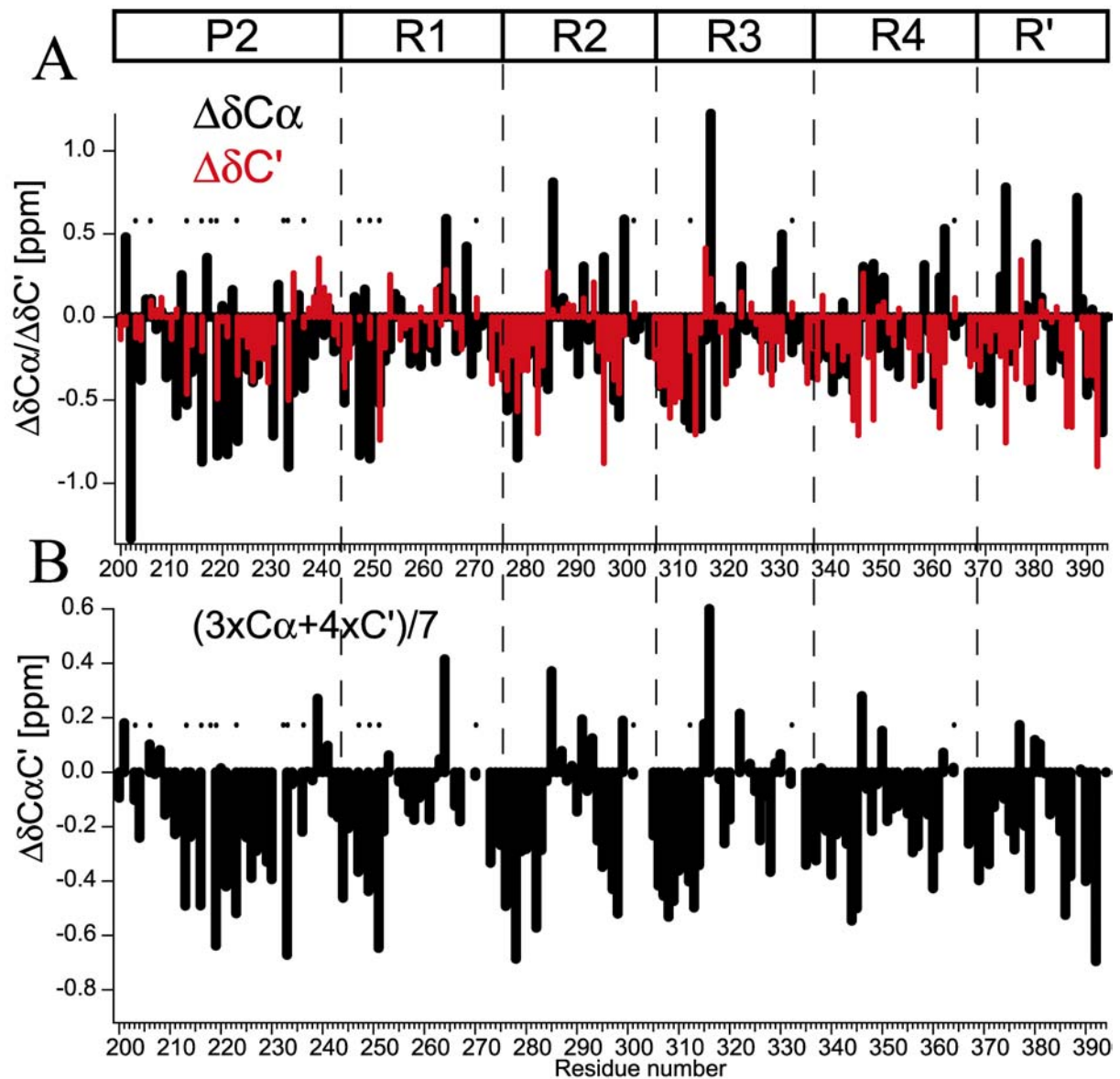
Fig. S3. Cᵅ and C' secondary chemical shifts. (A) C^α secondary chemical shifts (black) are compared to C' secondary chemical shifts (red). The two patterns are very similar, indicating that either C^α or C' chemical shifts can be used for detection of transient structure in unfolded proteins.(B) Average C^α/C' secondary chemical shifts calculated according to $(3C^\alpha+4C')/7$. Filled black circles indicate occurrence of proline residues.
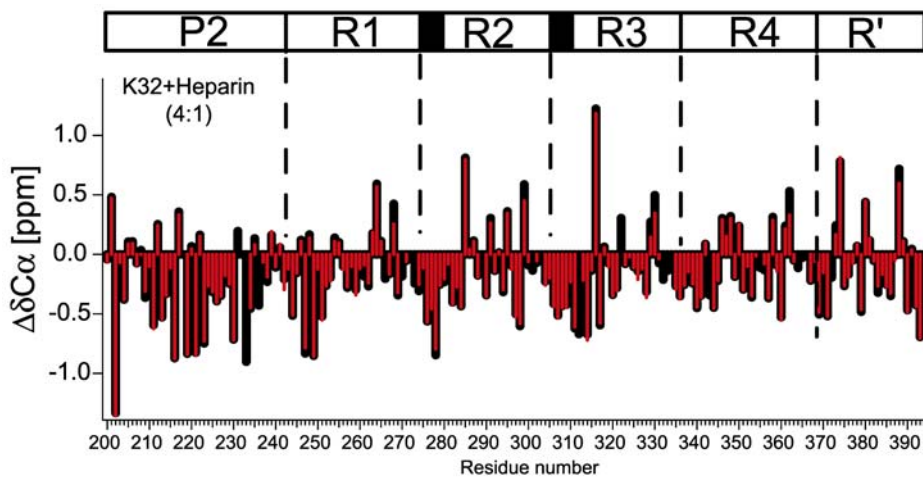
Figure 4 (suppl.)

Fig. S4. C^{α} secondary chemical shifts of K32 (100 μM) in the unbound state (black) and in the presence of heparin (25 μM) at 5 °C. The two patterns are almost identical. Thus, no change in secondary structure upon binding to the aggregation inducer heparin could be observed.
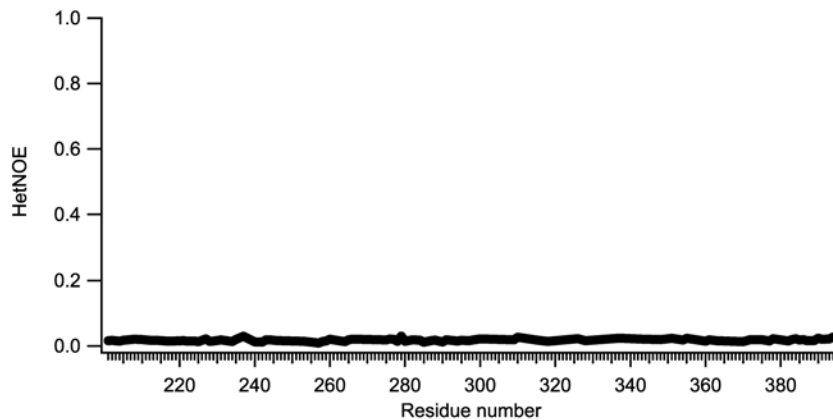
Figure 5 (suppl.)

Fig. S5. ^{1}H-^{15}N heteronuclear NOE values observed in K32 at a ^{1}H frequency of 800 MHz. All values were below 5%.

Residue number	Aa type	^{1}H [ppm]	^{15}N [ppm]	^{13}C [ppm]	C' [ppm]
200	pro			63.789	177.527
201	gly	8.569	109.806	44.9805	173.925
202	ser	8.216	116.945	56.568	
203	pro			63.7555	177.538
204	gly	8.551	109.403	44.991	174.043
205	thr	8.161	115.951	59.906	
206	pro			63.928	177.778
207	gly	8.693	109.895	45.257	174.483
208	ser	8.224	115.875	58.6355	175.006
209	arg	8.553	123.252	56.1675	176.568
210	ser	8.407	117.258	58.4855	174.569
211	arg	8.536	123.454	55.9775	176.356
212	thr	8.397	119.048	60.0525	
213	pro			63.2125	176.818
214	ser	8.561	117.332	58.259	174.153
215	leu	8.443	125.804	53.0115	
216	pro			62.8195	176.816
217	thr	8.491	118.818	60.157	
218	pro				
219	pro			62.8475	177.04
220	thr	8.393	115.718	62.027	174.996
221	arg	8.521	124.186	55.6955	175.924
222	glu	8.569	124.438	54.363	
223	pro			62.8935	176.763
224	lys	8.515	122.303	56.342	176.691
225	lys	8.519	124.361	56.164	176.459
226	val	8.344	123.397	62.028	175.705
227	ala	8.521	129.265	52.244	177.474
228	val	8.345	121.723	62.315	176.15
229	val	8.476	126.784	62.275	175.978
230	arg	8.667	126.964	55.7065	176.127
231	thr	8.448	119.91	59.9945	
232	pro				
233	pro			62.7095	176.721
234	lys	8.55	122.212	56.1955	176.694

235 ser	8.594	119.579	56.533	
236 pro			63.322	177.198
237 ser	8.569	116.554	58.547	174.941
238 ser	8.487	118.529	58.4005	174.58
239 ala	8.408	126.137	53.0015	178.172
240 lys	8.332	120.404	56.582	177.096
241 ser	8.334	117.135	58.638	174.837
242 arg	8.438	123.331	56.303	176.364
243 leu	8.243	123.062	55.228	177.4
244 gln	8.473	121.966	55.6965	176.028
245 thr	8.239	116.503	61.725	173.935
246 ala	8.432	128.444	50.6205	
247 pro			62.719	176.683
248 val	8.391	122.774	59.966	
249 pro			62.9295	176.623
250 met	8.556	122.425	53.191	
251 pro			63.1185	176.311
252 asp	8.53	121.037	53.9375	176.616
253 leu	8.403	124.13	55.4165	177.854
254 lys	8.359	120.629	56.8495	176.6
255 asn	8.325	118.807	53.2015	175.184
256 val	8.056	120.893	62.6305	176.373
257 lys	8.518	125.517	56.3315	176.763
258 ser	8.383	117.603	58.3995	174.499
259 lys	8.516	123.954	56.3445	176.717
260 ile	8.282	122.907	61.5035	176.918
261 gly	8.651	113.907	45.1155	174.183
262 ser	8.322	115.843	58.363	175.356
263 thr	8.442	116.14	62.235	174.923
264 glu	8.444	123.178	56.991	176.283
265 asn	8.524	119.612	53.392	175.37
266 leu	8.235	122.492	55.3865	177.567
267 lys	8.231	121.235	56.4865	176.417
268 his	8.268	120.214	55.924	
269 gln	8.409	123.398	53.358	
270 pro			63.5565	177.744
271 gly	8.78	110.515	45.358	
272 gly				

273 gly	8.408	108.75	45.0365	174.03
274 lys	8.237	120.922	56.194	176.747
275 val	8.303	122.773	62.4075	176.004
276 gln	8.614	125.788	55.4385	175.571
277 ile	8.47	124.71	60.997	176.129
278 ile	8.44	126.847	60.7355	175.714
279 asn	8.683	124.512	52.958	175.07
280 lys	8.49	123.408	56.598	176.47
281 lys	8.396	122.889	56.5095	176.551
282 leu	8.252	123.905	55.0485	176.772
283 asp	8.428	122.289	53.9205	176.509
284 leu	8.489	124.359	55.2065	177.969
285 ser	8.417	116.238	59.4805	174.632
286 asn	8.354	120.482	53.2945	175.355
287 val	8.022	120.55	62.8945	176.511
288 gln	8.544	124.106	55.944	176.267
289 ser	8.434	117.635	58.563	174.769
290 lys	8.514	123.566	56.4285	176.733
291 cys	8.44	120.491	58.9145	175.232
292 gly	8.612	112.006	45.2735	174.232
293 ser	8.355	116.084	58.5745	175.088
294 lys	8.576	123.35	56.5255	176.457
295 asp	8.258	120.553	54.5605	175.921
296 asn	8.342	118.733	53.283	175.108
297 ile	8.072	121.372	61.24	176.143
298 lys	8.413	125.761	56.009	176.102
299 his	8.462	122.342	56.087	174.792
300 val	8.274	124.999	59.7095	
301 pro			63.546	177.715
302 gly	8.762	110.736	45.3405	
303 gly				
304 gly			45.083	
305 ser	8.321	115.786	58.249	174.561
306 val	8.281	122.306	62.2655	175.992
307 gln	8.546	125.33	55.488	175.599
308 ile	8.405	124.851	61.018	175.764
309 val	8.318	126.454	61.957	175.499
310 tyr	8.583	126.887	57.9485	175.078

311 lys	8.257	126.518	53.58	
312 pro			62.802	176.859
313 val	8.301	121.151	62.411	175.664
314 asp	8.503	124.861	53.529	176.705
315 leu	8.681	125.894	55.5045	178.113
316 ser	8.47	116.343	59.8135	174.98
317 lys	8.003	122.209	56.0365	176.67
318 val	7.994	121.485	62.6125	176.579
319 thr	8.354	118.663	61.8355	174.619
320 ser	8.417	118.719	58.342	174.699
321 lys	8.558	123.768	56.4895	
322 cys			58.9145	175.269
323 gly	8.566	111.888	45.332	
324 ser	8.369	116.095	58.5335	174.962
325 leu	8.451	123.993	55.495	178.037
326 gly	8.393	109.009	45.249	173.808
327 asn	8.321	118.743	53.0985	175.36
328 ile	8.088	120.834	61.4475	175.963
329 his	8.417	123.133	55.7735	174.753
330 his	8.293	121.596	55.997	174.644
331 lys	8.488	125	54.127	
332 pro			63.4685	177.715
333 gly	8.74	110.49	45.273	
334 gly				
335 gly	8.465	108.897	45.0645	174.053
336 gln	8.343	120.004	55.66	176.012
337 val	8.33	122.333	62.315	176.004
338 glu	8.607	126.047	56.264	176.168
339 val	8.482	124.13	62.308	176.146
340 lys	8.615	126.851	56.1615	176.486
341 ser	8.501	118.114	58.226	174.579
342 glu	8.627	123.74	56.4865	176.342
343 lys	8.423	122.631	56.3185	176.486
344 leu	8.342	123.917	55.004	176.85
345 asp	8.392	121.443	53.98	176.09
346 phe	8.286	121.466	58.533	176.252
347 lys	8.275	122.011	56.9495	176.318
348 asp	8.201	120.236	54.52	176.182

349 arg	8.082	121.112	56.334	176.483
350 val	8.265	122.142	62.7775	176.459
351 gln	8.601	124.858	55.8265	176.096
352 ser	8.465	117.995	58.5135	174.531
353 lys	8.486	123.686	56.2805	176.711
354 ile	8.263	122.786	61.564	
355 gly	8.639	113.91	45.1895	174.167
356 ser	8.238	115.704	58.4385	174.464
357 leu	8.513	124.143	55.234	177.299
358 asp	8.237	120.363	54.513	
359 asn	8.349	118.856	53.2875	175.158
360 ile	8.121	120.981	61.284	176.478
361 thr	8.322	118.807	62.149	174.106
362 his	8.449	123.323	56.031	174.628
363 val	8.268	124.727	59.7505	
364 pro			63.567	177.744
365 gly	8.791	110.864	45.382	
366 gly				
367 gly			45.1415	173.974
368 asn	8.427	118.588	53.183	175.317
369 lys	8.383	122.141	56.3275	176.473
370 lys	8.442	123.639	56.361	176.486
371 ile	8.349	123.918	61.0035	176.256
372 glu	8.644	126.41	56.2065	176.521
373 thr	8.361	116.273	62.213	174.515
374 his			56.28	174.145
375 lys	8.347	122.973	56.366	176.491
376 leu	8.411	123.716	55.243	177.488
377 thr	8.162	115.1	61.759	174.982
378 phe	8.384	123.034	58.2095	175.604
379 arg	8.241	123.448	55.9795	176.001
380 glu	8.437	122.343	56.8385	176.479
381 asn	8.571	120.028	53.3275	175.194
382 ala	8.309	124.482	52.8875	177.902
383 lys	8.268	120.469	56.2795	176.52
384 ala	8.294	125.262	52.516	177.85
385 lys	8.423	121.104	56.4765	176.942
386 thr	8.235	114.901	61.6425	174.183

387 asp	8.395	122.702	54.1905	176.139
388 his	8.451	120.031	56.217	
389 gly	8.513	110.143	45.3485	173.876
390 ala	8.2	123.779	52.273	177.64
391 glu	8.458	120.494	56.445	176.252
392 ile	8.254	123.992	61.035	175.453
393 val	8.203	126.521	61.9075	174.946
394 tyr	8.004	130.717	59.757	

5   Highly Populated Turn Conformations in Natively Unfolded Tau Protein Identified from Residual Dipolar Couplings and Molecular Simulation

Marco D. Mukrasch[1†], Phineus Markwick[2†], Jacek Biernat[3], Martin von Bergen[3], Pau Bernado[2,4], Christian Griesinger[1], Eckhard Mandelkow[3], Markus Zweckstetter[1,5#] and Martin Blackledge[2#]

[1]Max Planck Institute for Biophysical Chemistry, Am Faßberg 11, 37077 Göttingen, Germany

[2]Institut de Biologie Structurale Jean-Pierre Ebel, CEA; CNRS; UJF UMR 5075, 41 Rue Jules Horowitz, Grenoble 38027, France

[3]Max-Planck-Arbeitsgruppen für strukturelle Molekularbiologie Hamburg, Notkestrasse 85, c/o DESY, 22067 Hamburg, Germany

[4]Current address : Institut de Recerca Biomèdica. Josep Samitier 1-5, 08028-Barcelona, Spain.

[5] DFG Research Center for the Molecular Physiology of the Brain (CMPB)
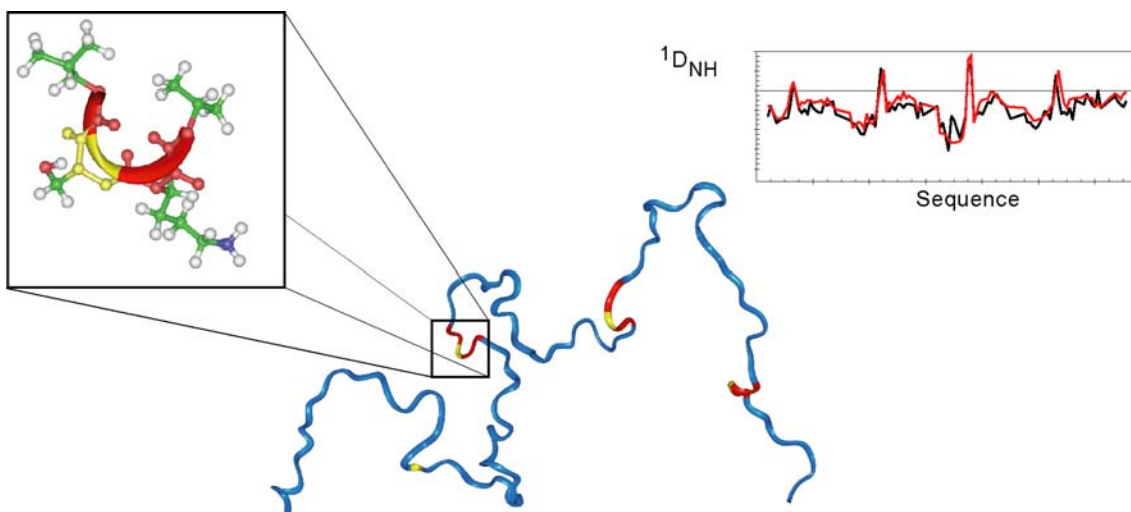
ABSTRACT

Tau, a natively unstructured protein that regulates the organization of neuronal microtubules, is also found in high concentrations in neurofibrillary tangles of Alzheimer's disease and other neurodegenerative disorders. The conformational transition between these vastly different healthy and pathological forms remains poorly understood. We have measured residual dipolar couplings (RDCs), J-couplings and nuclear Overhauser enhancement (nOe) in construct K18 of tau, containing all four repeat domains R1-R4. NH^N RDCs were compared with prediction based on a statistical model describing the intrinsic conformational sampling of unfolded proteins in solution. While local variation and relative amplitude of RDCs agrees with propensity-based prediction for most of the protein, homologous sequences in each repeat domain (DLKN, DLSN, DLSK and DKFD in repeats R1-R4) show strong disagreement characterized by inversion of the sign of the central couplings. Accelerated molecular dynamic simulations (AMD) in explicit solvent revealed strong tendencies to form turns, identified as type I β-turns for repeats R1, R2 and R3. Incorporation of the backbone dihedral sampling resulting from AMD into the statistical coil model closely reproduces experimental RDC values. These localized sequence-dependent conformational tendencies interrupt the propensity to sample more extended conformations in adjacent strands, and are remarkably resistant to local environmental factors, as demonstrated by the persistence of the RDC signature even under harsh denaturing conditions (8M urea). The role that this specific conformational behavior may play in the transition to the pathological form is discussed.

KEYWORDS : Natively unfolded proteins, Tau, NMR, Residual dipolar couplings, Molecular dynamics, Conformation

INTRODUCTION

Natively unfolded proteins play key roles in the development of neurodegenerative diseases,[1] often characterized by the transformation from soluble, physiological forms to aggregated, pathological forms of the same protein.[2] Amyloid plaques or neurofibrillary tangles (NFTs) found in brains of patients with Alzheimer's disease are fibrous assemblies made up of Aβ peptide[3] or microtubule associated protein (MAP) tau in the form of paired helical filaments (PHFs).[4] In its physiological form tau is an intrinsically unfolded protein believed to regulate the organization of neuronal microtubules.[5] The molecular mechanism associating the conformational behavior of tau in solution with the process of pathological aggregation remains poorly understood, principally due to the experimental difficulties encountered when studying unfolded polypeptide chains using classical tools of structural biology.

A number of isoforms of protein tau are found in Alzheimer PHFs, varying in length from 352 to 441 amino acids.[6] Three or four imperfect repeat domains are present in the C-terminal half of all isoforms. The repeat domains form the core of PHFs and have been proposed to be largely responsible for PHF assembly.[7] Although tau is essentially hydrophilic, two short, weakly hydrophobic hexapeptides occurring at the beginning of the repeat domains 2 and 3 are known to play an essential role in the formation of PHFs, and were subsequently proposed as seeds of aggregation (figure 1).[8] Recent studies of the repeat domains contained in constructs K18 and K19 used CD and FTIR spectroscopy[9] and subsequently NMR chemical shifts[10,11] to identify β-sheet propensities in these peptides. These regions were also shown to mediate the interaction with microtubules and polyanions.[10]

Nuclear magnetic resonance (NMR) is uniquely suited to the study of unfolded proteins in solution,[12] giving access to site-specific averages over all sampled conformations of the ensemble.[13-15] In particular residual dipolar couplings (RDCs)[16] report on time and ensemble-averaged conformations[17-19] and can be used to understand both the structure and dynamics of disordered proteins.[20,21] RDCs are sensitive to the presence of structure in flexible chains at levels that are difficult to detect using other techniques and offer an increasingly promising tool to determine quantitative levels of order in unfolded proteins.[22-25] Following on from previous NMR studies of tau protein in solution,[10,11,26,27] in this study we use RDCs to characterize conformational behavior in the K18 construct of the protein.

We recently developed a statistical coil model, termed Flexible-Meccano (FM) for the prediction of experimental properties of disordered proteins in solution.[28] FM describes the intrinsic conformational sampling of unfolded proteins by constructing an ensemble from randomly sampled residue-specific ϕ/ψ propensities present in a folded protein database. Close agreement was found between experimental and simulated RDCs for a number of unfolded proteins, establishing FM as a basic tool for studying unfolded proteins in solution.[29]

Although statistical sampling from structural databases is well suited to the study of highly disordered systems such as natively unfolded proteins, local conformational preferences that diverge from predicted behavior cannot easily be characterized from such an analysis. Examples of this kind of behavior are found here in four homologous regions of the construct K18 of tau protein, manifest as local inversion of the sign of measured RDCs. To study the molecular basis of these specific structural propensities we have complemented the FM approach with state-of-the-art molecular simulation techniques. While classical molecular dynamics (MD) calculations are routinely used to simulate fast stochastic motions in the sub-microsecond range in folded proteins, we have used a biased-potential simulation approach, known as accelerated MD,[30] to statistically sample the much larger conformational subspace available to unfolded proteins. The backbone dihedral angle distributions extracted from simulation are then incorporated into the FM molecular construction algorithm. This combination of molecular simulation and statistical conformational sampling provides rare insight into the structure and dynamics of tau protein, and holds great promise for the study of unfolded proteins in general.

RESULTS AND DISCUSSION

Tau aggregation from the healthy, unfolded form to pathological filament-forming PHFs is driven by a transition from unfolded to beta sheet structure.[31] Recent studies have identified two hexapeptides, located around the second and third repeat sequences in the core region of tau ([275]VQIINK[280] and

[306]VQIVYK[311] in repeats R2 and R3 respectively), that are sufficient for PHF formation, represent a minimal tau-tau interaction motif[9] and have been shown to mediate the interaction of tau with microtubules (figure 1).[10] Understanding the native behavior of the core domain of the intrinsically unfolded form of tau in solution is therefore critical to identifying the basis of this conformational transition. Here we have measured NH^N RDCs in strained gels,

interproton nuclear Overhauser enhancement (nOe) and $^3J_{NH-\alpha H}$ couplings from K18, a construct comprising all four repeat domains and therefore containing the key regions responsible for both normal and pathological activity (figure 2). Note that in this figure we present RDCs in an inverted form, to facilitate comparison with the other experimental measurements.
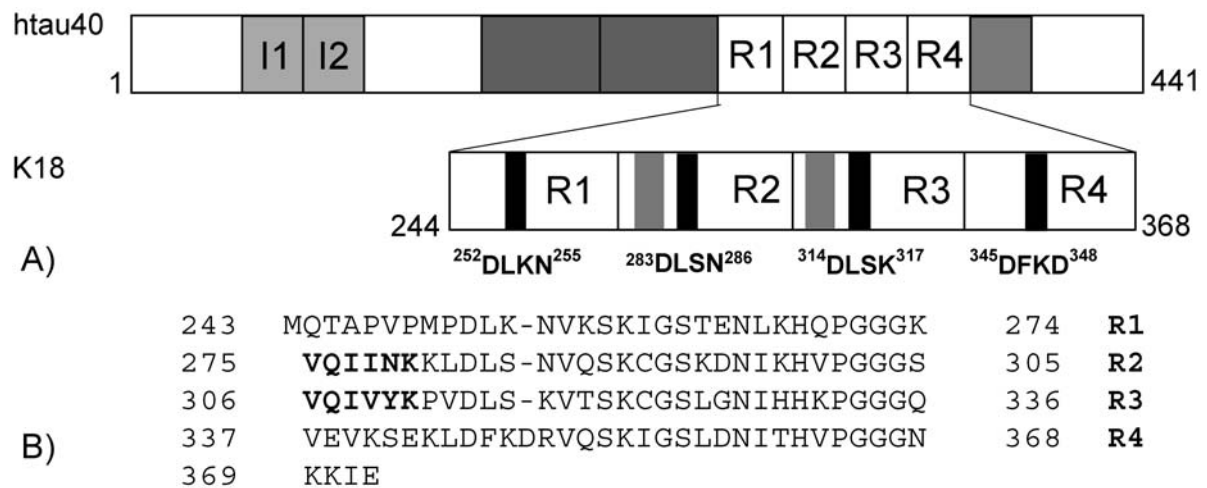
Figure 1. Tau protein and K18. A) Position of the K18 construct with respect to the htau40 isoform of tau. Tau contains four pseudorepeat domains (R1-R4) involved in binding microtubules and forming the core of PHFs. The position of the amino acids showing specific conformational behavior on the basis of RDCs is shown. The position of hexapeptides at the start of repeats R2 and R3 are shown as grey boxes. B) Primary sequence of the K18 construct, showing the position of repeat domains 1-4, containing 30-31 residues each. The position of hexapeptides at the start of repeats R2 and R3 are shown in bold.
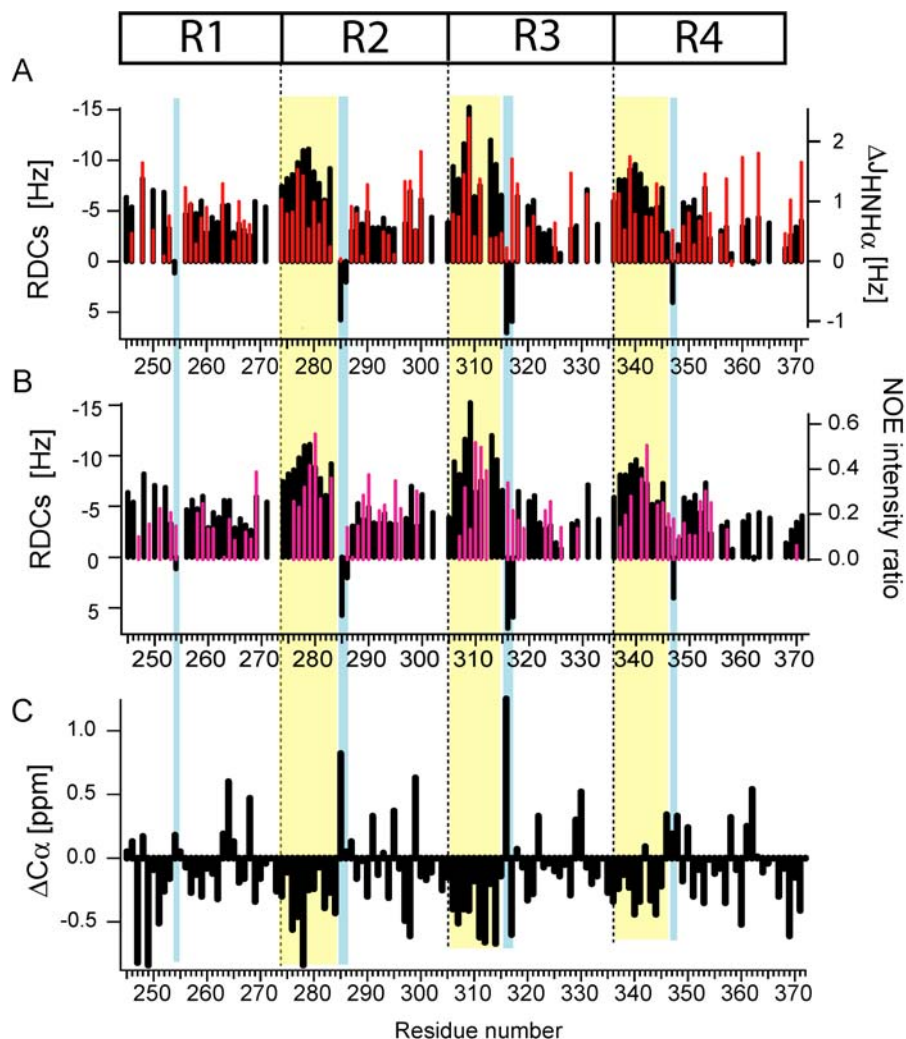
Figure 2. Summary of experimental data measured from the K18 construct of tau. Three regions exhibiting large negative RDC values (indicating extended structure) are highlighted in yellow. Inverted RDC values (turn propensity) are indicated in blue. A) RDCs measured in polyacrylamide gel (black) compared to secondary $^3J(H^NH^\alpha)$-coupling values (red). B) RDCs measured in polyacrylamide gel (black) compared to H^N_i-H^α_{i-1} NOE cross peak intensities (magenta) relative to diagonal cross peak intensity. C) C^α secondary chemical shift differences from random coil values,[10] indicating occurrence of secondary structure elements, are depicted as comparison.
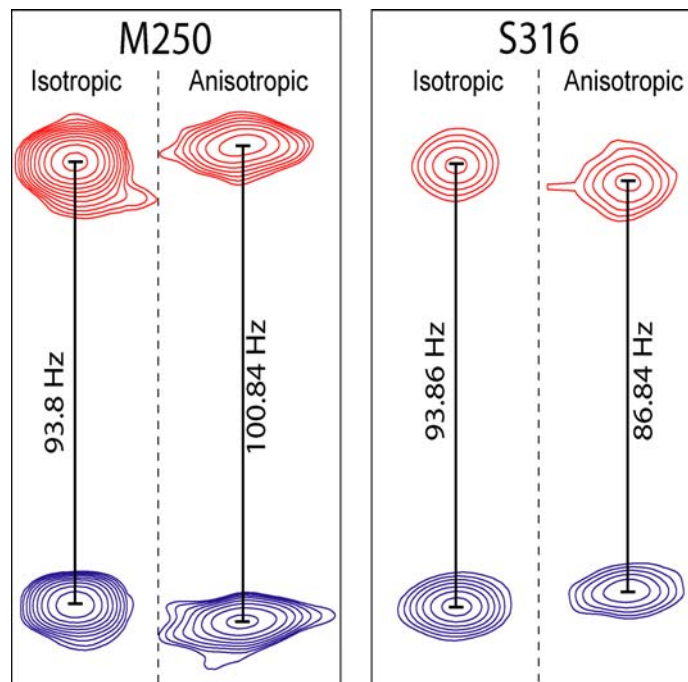
Figure 2D. Isotropic and anisotropic (aligned in polyacrylamide gel) doublets from K18.

The expected distribution of RDCs in unfolded proteins[21] is globally followed in K18, with negative couplings throughout the chain. The experimental data nevertheless present notable characteristics, with larger amplitude RDCs occurring in the four regions at the beginning of the repeats, 248-252, 275-283, 306-314 and 337-342. The two central strands correspond to the weakly hydrophobic repeat regions previously estimated to exhibit β-sheet propensities on the basis of CD, FTIR[9] and NMR secondary chemical shifts.[10] Large negative RDCs are associated with locally more extended conformations, due to the form of the angular probability function of the dipolar orientation governing RDC averaging, $\int P_2(\cos\theta)d\Omega$. In more extended parts of the chain the NH^N interaction direction will tend to be perpendicular to the external field that is also the direction of the longer axes of the anisotropic cavities in strained gels. This function becomes more negative when more β-extended structures are populated. Larger RDCs measured in K18 are therefore in qualitative agreement with β-sheet propensity in these regions. A similar distribution of RDCs is found when the protein is aligned in bacteriophage (supporting information), with small differences probably due to additional electrostatic alignment in this medium.[32] In the following we will discuss the somewhat simpler interpretation of gel-aligned RDCs. Importantly the current

results also indicate that all four repeat domains contain homologous sites {L253-K254, L284-S285, L315-S316 and L346-K347} exhibiting RDCs with inverted sign. The occurrence of such sign inversion in unfolded chains has been interpreted as an increase in local propensity to form turns or α-helical conformations.[22-24,33]

Comparison of experimental ^{3}J couplings (dependent on the distribution of ϕ angles) with random coil prediction confirms the presence of specific conformational behavior in these same regions. While positive $\Delta^3 J_{NH-\alpha H}$ ($J_{exp}-J_{random\ coil}$) values dominate throughout, indicating a tendency towards extended structure, low values, again indicative of turns, are found for K254, N285 and S316. Notably, despite following the general pattern of the measured RDCs elsewhere, sequential H^{α}_{i-1}-H^N_i nOes measured along the chain do not show evidence of differential behavior in these regions (vide infra).
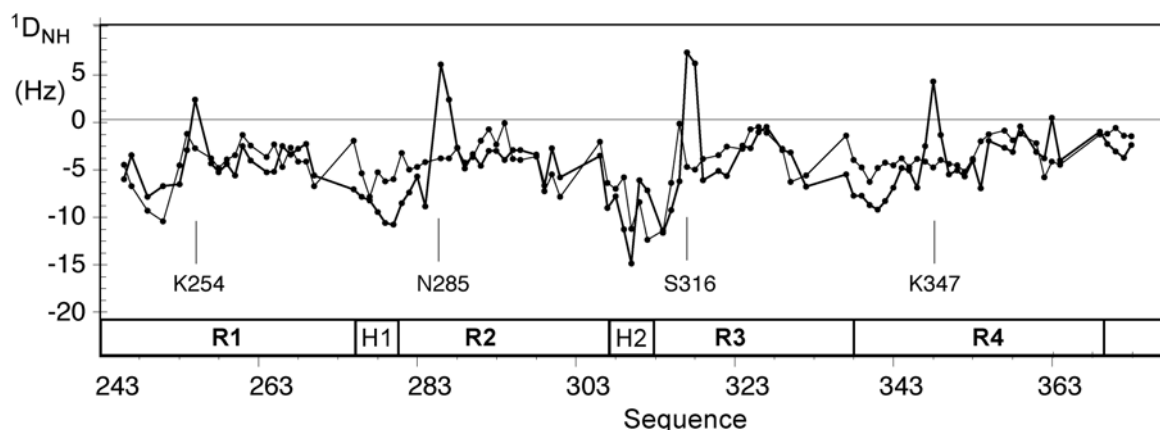
Figure 3. Residual Dipolar Couplings Measured in K18 Compared to FM simulation. Experimental NH^N RDCs from tau K18 construct aligned in polyacrylamide gel (thick line), compared to predicted NH^N RDCs using the statistical coil model FM (thin line). 50000 conformations were simulated and RDCs predicted using PALES. Average RDCs are uniformly scaled to reproduce experimental values. Only values for which experimental data are available are shown. The position of the domains R1-R4 and H1, H2 are indicated. Experimental error is estimated at 0.2Hz.

Comparison with Prediction using Flexible Meccano.

Two similar approaches have been developed to describe local conformational sampling in unfolded chains.[28,34] One of these approaches (FM) is used here to provide more detailed insight into the local conformational behavior of K18. FM can be used to predict RDCs in unfolded chains using statistical sampling of amino-acid specific conformations extracted from a structural database. RDCs simulated using this approach are compared to the experimentally measured values in figure 3. Simulated values are scaled by a common factor to match the experimental points. Both local variation and relative amplitude of RDCs along the sequence are broadly reproduced by prediction. Inverted couplings measured in the vicinity of homologous positions of the four regions L253-K254, L284-S285, L315-S316 and L346-K347 are however not predicted by the model. We conclude that conformational sampling in these regions is more complex and due to interactions that are not described by residue-specific propensities.

In an initial approach we modified the FM algorithm to search Ramachandran space at key amino acid positions. RDCs from the fragment 270-300 were extracted from FM simulations of the entire protein, in which the central amino acid, S285, sampled different conformational wells. Figure 4 illustrates the dependence of RDCs on ϕ/ψ sampling, with inverted signs of NH^N RDCs in β-extended and α-helical regions. Although this analysis verifies that turn conformations can give rise to the experimentally measured RDCs in these four regions, it is also evident that unique descriptions of conformational sampling cannot be extracted exclusively on the basis of NH^N RDCs. To gain further insight into the specific behavior of these regions and better understand the physical basis of the local conformational preferences we have therefore used MD simulation techniques. Due to the extensive conformational freedom available to unfolded proteins, it is not clear whether experimental parameters such as RDCs can be reproduced from standard MD. Here we have used accelerated MD (AMD) simulations in explicit water to predict the behavior of short peptides centered on the positions of interest.
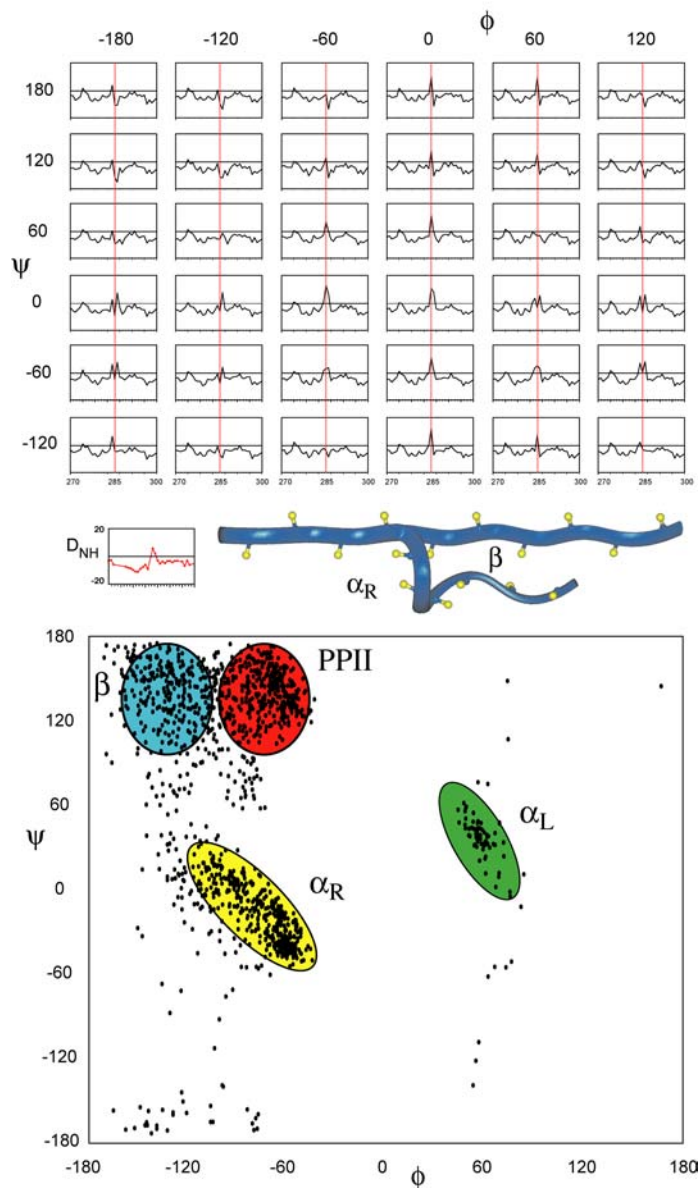
Figure 4. Backbone Conformational Dependence of NH[N] RDCs Top: Dependence of NH[N] RDCs in the range 271-300 on the local conformational sampling of residue S285. 50000 conformers were calculated in each case. S285 sampled distributions centred on the ϕ/ψ values shown, in Gaussian wells of width 10°. All other amino acids obeyed native propensities. Red line indicates the position of S285. The experimental data are shown in the inset (red). Also shown are effective orientations of NH vectors (yellow) in the presence of β-extended and α-helical conformations. Bottom: Ramachandran plot showing conformational distribution drawn from the structural database. The most populated conformational regions discussed in the text are indicated : Polyproline II (PPII), β-extended (β), right-handed a helix (α_R) and left-handed a helix (α_L).
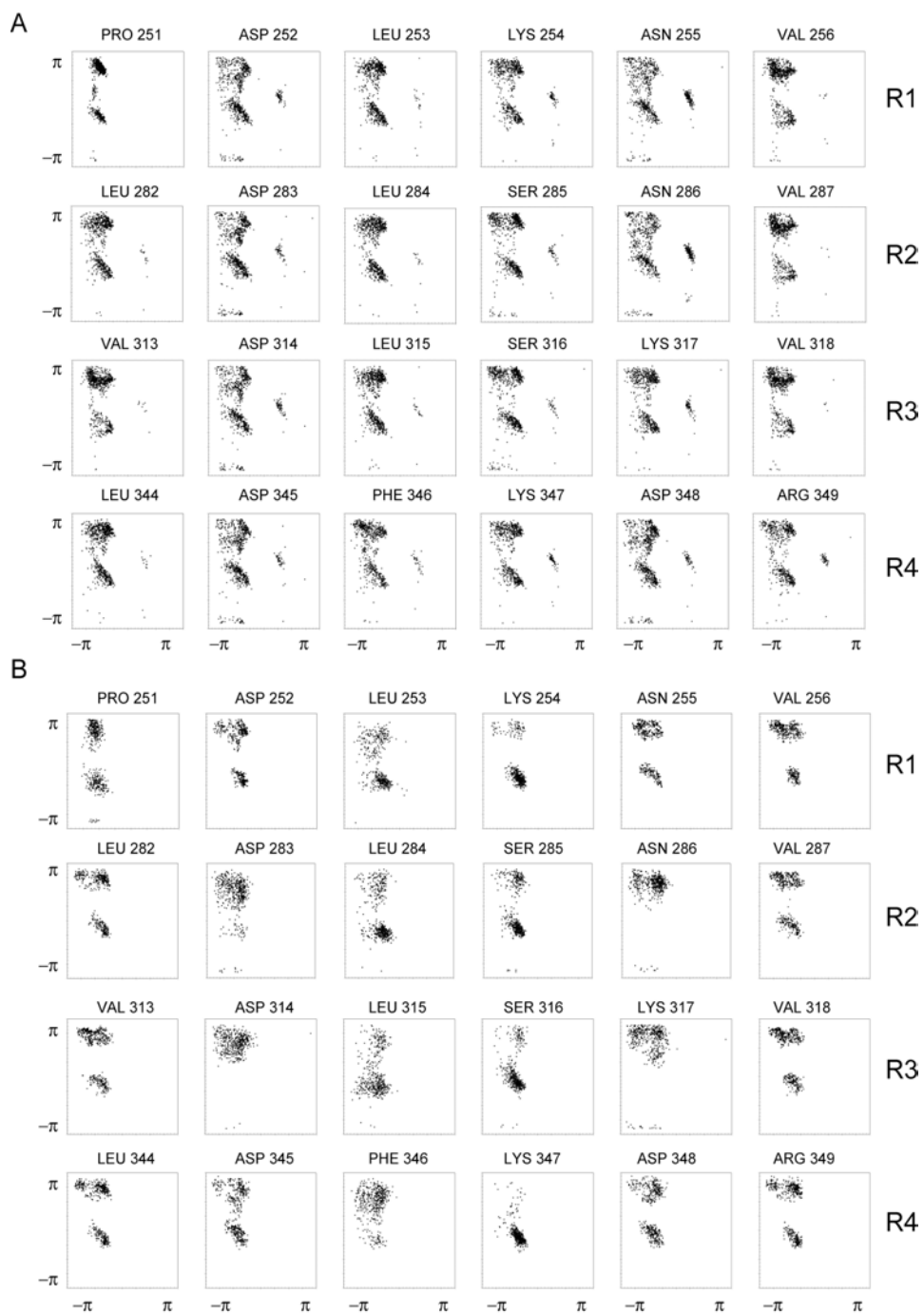
Figure 5. Conformational Sampling from AMD and FM Simulation. A) Conformational sampling from the FM simulation for amino acids in the vicinity of the regions exhibiting turn conformations; (251-256), (282-287), (313-318) and (344-349). B) Sampling from the AMD simulation for the same amino acids as shown in (A).

Accelerated Molecular Dynamics Simulations.

AMD uses biased potential sampling to enhance the probability of transition between low energy conformational states and therefore offers an efficient method for accessing both longer timescale motions and broader statistical sampling.[30]

Backbone dihedral sampling for regions in the vicinity of the proposed turns is shown in figure 5, and compared to the sampling present in the database-dependent 50000-strong FM ensemble. Before analyzing regions where specific local structures are suspected, we verified that conformational sampling from AMD generally reproduces the propensity-based populations in regions where the database conformations do reproduce experimental RDCs. Examples are shown in figure 5 where ϕ/ψ populations of the amino acids preceding and succeeding the regions of interest strongly resemble dihedral angle sampling extracted from the FM analysis. Histograms of the ψ-angle distribution for these amino acids are shown in figure 6. Although exceptions exist, in particular P251 where AMD predicts less extended sampling, for most of the amino acids examined the distributions are similar.

Figures 5 and 6 also reveals that certain amino acids in these four sequences show specific propensities that are significantly different to the native propensities (figure 5B and 6B). Conformational sampling indicative of type I beta turns for residues {D283, L284, S285, N286} and {D314, L315, S316, K317} is observed in repeats R2 and R3, with two consecutive conformations in the α_R region of Ramachandran space, preceded and succeeded by amino acids sampling more extended conformations. The same pattern is seen for repeat 1, with L253 and K254 populating the helical region, but preceding and following residues more closely resembling their native propensities. In contrast repeat R4 also samples a turn conformation, but only at the central residue K347. As the preceding residue tends to more extended conformation, this motif is closest to a type VIII beta turn. Since the turns are formed by transition from extended to α_R region it is not surprising that the H^{α}_{i-1}-H^{N}_{i} nOes are a poor indicator of this transition.

We can determine whether the conformational sampling observed from AMD is in agreement with the experimental data, by replacing the standard amino-acid specific propensities used in the FM algorithm with backbone conformations extracted from the trajectory. AMD populations shown in figure 5B were used to replace the propensity-based sampling (figure 5A) for the tetra-peptides 252-255, 283-286, 314-317 and 345-348. Database propensities were retained for all remaining residues, and 50000 conformers were constructed on the basis of this hybrid sampling. The results (figure 7) show that sampling from AMD is indeed in agreement with the experimental RDCs, at least for repeats R1-R3, indicating that

not only the conformations, but also their populations are accurately simulated. Importantly, the simulations predict that the configurations of the four regions involve specific conformational sampling in up to four sequential amino acids. Analysis of the AMD simulations failed to identify a unique interaction responsible for the propensity of this generic sequence (DLKN, DLSN and DLSK in repeats R1-R3 respectively) to induce the observed highly specific conformational properties. Rather a combination of van der Waals obstruction and transient hydrogen bonds were observed as principal factors. Nevertheless this striking result illustrates the power of combining MD simulation and FM-based statistical sampling.
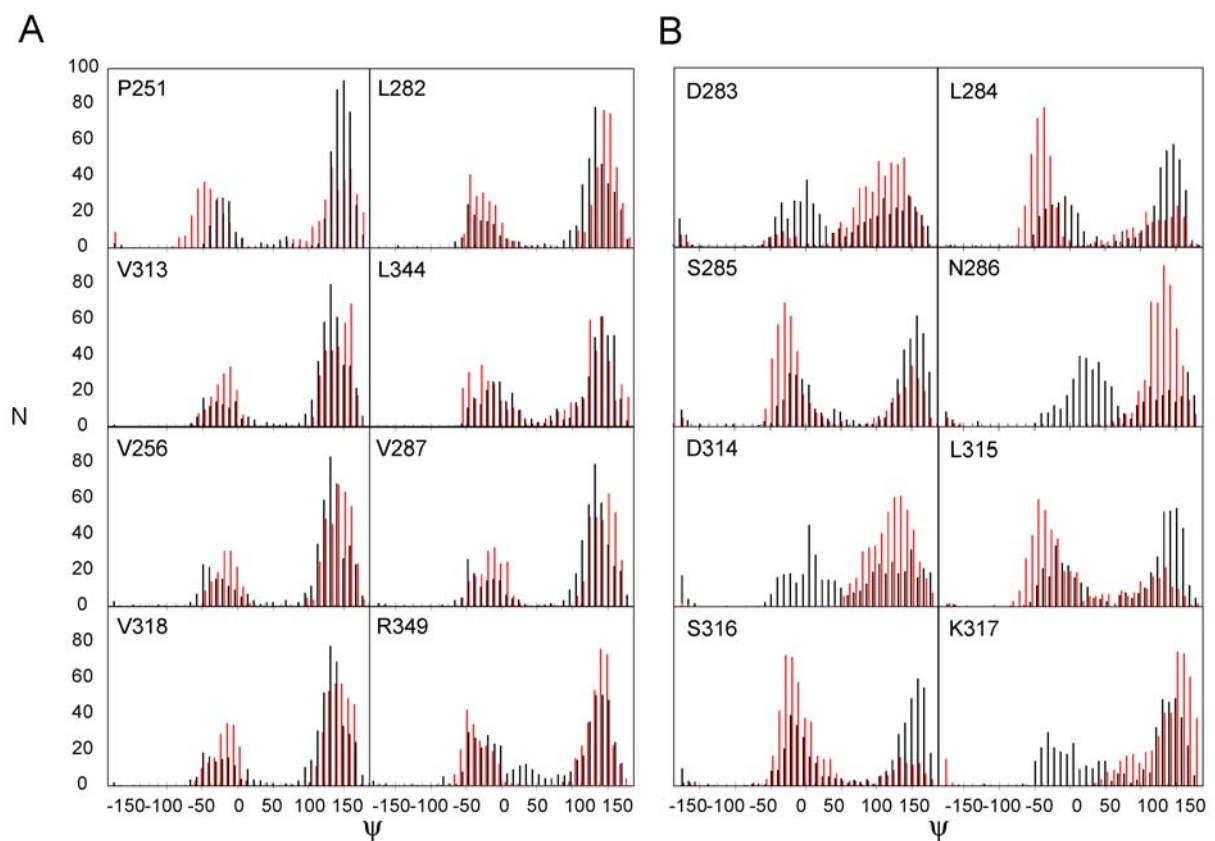
Figure 6. ψ Dihedral Angle Sampling from AMD and Amino-acid Specific Propensities. A) Histograms showing distribution of 500 ψ angles from FM (black) and AMD simulation (red) of the 8 N and C terminal amino acids of the regions shown in figure 5A (bin width 9°). B) Histograms showing distribution of 500 ψ angles from FM (black) and AMD simulation (red) of the 4 central amino acids of regions shown in figure 5A and 5B in repeats R2 and R3.

These observations agree with previous NMR studies, where chemical shift analysis identified propensity for turns in these regions, and slight β-sheet propensity in the strands preceding them.[10] The simulation shown in figure 6 explicitly incorporated additional β-strand conformations at the levels indicated in the previous publication (16% for the strand 274-283 (R2), 24% for strand 306-313 (R3), and 13% for strand 336-345 (R4)). Calculations run without these additional propensities resulted in slightly decreased couplings in these regions (supporting information). We have also run AMD simulations on these three strands and see a slightly higher propensity for extended conformations than found in the FM conformations (data not shown). ϕ-dihedral angle dependent $^3J_{NH-\alpha H}$ couplings also indicate the presence of turns (figure 2). We have predicted J-couplings from throughout the chain and compared these with experimental coupling constants (figure S4 supporting information). The results demonstrate reasonable correlation, both in the turn regions and in the rest of the chain. In addition H^{α}_{i-2}-H^{N}_{i} distances between Q276-I278, D283-S285, S285-V287, K309-V313 and D314-S316 were detected, indicating more compact structures in these regions, in agreement with turn conformations.

Finally to probe the stability of these observed structural propensities we have repeated RDC measurements on K18 dissolved in 8M urea. Remarkably the profile of experimental RDCs is very similar (supporting information), with sign inversion at the same positions. The sequence-dependent propensity to form turns is therefore remarkably stable, persisting even in the presence of extreme denaturing conditions.

Beta Turns in Tau –Inhibitor or Precursor of Filamentous Structure?

It is interesting to speculate on the role that these conformational properties may play in the context of the transition between healthy and pathological forms of tau. The second and third turn-regions, centered on S285 and S316, immediately follow strands of β-sheet propensity (274-283, 306-313) containing known aggregation-nucleation sites that are sufficient for formation of PHFs. Additional turn regions are expected to exist due to the GGG motif present in the terminal part of the 30 residue repeats, and this motif is preceded by some transient β-structure. Both repeats 2 and 3 therefore contain some propensity for sheet-turn-sheet-turn motifs in solution. Beta turns may play a role in disrupting the formation of amyloid fibrils,[35] in a similar way to proline residues. Indeed the insertion of a proline into the hexapeptide motif in repeat R3 has been shown to interrupt β-structure.[36] It will therefore be interesting to determine whether the observed turns are present in the aggregated form of tau, (some evidence exists for this on the basis of EPR of spin-labeled tau-aggregates[37]) or whether they represent an auto-inhibitory mechanism to avoid aggregation.

Long-range structural information reporting on the soluble form of tau is available from FRET measurements that have recently been used to demonstrate unusual proximity of sites 291 and 310 and 310 and 322.[38] This is in qualitative agreement with the presence of a turn at position 302 and the highly populated β-turn at position S316 described here, even in the presence of extended sampling either side of the motif. We have also calculated an effective radius of gyration from the ensemble shown here, equal to 35.5Å, that turns out to agree with experimentally derived values from SAXS studies (personal communication Dmitri Svergun).

CONCLUSIONS

Recent studies have shown the power of statistical coil models to describe the intrinsic conformational sampling of unfolded proteins. The question remained how one could address conformational sampling of disordered states when database approaches did not reproduce experimental data, due to more complex transient conformational sampling. Simulation using standard MD techniques presents a number of shortcomings, in particular restricted sampling that could fail to interrogate the vast phase space available to a disordered system. Here we have used biased potential approaches that allow broader statistical mechanical sampling of the conformational subspace to study the structure and dynamics of four repeat regions of tau whose conformational behavior clearly diverges from prediction based on simple amino-acid specific propensities.

Four peptides in the repeat domains, ^{252}DLKN^{255}, ^{283}DLSN^{286}, ^{314}DLSK^{317} and ^{345}DKFD^{348} show high propensities to form turns. AMD strongly indicates that these sequences fold locally, and provide otherwise inaccessible detail of the nature of the turn conformations, and the participating amino acids. The peptides in repeats 1-3 appear to adopt classical type I beta turns and reproduce experimental data very well, while the peptide in repeat 4 resembles a beta VIII turn in the simulation, but presents poorer reproduction of experimental data. This sequence-dependent structural propensity is remarkably resistant to local environmental factors, as demonstrated by the persistent turn behavior even under harsh denaturing conditions (8M urea). Importantly these turns all follow regions with β-sheet propensity, including hexapeptides occurring at the beginning of the repeat domains R2 and R3 previously identified as potential seeds of aggregation. Whether the strong propensity to

form turns represents an inhibitory mechanism present in the healthy form, to avoid formation of continuous β-fibrils for example, or whether these structured regions are present in the pathological form, remains an open, and crucially important question.

METHODS

Experimental NMR Measurements

K18 protein expression and backbone assignment has been described.[10] ^{1}H-^{15}N residual dipolar couplings where measured in 7% uncharged polyacrylamide gels and in Pf1 phages (5 mg/ml). The sequence of an IPAP-HSQC (16 scans, 1.2 ms as relaxations delay) was used 37) and measured on a Bruker 800 DRX spectrometer. NOESY-HSQC (4 scans, relaxation delay: 1.3 ms, mixing time 120 ms) was measured on a Bruker DRX 800 spectrometer. Spectra were recorded at 5°C and processed and analyzed using NMRPipe[40] and Sparky 3.[41] ^{3}J-H^N_iH$^\alpha_{i-1}$ couplings were measured using quantitative J correlation (intensity modulated HSQC) on a Bruker 800 DRX spectrometer (32 scans, relaxation delay 1.2 ms, 2τ = time for evolution of ^{3}J$_{HNHa}$: 18 ms).[42] Couplings were evaluated by using the relation S$_{cross}$/S$_{diag}$ = cos(π^{3}J$_{HNHa}$2τ). Random coil values were subtracted from the couplings to gain direct indication of possible secondary structure elements.[43]

Molecular Dynamics Simulations

Accelerated Molecular Dynamic (AMD) simulations[30] use biased potential sampling to enhance the probability of transition between low energy conformational states. The methods have been presented previously, and will be briefly described here. Acceleration of dynamic events is provoked by defining a reference or 'boost' energy, E$_b$, lying above the minimum of the potential energy surface. If the potential energy V(r) lies below this boost energy, a bias potential is added to the actual potential, thus accelerating exchange between low energy conformational states, and in the case of unfolded proteins allowing more efficient conformational sampling. The energy modification is given by

$$\Delta V(r) = \frac{\left(E_b - V(r)\right)^2}{\alpha + \left(E_b - V(r)\right)} \tag{1}$$

The extent of acceleration is determined by the choice of the boost energy and the acceleration parameter, α. During the course of the simulation the forces are recalculated for the modified potential.

AMD simulations were performed for the 15-residue fragments associated with the four regions of interest using an in-house modified version of the sander module in AMBER8.[44] Each system was solvated by approximately 4000 TIP3P water molecules[45] in a periodic box and the ff99SB force-field was employed for the solute.[46] Simulations were carried out at 300K using a value of 2.0 ps^{-1} for the collision frequency and a time-step of 2 fs. All bonds involving hydrogens were constrained using the SHAKE algorithm.[47] A cut-off of 10 Å was used for non-bonded interactions and long-range interactions were treated with the particle mesh Ewald (PME) method.[48]

AMD simulations were performed for each system for 15.10^6 steps, and structures collected at 100-step intervals. Acceleration was applied to the torsion force-field potential only. The boost energy was set 800 kcal.mol^{-1} above the average dihedral angle energy (obtained from an initial 500 ps MD simulation of the system) and the acceleration parameter (α) at 200 kcal.mol^{-1}. AMD simulations were used to calculate free energy surfaces for the backbone dihedral angles. This procedure was repeated starting from multiple different initial peptide structures using the same of level of acceleration in order to identify the lowest energy regions of conformational space.

All ϕ/ψ pairs were collected for each residue. 2-dimensional ϕ/ψ normalized histograms were constructed as follows: Ramachandran space was divided into 10° by 10° bins. Each ϕ/ψ pair was allocated appropriately. Canonical Boltzmann distributions were obtained by multiplying each ϕ/ψ point by its Boltmann weighting factor ($e^{\beta\Delta E}$, where $\Delta E = (E_b-V)^2/(E_b-V+\alpha)$. Free energy was calculated using $\Delta G = -RTln(N_i/N_0)$ where N_i is the population of a particular bin, N_0 is the most populated bin, and the resulting global free energy minimum by default is always 0 kcal.mol^{-1}. Free energy surfaces were interpolated, and a random number generator used to obtain a sample of 500 ϕ/ψ points that accurately represent the Boltzmann weighted ϕ/ψ population.

Generation of the Conformational Ensemble and Prediction of RDCs

Flexible-Meccano (FM) uses a Monte-Carlo sampling technique based on amino-acid propensity and sidechain volume. The details of the algorithm have been presented elsewhere.[28] Alignment tensors for each conformer were calculated using PALES, an atomic resolution approach to alignment tensor prediction.[49] RDCs were calculated from throughout the molecule using the same program.

Incorporation of Specific Ramachandran Sampling

FM calculations were also performed using specific ϕ/ψ distributions for the four amino acids K254, S285, S316 and K347 in place of the standard residue-specific distributions. Gaussian distributions with standard deviation of 10° centered on values ranging from -180° to +180° in steps of 60° were used for both ϕ and ψ. In total 36 entire FM simulations were performed. Calculations were also performed using 2000 ϕ/ψ pairs for residues extracted from the accelerated Molecular Dynamics simulations of four quindecapeptides with amino acids K254, S285, S316 and K347 in the central position. The effective radius of gyration was calculated from the ensemble using previously described methods.[28]

ACKNOWLEDGEMENTS

SUPPORTING INFORMATION
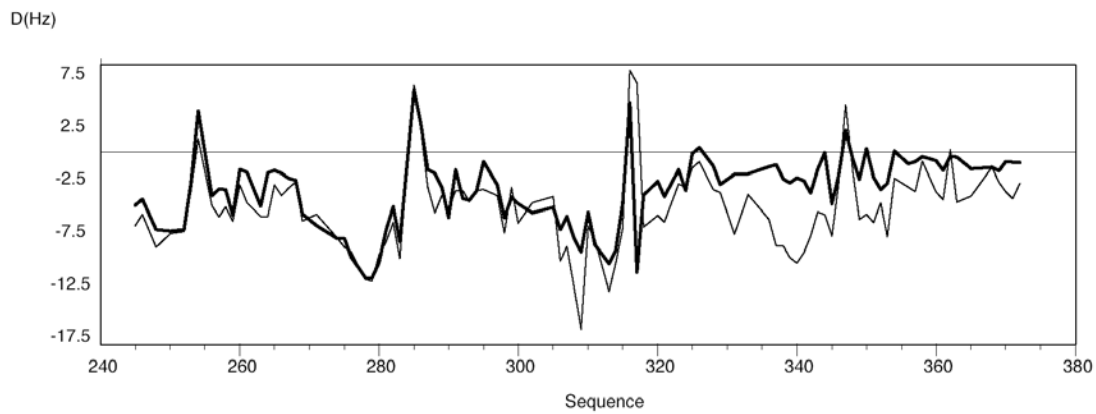
Figure 1. Comparison of RDCs measured in Tau K18 aligned in uncharged polyacrylamide gel (thinline) and bacteriophage (thick line).
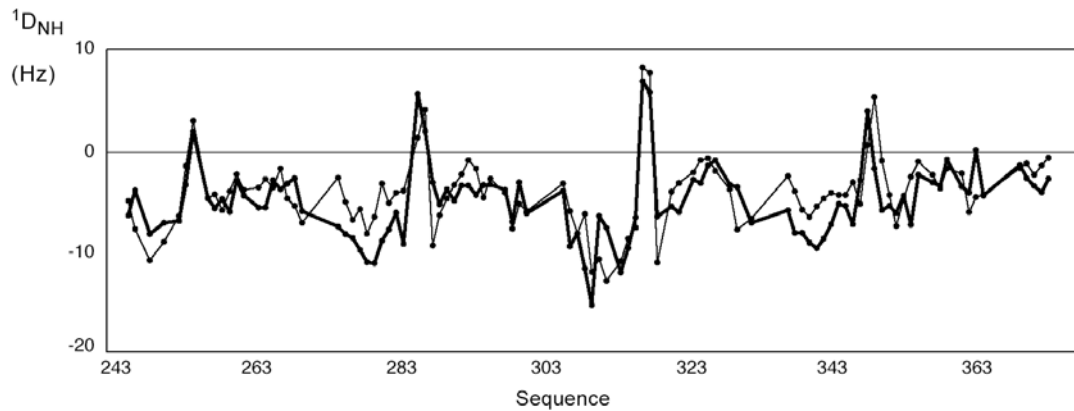
Figure 2. Prediction of NH-N RDCs from Tau K18 construct using the combined statistical coil/ Molecular dynamics model (thin line) compared to experimental values (thick). Conditions as in figure 6,except that additional beta sheet propensities predicted in a previous study were not included.
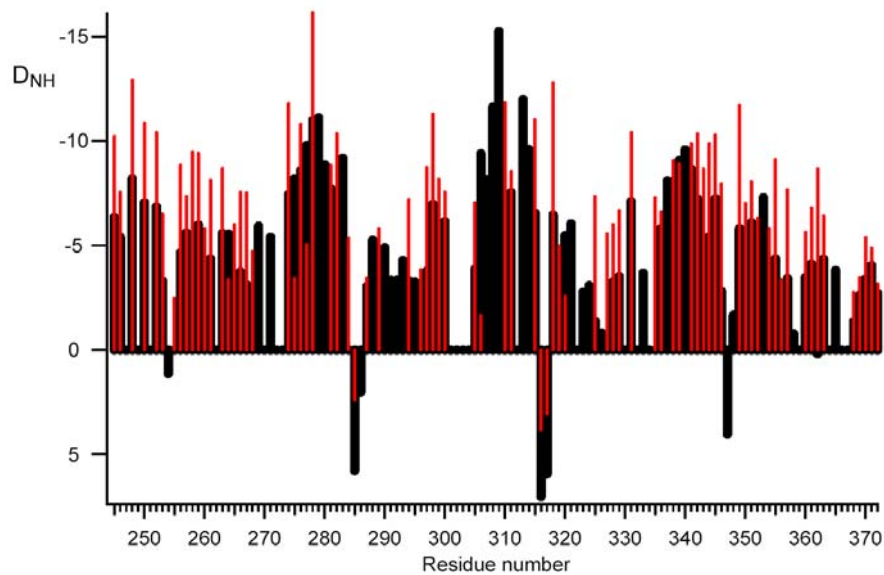
Figure 3. Comparison of measured NH RDCs from K18 dissolved in standard buffer (black) and 8M Urea (red). Both were aligned in Polyacrylamide gel. Standard buffer refers to the experimental conditions described in the Methods section.
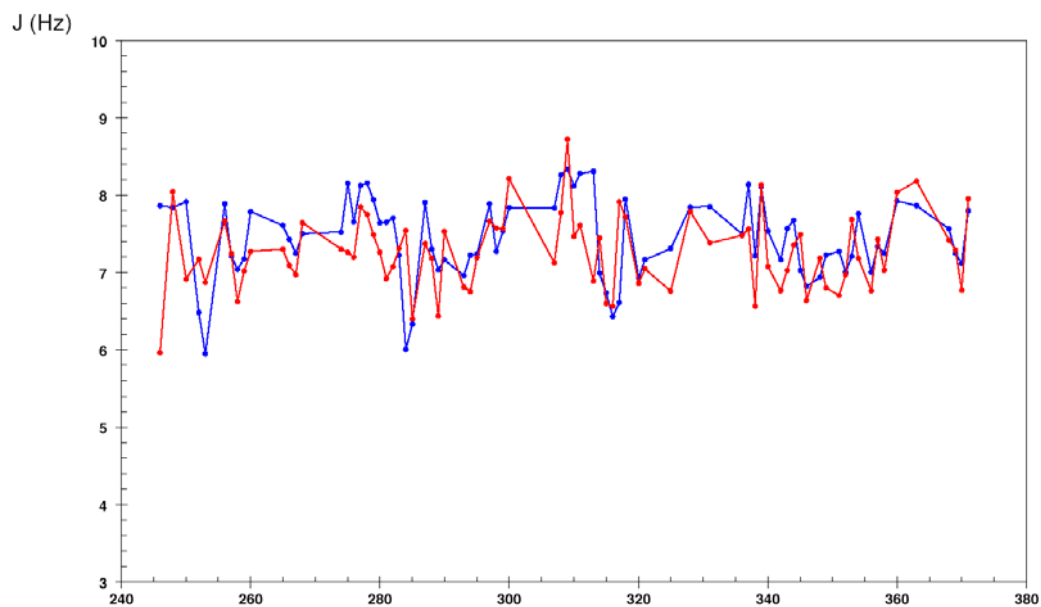
Figure 4. Comparison of measured (red) 3J HNHA couplings with values calculated from the FM ensemble (blue) using known Karplus type relationships (1).

(1) Pardi A, Billeter M, Wüthrich K (1984) J Mol Biol 180 : 741-751

REFERENCES

[1]) Dobson, C.M. Phil Trans Roy Soc ser B, 2001, 356, 133–145

[2]) Kelly, J.W. Curr Opin Struct Biol 1998, 8, 101–106

[3]) Koo, E.H.; Lansbury, P.T. Jr; Kelly, W. Proc Natl Acad Sci USA 1999, 96, 9989-9990

[4]) Mandelkow, E.-M.; Mandelkow, E. Trends, Cell Biol, 1998, 8, 425-427

[5]) Gustke, N.; Trinczek, B.; Biernat, J.; Mandelkow, E.-M.; Mandelkow, E. Biochemistry, 1994, 33, 9511-9522

[6]) Trinczek, B.; Biernat, J.; Baumann, K.; Mandelkow, E.-M.; Mandelkow, E. Mol. Biol. Cell, 1995, 6, 1887-1902

[7]) Wille, H.; Drewes, G.; Biernat, J.; Mandelkow, E.-M.; Mandelkow E. J. Cell. Biol, 1995, 118, 573-584

8) von Bergen, M.; Barghorn, S.; Li, L.; Marx, A.; Biernat, J.; Mandelkow, E-M.; Mandelkow, E. J Biol Chem 2001, 276, 48165-48174

9) von Bergen, M.; Freidhoff, P.; Biernat, J.; Heberle, J.; Mandelkow, E-M.; Mandelkow, E. Proc Natl Acad Sci USA, 1995, 97, 5129-5134

10) Mukrasch, M.; Biernat, J.; von Bergen, M.; Griesinger, C.; Mandelkow, E.; Zweckstetter, M. J. Biol. Chem. 2005, 280, 24978-24986

11) Eliezer, D.; Barré, P.; Kobaslija, M.; Chan, D.; Li, X.; Heend, L. Biochemistry, 2005, 44, 1026-1036

[12]) Dyson, H.J.; Wright, P.E. Chem. Rev. 2004, 104, 3607-3622

[13]) Wirmer, J.; Schlörb, C.; Schwalbe, H. in Protein Folding Handbook, Part I, Vol. I Buchner, Johannes / Kiefhaber, Thomas (eds) Wiley VCH 2005.

14) Dedmon, M.M.; Lindorff-Larsen, K.; Christodoulou, J.; Vendruscolo, M.; Dobson, C.M. J.Am.Chem.Soc. 2005, 127, 476-477

15) Choy, W. Y., Forman-Kay, J. D. J. Mol. Biol. 2001, 308, 1011-32.

[1]6) Tjandra, N.; Bax A., Science, 1997, 278, 1111-1114

[1]7) Prestegard, J.H.; al-Hashimi, H.M.; Tolman, J.R. Q Rev Biophys 2000, 33, 371-424

[1]8) Blackledge, M Progr. N.M.R. Spectr. 2005, 46, 23-61

[1]9) Meiler, J.; Prompers, J.J.; Peti, W.; Griesinger, C.; Bruschweiler, R. J.Am.Chem.Soc. 2001, 123, 6098-6107

[20]) Shortle, D.; Ackerman, M.S. Science, 2001, 293, 487-489

[21]) Louhivouri, M.; Pääkkönen, K.; Fredriksson, K.; Permi, P.; Lounila, J.; Annila, A J.Am.Chem.Soc. 2003, 125, 15647-15650

22) Fieber, W.; Kristjansdottir, S.; Poulsen, F.M., J.Mol.Biol. 2004, 339, 1191-1199

23) Mohana-Borges, R.; Goto, N.K.; Kroon, G.J.A.; Dyson, H.J.; Wright, P.E. J.Mol.Biol. 2004, 34, 1131-1142

24) Meier, S.; Güthe, S.; Kiefhaber, T.; Grzesiek, S. J.Mol.Biol. 2004, 344, 1051

25) Bertoncini, C.W.; Jung, Y.S.; Fernandez, C.O.; Hoyer, W.; Griesinger, C.; Jovin, T.M.; Zweckstetter, M. Proc.Natl.Acad.Sci. 2005, 102, 1430-1435

26) Landrieu, I.; Lacosse, L.; Leroy, A.; Wieruszeski, J-M.; Trivelli, X.; Sillen, A.; Sibille, N.; Schwalbe, H.; Saxena, K.; Langer, T.; Lippens, G. J.Am.Chem.Soc. 2005, 128, 3575-3583

27) Sibille, N.; Sillen, A.; Leroy, A.; Wieruszeski, J-M.; Mulloy, B.; Landrieu, I.; Lippens, G. Biochemistry 2006, 45, 12560-12572

28) Bernado, P.; Blanchard, L.; Timmins, P.; Marion, D.; Ruigrok, R.W.H.; Blackledge, M. Proc.Natl.Acad.Sci. USA 2005, 102, 17002-17007

29) Bernado, P.; Bertoncini, C.W.; Griesinger, C.; Zweckstetter, M.; Blackledge, M. J.Am.Chem.Soc. 2005, 127, 17968-17969

30) Hamelberg, D.; McCammon, J.A. J.Am.Chem.Soc. 2005, 127, 13778-13779

31) von Bergen, M.; Barghorn, S.; Niernat, J.; Mandelkow, E.-M.; Mandelkow, E. Biochem.Biophys.Acta. 2005, 1739, 158-166

32) Skora, L.; Cho, M.K.; Kim, H.Y.; Becker, S.; Fernandez, C.O.; Blackledge, M.; Zweckstetter, M. Angew. Chem. Int. Ed., 2006, 45, 7012-7015

[33]) Louhivouri, M.; Fredriksson, K.; Pääkkönen, K.; Permi, P.; Annila, A J.Biomol.NMR 2004, 29, 517-524

34) Jha, A.K.; Colubri, A.; Freed, K.; Sosnick, T Proc.Natl.Acad.Sci. (USA) 2005, 102, 13099-13104

35) Hosia, W.; Bark, N.; Liepinsh, E.; Tjernberg, A.; Persson, B.; Hallen, D.; Thyberg, J.; Johansson, J.; Tjernberg, L, Biochemistry 2004, 43, 4655-4661

36) von Bergen, M.; Barghorn, S.; Li, L.; Marx, A.; Biernat, J.; Heberle, J.; Mandelkow, E.-M.; Mandelkow, E. J.Biol.Chem. 2001, 276, 48165-48174

[37]) Margittai, M.; Langen, R Proc.Natl.Acad.Sci. (USA) 2004, 101, 10278-10283

38) Jeganathan, S.; von Bergen, M.; Brutlach, H.; Steinhoff, H.-J.; Mandelkow E. Biochemistry 2006, 45, 2283-2293

39) Kontaxis, G.; Bax A J.Biomol. NMR 2001, 20, 77-82

40) Delaglio, F.; Grzesiek, S.; Vuister, G.W.; Zhu, G.; Pfeifer, J.; Bax, A J.Biomol.NMR, 1995, 6, 277-293

41) Goddard, T.D.; Kneller, D.G. SPARKY 3, University of California, San Francisco

42) Permi, P.; Kilpeläinen, I.; Annila, A.; Heikkinen, S. J. Biomol. NMR, 2000, 16, 29-37

43) Plaxco, K.W.; Morton, C.J.; Grimshaw, S.B.; Jones, J.A.; Pitkeathly, M.; Campbell, I.D.; Dobson, C.M J.Biomol.NMR 1997, 10, 221-230

44) Case D.A. et al 2004, AMBER 8, University of California, San Francisco

45) Jorgensen, W.L.; Chandrasekhar, J.; Madura J.D.; Impey, R.W.; Klein, M.L. J.Chem.Phys 1983, 79, 926-935

46) Cornell, W.D.; Cieplak, P.; Bayly, C.I.; Gould, I.R.; Merz, K.M.; Ferguson, D.M.; Spellmeyer, D.C.; Fox, T.; Caldwell, J.W.; Kollman, P.A. J.Am.Chem.Soc. 1995, 117, 5179-5197

47) Ryckaert, J.-P.; Ciccotti, G.; Berendsen, H.J.C. J.Comput.Phys. 1977, 23, 327-341

[48]) Cheatham, T.E.; Miller, J.L.; Fox, T.; Darden, T.A.; Kollman, P.A. J.Am.Chem.Soc. 1995, 117, 4193-4194

49)   Zweckstetter,   M.;   Bax,   A.   J.Am.Chem.Soc.   2000,   122,   3791-3792

6 Structural Polymorphism of 441 Residue Tau at Atomic Resolution

Marco D. Mukrasch‡, Sadasivam Jeganathan¶, Jacek Biernat¶, Eva-Maria Mandelkow¶, Christian Griesinger‡, Eckhard Mandelkow¶, Markus Zweckstetter‡

From the ‡Department for NMR-based Structural Biology, Max Planck Institute for Biophysical Chemistry, Am Fassberg 11, 37077 Göttingen, Germany and the ¶Max Planck Unit for Structural Molecular Biology, c/o DESY, Notkestrasse 85, 22607 Hamburg, Germany

ABSTRACT

Htau40 is with 441 residues the longest spliceform of the tau protein, which is one of the most essential microtubule-associated proteins in neurons. In its pathological state tau forms aggregates that are key markers in the course of Alzheimer's disease. Its complete residual description by state-of-the-art NMR spectroscopy was not accessible until now, due to its size. Here, we report the first complete resonance assignment for backbone amide protons and C^α atoms of htau40. This assignment made it feasible to elucidate transient β-structure in the regions ^{274}Lys-Leu^{284}, ^{305}Ser-Asp^{315} and ^{336}Gln-Asp^{345}, α-helical propensity in ^{114}Leu-Thr^{123} and ^{428}Leu-Ala^{437} and poly-proline helix in ^{175}Thr-Ser^{184}, ^{217}Thr-Lys^{224}, ^{234}Lys-Ala^{239}. The regions ^{214}Ser-Lys^{240}, ^{243}Leu-Ile^{260}, ^{274}Lys-Gln^{288} and ^{297}Ile-Val^{318} were identified as the strongest binding sites for microtubules. Thus, all β-structural elements that constitute seeds of PHF aggregation are localized within the microtubule-binding region, which were completely found in the core of htau40 fibrils. The core spans from residue Gly^{207} to Asp^{402}, as we determined with the help of HR-MAS NMR spectroscopy. Characterization of the "fuzzy coat" showed that the complete C-terminal part and a region starting with Glu^{115} are particularly strongly attached to the PHF core. Furthermore, analysis of backbone dynamics of monomeric htau40 revealed a significantly higher conformational rigidity for the region constituting the core of PHFs than for the rest of tau. Our results emphasize strongly the structural, dynamical and functional difference between the microtubule-binding domain and its surroundings in the monomeric, microtubule-associated and fibril state of tau, which could help to understand its complex behaviour in biological and pathological processes.

INTRODUCTION

The tau protein is one of the essential microtubule-associated proteins (MAPs) in neurons. It is necessary for neurite outgrowth and maintenance of metabolic processes in neurons (1-3). However, it plays its most prominent role in the Alzheimer's disease (AD), where it aggregates to paired helical filaments (PHFs) which form so-called neurofibrillary tangles

(NFTs). Intracellular NFTs constitute the most significant marker in the course of AD besides the extracellular β-amyloid plaques (4). The tau protein (Fig. 1) exists in six different isoforms ranging from 352 up to 441 residues in size. All encompass in the C-terminal half (assembling domain) a repeat domain (R1-R4), that consists of three/four pseudorepeat-sequences (~31 residues each). Repeats R2 and R3 contain two hexapeptide motives (^{275}VQIINK^{280} and ^{306}VQIVYK^{311}), that populate β-structure propensity and are essential for tau aggregation (5-10). In pronase digestion experiments with PHFs it was demonstrated that this repeat domain forms the core of AD fibrils. The basic R1-R4 region is flanked by an acidic N-terminal projection domain containing no, one or two insertions and a C-terminal domain, which both form the 'fuzzy coat' surrounding the fibril core in PHFs (11-15). The role of the N-and C-terminal part of the protein, which in antibody and FRET assays (16-21) were found to fold back onto R1-R4, was described mainly as inhibiting aggregation. Hardly any structural features could be observed for the N-terminal half, whereas the occurrence of an amphipatic α-helix was postulated for the sequential part 423-441 (22). Most of the present data about structural and functional behaviour of tau were collected with the help of biochemical and biophysical methods that do not allow atomic resolution (7, 8, 21, 23-29) as tau is not amenable for crystallography. NMR spectroscopy is the only method providing atomic resolution, which can give a detailed description of residual order and three-dimensional structure of intrinsically disordered proteins (IDPs). During the last years several publications reported either complete assignments of smaller tau constructs containing only sections of complete tau isoforms (5, 6, 30-34) or a partial assignment (40-50%) of the largest tau isoform htau40 (35, 36). However, to obtain a complete picture of the structure and function of tau in its monomeric, MT-bound or fibril state, a complete assignment of the resonances of tau is required.

Htau40 is the biggest of the six neuronal isoforms, which are involved in the formation of PHFs during dementia like Alzheimer's disease. It contains all four repeat domains and the two N-terminal inserts. The spectra were recorded at a temperature of 5°C and a pH-value of 6.9. Despite its size of 441 residues (45,850 Da), which would require the use of TROSY sequences (37-39) in the case of folded proteins, all resonances were sharp. This is caused by the high conformational flexibility of tau and its almost complete lack of any secondary structure elements, which results in T2 relaxation time values of ~200 ms on average. Despite advantageous dependence of line width and protein size for IDPs, the NMR analysis of them became only feasible during the last decade by the development of powerful high-field spectrometers and multidimensional heteronuclear NMR experiments with high-

resolution. The major obstacle consists of the small signal dispersion in the proton dimension, which causes high signal overlap. Furthermore, regarding the tau repeat domains, the amino acid sequence is highly repetitive. Together with the strong frequency degeneration for each amino acid unambiguous resonance assignment is a major challenge. On average, for each amino acid i more than five other residues could be identified having C^α chemical shift frequencies in a range of $\pm$ 0.05 ppm around the C^α value for i. The groups of G. Lippens (35, 36) and D. Eliezer (32) reported either partial assignment of htau40 (~40%) or assignment of a smaller construct K19, which consists only of three repeats (R1, R3 and R4). In a previous publication, our group extended their work to all four repeats (K18) (6) and the two flanking domains P2 and R' (K32) (5). Nevertheless, the detailed description for each residue of the entire construct htau40 was not available, yet.

Here, we report the assignment of htau40 monomers in solution at 5°C and 20°C and extract information about secondary structure and backbone dynamics. In the N- and C-terminal parts α-helical propensity was detected for the residues ^{114}Leu-Thr^{123} and even more pronounced for ^{428}Leu-Ala^{437}, whereas β-structure was detected for repeats R2, R3 and R4 in agreement with the investigation of shorter constructs. Additionally, we monitored in detail the binding sites of htau40 for microtubules with chemical shift perturbation experiments, which identified the largest contributions to the binding strength in the regions P2, R1, R2 and R3 (5, 40). With the help of HR-MAS NMR spectroscopy we showed that tau regions containing β-structure and higher backbone rigidity constitute the core of PHFs. Furthermore, intensity differences of the so-called 'fuzzy coat' (41-43) indicated stronger attachment to the fibril core for the C-terminal flexible parts. Our data eventually contribute to a more detailed picture of tau polymorphism, which might lead to a better understanding of processes underlying dementias, like Alzheimer's disease.
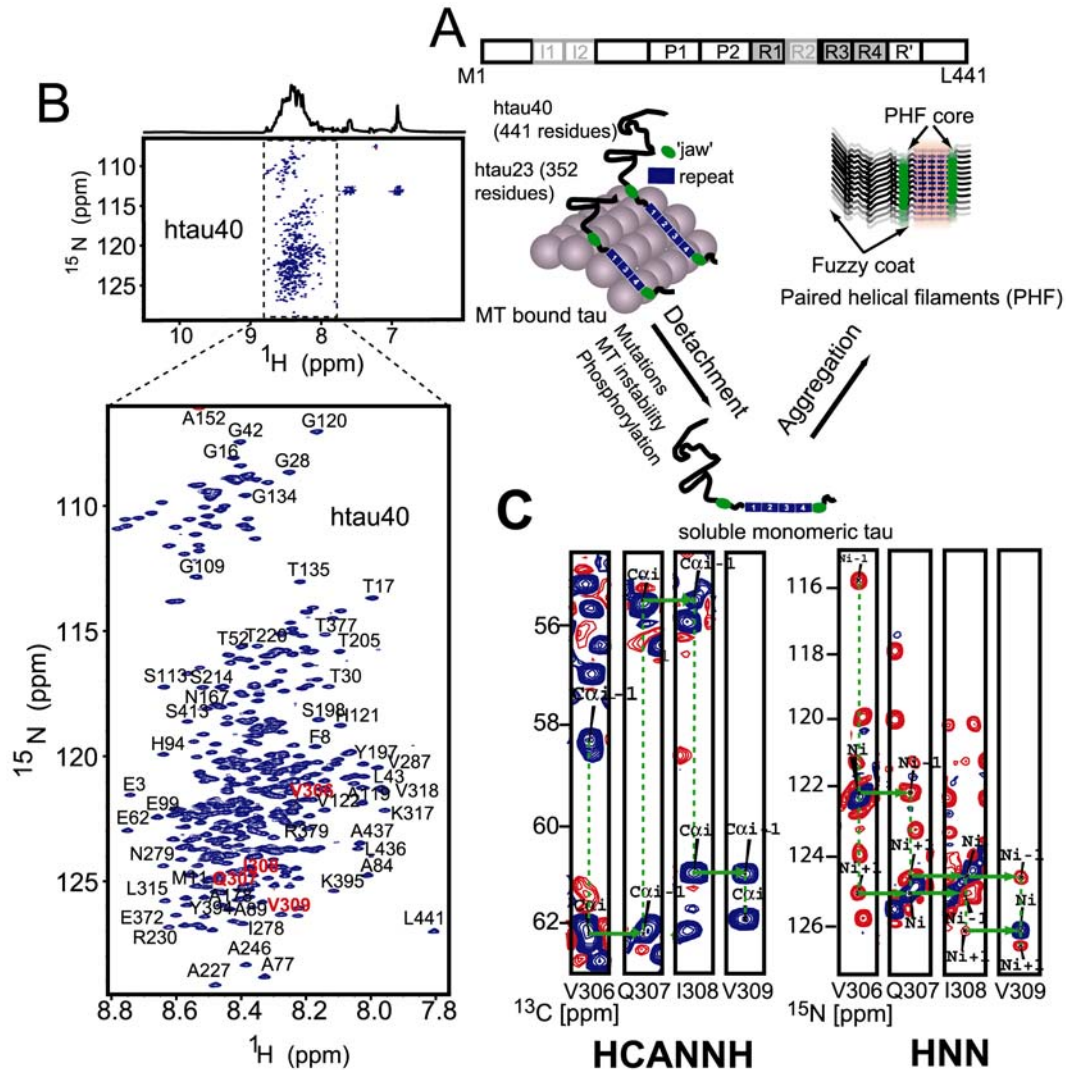
Figure 1

Figure 1: Structural polymorphism of 441 residue htau40. A: Scheme depicting tau's transition from its biological function to its pathological role. As long as tau is bound to MTs, the aggregation prone segment of tau is blocked. Phosphorylation, mutations or MT instability can lead to a rise of concentration of the soluble monomeric form, which is then prone to aggregate into PHFs. Differential splicing of the tau gene is illustrated by pale exonic parts in the htau40 domain scheme. B: Two-dimensional ^{1}H, ^{15}N correlation spectrum of htau40 at 5 °C. Due to lack of any three-dimensional structure strongly reduced chemical shift dispersion in the ^{1}H-dimension is observable. Assignment strategy is demonstrated for residues highlighted in red. C: Two dimensional strips from 3D (HA)CANNH and HNN spectra for residues Val^{306} (^{1}H:8.243 ppm ^{15}N: 122.2 ppm ^{13}C$^\alpha$: 62.21 ppm), Gln^{307} (^{1}H: 8.505 ppm ^{15}N: 125.243 ppm ^{13}C$^\alpha$: 55.41 ppm), Ile^{308} (^{1}H: 8.361 ppm ^{15}N: 124.765 ^{13}C$^\alpha$: 60.91 ppm) and Val^{309} (^{1}H: 8.276 ppm ^{15}N: 126.338 ppm ^{13}C$^\alpha$: 61.84 ppm) are shown. Connectivities are marked by green arrows.

EXPERIMENTAL PROCEDURES

Expression and isotopic labeling of recombinant tau constructs: Human tau constructs were expressed in the vector pNG2 (a derivative of pET-3a, Merck-Novagen, Darmstadt) in E.coli strain BL21(DE3) as described (44). Htau40 is the longest neuronal tau spliceform which can be found in brain lesions, called neurofibrillary tangles, in Alzheimer's disease. It contains 441 amino acids. K32 comprises residues (M)S198-Y394, equivalent to the 4 repeats and the two flanking regions (198 residues). K10 consists of the repeats R1, R3, R4 with the flanking region R' and the C-terminal part (168 residues). K25 encompasses the whole N-terminal half auf htau40 (M1-Q244) without inserts I1 and I2 (185 residues). The expressed proteins were purified from bacterial extracts by making use of the heat stability of the protein and by FPLC SP-Sepharose chromatography (Amersham Biosciences). In order to label the tau proteins with ^{15}N and ^{13}C stable isotopes, the E. coli cultures expressing the different tau constructs were grown on rich growth medium based on chemolithoautotrophic bacteria labeled with ^{13}C and ^{15}N isotopes (Silantes, Munich). Protein samples uniformly enriched in ^{15}N were prepared by growing E. coli bacteria in minimal medium containing 1g L^{-1} of $^{15}NH_4Cl$.

The cell pellets were resuspended in boiling-extraction buffer (50 mM MES, 500 mM NaCl, 1 mM $MgCl_2$, 1 mM EGTA, 5 mM DTT, pH 6.8) complemented with a protease inhibitor cocktail. The cells were disrupted with a French pressure cell and subsequently boiled for 20 min. The soluble extract was isolated by centrifugation, the supernatant was dialyzed against two changes of cation exchange chromatography buffer A (20 mM MES, 50 mM NaCl, 1 mM EGTA, 1 mM $MgCl_2$, 2 mM DTT, 0.1 mM PMSF, pH 6.8) and loaded on an FPLC SP-Sepharose column. The proteins were eluted by a linear gradient of cation exchange chromatography buffer B (20 mM MES, 1 M NaCl, 1 mM EGTA, 1 mM $MgCl_2$, 2 mM DTT, 0.1 mM PMSF, pH 6.8). In the second purification step, the tau breakdown products were removed by applying the gel filtration column Superdex G75 with PBS buffer (137 mM NaC1, 3 mM KCI, 10 mM Na_2HP0_4, 2 mM KH_2PO_4, pH 7.4 with 1 mM DTT). NMR samples contained 0.9 to 0.5 mM ^{15}N- or $^{15}N/^{13}C$-labeled protein in 90% H_2O/10% D_2O, 50 mM phosphate buffer pH 6.8 with 1 mM DTT.

Microtubule preparation: Porcine brain tubulin was purified as described (44, 45) and incubated at concentrations higher than 200 μM in microtubule assembly buffer (100 mM Pipes pH 6.9, 1 mM EDTA, 1 mM MgSO$_4$, 1 mM DTT) in the presence of 1 mM GTP at 37° C for 5 minutes. After addition of 100 μM Paclitaxel (Sigma-Aldrich Chemie, Munich, Germany) the polymerisation was performed for 20 min at 37° C. The integrity of microtubules was checked by standard negative stain electron microscopy.

NMR Spectroscopy: NMR spectra were acquired at 5°C on a Bruker Avance 900 spectrometer equipped with a cryo-probe. Aggregation did not occur under these low temperature conditions. Three-dimensional (HA)CANNH (46) (100 (F1) x 72 (F2) x 1 K (F3) complex data points) and HNN (47) (100 (F1) x 100 (F2) x 1 K (F3) complex data points) experiments (4 scans, 1.2 s recovery delay, for each experiment roughly 1day measurement time) were collected to obtain sequence-specific assignments for the backbone of K32, K10, K25 and finally htau40. NMR data were processed and analyzed using NMRPipe (48) and Sparky 3 (T. D. Goddard and D. G. Kneller, SPARKY 3, University of California, San Francisco). The already available assignment of K18 (6) was used to accelerate analysis of K32 spectra (5). Assignment of K10 and K25 together lasted roughly 2 weeks. All these assignment data assisted the final assignment of htau40. These results were transferred to spectra recorded at 20 °C and 28 °C by performing a temperature titration, in which the temperature was raised in small steps (2-3 °C) and recording 3D-(HA)CANNH spectra at 20 °C and 28 °C. Secondary shift values were calculated as the differences between measured C$^\alpha$ chemical shifts and the empirical random coil value for the appropriate amino acid type. Using the program NMRView Version 5 (49, 50), random-coil values for the primary sequence of htau40 were generated (50, 51). Random coil values for histidines, glutamates and aspartates were taken from (52-54), as the chemical shifts of these residues are particularly sensitive to pH and the pH in the studies by Wishart et al. (pH 5) is more similar to the one used here (pH 6.9). Furthermore, correction factors for residues occurring in the sequence before a proline residue were also taken from Wishart et al. (54). To estimate the β-sheet propensity in contiguous segments of tau, the observed C$^\alpha$ chemical shifts were normalized by the empirically determined secondary shift expected for that residue type in a fully β-sheet conformation (55), summed and normalized by the number of residues in the segment (56).

For tau-MT titrations NMR samples contained 274 μM uniformly ^{15}N, ^{13}C-labeled htau40. The complex formation was monitored at 20 °C for MT concentrations (αβ-tubulin dimers) of 137 μM by recording ^{15}N-HSQC spectra, in which changes of signal assignment caused by the presence of MTs and different buffer conditions were tracked with the help of a 3D-(HA)CANNH experiment. The whole experiment took roughly 1 day. Analysis of MTs showed that the microtubule fraction used for the experiment remained stable over the entire duration of the experiment.

One-bond N-H RDCs (D$_{NH}$) were determined by using the 2D inphase-antiphase (IPAP)-HSQC (57). D$_{NH}$ values were calculated as the difference between splittings measured in the isotropic phase and in a sample, in which htau40 had been aligned in 5 mg/ml Pf1 bacteriophage (Asla, Riga, Latvia) (deuterium splitting 4.3 Hz) . RDCs were not corrected for the negative gyromagnetic ratio of ^{15}N.

^{15}N R$_{1\rho}$ relaxation rates were measured with pulse sequences based on Farrow et al. (58, 59) at 5°C on a Bruker Avance 700 MHz spectrometer. For R$_{1\rho}$ the spinlock frequency was 2 kHz and the relaxation periods 20, 100, 220 and 300 ms. Relaxation times were calculated by fitting a exponential function to the decaying signal integrals with subsequent fitting error estimation.

^{3}J(H^N_iH$^\alpha_{i-1}$)- couplings were measured using quantitative J correlation (intensity modulated HSQC) on a Bruker 900 Avance spectrometer (32 scans, relaxation delay 1.2 ms, 2τ = time for evolution of ^{3}J$_{HNH\alpha}$: 18 ms). (60) Couplings were evaluated by using the relation S$_{cross}$/S$_{diag}$ = cos(π^3J$_{HNH\alpha}2\tau$). Random coil values were subtracted from the couplings to gain direct indication of possible secondary structure elements (61).

Htau40 fibrils were investigated with Bruker 900 MHz HR-MAS probehead at a spinning frequency of 4.2 KHz and a temperature of 28 °C. The sample of ca. 60 μl contained roughly 7 mg of (uniformly ^{15}N/^{13}C labelled) htau40 fibrils. The fibrils were pelletted twice by ultracentrifugation for 1 h to remove non-fibrillous components. The pellet was resolved in 50 mM sodium phosphate buffer (pH 6.9) with 1 mM DTT and 10 % D$_2$O. With the help of a diffusion-ordered 1D-NMR experiment (BPP-LED (62)) diffusion velocity of htau40 fibril

could be distinguished from monomeric htau40. Furthermore, the fibril quality was checked on PAGE and by cryo-EM.

RESULTS

Backbone assignment of htau40

By combining the high-resolution 3D (HA)CANNH (46) and 3D HNN (47) experiments at high-field (900 MHz with cryo probehead), we could unambiguously assign all backbone resonances of htau40. As already reported for the construct K32 (5), residues Gly^{272}, Gly^{303}, Gly^{334}, Gly^{366} (surrounded by two glycines in the sequence motif PGGG, which occurs at the C-terminal end of each repeat region) and Gly^{304}/Gly^{335} were identified in the spectra, however, their unambiguous assignment was not possible due to extreme resonance overlap. Furthermore, the resonances originating from Met^1 and Ala^2 were not detectable due to fast exchange near to the N-terminal end. Thus, more than 98% of htau40 were identified, excluding proline residues for which more than 83% of C^α frequencies were found. Using the constructs K32 (P2/R1-R4/R'), K10 (C-terminal-half with R2) and K25 (N-terminal half without I1/I2) helped additionally to resolve cases of strong or complete signal overlap (Supporting information).

Residual structure propensity in htau40

NMR spectroscopy provides different tools to detect residual secondary structure. We made use of C^α secondary chemical shifts, $^3J(H^NH^\alpha)$ couplings and residual dipolar couplings (RDCs).

C^α secondary chemical shifts are very sensitive probes for secondary structure in folded and unfolded proteins. Small but distinct deviations from random-coil values (50-52, 55)) indicate the occurrence of β-sheet and α-helical propensity. We already published secondary chemical shifts for K18 and K32 (5, 6, 30, 31). Comparison of the corresponding region in htau40 showed that the secondary structure of these parts did not change upon completion of the molecule by the N-terminal part (Met^1-Tyr^{197}) and the C-terminal part (Tyr^{394}-Leu^{441}) (supporting information). Thus, we observed again continuous stretches (containing 7-11

residues) with negative secondary chemical shifts, in particular ^{274}Lys-Leu^{284} (R1/R2), ^{305}Ser-Asp^{315} (R2/R3) and ^{336}Gln-Asp^{345} (R3/R4) (Fig. 2), which indicated a propensity for β-structure. Quantitative analysis resulted in populations of β-structure of 22% for ^{274}Lys-Leu^{284}, 25% for ^{305}Ser-Asp^{315} and 19% for ^{336}Gln-Asp^{345} Additional sites within the repeat domains with β-structure content were ^{256}Val-Ser^{262} (12%) and ^{351}Gln-Leu^{357} (12%), which were located roughly in the center of repeats R1 and R3. Continuous stretches of negative C$^\alpha$ secondary chemical shifts consisting of more than 4 amino acids located in sequential parts outside R1-R4 were ^{86}Gly-Gln^{92} (17%), ^{128}Val-Lys^{132} (11%), ^{161}Gly-Ala^{166} (17%) and ^{224}Lys-Arg^{230} (18%). Thus, the strongest content of β-structure within the entire sequence of htau40 was found in the two regions ^{274}Lys-Leu^{284} (R1/R2) and ^{305}Ser-Asp^{315} (R2/R3) encompassing the two hexapapeptides ^{275}VQIINK^{280} and ^{306}VQIVYK^{311}. Continuous stretches of positive secondary chemical shifts indicate the occurrence of α-helical propensity. This secondary structure element was completely absent from the sequential region P1-R', whereas we could detect it for ^{114}Leu-Thr^{123} (in between insert 2 (I2) and the proline-rich region P2) and ^{428}Leu-Ala^{437} in immediate proximity to the C-terminus. The population of α-helical propensity could be quantified: 18% for ^{114}Leu-Thr^{123} and 25% for ^{428}Leu-Ala^{437}. Htau40 did not exhibit any temperature dependence concerning residual structure elements. The pattern of secondary chemical shifts found at 5°C was identical to the pattern at 20°C (supporting information).
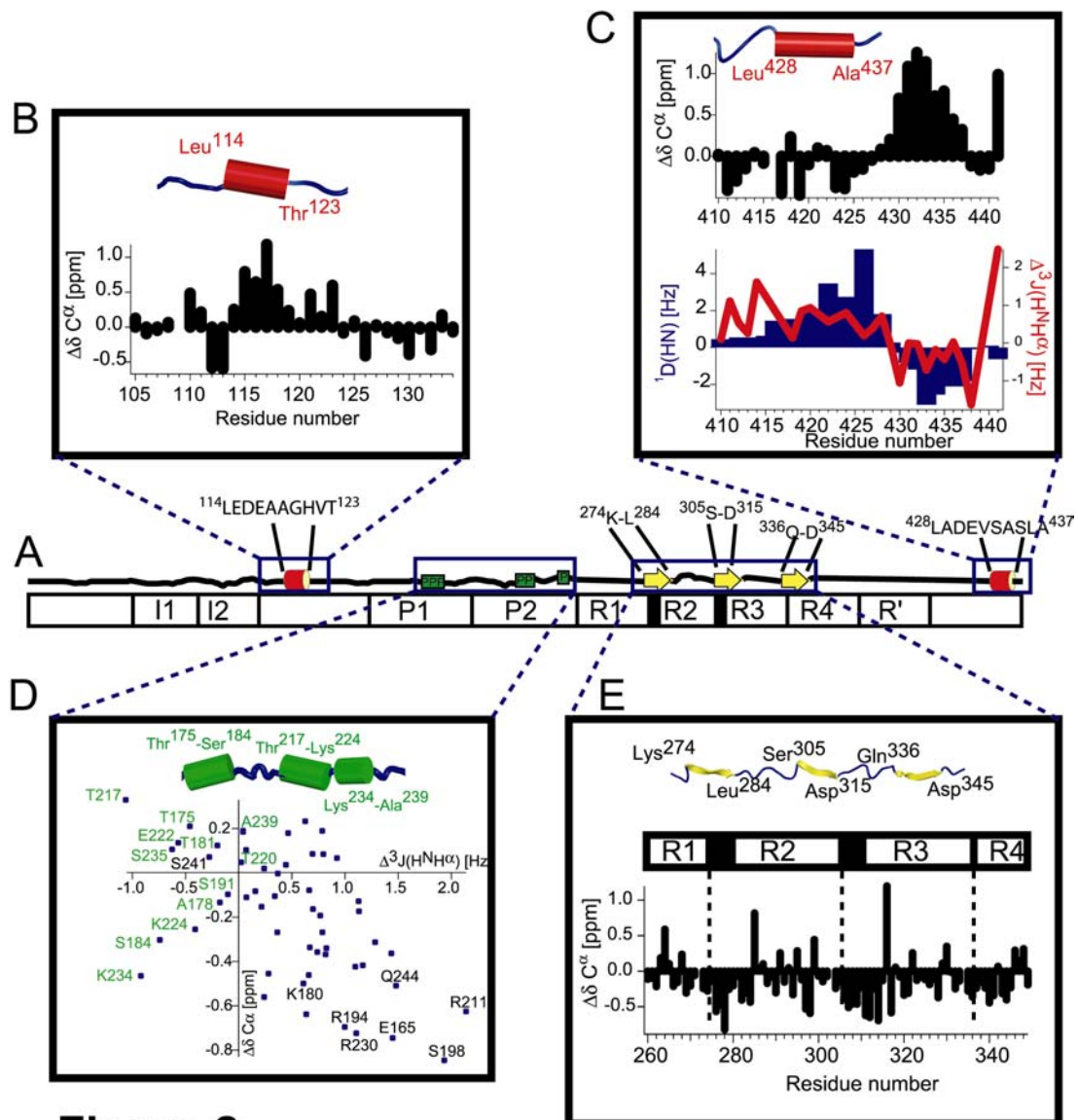
Figure 2: Structural properties of monomeric htau40 in solution. **A:** 338 out of 441 residues of htau40 assume random-coil conformation. **B:** ^{114}Leu-Thr^{123} exhibits α-helical propensity (positive $\Delta\delta C^\alpha$). **C:** ^{428}Leu-Ala^{437} contains α-helical character (positive $\Delta\delta C^\alpha$, negative ^{1}D(HN) couplings and negative differences ($\Delta^3 J_{NH-\alpha H}$) between $^3 J_{NH-\alpha H}$-couplings and random-coil values (61). **D:** poly-proline helical tendency for ^{175}Thr-Ser^{184}, ^{217}Thr-Lys^{224}, ^{234}Lys-Ala^{239} (negative $\Delta^3 J(H^N H^\alpha)$-coupling values and negative $\Delta\delta C^\alpha$). **E:** ^{274}Lys-Leu^{284}, ^{305}Ser-Asp^{315} and ^{336}Gln-Asp^{345} populate transiently β-structure as indicated by negative ΔC^α. The estimated error is 0.2 Hz for ^{1}D(HN) and 0.4 Hz for $\Delta^3 J_{NH-\alpha H}$-couplings.

Comparison of experimental ^{3}J-couplings (dependent on the distribution of ϕ angles) with random coil prediction confirmed the presence of specific conformational behavior in

these same regions. While positive $\Delta^3J_{NH-\alpha H}$ (J_{exp}–$J_{random\ coil}$) values indicate a tendency towards extended structure and β-structure, low or even negative values indicate turns or helical propensity. The largest coupling values were detected for the region of [306]Val-Asp[315] (supporting information). The region of the second strongest β-structure content ([274]Lys-Leu[284]) also exhibited positive $\Delta^3J_{NH-\alpha H}$ (J_{exp}–$J_{random\ coil}$) values, but the effect was not very pronounced. Positive values were clearly dominant in the entire htau40 indicating the overall extended chain conformation of an unfolded protein. In contrast, negative $\Delta^3J_{NH-\alpha H}$ (J_{exp}–$J_{random\ coil}$) values or values close to zero were found in regions, in which also secondary chemical shifts indicated the occurrence of α-helix ([114]Leu-Thr[123] and [428]Leu-Ala[437]). Furthermore, small ^3J-coupling values were detectable for the two proline-rich regions P1 and P2: Thr[175], Ala[178], Thr[181], Ser[184], Thr[217], Thr[220], Glu[222], Lys[224], Lys[234] and Ser[235] (Fig. 2).At the same time some of these residues also exhibited negative secondary chemical shifts. Negative $\Delta^3J_{NH-\alpha H}$ and negative $\Delta\delta C^\alpha$ values can only be reconciled by a polyproline II helix. In P2 a stretch of positive $\Delta^3J_{NH-\alpha H}$ (J_{exp}–$J_{random-coil}$) values, which was sandwiched by negative values, was identical to the region of [224]Lys-Arg[230] exhibiting β-structure propensity as indicated by C^α secondary chemical shifts.
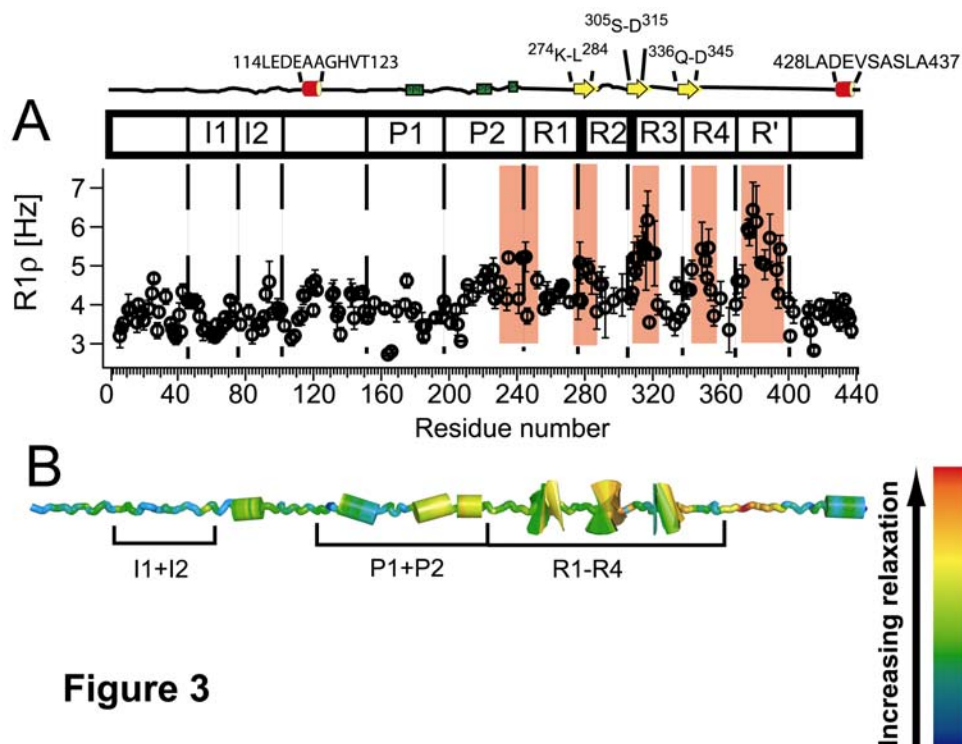
Figure 3: Backbone dynamics of monomeric tau. **A**: ^{15}N R1ρ relaxation rates: Stretches exhibiting increased backbone rigidity resulting in higher relaxation rates are highlighted in red. **B**: ^{1}H, ^{15}N RDCs: The regions P1-R' show the largest couplings. The estimated error is 0.2 Hz. **C**: htau40 molecular model with the R1ρ relaxation information.

As another tool for determining residual structure we used N-H residual dipolar couplings (RDCs), which can be measured in partially aligned media, such as solutions of Pf1 bacteriophages. In an anisotropic environment dipolar couplings report on the averaging of the orientation of the one-bond internuclear vector with respect to the magnetic field axis. In contrast to a smooth bell-like coupling profile (63) but in agreement with both models of random-coils that take the sequence information into account and with findings on other intrinsically unfolded proteins such as α-synuclein (64, 65), we could detect distinct distribution of negative and positive RDC values (Fig. 3). Comparison to RDCs measured for K18 (supporting information) (scaled by a factor of 2.8) indicated a high degree of correlation between the coupling profile of K18 and the corresponding region in htau40. Due to strong signal overlap no significant negative RDC values could be identified, as were found in K18 and K32 (indicating turn propensity) within the repeat domains. The overall distribution of RDC values clearly showed that the strongest couplings were located within the region P1-R',

where several coupling values above 10 Hz were observed. The complete N-terminal half and the C-terminal part (^{390}Ala-Leu^{441}) exhibited rather low coupling values, which are all below 6 Hz and in many cases even around 1 Hz. The region of ^{305}Ser-Asp^{315}, which contained the strongest β-structure propensity according to secondary chemical shifts and $^3J(H^NH^\alpha)$ couplings showed the highest RDC values in full agreement with the other aforementioned NMR data.

Furthermore, a stretch of negative RDC values in ^{430}Asp-Leu^{441} matched exactly the region with α-helical propensity revealed by secondary chemical shifts and $^3J(H^NH^\alpha)$ couplings. This was the only region where turn or helix were detected.

RDCs are sensitive to motion on all timescales between pico- and milliseconds and also contain structural information, whereas ^{15}N R1ρ spin relaxation rates, for which chemical exchange is refocused, reflect backbone dynamics on timescales between pico-nanoseconds (66). Instead of a bell-like profile of R1ρ relaxation rates, as would be expected for a completely unfolded protein, we detected sites with restricted backbone mobility on the corresponding time scales, which resulted in higher relaxation rates. The region of P2-R' indicated the highest R1ρ rates. In particular the following sites (> 5Hz): ^{309}Val-Lys^{321} (R3), ^{343}Lys-Lys^{353} (R4) and ^{372}Glu-Lys^{395} (R'). In P2, R1 and R2 reduced backbone mobility was probed for the residues: Ser^{235}, Leu^{243}, Thr^{245}, Ile^{277}, Asn^{279} and Leu. ^{282} The reason for faster relaxation in R2, R3 and R4 is the presence of partial β-structure character in these repeats, whereas no structural propensity could be detected for R', which exhibited the highest relaxation rates. Zones with higher relaxation rates in P2 and R1 correlated well with the poly-proline helix character for P2. No particular backbone rigidity was detected for P1 with T1ρ spin relaxation as no high RDC values were observed.

Htau40-microtubule interactions
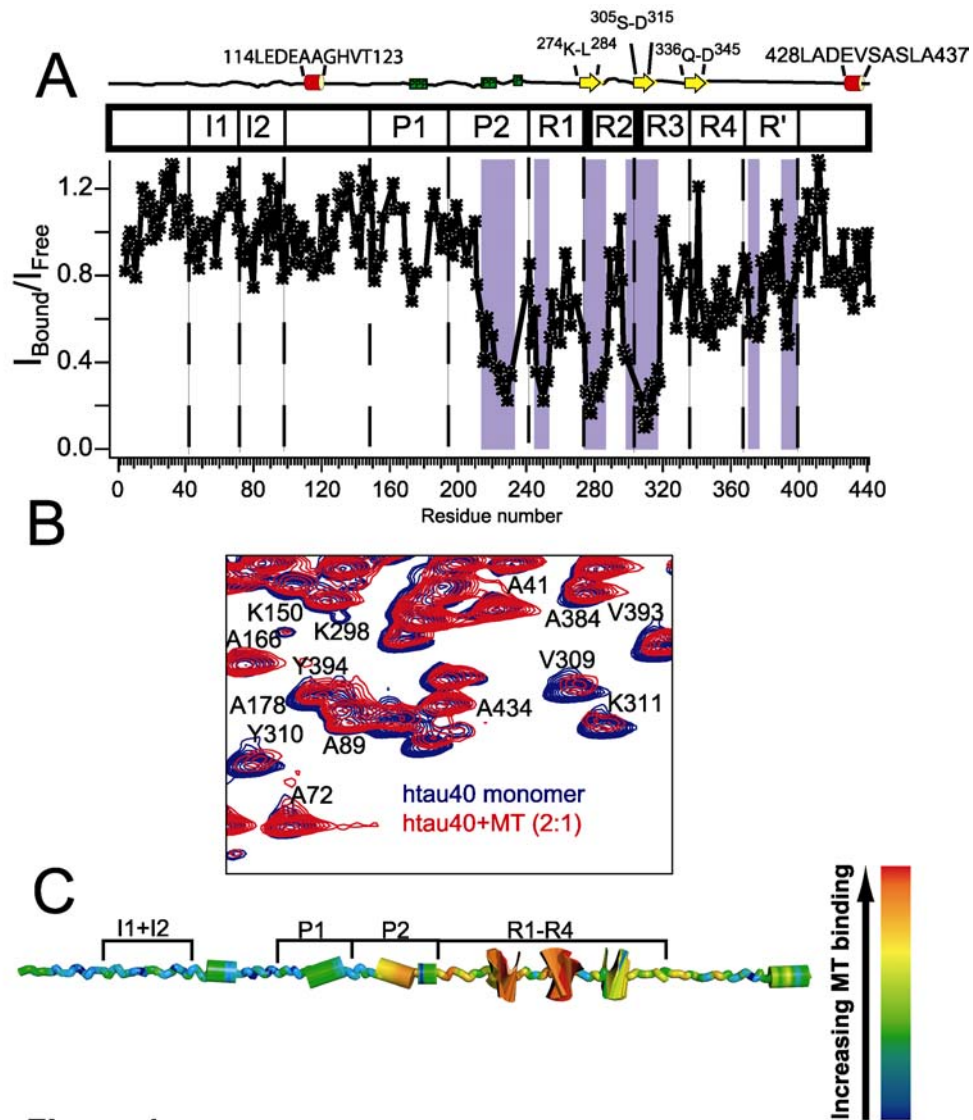
Figure 4: Atomic resolution characterization of MT - htau40 interaction. For sequential alignment monomeric htau40 as cartoon with structural propensities is depicted at the top. **A**: Intensity profile for htau40 in the MT bound state at 20 °C. Low intensity ratios indicate strong binding to MTs. Strongest binding sites are marked by blue boxes. **B**: Part of two overlaid HSQC spectra for the free unbound htau40 monomer (blue) and the bound form (red). The concentration ratio between htau40 and MT is 2:1 (274 μM : 137 μM). One can recognize the intensity loss and chemical shifts change for residues binding strongly to MTs. **C**: Htau40 molecular model indicating regions of high MT affinity in blue (/green). Weaker binding sites are depicted in yellow or red.

NMR signals of backbone amides constitute excellent probes to detect interactions with potential binding partners (67). We applied chemical shift perturbation mapping and made use of changes in peak position and intensity to quantify the strength of interactions with potential binding sites in htau40. The spectra of htau40 were recorded in the presence of taxol stabilized microtubules (MTs) in a tau : MT ratio of 2:1. Thus we avoided the problem of probing unspecific binding sites in htau40, which could occur at an excess of MTs. We measured at a temperature of 20 °C to ensure MT stability over a time interval of ~1 day for recording 3D-(HA)CANNH experiments. These experiments helped us to resolve ambiguities of the assignment caused by the presence of MTs as ligand. The overall signal intensity was decreased immediately upon addition of MTs, because completely bound htau40 is no longer detectable due to extreme shortening of relaxation times which results in strong line-broadening beyond our detection level. Nevertheless, chemical shift changes, indicating weak or intermediate interaction, and additional exchange-induced broadening, caused by strong MT-binding, of specific regions of htau40 were observed. There was a very good correlation between the two parameters (supporting information). The following regions indicated the strongest interactions with MTs (Fig. 4): ^{214}Ser-Lys^{240}, ^{243}Leu-Ile^{260}, ^{274}Lys-Gln^{288} and ^{297}Ile-Val^{318}. Thus, the regions P2, R1, R2 and R3 were significantly involved in the binding to microtubules which was accompanied by a loss of the amide signals to less than 20%. For the regions R4 and R' the intensity of the amide resonances was reduced to around 40% indicating a weaker binding. In region R', which was postulated to be one of the 'jaw' regions facilitating the tight binding of tau to MTs, the two regions ^{371}Ile-Arg^{379} and ^{393}Val-Val^{399} showed the most significant effect concerning signal broadening. The chemical shift difference in R' was most evident for the sequential part ^{392}Ile-Val^{399}, which correlated quite well with the signal intensity drop at the same site.

Interestingly, several residues within almost the entire N-terminal half showed signal ratios higher than 1, which indicated a rise of signal intensity of this region upon MT binding in contrast to the overall intensity drop dominating the C-terminal part.

Htau40 fibrils investigated with HR-MAS NMR spectroscopy
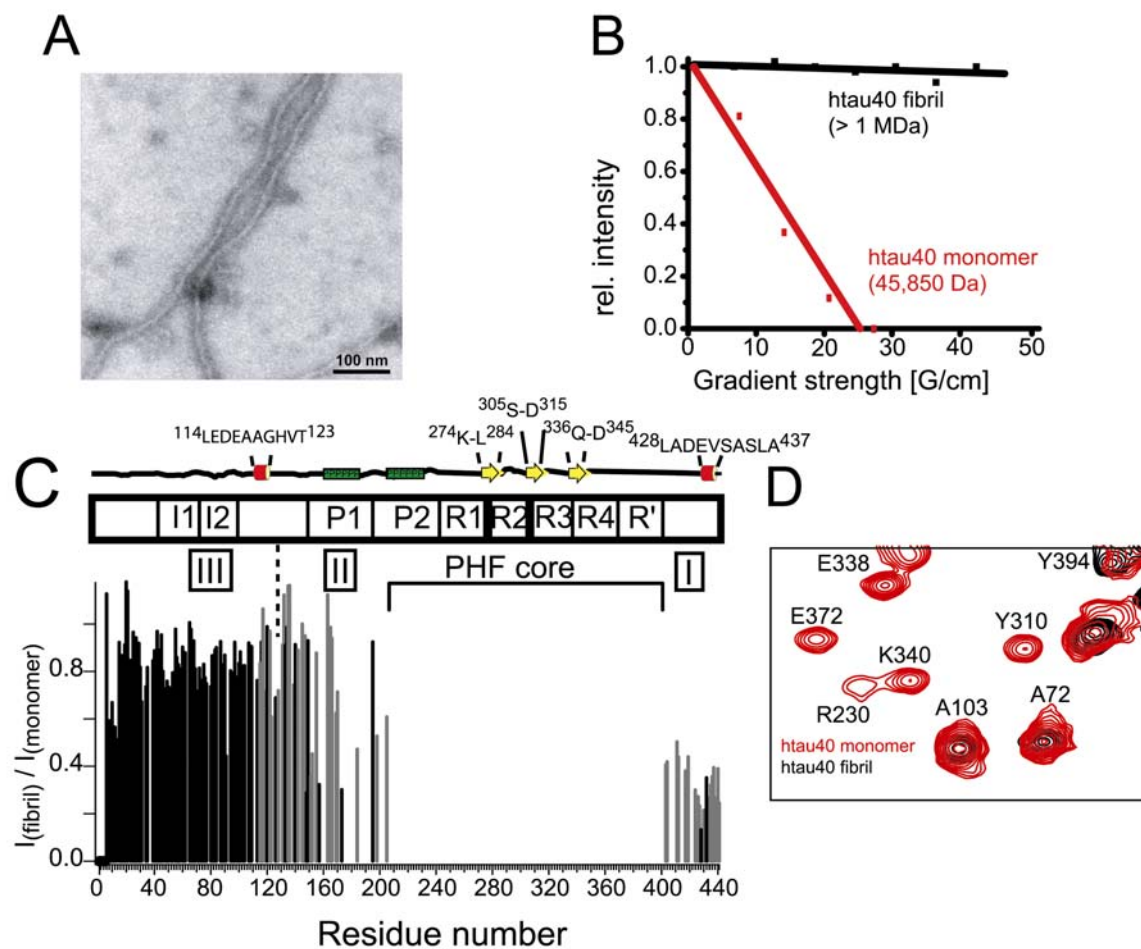
Figure 5: Structural polymorphism in htau40 PHFs. **A**: Electron microscopy picture of bona fide htau40 fibrils. **B**: Relative signal intensity loss as measure for diffusion velocities in dependence of molecular mass for monomeric htau40 (red) and htau40 fibril (black). **C**: Intensity ratio of signals originating from htau40 fibril and htau40 monomer at 28 °C. No signal intensity is available for residues located in the rigid PHF core. In contrast, the flexible 'fuzzy coat' can be classified according to signal intensity and ^{15}N chemical shift differences into domains I, II and III. Grey highlights residues with $\Delta\delta^{15}N$ higher than 0.025 ppm. Monomeric htau40 as cartoon with residual structure element is depicted at the top.

HR-MAS detects signals that have all properties of signals stemming from molecules in solution, namely averaged out anisotropic interactions such as chemical shift anisotropy or dipolar couplings. They also have relaxation properties characteristic of fast tumbling (ps to ns time scale). The only difference is their behavior in sequences that probe translational

diffusion of the molecules. Here they behave like a macromolecular assembly. HR-MAS is therefore optimally suited to detect signals from mobile parts of macromolecular assemblies. Parts of the molecule that tumble slower (slower than μs) cannot be detected because they are broadened by dipolar couplings that are not averaged out at the moderate decoupling powers applied in a HR-MAS probe.

Samples of htau40 fibril (^{15}N,^{13}C-labeled) were measured at a temperature of 28 °C and a spinning frequency of 4.2 KHz. At these conditions we could obtain sharp resonances for the mobile residues, which allowed us to record [^{1}H, ^{15}N]-HSQC spectra. The mobile parts encompassed the whole N-terminal region up to residue Thr^{205} and the C-terminal part from Thr^{403} until Leu^{441}. The measured signal intensity of the fibril was normalized by the corresponding intensities of monomeric htau40 measured at identical conditions. Interestingly, the overall intensity ratio for the C-terminal parts was roughly only the half of the N-terminal parts, reflecting the fact, that this region must be more rigid. No signals (not even resonances of the **PGGG**-motives) could be detected for the repeat domain R1-R4, which emphasized its incorporation into the fibril core. The regions P2 and R' exhibited little backbone mobility as well. Furthermore, according to particularly high ^{15}N chemical shift differences between monomeric and fibrous state the regions from residue Glu^{115} to the fibril core and the complete observable C-terminal part had to experience a change in their chemical environment caused by the fibril core. A LED diffusion experiment (62) indicated the difference of the diffusion velocity between the htau40 monomer with a hydrodynamic radius of ca. 65 ± 2 Å (DOSY measurement (68), theoretically determined value ca. 71 Å (69)) and the htau40 fibril. Thus, the NMR resonances, measured for PHF samples, originated from molecular species with a mass of more than 1 MDa. Furthermore, no signal intensity of residues within the repeat domain could be detected. Therefore, detected signals from flexible parts could not be caused by free htau40 monomer.

DISCUSSION

Htau40 is for several reasons a very interesting protein to investigate. First, its sheer size is challenging for an NMR spectroscopist, because complete assignment of an unfolded protein of this length was never achieved before. Second, the tau protein is a member of the class of intrinsically disordered proteins (IDP), whose high significance for pathological processes, e.g. aggregopathies (like Parkinson's disease, Alzheimer's disease (AD)) was more and more elucidated during the recent years (70-75). Aggregates (NFTs) of hyperphosphorylated tau are the most significant hallmark concerning occurrence and course of Alzheimer's disease besides β-amlyoid plaques (4). Appearance of cytosolic NFTs correlates better with the different states of AD than the extracellular β-amyloid plaques. Third, tau is one of the essential microtubule associated proteins (MAPs) in neurons (76). Here, it is necessary for maintenance of cell metabolism, enabling neurite outgrowth and synaptic function.

The exact molecular nature of all processes, biological and pathological ones, is still only roughly understood. Techniques that report bulk properties such as CD or UV/VIS spectroscopy accompanied by immunobiological assays were applied to tau (7, 9, 28, 29, 77). Although these techniques could already elucidate some characteristics of tau concerning residual structure, MT binding and PHFs, none of them was capable of providing any structural or dynamic data with atomic resolution without severe protein modifications, like mutations for example. Since IDPs are highly dynamic, NMR spectroscopy is the only technique to provide information on the structure and dynamics of tau with atomic resolution.

This prompted us to apply state-of-the-art liquid-state NMR spectroscopy to shed light onto structural and dynamic aspects of the htau40 monomer, which is the biggest tau isoform in the human central nervous system. Furthermore, its role in physiological processes (aggregation and MT binding) aroused our interest. The basis for all further work with NMR spectroscopy is the backbone assignment of a protein. Accomplishing this assignment for tau is a big challenge, which is put into evidence by several publications that either achieved only partial assignment (40-50%) of full length tau (35, 36, 78) or resorted to fragments of tau that were at least a factor of 2 smaller than full length tau (5, 6, 32). There are three major obstacles: (1) the very low signal dispersion in the ^{1}H- dimension (< 1 ppm) in comparison to folded proteins, (2) the high degree of frequency degeneration (on average ca. five possible

C^α-connectivities for each residue) caused by repetitive amino acid sequences at least in the four repeats R1 to R4 and (3) the absence of pronounced tertiary structure. We combined 3D-NMR spectroscopy on high field NMR spectrometers with measurements of different tau fragments (K10, K25 and K32) to obtain the complete backbone assignment of htau40. Apart from MAP2 (~1860 residues) and titin (length of disordered titin region is 2174 residues), htau40 is one of the biggest unfolded proteins (7, 79, 80) as indicated in the protein databank DISPROT (81). Up to now, backbone assignment was only feasible for proteins, which are by more than the factor of 2 smaller than htau40, like K32 (5) or HIV-1 protease precursor (82). Our work shows, that this class of proteins is only accessible for NMR spectroscopy as high-resolution structure technique. The assignment could be accomplished by conventional three-dimensional NMR spectroscopy. No experiments with reduced dimensionality, like APSY (83), were necessary.

To apply the assignment on essential questions concerning structural polymorphism that underlies the role of htau40 in biological and physiological processes, we determined residual structure elements with the help of secondary chemical shifts, $^3J(H^N H^\alpha)$-couplings and RDCs. Furthermore, we also probed backbone dynamics by measuring R1ρ relaxation rates. The overall picture we get is that the microtubule-binding region (MTBR) is structurally different to the rest of the molecule. We detected β-structure propensity in the regions ^{274}Lys-Leu^{284}, ^{305}Ser-Asp^{315} and ^{336}Gln-Asp^{345}, which are all located in the repeat domain (R2-R4). The rest of the molecule contains only some stretches of relatively weak β-structure or extended chain character. The whole N-terminal half (^{1}Met- Ile^{151}) is very flexible (17) lacking any real structural propensity apart from a stretch of partial α-helical character for ^{114}Leu-Thr^{123}. A second, but more populated, site of α-helix propensity is located in the C-terminal part of htau40 (^{428}Leu-Ala^{437}). This correlates well with the identification of an α-helix in the peptide ^{423}Pro-Leu^{441} by Esposito et al. (22). We want to underline here, that the measurements for determining secondary structure propensity were performed in the absence of any secondary structure inducing agents, like micelles or TFE ((2,2,2)-trifluor-ethanol) (22, 33, 77). The latter sometimes induce secondary structures that are not observed in water (84). Determination of backbone dynamics confirmed the characteristic differences between MTBR, which shows the highest RDC values and R1ρ rates (> 5 Hz), and the flanking regions with mostly small dipolar coupling values (~1Hz) and R1ρ rates (3-4 Hz). Furthermore, we could measure poly-proline helix character in P1 and P2 (^{175}Thr-Ser^{184}, ^{217}Thr-Lys^{224}, ^{234}Lys-Ala^{239}). This matches the results by Bielska et al. (85) proposing

significant poly-proline (II) helix in the same regions upon phosphorylation of certain sites. We could observe higher backbone rigidity indicated by stronger RDCs and higher R1ρ relaxation rates for the regions P2-R', which can be explained in case of the four repeat regions by their relatively high content of β-structure. Detection of negative RDC values in the C-terminal region, already identified as region with partial α-helical character, emphasizes that RDCs can help to detect residual structure elements. Nevertheless, no significant negative RDC values could be observed in the second region, for which secondary chemical shifts propose a weaker occurrence of α-helical character. To analyze the influence of these structural data we examined interaction of htau40 with taxol-stabilized microtubules (MTs) and htau40 when it is part of bona fide PHFs.

We detected the following main binding sites for the regions P2 and R1-R3: [214]Ser-Lys[240], [243]Leu-Ile[260], [274]Lys-Gln[288] and [297]Ile-Val[318]. The affinity of R4 and R' was weaker than for the aforementioned strongest binding sites. The residues showing the strongest binding in R4 and R' were [371]Ile-Arg[379] and [393]Val-Val[399]. This confirms the 'jaws' model, in which the bite of P2 is about twice as stronger as that of R4 and R' (40). This is different from the binding behavior of K32 (5), for which the contribution to the MT-interaction of R' and P2 were in a rather similar range. A similiar experiment to monitor binding-sites of tau for MTs has also been performed by the group of G. Lippens (86). In their publication the binding epitopes could not be characterized with the same resolution achieved in this study, since only 40 to 50% of the resonances were assigned. In contrast to (86), in our experiments we chose a concentration ratio of tau : tubulin of 2:1 that exludes unspecific binding of MT to tau. The substoichiometrical concentration of tubulin also ensures that differences in the observation of MT induced chemical shifts and effects on the intensity of NMR signals of tau can be interpreted as on-pathway encounter binding of MT to tau. The group of G. Lippens detects tau-MT interactions for the regions between residues 100 to 200 and for the last ca. 40 residues at the C-terminal end. This is probably caused by unspecific tau-MT interactions due to high excess of microtubules (86). We clearly see no significant signal intensity loss for the complete N-terminal part up to residue number 200. Regions outside the MTBR show only minor effects, such as increasing signal intensities in the N-terminal part of htau40. These stronger signal intensities could be caused by release of some intramolecular long-range interaction as described by (16, 17, 21). This issue needs to be further clarified, for example with the help of paramagnetic spinlabel measurements, which are already in progress. Furthermore, in contrast to PHFs, we were still able to detect signal intensity for residues within the MTBR, in particular for amino acids being located between the strong binding

sites. Therefore, we could not observe any aggregation at the surface of MTs upon MT binding, resembling PHF formation. This means, that tau exhibits also in the MT-bound state a mainly unfolded and very flexible character instead of high backbone rigidity (87).

HR-MAS measurements of htau40 PHFs showed that PHFs can be subdivided into a rigid core and a flexible 'fuzzy coat'. We could also detect regional differences within the "fuzzy coat". The reproducibility of the PHF intensity profile was satisfying (Supporting information). This implies that different batches of PHFs are morphologically highly similar. Opposite to findings for amyloid-β-peptide, no significant polymorphism for different tau fibril samples could be detected (88). According to our observations the region between Thr^{205} and Thr^{403} exhibits high rigidity, which causes signal loss for this range of the protein. Even sequential motives, which are supposed to be highly flexible like the **PGGG** region are not recognizable in any spectrum. The remaining peaks originate completely from the flexible regions surrounding the PHF core. These regions constitute the so-called "fuzzy coat" and behave almost identically to the htau40 monomer. Further characterization of the "fuzzy coat" was possible on the basis of comparison between chemical shift differences and intensity ratios. Thus, the first 114 residues do not show any significant signal broadening or chemical shift changes. In contrast, the N-terminal part of the "fuzzy coat" starting with Glu^{115} exhibits chemical shift differences of more than 0.025 ppm, which can be caused by interactions with the PHF core. Lower intensity ratios and chemical shift differences of more than 0.025 ppm for the flexible residues at the C-terminal side indicate that this part is more tightly bound to the PHF core than the N-terminal part. This was also found by von Bergen et al. (15) with enzymatic digestion.

Thus, the part of htau40 monomer, for which we detected the highest content of β-structure character accompanied by the most restrained backbone dynamics (high R1ρ rates for ^{309}Val-Lys^{321} (R3), ^{343}Lys-Lys^{353} (R4) and ^{372}Glu-Lys^{395} (R')), constitutes the rigid core of the PHFs, which is beyond our detection limit. This region of htau40 contains all aggregation-prone elements. In contrast, parts of the monomer (^{1}Met-Asp^{146}, ^{400}Ser-Leu^{441}) which are highly flexible or even show partial α-helical propensity cannot be incorporated into the fibril, because they lack any seeds of aggregation, which are limited virtually entirely to the MTBR. We were able to demonstrate that structural and dynamical behaviour in the htau40 monomer determines the process of aggregation, which affects sequential tau regions to a different extent. One can speculate that the flexible parts of tau could even function as inhibitors of aggregation or counterparts to the aggregation prone repeat domains as was found by the group of Binder (17, 19, 20, 89). In studies with conformational sensitive antibodies it was

found, that certain long-range interactions between the N-terminal parts and the MTBR can suppress formation of PHFs (17). For this effect the C-terminal part, in particular the stretch with α-helical content, is essential, which is in close proximity to the N-terminal end as indicated by antibody and FRET experiments (16, 24, 25, 27). Phosphorylation plays an important role concerning MT binding and PHF aggregation. It is widely known, that phosphate groups within the four repeat regions (Ser^{262}, Ser^{293}, Ser^{324}, Ser^{356}) cause detachment of MTs, whereas aggregation rates are remarkably reduced. In contrast, phosphorylation in the flanking regions, such as Thr^{212}, Ser^{214}, Thr^{217}, Thr^{231}, Ser^{396}, Ser^{404}, accelerates formation of fibrils (90-93). Conformational changes upon phosphorylation should be responsible for release of tau from MTs. Phosphorylation could induce more strongly pronounced poly-proline helices in the two proline-rich domains P1 and P2 (^{175}Thr-Ser^{184}, ^{217}Thr-Lys^{224}, ^{234}Lys-Ala^{239}) (85). As was also found in the case of the N-terminal mutation R5L (89, 94) loss of flexibility in the N-terminal part can already enhance aggregation tendency. We emphasized in the current work that flexibility and conformational differences (e.g. those between α-helix and β-structure) play an important role concerning inducing fibrillization. One could conclude that, rigidification of the protein backbone, eventually accompanied by side-chain effects, caused by mutation (17) or phosphorylation (95), reduces the quantity of aggregation-resistant conformations and therefore promote formation of PHFs.

In our experiments we demonstrated, that NMR spectroscopy as only high-resolution technique can also handle particularly demanding biological systems as intrinsically unfolded proteins. We could overcome the major obstacles of assigning the amide backbone resonances of the biggest tau isoform htau40, which is especially interesting, because it is involved in several dementia like Alzheimer's disease. Thus, NMR spectroscopy is able to make an important contribution to elucidate the molecular basis causing these diseases. We demonstrated that it is possible to achieve a detailed description of residual structure elements and dynamic behaviour of htau40 for different states of tau polymorphism: monomer, MT-bound state and PHF fibrils. We could also show the correlation between these data and biological and pathological effects, which should be all encoded already in the monomeric state. One can expect that combination or creation of new high-resolution multidimensional NMR experiments and the ongoing development of high-field NMR spectrometers will further expand size limits for NMR spectroscopy in dealing with the class of IDPs, which would help to understand the underlying principles of aggregopathies.

ACKNOWLEDGEMENT

The abbreviations used are: AD = Alzheimer's disease, FRET = Fluorescence resonance energy transfer, HR-MAS = high resolution magic angle spinning, IDP = intrinsically disordered protein, MAP = microtubule-associated protein, MTs = microtubules, MTBR = microtubule-binding regions

REFERENCES

1. Garcia, M. L. & Cleveland, D. V. (2001) *Curr. Opin. Cell Biol.* **13,** 41-48.

2. Cassimeris, L. (1999) *Curr. Opin. Cell Biol.* **11,** 134-141.

3. Cassimeris, L. & Spittle, C. (2001) *Internatl. Rev. Cyt., Vol 210* **210,** 163-226.

4. Braak, H. & Braak, E. (1991) *Acta Neuropath.* **82,** 239-259.

5. Mukrasch, M. D., von Bergen, M., Biernat, J., Fischer, D., Griesinger, C., Mandelkow, E. & Zweckstetter, M. (2007) *J. Biol. Chem.* **282,** 12230-9.

6. Mukrasch, M. D., Biernat, J., von Bergen, M., Griesinger, C., Mandelkow, E. & Zweckstetter, M. (2005) *J. Biol. Chem.* **280,** 24978-24986.

7. von Bergen, M., Barghorn, S., Biernat, J., Mandelkow, E. M. & Mandelkow, E. (2005) *Biochim. Biophys. Acta* **1739,** 158-166.

8. von Bergen, M., Barghorn, S., Li, L., Marx, A., Biernat, J., Mandelkow, E. M. & Mandelkow, E. (2001) *J. Biol. Chem.* **276,** 48165-48174.

9. von Bergen, M., Friedhoff, P., Biernat, J., Heberle, J., Mandelkow, E. M. & Mandelkow, E. (2000) *Mol. Biol. Cell* **11,** 363A-363A.

10. Inouye, H., Sharma, D., Goux, W. J. & Kirschner, D. A. (2006) *Biophys. J.* **90,** 1774-89.

11. Lee, G., Cowan, N. & Kirschner, M. (1988) *Science* **239,** 285-8.

12.   Goedert, M., Spillantini, M. G., Jakes, R., Rutherford, D. & Crowther, R. A. (1989) *Neuron* **3,** 519-26.

13.   Goedert, M. & Crowther, R. A. (1989) *Neurobiol. Aging* **10,** 405-406.

14.   Goedert, M. (1996) *Neurobiol. Alzheimer's Dis.* **777,** 121-131.

15.   von Bergen, M., Barghorn, S., Muller, S. A., Pickhardt, M., Biernat, J., Mandelkow, E. M., Davies, P., Aebi, U. & Mandelkow, E. (2006) *Biochemistry* **45,** 6446-57.

16.   Jeganathan, S., von Bergen, M., Brutlach, H., Steinhoff, H. J. & Mandelkow, E. (2006) *Biochemistry* **45,** 2283-2293.

17.   Horowitz, P. M., LaPointe, N., Guillozet-Bongaarts, A. L., Berry, R. W. & Binder, L. I. (2006) *Biochemistry* **45,** 12859-12866.

18.   Guillozet-Bongaarts, A. L., Garcia-Sierra, F., Reynolds, M. R., Horowitz, P. M., Fu, Y. F., Wang, T. Y., Cahill, M. E., Bigio, E. H., Berry, R. W. & Binder, L. I. (2005) *Neurobiol. Aging* **26,** 1015-1022.

19.   Berry, R. W., Abraha, A., Lagalwar, S., LaPointe, N., Gamblin, T. C., Cryns, V. L. & Binder, L. I. (2003) *Biochemistry* **42,** 8325-8331.

20.   Horowitz, P. M., Patterson, K. R., Guillozet-Bongaarts, A. L., Reynolds, M. R., Carroll, C. A., Weintraub, S. T., Bennett, D. A., Cryns, V. L., Berry, R. W. & Binder, L. I. (2004) *J. Neurosci.* **24,** 7895-7902.

21.   Binder, L. I., Guillozet-Bongaarts, A. L., Garcia-Sierra, F. & Berry, R. W. (2005) *Biochim. Biophys. Acta* **1739,** 216-223.

22.   Esposito, G., Viglino, P., Novak, M. & Cattaneo, A. (2000) *J. Peptide Sci.* **6,** 550-559.

23.   Carmel, G., Mager, E. M., Binder, L. I. & Kuret, J. (1996) *J. Biol. Chem.* **271,** 32789-32795.

24.   Jicha, G. A., Lane, E., Vincent, I., Otvos, L., Hoffmann, R. & Davies, P. (1997) *J. Neurochem.* **69,** 2087-2095.

25.   Jicha, G. A., Bowser, R., Kazam, I. G. & Davies, P. (1997) *J. Neurosci. Res.* **48,** 128-132.

26.   Jicha, G. A., Berenfeld, B. & Davies, P. (1999) *J. Neurosci. Res.* **55,** 713-23.

27.   Jicha, G. A., Rockwood, J. M., Berenfeld, B., Hutton, M. & Davies, P. (1999) *Neurosci. Lett.* **260,** 153-6.

28.   von Bergen, M., Barghorn, S., Jeganathan, S., Mandelkow, E. M. & Mandelkow, E. (2006) *Neurodegener. Dis.* **3,** 197-206.

29.   Barghorn, S., von Bergen, M., Li, L., Biernat, J., Mandelkow, E. M. & Mandelkow, E. (2002) *Neurobiol. Aging* **23,** S528-S528.

30.   Fischer, D., Mukrasch, M. D., Bergen, M. V., Klos-Witkowska, A., Biernat, J., Griesinger, C., Mandelkow, E. & Zweckstetter, M. (2007) *Biochemistry* **46,** 2574-2582.

31.   Mukrasch, M. D., Markwick, P., Biernat, J., Bergen, M., Bernado, P., Griesinger, C., Mandelkow, E., Zweckstetter, M. & Blackledge, M. (2007) *J. Am. Chem. Soc.* **129,** 5235-43.

32.   Eliezer, D., Barre, P., Kobaslija, M., Chan, D., Li, X. H. & Heend, L. (2005) *Biochemistry* **44,** 1026-1036.

33. Barre, P. & Eliezer, D. (2006) *J. Mol. Biol.* **362,** 312-26.

34. Daniela Fischer, M. M., Martin von Bergen, Aleksandra Klos-Witkowska, Jacek Biernat, Christian Griesinger, Eckhard Mandelkow, Markus Zweckstetter (2006) *Biochemistry*.

35. Lippens, G. (2004) *Chembiochem* **5,** 256-256.

36. Smet, C., Leroy, A., Sillen, A., Wieruszeski, J. M., Landrieu, I. & Lippens, G. (2004) *Chembiochem* **5,** 1639-1646.

37. Salzmann, M., Pervushin, K., Wider, G., Senn, H. & Wuthrich, K. (1998) *Proc. Natl. Acad. Sci. U. S. A.* **95,** 13585-13590.

38. Pervushin, K., Riek, R., Wider, G. & Wuthrich, K. (1998) *J. Am. Chem. Soc.* **120,** 6394-6400.

39. Salzmann, M., Wider, G., Pervushin, K., Senn, H. & Wuthrich, K. (1999) *J. Am. Chem. Soc.* **121,** 844-848.

40. Preuss, U., Biernat, J., Mandelkow, E. M. & Mandelkow, E. (1997) *J. Cell Sci.* **110,** 789-800.

41. Wischik, C. M., Novak, M., Edwards, P. C., Klug, A., Tichelaar, W. & Crowther, R. A. (1988) *Proc. Natl. Acad. Sci. U. S. A.* **85,** 4884-4888.

42. Wischik, C. M., Novak, M., Thogersen, H. C., Edwards, P. C., Runswick, M. J., Jakes, R., Walker, J. E., Milstein, C., Roth, M. & Klug, A. (1988) *Proc. Natl. Acad. Sci. U. S. A.* **85,** 4506-4510.

43. Goedert, M., Wischik, C. M., Crowther, R. A., Walker, J. E. & Klug, A. (1988) *Proc. Natl. Acad. Sci. U. S. A.* **85,** 4051-4055.

44. Gustke, N., Trinczek, B., Biernat, J., Mandelkow, E. M. & Mandelkow, E. (1994) *Biochemistry* **33,** 9511-9522.

45. Mandelkow, E. M., Herrmann, M. & Ruhl, U. (1985) *J. Mol. Biol.* **185,** 311-327.

46. Zweckstetter, M. & Bax, A. (2001) *J. Am. Chem. Soc.* **123,** 9490-9491.

47. Panchal, S. C., Bhavesh, N. S. & Hosur, R. V. (2001) *J. Biomol. NMR* **20,** 135-147.

48. Delaglio, F., Grzesiek, S., Vuister, G. W., Zhu, G., Pfeifer, J. & Bax, A. (1995) *J. Biomo. NMR* **6,** 277-293.

49. Johnson, B. A. & Blevins, R. A. (1994) *J. Biomol. NMR* **4,** 603-614.

50. Schwarzinger, S., Kroon, G. J. A., Foss, T. R., Wright, P. E. & Dyson, H. J. (2000) *J. Biomol. NMR* **18,** 43-48.

51. Schwarzinger, S., Kroon, G. J. A., Foss, T. R., Chung, J., Wright, P. E. & Dyson, H. J. (2001) *J. Am. Chem. Soc.* **123,** 2970-2978.

52. Wishart, D. S. & Sykes, B. D. (1994) *J. Biomol. NMR* **4,** 171-80.

53. Wishart, D. S. & Sykes, B. D. (1994) *Nucl. Magn. Res., Pt C* **239,** 363-392.

54. Wishart, D. S., Bigam, C. G., Holm, A., Hodges, R. S. & Sykes, B. D. (1995) *J. Biomol. NMR* **5,** 67-81.

55. Wishart, D. S. & Sykes, B. D. (1994) *Methods Enzymol.* **239,** 363-92.

56. Bussell, R. & Eliezer, D. (2001) *J. Biol. Chem.* **276,** 45996-46003.

57. Ottiger, M., Delaglio, F. & Bax, A. (1998) *J. Magn. Res.* **131,** 373-378.

58. Farrow, N. A., Muhandiram, R., Singer, A. U., Pascal, S. M., Kay, C. M., Gish, G., Shoelson, S. E., Pawson, T., Formankay, J. D. & Kay, L. E. (1994) *Biochemistry* **33,** 5984-6003.

59. Farrow, N. A., Muhandiram, R., Singer, A. U., Pascal, S. M., Kay, C. M., Gish, G., Shoelson, S. E., Pawson, T., Forman-Kay, J. D. & Kay, L. E. (1994) *Biochemistry* **33,** 5984-6003.

60. Permi, P., Kilpelainen, I., Annila, A. & Heikkinen, S. (2000) *J. Biomol. NMR* **16,** 29-37.

61. Plaxco, K. W., Morton, C. J., Grimshaw, S. B., Jones, J. A., Pitkeathly, M., Campbell, I. D. & Dobson, C. M. (1997) *J. Biomol. NMR* **10,** 221-230.

62. Wu, D. H., Chen, A. D. & Johnson, C. S. (1995) *J. Magn. Res. Series A* **115,** 260-264.

63. Louhivuori, M., Paakkonen, K., Fredriksson, K., Permi, P., Lounila, J. & Annila, A. (2003) *J. Am. Chem. Soc.* **125,** 15647-15650.

64. Bernado, P., Bertoncini, C. W., Griesinger, C., Zweckstetter, M. & Blackledge, M. (2005) *J. Am. Chem. Soc.* **127,** 17968-9.

65. Bertoncini, C. W., Jung, Y. S., Fernandez, C. O., Hoyer, W., Griesinger, C., Jovin, T. M. & Zweckstetter, M. (2005) *Proc. Natl. Acad. Sci. U. S. A.* **102,** 1430-1435.

66. Palmer, A. G., 3rd, Kroenke, C. D. & Loria, J. P. (2001) *Methods Enzymol.* **339,** 204-38.

67. Craik, D. J. & Wilce, J. A. (1997) *Methods Mol. Biol.* **60,** 195-232.

68. Jones, J. A., Wilkins, D. K., Smith, L. J. & Dobson, C. M. (1997) *J. Biomol. NMR* **10,** 199-203.

69. Wilkins, D. K., Grimshaw, S. B., Receveur, V., Dobson, C. M., Jones, J. A. & Smith, L. J. (1999) *Biochemistry* **38,** 16424-16431.

70. Goedert, M. (1999) *Philos. Trans. R. Soc. Lond. B. Biol. Sci.* **354,** 1101-1118.

71. Lee, V. M. Y., Goedert, M. & Trojanowski, J. Q. (2001) *Ann. Rev. Neurosci.* **24,** 1121-1159.

72. Gamblin, T. C., Berry, R. W. & Binder, L. I. (2003) *Biochemistry* **42,** 15009-15017.

73. Mandelkow, E. M. (2004) *Neurobiol. Aging* **25,** S24-S24.

74. Delacourte, A. (2005) *Folia Neuropathol.* **43,** 244-257.

75. Trojanowski, J. Q. (2006) *Movement Dis.* **21,** S5-S5.

76. Schoenfeld, T. A. & Obar, R. A. (1994) in *Internatl. Rev. Cyt., Vol 151*, Vol. 151, pp. 67-137.

77. Tokimasa, M., Minoura, K., Hiraoka, S., Tomoo, K., Sumida, M., Taniguchi, T. & Ishida, T. (2005) *FEBS Lett.* **579,** 3481-3486.

78. Smet, C., Sambo, A. V., Wieruszeski, J. M., Leroy, A., Landrieu, I., Buee, L. & Lippens, G. (2004) *Biochemistry* **43,** 2032-2040.

79. Romero, P., Obradovic, Z., Li, X. H., Garner, E. C., Brown, C. J. & Dunker, A. K. (2001) *Proteins-Struct. Funct. Genet.* **42,** 38-48.

80. Dunker, A. K., Lawson, J. D., Brown, C. J., Williams, R. M., Romero, P., Oh, J. S., Oldfield, C. J., Campen, A. M., Ratliff, C. R., Hipps, K. W., Ausio, J., Nissen, M. S.,

Reeves, R., Kang, C. H., Kissinger, C. R., Bailey, R. W., Griswold, M. D., Chiu, M., Garner, E. C. & Obradovic, Z. (2001) *J. Mol. Graphics & Modelling* **19,** 26-59.

81. Sickmeier, M., Hamilton, J. A., LeGall, T., Vacic, V., Cortese, M. S., Tantos, A., Szabo, B., Tompa, P., Chen, J., Uversky, V. N., Obradovic, Z. & Dunker, A. K. (2007) *Nucl. Acids Res.* **35,** D786-D793.

82. Chatterjee, A., Mridula, P., Mishra, R. K., Mittal, R. & Hosur, R. V. (2005) *J. Biol. Chem.* **280,** 11369-78.

83. Hiller, S., Fiorito, F., Wuthrich, K. & Wider, G. (2005) *Proc. Natl. Acad. Sci. U. S. A.* **102,** 10876-10881.

84. Quarzago, D. & Moroder, L. (1994) *Lett. Peptide Sci.* **1,** 171-177.

85. Bielska, A. A. & Zondlo, N. J. (2006) *Biochemistry* **45,** 5527-5537.

86. Sillen, A., Barbier, P., Landrieu, I., Lefebvre, S., Wieruszeski, J. M., Leroy, A., Peyrot, V. & Lippens, G. (2007) *Biochemistry* **46,** 3055-3064.

87. Santarella, R. A., Skiniotis, G., Goldie, K. N., Tittmann, P., Gross, H., Mandelkow, E. M., Mandelkow, E. & Hoenger, A. (2004) *J. Mol. Biol.* **339,** 539-553.

88. Tycko, R. (2000) *Curr. Opin. Chem. Biol.* **4,** 500-6.

89. Gamblin, T. C., Berry, R. W. & Binder, L. I. (2003) *Biochemistry* **42,** 2252-2257.

90. Wang, J. Z., Grundke-Iqbal, I. & Iqbal, K. (2007) *Eur. J. Neurosci.* **25,** 59-68.

91. Illenberger, S., Zheng-Fischhofer, Q., Preuss, U., Stamer, K., Baumann, K., Trinczek, B., Biernat, J., Godemann, R., Mandelkow, E. M. & Mandelkow, E. (1998) *Mol. Biol. Cell* **9,** 1495-512.

92. Zheng-Fischhofer, Q., Biernat, J., Mandelkow, E. M., Illenberger, S., Godemann, R. & Mandelkow, E. (1998) *Eur. J. Biochem.* **252,** 542-52.

93. Biernat, J., Gustke, N., Drewes, G., Mandelkow, E. M. & Mandelkow, E. (1993) *Neuron* **11,** 153-163.

94. Poorkaj, P., Muma, N. A., Zhukareva, V., Cochran, E. J., Shannon, K. M., Hurtig, H., Koller, W. C., Bird, T. D., Trojanowski, J. Q., Lee, V. M. Y. & Schellenberg, G. D. (2002) *Ann. Neurol.* **52,** 511-516.

95. Hagestedt, T., Lichtenberg, B., Wille, H., Mandelkow, E. M. & Mandelkow, E. (1989) *J. Cell Biol.* **109,** 1643-1651.

SUPPORTING INFORMATION
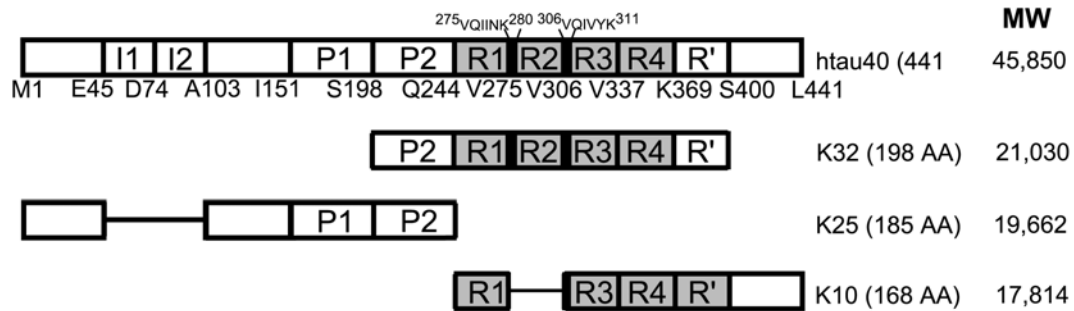
Figure 1 suppl.

Figure 1 supplemental: Schematic overview of tau constructs K10, K25, K32 and htau40. The hexapeptide sequences are highlighted by thick black bars.
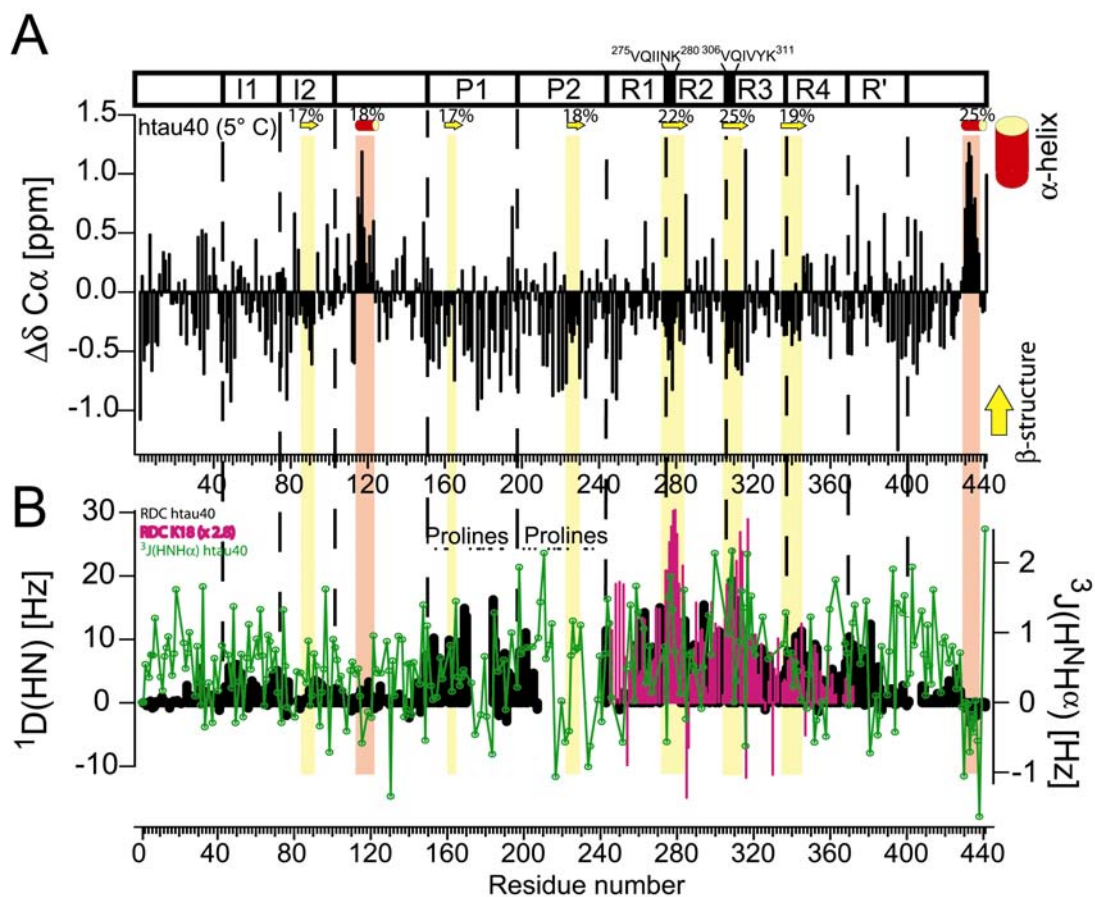
Figure 2 supplemental: Identification of residual structures (at 5 °C) by C^{α} secondary chemical shifts, $^{3}JH^{N}H^{\alpha}$-couplings and RDCs. Stretches with β-structure and α-helical propensity are highlighted by yellow and red boxes, respectively. **A:** Continuous negative and positive ΔC^{α} values indicate β-structure and α-helix propensity, which is quantified in % for each of these amino-acid stretches. **B**: $\Delta^{3}JH^{N}H^{\alpha}$ (green) and $^{1}D(HN)$ (black) couplings ^{15}N for htau40 at 5 °C. K18 RDCs multiplied with 2.8 (pink) are shown as comparison. All RDCs were measured using identical concentrations of Pf1 phages as alignment medium.
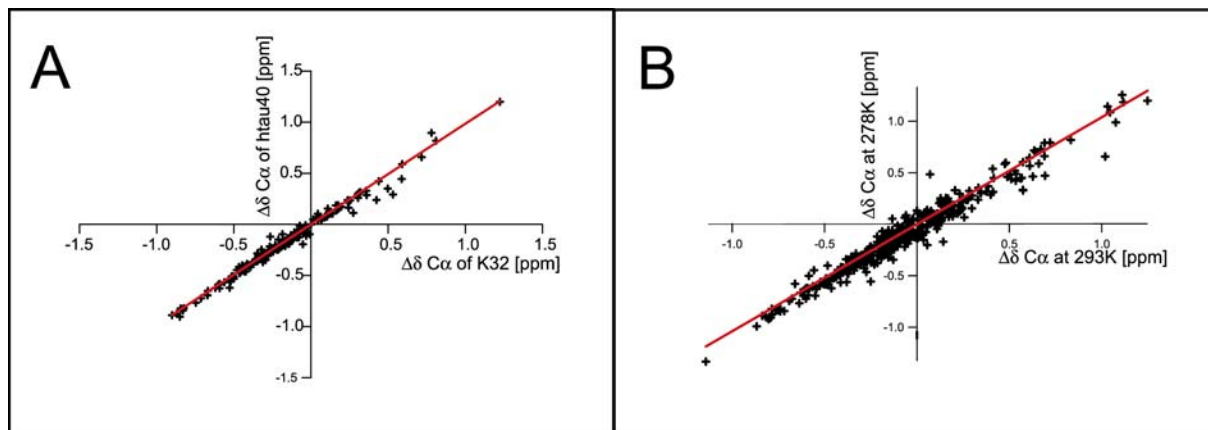
Figure 3 suppl.

Figure 3 supplemental: C$^\alpha$ secondary chemical shifts of htau40 at different conditions. **A:** High degree of correlation between ΔC$^\alpha$ values for htau40 and K32 indicates that additional sequential parts do not cause any structural change between htau40 and K32. **B:** ΔC$^\alpha$ values for htau40 at 5 °C and 20 °C correlate with each other. Thus, temperature differences have virtually no effect on secondary chemical shifts and occurrence of residual structure elements.
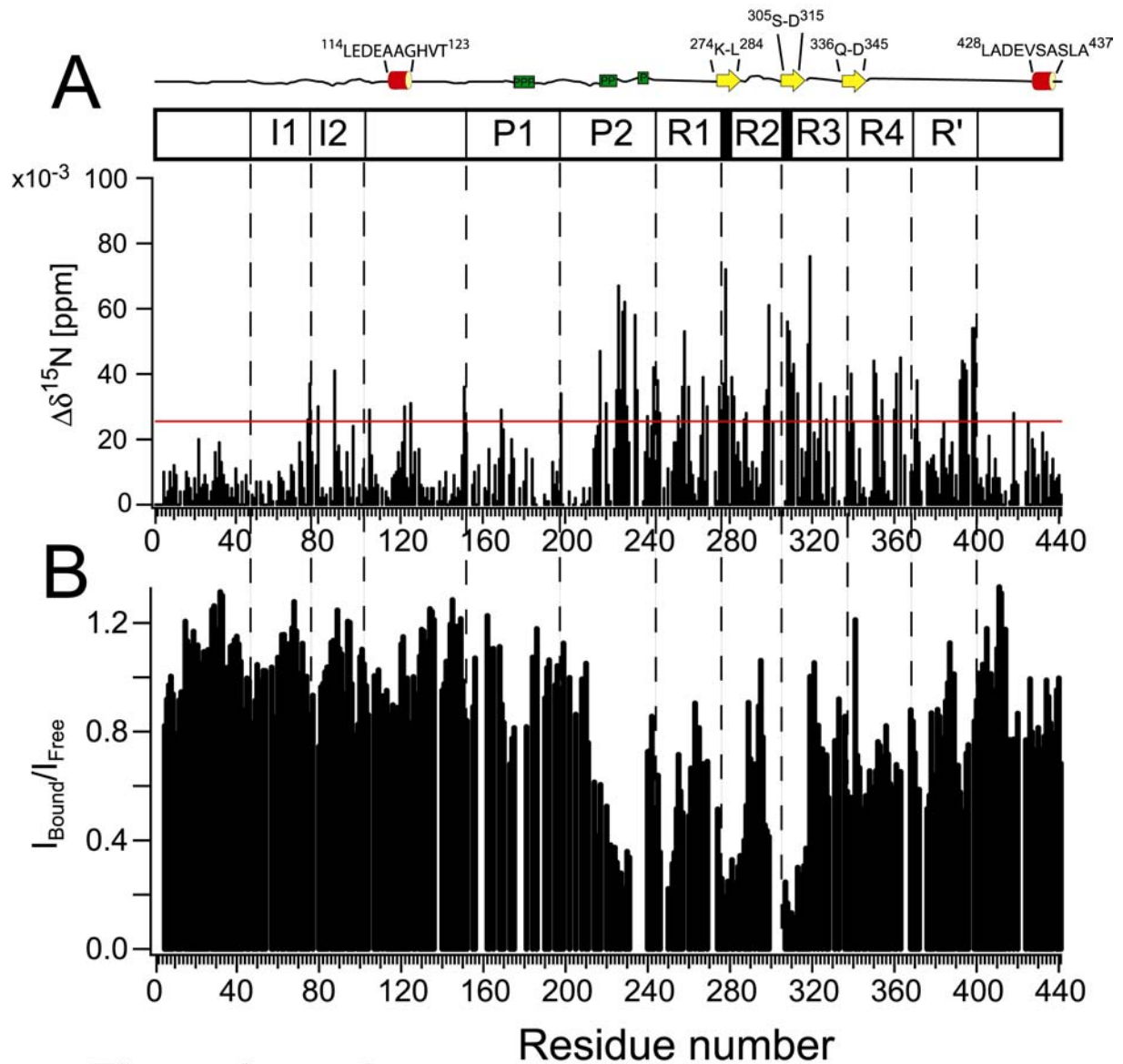
Figure 4 supplemental: Localization of MT binding sites in htau40 with the help of chemical shift perturbation mapping. **A:** ^{15}N chemical shift differences. An averaged estimated error (0.025 ppm) is shown as red line. Shift differences below this value are not significant. **B:** Intensity ratio between signals originating of htau40 in bound and in free state.
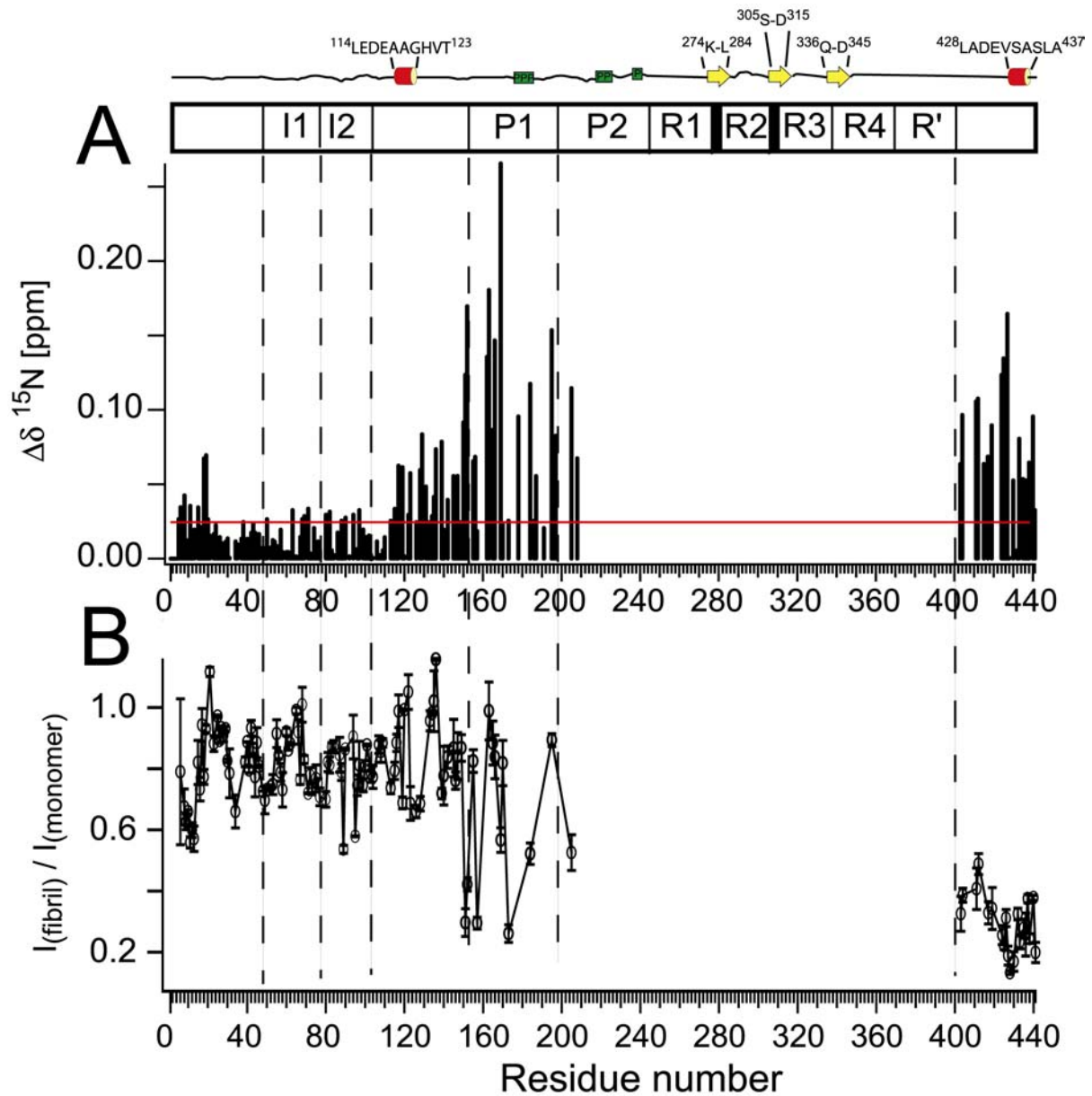
Figure 5 supplemental: Analysis of htau40 fibrils, for which only resonances for residues in the flexible 'fuzzy coat' are available. A: Chemical shift changes between monomeric htau40 and htau40 fibrils at 28 °C. Significantly high $\Delta\delta^{15}N$ values for the complete C-terminal part and residues 130-205. B: Profile of intensity ratios between monomeric htau40 and the average of two different PHF samples with error bars at 28 °C. The intensity profile could be reproduced.

Table with assigned ^1H, $^{13}C^\alpha$ and ^{15}N frequencies in ppm for htau40 at 278K and 293K.

Residue number	Aa type	^{1}H (278K)	^{15}N (278K)	^{13}C$^\alpha$ (278K/293K)	^{1}H (293K)	^{15}N (293K)
2	Ala			51.6		
3	Glu	8.742	121.556	54.33	8.656	121.54
4	Pro			63.11		
5	Arg	8.526	121.978	56	8.406	121.541
6	Gln	8.571	122.837	55.7	8.464	122.415
7	Glu	8.525	122.665	56.88		
8	Phe	8.17	119.62	57.4	8.051	119.381
9	Glu	8.269	122.554	56.42	8.207	122.243
10	Val	8.287	122.388	62.34	8.157	121.734
11	Met	8.537	125.204	55.22	8.424	124.724
12	Glu	8.477	122.879	56.55	8.38	122.54
13	Asp	8.404	121.724	54.17	8.317	121.435
14	His	8.428	120.121	55.83		
15	Ala	8.374	124.505	53.1	8.279	124.317
16	Gly	8.422	108.078	45.42	8.329	107.8
17	Thr	7.994	113.676	62.11	7.917	113.496
18	Tyr	8.339	122.803	58.31	8.234	122.493
19	Gly	8.375	110.899	45.25	8.288	110.601
20	Leu	8.138	121.331	55.41	8.041	121.254
21	Gly	8.476	109.4	45.33	8.383	109.146
22	Asp	8.231	120.475	54.28	8.158	120.343
23	Arg	8.323	121.347	56.26	8.227	121.07
24	Lys	8.445	122.246	56.61	8.354	122.059
25	Asp	8.388	120.556	54.3	8.31	120.414
26	Gln	8.342	120.463	56.03	8.257	120.266
27	Gly	8.479	109.514	45.42	8.399	109.318
28	Gly	8.25	108.648	45.16	8.174	108.481
29	Tyr	8.107	120.311	58.07	8.023	120.085
30	Thr	8.129	117.223	61.81	8.044	116.694
31	Met	8.331	123.11	55.5	8.233	122.774
32	His	8.505	120.869	55.96	8.374	120.653

33 Gln	8.455	122.647	55.76	8.35	122.26
34 Asp	8.601	122.124	54.72	8.502	121.86
35 Gln	8.412	120.309	55.7	8.313	120.085
36 Glu	8.522	122.458	56.89		
37 Gly	8.464	110.159	45.13	8.363	109.843
38 Asp	8.287	120.693	54.33	8.222	120.556
39 Thr	8.241	114.908	62.26	8.154	114.56
40 Asp	8.43	122.914	54.57	8.346	122.705
41 Ala	8.297	125.185	53.2	8.199	124.878
42 Gly	8.402	107.432	45.37	8.339	107.24
43 Leu	7.968	121.285	55.19	7.896	121.184
44 Lys	8.278	122.388	56.08	8.189	122.057
45 Glu	8.39	122.141	56.15	8.288	121.742
46 Ser	8.516	119.128	56.45	8.39	118.662
47 Pro			63.06		
48 Leu	8.349	122.488	55.23	8.232	122.107
49 Gln	8.434	121.982	55.29	8.311	121.563
50 Thr	8.373	119.418	60.05	8.243	118.785
51 Pro			63.23		
52 Thr	8.397	115.61	61.99	8.27	115.047
53 Glu	8.565	123.593	56.4	8.465	123.262
54 Asp	8.487	121.894	54.41	8.385	121.651
55 Gly	8.502	110.403	45.46	8.404	110.065
56 Ser	8.24	115.948	58.71	8.173	115.744
57 Glu	8.569	122.539	56.22	8.475	122.421
58 Glu	8.499	123.93	54.27	8.398	123.602
59 Pro			63.5		
60 Gly	8.676	110.281	45.17	8.568	109.888
61 Ser	8.262	115.787	58.52	8.174	115.568
62 Glu	8.75	122.982	56.84	8.658	122.814
63 Thr	8.275	115.097	61.82	8.177	114.73
64 Ser	8.372	118.241	58.47	8.287	117.978
65 Asp	8.41	122.785	54.33	8.33	122.568
66 Ala	8.231	124.501	52.84	8.144	124.286
67 Lys	8.319	120.304	56.17	8.217	119.972
68 Ser	8.307	117.169	58.22	8.21	116.805
69 Thr	8.273	119.04	59.93	8.158	118.567
70 Pro			63.2		

71 Thr	8.437	115.964	61.87	8.307	115.3
72 Ala	8.488	126.961	52.6	8.36	126.545
73 Glu	8.41	120.305	56.55	8.321	119.975
74 Asp	8.378	121.871	54.27	8.285	121.488
75 Val	8.174	120.739	62.19	8.057	120.219
76 Thr	8.324	118.997	62.02	8.212	118.175
77 Ala	8.326	128.835	50.61	8.189	128.347
78 Pro			62.75		
79 Leu	8.426	123.053	55.1	8.304	122.663
80 Val	8.246	122.202	62.14	8.107	121.493
81 Asp	8.497	124.973	54	8.375	124.53
82 Glu	8.61	123.328	57.06	8.485	122.855
83 Gly	8.501	109.417	45	8.433	109.313
84 Ala	8.009	124.776	50.85	7.935	124.605
85 Pro			63.58		
86 Gly	8.527	109.15	45.19	8.423	108.868
87 Lys	8.141	120.993	56.39	8.052	120.743
88 Gln	8.469	122.02	55.73	8.365	121.592
89 Ala	8.436	126.139	52.5	8.319	125.772
90 Ala	8.335	123.682	52.23	8.213	123.352
91 Ala	8.312	123.736	52.21	8.19	123.422
92 Gln	8.42	121.134	53.44	8.287	120.763
93 Pro					
94 His	8.639	119.932	55.83	8.49	119.648
95 Thr	8.191	117.175	61.78	8.052	116.478
96 Glu	8.583	124.136	56.18	8.464	123.835
97 Ile	8.41	124.715	58.6	8.265	124.144
98 Pro			63.08		
99 Glu	8.658	122.45	56.97	8.549	122.07
100 Gly	8.602	110.846	45.25	8.492	110.473
101 Thr	8.092	114.192	61.86	8.008	113.921
102 Thr	8.357	117.232	61.77	8.254	116.741
103 Ala	8.522	126.867	52.8	8.412	126.532
104 Glu	8.452	120.454	56.85	8.365	120.142
105 Glu	8.395	122.333	56.53	8.295	121.934
106 Ala	8.376	125.335	52.78	8.262	124.97
107 Gly	8.399	108.382	45.2	8.31	108.088
108 Ile	8.061	119.852	61.48	7.95	119.513

109 Gly	8.538	112.827	45.09	8.432	112.482
110 Asp	8.231	120.609	54.68	8.158	120.343
111 Thr	8.267	117.401	60.02	8.16	116.901
112 Pro			63.16		
113 Ser	8.637	117.242	57.99	8.497	116.762
114 Leu	8.548	124.773	55.77	8.412	124.59
115 Glu	8.435	120.926	57.19	8.358	120.78
116 Asp	8.247	121.456	54.85	8.168	121.148
117 Glu	8.398	122.153	57.58	8.331	121.959
118 Ala	8.245	123.749	53.24	8.185	123.603
119 Ala	8.026	121.885	53.12	7.955	121.772
120 Gly	8.166	107.023	45.42	8.11	106.855
121 His	8.093	118.776	55.97	8.04	118.795
122 Val	8.142	122.163	62.74	8.034	121.557
123 Thr	8.349	119.17	62.53	8.221	118.347
124 Gln	8.461	123.348	56.09	8.342	122.864
125 Ala	8.381	125.194	52.88	8.244	124.575
126 Arg	8.288	120.161	56.23	8.186	119.707
127 Met	8.38	122.153	55.58	8.278	121.693
128 Val	8.239	122.282	62.39	8.126	121.682
129 Ser	8.464	120.202	58.38	8.352	119.723
130 Lys	8.509	124.131	56.37	8.393	123.805
131 Ser	8.403	117.449	58.52	8.308	117.093
132 Lys	8.548	123.746	56.64	8.443	123.456
133 Asp	8.3	120.916	54.38	8.229	120.767
134 Gly	8.386	109.57	45.53	8.306	109.325
135 Thr	8.217	113.031	62.29	8.146	112.955
136 Gly	8.623	111.594	45.42	8.532	111.387
137 Ser	8.3	115.917	58.61		
138 Asp	8.497	122.332	54.5	8.418	122.202
139 Asp	8.235	121.037	54.66	8.185	120.867
140 Lys	8.269	121.228	56.73	8.188	120.993
141 Lys	8.146	121.301	56.43	8.067	120.968
142 Ala	8.223	124.899	52.6	8.125	124.571
143 Lys	8.357	120.888	56.37	8.238	120.566
144 Gly	8.451	109.997	45	8.363	109.843
145 Ala	8.348	124.008	52.92	8.239	123.86
146 Asp	8.346	118.823	54.23	8.278	118.801

147 Gly	8.317	109.058	45.6	8.256	108.894
148 Lys	8.13	120.519	56.3	8.085	120.378
149 Thr	8.275	116.603	62.46	8.157	115.912
150 Lys	8.459	125.478	56.21	8.339	124.891
151 Ile	8.294	123.778	60.81	8.155	123.076
152 Ala	8.528	129.586	52.21	8.408	129.114
153 Thr	8.347	117.785	59.99	8.191	117.082
154 Pro			63.17		
155 Arg	8.61	122.372	56.39	8.486	121.944
156 Gly	8.51	110.72	44.95	8.403	110.418
157 Ala	8.174	123.796	52.01	8.069	123.622
158 Ala	8.398	125.354	50.4	8.27	124.97
159 Pro					
160 Pro			63.27		
161 Gly	8.542	109.168	45.17	8.438	108.875
162 Gln	8.22	120	55.74	8.132	119.81
163 Lys	8.559	123.379	56.67	8.443	122.944
164 Gly	8.559	110.53	45.21	8.447	110.194
165 Glu	8.269	119.993	55.66	8.189	119.842
166 Ala	8.512	125.659	52.83	8.406	125.342
167 Asn	8.476	117.946	53.24	8.375	117.695
168 Ala	8.284	124.443	52.74	8.188	124.199
169 Thr	8.197	114.242	62.18	8.091	113.704
170 Arg	8.37	124.504	55.87	8.261	124.036
171 Ile	8.388	125.208	58.62	8.244	124.575
172 Pro			63.04		
173 Ala	8.466	124.932	52.28	8.336	124.602
174 Lys	8.44	121.432	56.15	8.314	121.001
175 Thr	8.351	119.508	60.01	8.205	118.815
176 Pro					
177 Pro			62.56		
178 Ala	8.461	125.96	50.37	8.33	125.657
179 Pro			62.75		
180 Lys	8.556	122.31	56.23	8.438	121.909
181 Thr	8.307	118.966	59.92	8.164	118.299
182 Pro					
183 Pro			62.92		
184 Ser	8.564	116.703	58.31	8.438	116.278

185 Ser	8.504	118.102	58.49	8.382	117.731
186 Gly	8.393	110.762	44.94	8.313	110.577
187 Glu	8.244	121.881	54.24	8.157	121.734
188 Pro					
189 Pro			62.77		
190 Lys	8.591	122.306	56.15	8.478	121.965
191 Ser	8.46	117.233	58.55	8.334	116.816
192 Gly	8.54	111.132	45.21	8.437	110.868
193 Asp	8.215	120.455	54.49	8.158	120.343
194 Arg	8.543	122.397	55.95	8.428	121.967
195 Ser	8.455	117.231	59.38	8.364	116.923
196 Gly	8.479	110.83	45.23	8.378	110.561
197 Tyr	8.022	120.319	58.05	7.959	120.103
198 Ser	8.159	118.542	57.8	8.09	118.084
199 Ser	8.36	119.167	56.49	8.256	118.872
200 Pro					
201 Gly	8.494	109.638	44.99	8.399	109.318
202 Ser	8.164	116.936	56.59	8.088	116.733
203 Pro			63.77		
204 Gly	8.501	109.44	45	8.4	109.044
205 Thr	8.096	115.806	59.88	8.004	115.614
206 Pro			63.92		
207 Gly	8.644	109.856	45.25		
208 Ser	8.177	115.816	58.67	8.111	115.642
209 Arg	8.508	123.145	56.17	8.413	122.876
210 Ser	8.359	117.135	58.48	8.268	116.775
211 Arg	8.489	123.362	55.94	8.387	123.063
212 Thr	8.355	118.934	60.03	8.235	118.339
213 Pro			63.12		
214 Ser	8.518	117.249	58.25	8.381	116.729
215 Leu	8.394	125.7	52.97	8.249	125.397
216 Pro			62.81		
217 Thr	8.443	118.708	60.13	8.278	117.935
218 Pro					
219 Pro			62.85		
220 Thr	8.349	115.602	62.01	8.205	114.97
221 Arg	8.473	124.09	55.7	8.351	123.695
222 Glu	8.531	124.376	54.34	8.414	123.961

223	Pro			62.87		
224	Lys	8.478	122.269	56.37	8.365	121.795
225	Lys	8.475	124.227	56.14	8.351	123.695
226	Val	8.299	123.259	62	8.159	122.533
227	Ala	8.478	129.155	52.23	8.36	128.628
228	Val	8.296	121.597	62.27	8.15	120.982
229	Val	8.424	126.597	62.25	8.284	125.775
230	Arg	8.623	126.842	55.7	8.498	126.273
231	Thr	8.405	119.796	59.97	8.261	119.098
232	Pro					
233	Pro			62.72		
234	Lys	8.509	122.124	56.19	8.388	121.711
235	Ser	8.546	119.418	56.51	8.407	118.87
236	Pro			63.33		
237	Ser	8.527	116.463	58.55	8.414	116.041
238	Ser	8.441	118.455	58.41	8.289	117.995
239	Ala	8.366	126.054	53.03	8.242	125.358
240	Lys	8.286	120.266	56.61	8.184	119.943
241	Ser	8.286	117.009	58.65	8.18	116.58
242	Arg	8.39	123.234	56.29	8.298	122.939
243	Leu	8.194	122.892	55.24	8.119	122.652
244	Gln	8.424	121.809	55.7	8.331	121.48
245	Thr	8.193	116.352	61.71	8.084	115.739
246	Ala	8.384	128.351	50.6	8.258	127.907
247	Pro			62.71		
248	Val	8.345	122.69	59.94	8.186	122.04
249	Pro			62.88		
250	Met	8.513	122.348	53.18	8.378	121.987
251	Pro			63.08		
252	Asp	8.488	120.925	53.95	8.371	120.482
253	Leu	8.35	124.011	55.39	8.204	123.556
254	Lys	8.318	120.632	56.82	8.232	120.37
255	Asn	8.296	118.826	53.17	8.223	118.592
256	Val	8.021	120.818	62.61	7.923	120.328
257	Lys	8.478	125.426	56.34	8.367	124.805
258	Ser	8.344	117.537	58.4	8.213	117.001
259	Lys	8.477	123.902	56.29	8.337	123.512
260	Ile	8.242	122.804	61.49	8.123	122.231

261 Gly	8.611	113.815	45.2	8.494	113.346
262 Ser	8.286	115.781	58.41	8.199	115.583
263 Thr	8.405	116.102	62.25	8.297	115.739
264 Glu	8.403	123.083	56.99	8.344	122.865
265 Asn	8.478	119.525	53.39	8.385	119.23
266 Leu	8.189	122.402	55.38	8.085	122.188
267 Lys	8.191	121.115	56.49	8.111	120.898
268 His	8.271	119.896	55.74	8.139	119.769
269 Gln	8.403	123.315	53.39	8.273	122.957
270 Pro			63.53		
271 Gly	8.758	110.535	45.35	8.622	110.138
272 Gly					
273 Gly	8.375	108.736	45.04	8.287	108.555
274 Lys	8.201	120.879	56.22	8.117	120.708
275 Val	8.263	122.663	62.39	8.137	121.972
276 Gln	8.569	125.682	55.43	8.456	125.148
277 Ile	8.427	124.615	60.98	8.294	124.034
278 Ile	8.395	126.705	60.76	8.266	125.966
279 Asn	8.64	124.389	52.95	8.518	123.852
280 Lys	8.451	123.328	56.63	8.32	122.847
281 Lys	8.354	122.701	56.52	8.262	122.383
282 Leu	8.199	123.734	55.04	8.122	123.439
283 Asp	8.383	122.155	53.9	8.295	121.884
284 Leu	8.445	124.286	55.21	8.311	123.879
285 Ser	8.377	116.159	59.49	8.311	115.904
286 Asn	8.31	120.417	53.29	8.245	120.208
287 Val	7.977	120.464	62.88	7.894	119.963
288 Gln	8.504	124.017	55.95	8.396	123.496
289 Ser	8.392	117.57	58.52	8.273	117.102
290 Lys	8.473	123.501	56.47	8.366	123.188
291 Cys	8.41	120.309	58.87	8.31	119.975
292 Gly	8.575	111.921	45.26	8.477	111.631
293 Ser	8.309	115.993	58.61	8.212	115.686
294 Lys	8.54	123.307	56.51	8.438	123.034
295 Asp	8.215	120.455	54.49	8.157	120.454
296 Asn	8.305	118.689	53.26	8.241	118.603
297 Ile	8.025	121.266	61.21	7.93	120.819
298 Lys	8.374	125.624	56.02	8.269	125.081

299 His	8.46	122.01	55.94	8.314	121.604
300 Val	8.265	124.793	59.73	8.119	124.101
301 Pro			63.53		
302 Gly	8.752	110.794	45.34	8.604	110.366
303 Gly					
304 Gly			45.07		
305 Ser	8.287	115.766	58.31	8.199	115.583
306 Val	8.243	122.2	62.29	8.126	121.682
307 Gln	8.505	125.243	55.49	8.395	124.687
308 Ile	8.361	124.765	60.99	8.224	124.081
309 Val	8.276	126.338	61.92	8.152	125.535
310 Tyr	8.538	126.748	57.92	8.392	126.067
311 Lys	8.225	126.381	53.58	8.13	125.804
312 Pro			62.82		
313 Val	8.262	121.086	62.38	8.138	120.448
314 Asp	8.464	124.788	53.51	8.337	124.266
315 Leu	8.634	125.794	55.51	8.48	125.265
316 Ser	8.432	116.278	59.79	8.371	116.009
317 Lys	7.956	122.168	56.05	7.893	121.863
318 Val	7.957	121.408	62.6	7.861	120.674
319 Thr	8.31	118.551	61.83	8.181	117.714
320 Ser	8.379	118.669	58.34	8.255	118.282
321 Lys	8.517	123.716	56.46	8.398	123.337
322 Cys	8.41	120.309	58.87	8.31	119.975
323 Gly	8.529	111.79	45.28	8.43	111.503
324 Ser	8.322	116.007	58.49	8.232	115.829
325 Leu	8.419	123.944	55.48	8.307	123.724
326 Gly	8.353	108.932	45.2	8.275	108.664
327 Asn	8.286	118.696	53.02	8.213	118.581
328 Ile	8.05	120.783	61.39	7.943	120.332
329 His	8.431	122.993	55.61	8.304	122.663
330 His	8.363	121.349	55.85	8.226	121.005
331 Lys	8.501	124.959	54.19	8.338	124.527
332 Pro			63.43		
333 Gly	8.715	110.48	45.27	8.589	110.147
334 Gly					
335 Gly			45.05		
336 Gln	8.307	119.955	55.65	8.222	119.834

337 Val	8.287	122.24	62.33	8.171	121.678
338 Lys	8.567	125.959	56.25	8.462	125.447
339 Val	8.437	124	62.32	8.3	123.397
340 Lys	8.574	126.773	56.17	8.457	126.213
341 Ser	8.462	118.047	58.23	8.341	117.624
342 Glu	8.585	123.669	56.47	8.499	123.413
343 Lys	8.381	122.593	56.34	8.28	122.19
344 Leu	8.297	123.784	55.05	8.181	123.555
345 Asp	8.354	121.388	53.97	8.257	121.176
346 Phe	8.247	121.456	58.53	8.142	120.982
347 Lys	8.237	121.91	56.92	8.157	121.734
348 Asp	8.165	120.247	54.51	8.103	120.033
349 Arg	8.052	121.094	56.33	8.007	120.761
350 Val	8.225	122.049	62.78	8.097	121.319
351 Gln	8.556	124.754	55.77	8.436	124.093
352 Ser	8.426	117.92	58.52	8.295	117.361
353 Lys	8.442	123.62	56.28	8.327	123.27
354 Ile	8.219	122.672	61.59	8.102	122.074
355 Gly	8.592	113.801	45.19	8.473	113.312
356 Ser	8.202	115.67	58.46	8.116	115.448
357 Leu	8.47	124.085	55.24	8.36	123.848
358 Asp	8.199	120.294	54.51	8.136	120.083
359 Asn	8.306	118.831	53.25	8.226	118.389
360 Ile	8.076	120.892	61.26	7.986	120.479
361 Thr	8.277	118.685	62.12	8.175	118.042
362 His	8.429	122.999	55.79	8.304	122.663
363 Val	8.26	124.637	59.73	8.111	123.958
364 Pro			63.54		
365 Gly	8.781	110.906	45.38	8.631	110.467
366 Gly					
367 Gly			45.11		
368 Asn	8.396	118.57	53.17	8.311	118.455
369 Lys	8.347	122.092	56.32	8.246	121.784
370 Lys	8.405	123.562	56.35	8.304	123.128
371 Ile	8.306	123.828	61	8.174	123.164
372 Glu	8.6	126.361	56.18	8.505	125.844
373 Thr	8.323	116.273	62.13	8.204	115.606
374 His	8.486	121.781	56.39	8.372	121.43

375 Lys	8.357	123.01	56.51	8.195	122.433
376 Leu	8.387	123.756	55.2	8.253	123.295
377 Thr	8.141	115.137	61.72	8.019	114.721
378 Phe	8.367	122.964	58.19	8.228	122.6
379 Arg	8.22	123.327	56.01	8.133	122.896
380 Glu	8.395	122.333	56.82	8.337	121.969
381 Asn	8.536	120.035	53.34	8.433	119.763
382 Ala	8.284	124.443	52.75	8.194	124.285
383 Lys	8.223	120.475	56.35	8.136	120.091
384 Ala	8.25	125.211	52.52	8.15	124.891
385 Lys	8.377	121.104	56.49	8.273	120.774
386 Thr	8.21	115.185	61.71	8.111	114.773
387 Asp	8.367	122.834	54.1	8.285	122.623
388 His	8.469	120.202	56.16	8.33	119.788
389 Gly	8.513	110.042	45.39	8.427	109.923
390 Ala	8.156	123.677	52.32	8.07	123.544
391 Glu	8.411	120.45	56.5	8.338	120.091
392 Ile	8.256	123.73	61.05	8.116	122.981
393 Val	8.221	126.08	61.98	8.079	125.183
394 Tyr	8.511	126.418	58.21	8.344	125.588
395 Lys	8.113	125.388	55.36	8.052	124.621
396 Ser	8.398	119.796	56.65	8.277	119.234
397 Pro			63.06		
398 Val	8.278	121.616	62.52	8.144	120.928
399 Val	8.407	125.748	61.97	8.255	124.871
400 Ser	8.527	120.639	58.43	8.393	120.049
401 Gly	8.53	111.573	45.26	8.417	111.233
402 Asp	8.268	120.577	54.33	8.2	120.441
403 Thr	8.247	114.666	61.58	8.139	114.216
404 Ser	8.354	120.166	57	8.269	119.836
405 Pro			63.07		
406 Arg	8.526	121.978	56	8.406	121.541
407 His	8.397	120.183	56	8.304	119.966
408 Leu	8.295	124.127	55.07	8.173	123.597
409 Ser	8.359	116.454	58.35	8.24	116.09
410 Asn	8.513	121.017	53.27	8.416	120.714
411 Val	8.098	120.133	62.35	7.997	119.668
412 Ser	8.49	119.848	58.27	8.377	119.33

413 Ser	8.565	118.615	58.61	8.437	118.235
414 Thr	8.238	115.079	62.18	8.157	114.843
415 Gly	8.355	111.306	45.26	8.286	111.067
416 Ser	8.183	115.843	58.2	8.111	115.642
417 Ile	8.283	122.388	61.23	8.176	121.998
418 Asp	8.369	124.055	54.44	8.284	123.687
419 Met	8.298	121.236	55.34	8.188	120.87
420 Val	8.179	121.757	62.45	8.07	121.161
421 Asp	8.444	123.941	54.3	8.341	123.517
422 Ser	8.212	117.299	56.47	8.099	116.869
423 Pro			63.39		
424 Gln	8.525	120.776	55.75	8.418	120.344
425 Leu	8.3	124.13	55.15	8.168	123.612
426 Ala	8.359	125.156	52.66	8.242	124.727
427 Thr	8.177	114.065	61.92	8.045	113.433
428 Leu	8.316	124.884	55.51	8.196	124.572
429 Ala	8.306	124.41	53.05	8.212	124.302
430 Asp	8.237	119.565	54.9	8.156	119.316
431 Glu	8.315	121.514	57.49	8.269	121.135
432 Val	8.207	121.752	63.84	8.104	121.144
433 Ser	8.361	118.52	59.62	8.27	118.227
434 Ala	8.334	125.84	53.6	8.238	125.573
435 Ser	8.117	114.491	59.42	8.045	114.151
436 Leu	8.038	123.701	55.88	7.966	123.479
437 Ala	8.032	123.487	53.06	7.972	123.354
438 Lys	8.07	119.9	56.59	7.999	119.669
439 Gln	8.235	120.961	56.03	8.175	120.769
440 Gly	8.378	110.511	45.28	8.307	110.338
441 Leu	7.804	127.015	56.46	7.701	126.982

7   Curriculum vitae

Seit August 2003	Promotion in Göttingen am Max-Planck-Institut für biophysikalische Chemie bei Prof. C. Griesinger unter der Betreuung von Dr. M. Zweckstetter

- Thema der Dissertation: Untersuchung des Tau-Proteins mit Hilfe von *NMR-Spektroskopie*
- Förderung durch ein Stipendium des Boehringer Ingelheim Fonds
- Stipendiat des DFG Graduiertenkollegs GRK 782 "Spectroscopy and Dynamics of Molecular Aggregates, Chains, Coils and Networks" (Vorträge beim Bunsenkolloquium 2005 und bei der Evaluierung durch die DFG 2006)

Oktober 2002 - April 2003	Diplomarbeit am Institut für biophysikalische Chemie der Johann Wolfgang Goethe-Universität bei Prof. H. Rüterjans unter der Betreung von PD C. Lücke Titel: Untersuchung der löslichen Cu_A-Domäne aus der Untereinheit II der ba_3 Cytochrom c Oxidase von *Thermus thermophilus* mit Hilfe der NMR Spektroskopie
2000 – 2003	Hauptstudium des Studienganges Biochemie an der Johann Wolfgang Goethe-Universität Nebenfächer: Organische Chemie und Informatik
1998 – 2000	Grundstudium des Studienganges Biochemie an der Johann Wolfgang Goethe-Universität
1997 – 1998	Zivildienst in den Höchster Kliniken im Zentral-OP
1997	Allgemeine Hochschulreife Auszeichnung mit dem Karl von Frisch – Preis im Fach Biologie
23.05.1978	Geboren in Frankfurt am Main/Höchst

Publikationen

- Fischer, D., **Mukrasch, M. D.**, Bergen, M. V., Klos-Witkowska, A., Biernat, J., Griesinger, C., Mandelkow, E., and Zweckstetter, M. (2007). Structural and Microtubule Binding Properties of Tau Mutants of Frontotemporal Dementias. *Biochemistry 46*, 2574-2582.

- **Mukrasch, M. D.**, Biernat, J., von Bergen, M., Griesinger, C., Mandelkow, E., and Zweckstetter, M. (2005). Sites of tau important for aggregation populate beta-structure and bind to microtubules and polyanions. *J. Biol. Chem. 280*, 24978-24986.

- **Mukrasch, M. D.**, Lucke, C., Lohr, F., Maneg, O., Ludwig, B., and Ruterjans, H. (2004). Letter to the Editor: Complete H-1, N-15 and C-13 assignment of the soluble domain of the ba(3) oxidase subunit II of Thermus thermophilus in the reduced state. *J. Biomol. NMR 28*, 297-298.

- **Mukrasch, M. D.**, Markwick, P., Biernat, J., Bergen, M., Bernado, P., Griesinger, C., Mandelkow, E., Zweckstetter, M., and Blackledge, M. (2007a). Highly populated turn conformations in natively unfolded tau protein identified from residual dipolar couplings and molecular simulation. *J. Am. Chem. Soc. 129*, 5235-5243.

- **Mukrasch, M. D.**, von Bergen, M., Biernat, J., Fischer, D., Griesinger, C., Mandelkow, E., and Zweckstetter, M. (2007b). The "jaws" of the tau-microtubule interaction. *J. Biol. Chem. 282*, 12230-12239.

- Muresanu, L., Pristovsek, P., Lohr, F., Maneg, O., **Mukrasch, M. D.**, Ruterjans, H., Ludwig, B., and Lucke, C. (2006). The electron transfer complex between cytochrome c552 and the CuA domain of the Thermus thermophilus ba3 oxidase. A combined NMR and computational approach. *J. Biol. Chem. 281*, 14503-14513.

Konferenzen

- **Marco D. Mukrasch**, Jacek Biernat, Martin von Bergen, Christian Griesinger, Eckhard Mandelkow and Markus Zweckstetter: The repeat domain of the tau protein at high resolution. Seeds of aggregation and binding to polyanions and microtubules. **21st International Conference on Magnetic Resonance in Biological Systems, Hyderabad (Indien), 2005** - Präsentation

- **Marco D. Mukrasch**, Phineus Markwick, Jacek Biernat, Martin von Bergen, Pau Bernado, Daniela Fischer, Christian Griesinger, Eckhard Mandelkow, Martin Blackledge, Markus Zweckstetter : Study of the Conformational Behaviour of the Tau Protein using Residual Dipolar Couplings, Paramagnetic Relaxation Enhancement and Molecular Simulation. **47th ENC, Asilomar (Kalifornien), 2006** – Poster